Kaon matrix elements and *CP* violation from quenched lattice QCD: The 3-flavor case

T. Blum,[1] P. Chen,[2] N. Christ,[2] C. Cristian,[2] C. Dawson,[3] G. Fleming,[2,*] R. Mawhinney,[2] S. Ohta,[4,1] G. Siegert,[2] A. Soni,[3] P. Vranas,[5] M. Wingate,[1,*] L. Wu,[2] and Y. Zhestkov[2]

[1]*RIKEN-BNL Research Center, Brookhaven National Laboratory, Upton, New York 11973, USA*

[2]*Physics Department, Columbia University, New York, New York 10027, USA*

[3]*Physics Department, Brookhaven National Laboratory, Upton, New York 11973, USA*

[4]*Institute for Particle and Nuclear Studies, KEK, Tsukuba, Ibaraki, 305-0801, Japan*

[5]*IBM Research, Yorktown Heights, New York 10598, USA*

(Received 19 July 2002; published 30 December 2003)

We report the results of a calculation of the $K\rightarrow\pi\pi$ matrix elements relevant for the $\Delta I=1/2$ rule and ϵ'/ϵ in quenched lattice QCD using domain wall fermions at a fixed lattice spacing $a^{-1}\sim 2$ GeV. Working in the three-quark effective theory, where only the *u*, *d*, and *s* quarks enter and which is known perturbatively to next-to-leading order, we calculate the lattice $K\rightarrow\pi$ and $K\rightarrow|0\rangle$ matrix elements of dimension six, four-fermion operators. Through lowest order chiral perturbation theory these yield $K\rightarrow\pi\pi$ matrix elements, which we then normalize to continuum values through a nonperturbative renormalization technique. For the ratio of isospin amplitudes $|A_0|/|A_2|$ we find a value of 25.3 ± 1.8 (statistical error only) compared to the experimental value of 22.2, with individual isospin amplitudes 10%–20% below the experimental values. For ϵ'/ϵ, using known central values for standard model parameters, we calculate $(-4.0\pm 2.3)\times 10^{-4}$ (statistical error only) compared to the current experimental average of $(17.2\pm 1.8)\times 10^{-4}$. Because we find a large cancellation between the $I=0$ and $I=2$ contributions to ϵ'/ϵ, the result may be very sensitive to the approximations employed. Among these are the use of quenched QCD, lowest order chiral perturbation theory, and continuum perturbation theory below 1.3 GeV. We also calculate the kaon *B* parameter B_K and find $B_{K,\overline{\mathrm{MS}}}(2\ \mathrm{GeV})=0.532(11)$. Although currently unable to give a reliable systematic error, we have control over statistical errors and more simulations will yield information about the effects of the approximations on this first-principles determination of these important quantities.

DOI: 10.1103/PhysRevD.68.114506 PACS number(s): 11.15.Ha, 11.30.Er, 12.38.Gc, 12.39.Fe

I. INTRODUCTION

The experimental observation of *CP* violation in kaon decays [1–5] presents a continuing challenge to theoretical calculations within the standard model and its possible extensions. The standard model allows *CP* violation through the single avenue set down by Kobayashi and Maskawa almost 30 years ago [6], but a quantitative comparison between theory and experiment requires the calculation of well-defined electroweak interactions involving quarks, when the quarks are bound into kaons and pions. These ''weak matrix elements'' can be calculated from first principles using the techniques of lattice QCD, although many technical difficulties have impeded the realization of this goal. A large number of analytical and phenomenological techniques have also been employed to estimate these matrix elements and these are reviewed in [7]. The work described in this paper represents a complete calculation of the matrix elements, using the approximations described below, that determines the amplitudes A_0 and A_2 which describe two pion decays of kaons, both their magnitudes, and their *CP*-violating phases. We also calculate the kaon *B* parameter B_K which enters standard model predictions for the *CP* violation effects first seen by Cronin and Fitch [1].

A major approximation made in this work is the use of quenched lattice QCD in the evaluation of the matrix elements and the determination of their normalizations. This truncation of the full theory reduces the required computer power markedly, but is an uncontrolled approximation. In most cases where quenched results are compared with experimental values, agreement is at or better than the ~25% level, but there is no convincing argument that such an agreement must be uniformly good for all low-energy hadronic phenomena. It should be stressed that, if the necessary computer power were available to generate an ensemble of dynamical fermion lattices, the numerical work and analysis in this paper could be easily redone, yielding values without the approximation of quenching.

Almost all attempts to calculate the matrix elements needed for *CP* violation using lattice QCD have been done in the quenched approximation. The first lattice calculations using Wilson fermions were unsuccessful [8,9], primarily due to the lack of chiral symmetry on the lattice. Staggered fermions do provide a remnant chiral symmetry on the lattice and a calculation of the matrix elements studied here has been done [10]. To match continuum and lattice operators for staggered fermions, perturbation theory was used [11]. Because of the large size of the one-loop perturbative corrections for unimproved staggered fermions, the matching introduces large uncertainties. The current calculation uses domain wall fermions, which have controllable chiral symmetry breaking at finite lattice spacing, and a nonperturbative renormalization technique to relate lattice quantities to the continuum.

*Present address: Physics Department, The Ohio State University, Columbus, OH 43210.

The electroweak physics responsible for $K\to\pi\pi$ decays is readily described by an effective weak Hamiltonian, valid for low energy processes, which is given by four-quark operators multiplied by perturbatively calculable Wilson coefficients. In Sec. II, we give our notation for the effective Hamiltonian and the operator basis we will use. We discuss both the three-quark effective Hamiltonian, where *u*, *d*, and *s* quarks can appear, and the four-quark Hamiltonian, which includes the *c* quark. The Wilson coefficients are known in both cases, although the three-quark case requires using continuum perturbation theory down to a scale below the charm quark mass, $m_c \approx 1.3$ GeV. The $\mathrm{SU}(3)_L \otimes \mathrm{SU}(3)_R$ quantum numbers of the operators are given, since these determine their mixing under renormalization and their behavior in the chiral limit. In this section we also give the relations between the matrix elements we calculate and the quantities ϵ' and ϵ.

A second approximation made in this work is the use of primarily lowest order chiral perturbation theory in the determination of the desired $K\to\pi\pi$ matrix elements [12]. We evaluate $K\to\pi$ and $K\to|0\rangle$ matrix elements in quenched lattice QCD and then use lowest-order, full QCD chiral perturbation theory to determine $K\to\pi\pi$ matrix elements. This is reviewed in Sec. III. Thus our calculation is strictly an evaluation of the relevant matrix elements for small quark masses. The effects of quenching on lowest order full QCD chiral perturbation theory and the chiral limit of quenched QCD are still subjects where analytic understanding is limited. We address quenching effects in our results where analytic calculations offer guidance as to the mass dependence expected in quenched amplitudes. However, in general, such phenomena are neglected in the quenched approximation and their presence serves as a measure of the size of systematic error. Once we have determined values for the $K\to\pi\pi$ matrix elements valid in the region of small quark mass, we then use the known chiral logarithms in full QCD to extrapolate to the physical kaon mass. The size of these next-to-leading-order, chiral logarithms provides an indication of the importance of the other next-to-leading-order terms which we do not include in our extrapolation. Terms of this type, i.e., $m^2\ln(m^2)$ where *m* is a pseudoscalar mass, we will refer to as conventional chiral logarithms. Similar $m^2\ln(m^2)$ terms also occur in the quenched theory, along with the more singular quenched chiral logarithms [13–15] discussed in Sec. III.

To employ chiral perturbation theory as discussed in the previous paragraph, it is important to use a lattice fermion formulation which preserves chiral symmetry for the low energy physics. (The presence of chiral symmetry also simplifies operator mixing and renormalization, which we discuss shortly.) A major theoretical advance in this area [16] is provided by the domain wall [16–18]and overlap fermion [19,20] formulations of lattice fermions. Here we use the domain wall fermion formulation, which has been shown, even for the quenched theory, to have small chiral symmetry breaking effects for currently accessible values for the length of the introduced fifth dimension [21,22]. In Sec. IV we discuss the features of domain wall fermions relevant for this calculation, paying particular attention to the nonuniversal character of the chiral symmetry breaking for power divergent operators and the topological near-zero modes present in quenched calculations at finite volume. This discussion will be important for understanding the chiral limit of our matrix elements and in the subtraction of power divergent terms from them.

In Sec. V we discuss the basic parameters of our numerical calculations. Then in Sec. VI we present further tests of the chiral properties of domain wall fermions, in particular extending the results of [21] to the case of Ward-Takahashi identities involving power divergent operators. Here we also determine the size of quenched chiral logarithm effects in our simulations. The numerical examples in this section complement the theoretical explanations in Sec. IV.

The continuum perturbation theory calculations of the Wilson coefficients for the low energy effective Hamiltonian have been done to next-to-leading order [23,24]. Using the results from these calculations, we must evolve the Wilson coefficients to the scale where we have renormalized our lattice operators. This is discussed in Sec. VII and involves some subtlety due to the matching between the Wilson coefficients calculated in full QCD and our quenched operators. In addition, we must also incorporate perturbatively calculated matching factors to move from the modified minimal subtraction ($\overline{\mathrm{MS}}$) scheme used in the continuum to the regularization independent scheme used for our lattice operators.

To handle the renormalization of lattice operators, we employ another major theoretical advance of recent years, the nonperturbative renormalization (NPR) technique. In this method one adopts a renormalization scheme for defining renormalized operators that is independent of the regularization. Such a scheme can then be implemented in both perturbation theory (where dimensional regularization is typically used) and in a nonperturbative lattice calculation. This NPR approach avoids the use of lattice perturbation theory and the attendant worries about its accuracy. In principle, NPR permits the use of perturbation theory to be restricted to short distances where its validity is more certain. Of the two most developed approaches to NPR, the Schroedinger functional [25] and momentum-space based RI method [26], we have adopted the latter method since much important analytical work for the kaon system has already been done supporting this approach. In Sec. VIII, we discuss in some detail how we have implemented this technique for the $\Delta S=1$ operators of primary interest in this paper. This represents one of the most complicated cases where this technique has been used to date and we have only removed mixings with the dominant lower-dimensional operators. It is worth noting that this technique is particularly well suited for use with domain wall fermions, since the definition of the regularization independent scheme involves off-shell quark fields. For domain wall fermions the suppression of explicit chiral symmetry breaking and the consequent elimination of order *a* lattice spacing errors occurs both on- and off-shell.

In Sec. IX, we discuss the precise quantities that we measure on the lattice to determine $K\to\pi$ and $K\to|0\rangle$ matrix elements. We have used standard ratios of lattice Green's functions to measure these matrix elements, but the presence of topological near-zero modes leads to preferred choices for the factors in the ratio to minimize the effects of zero modes.

The tables referred to in Sec. IX report our bare lattice values for these quantities.

We can now use our lattice results for the bare $K\to\pi$ and $K\to|0\rangle$ matrix elements to evaluate the chiral perturbation theory constants which determine $K\to\pi\pi$ matrix elements. In Sec. X we discuss the $\Delta I=3/2$ matrix elements, where the chiral perturbation theory constants come directly from $K\to\pi$ matrix elements. Depending on the operator involved, these operators can vanish or be nonzero in the chiral limit. We find that it is important to know the coefficients of the conventional chiral logarithm terms from analytic calculations in order to determine the chiral perturbation theory constants.

In Sec. XI, we perform a similar analysis of our lattice data to determine the chiral perturbation theory constants for $\Delta I=1/2$ matrix elements. This case is more subtle numerically, since it involves the cancellation of unphysical, power divergent effects between $K\to\pi$ and $K\to|0\rangle$ matrix elements in the determination of the desired physical chiral perturbation theory constants. For one group of operators, we can check this cancellation by using the Wigner-Eckart theorem to relate $\Delta I=1/2$ constants, which involve subtractions, to $\Delta I=3/2$ constants, which do not. We find the agreement expected. The end result of our numerical determinations are the values given in Table XXXVIII. These are lattice values from a quenched calculation, using the formulas from chiral perturbation theory for full QCD.

In Sec. XII we discuss how to take these final lattice values and calculate physical quantities. In the spirit of the quenched approximation we take these quenched results as an approximation for the desired full QCD quantities. In particular, for $K\to\pi\pi$ matrix elements which vanish in the chiral limit, we take our quenched values for the slope with respect to quark mass of these matrix elements as the value for the slope for the full QCD matrix elements. For $K\to\pi\pi$ matrix elements which are nonzero in the chiral limit, the chiral limit value in the quenched theory is used as the chiral limit value in the full theory. We can then determine physical matrix elements at the kaon mass by extrapolating in lowest order chiral perturbation theory. Since the chiral logarithms are known, we can also extrapolate including the effects of the logarithms. This is not a complete higher order chiral perturbation theory calculation, but gives an indication of the size of the effects entering at next order.

In Sec. XIII we combine the matrix elements, Wilson coefficients, nonperturbative renormalization, and central values for standard model parameters to give physical values for $\mathrm{Re}(A_0)$, $\mathrm{Re}(A_2)$ and their ratio, which reflects the $\Delta I=1/2$ rule. Figures 29, 30, and 31 show our results for the various extrapolations, along with the physical values. The general agreement with the experimental values is quite good, in spite of the many approximations in the calculation. We also report our results for the kaon B parameter, B_K, at the end of this section.

Section XIV also combines matrix elements, Wilson coefficients, nonperturbative renormalization, and central values for standard model parameters, but now the values for $\mathrm{Im}(A_0)$, $\mathrm{Im}(A_2)$, and $\mathrm{Re}(\epsilon'/\epsilon)$ are the focus. Figures 35 and 36 show $\mathrm{Im}(A_0)$ and $\mathrm{Im}(A_2)$ and Fig. 38 shows $\mathrm{Re}(\epsilon'/\epsilon)$. For $\mathrm{Re}(\epsilon'/\epsilon)$, a large cancellation is occurring between individual isospin contributions, as can be seen in Fig. 39. It is important to note that the magnitudes of each of the two individual isospin terms are very similar to the experimental value for $\mathrm{Re}(\epsilon'/\epsilon)$. We would like to point out that even though in principle lattice techniques allow a calculation of ϵ'/ϵ, here we have used experimental information regarding the phases of ϵ' and ϵ in our calculation of $\mathrm{Re}(\epsilon'/\epsilon)$.

Table XLIX gives our final values for the physical quantities $\mathrm{Re}(A_0)$, $\mathrm{Re}(A_2)$, $\mathrm{Re}(A_0)/\mathrm{Re}(A_2)$, and $\mathrm{Re}(\epsilon'/\epsilon)$. Our conclusions are given in Sec. XV and the five Appendixes contain further details about our conventions, the decomposition of operators into irreducible representations of $\mathrm{SU}(3)_L\otimes\mathrm{SU}(3)_R$, and other definitions used in the text.

II. GENERAL ANALYTIC FRAMEWORK

A. $K\to\pi\pi$ in the standard model

At energies below the electroweak scale, the weak interactions can be described by local four-fermion operators due to the essentially point-like character of the vector boson interactions for low energies. Simple charged vector boson exchange produces current−current operators, with both currents left-handed, of the form $(\bar{q}q')_{(V-A)}\,(\bar{q}''q''')_{(V-A)}$. Additional low-energy four-fermion operators arise from more complicated standard model processes involving loops with heavy particles, including the vector bosons and the top quark. The naive suppression of these nonexchange operators, due to the large masses in the loop propagators and additional powers of the couplings, is offset somewhat by the large phase space for the loop integrals and the large logarithms which appear due to the disparity between GeV scale hadronic physics and these heavy masses. The operator product expansion and the renormalization group provide the framework for understanding such logarithmic enhancements and, coupled with continuum perturbation theory, provide a way to calculate these logarithmic effects. Such calculations yield the low-energy four-fermion operators' Wilson coefficients, which encapsulate the high energy physics in the low-energy effective theory.

Thus for energies well below the electroweak scale but above the bottom quark mass, we have an effective weak Hamiltonian with four-fermion interactions, where the coefficients of a given operator depend on μ, m_t, m_W, m_Z, α_s, α, and the elements of the Cabibbo-Kobayashi-Maskawa (CKM) matrix, V_{lm}. The four-fermion interactions can involve all quark fields, except the top, giving the Hamiltonian the generic form

$$\mathcal{H}_{\mathrm{eff}}=\frac{G_F}{\sqrt{2}}\sum_i A_i(\mu,m_t,m_W,m_Z,\alpha_s,\alpha,V_{lm})\times(\bar{q}_i\Gamma_i q_i')(\bar{q}_i''\Gamma_i' q_i''').\quad(1)$$

The scale μ which appears in this equation is introduced through the normalization condition required to define the composite four-fermion operators, whose dependence on μ is not shown. The explicit μ dependence of the coefficients A_i cancels the μ dependence implicit in these operators. In

studying physics at energy scales well below the bottom quark mass, we can remove the bottom quark from the operators that appear in $\mathcal{H}_{\rm eff}$, renormalizing at a scale μ which is generally chosen near the scale of the physics under consideration. Of course, the Wilson coefficients A_i must now depend explicitly on the bottom quark mass, m_b. A similar elimination of the charm degrees of freedom can be achieved if $\mathcal{H}_{\rm eff}$ is specialized to a form valid for energies well below the charm quark mass.

Following the general discussion above, one can determine the terms in the low-energy effective Hamiltonian relevant to particular processes, such as the $\Delta S=1$, $\Delta D=-1$ case of primary interest in this study. The terms arising from simple vector boson exchange, which should play a dominant role in the $\Delta I=1/2$ rule because of their large Wilson coefficients, were first discussed in [27,28], where it was also found that the A_i coefficients for these terms could explain some of the enhancement given by the $\Delta I=1/2$ rule. Subsequently, additional low-energy terms arising from standard model graphs involving loops were identified [29,30] and their importance for CP violation in the full six-quark standard model emphasized in Refs. [31–33]. These additional low-energy four-quark operators are referred to as penguin operators and are further refined into QCD and electroweak penguin operators. Historically attention was first focused on the QCD penguins, since the electroweak penguins are suppressed by a power of the electroweak coupling α. However, as reviewed below, the electroweak penguins are important for CP violation in the standard model since they are nonzero to lowest order in the light quark masses, are enhanced by the $\Delta I=1/2$ rule, and enter with coefficients that increase with the top quark mass.

For our calculations, the energy scale that can be used in the effective theory must be well below m_b, since we will work on a lattice with $a^{-1}\sim 2$ GeV. We do, however, have the ability to work both with an effective theory valid for energies at or above m_c (a four-flavor theory) and with a three-flavor theory that is only valid for energies below m_c. Thus we will actually deal with two effective Hamiltonians for $\Delta S=1$ processes. For clarity, we will denote the four-flavor $\Delta S=1$ effective Hamiltonian valid for energies below m_b by $\mathcal{H}_c^{(\Delta S=1)}$ and use $\mathcal{H}^{(\Delta S=1)}$ for the three-flavor theory valid only for energies below m_c. Note, the renormalization scale μ that appears in $\mathcal{H}_c^{(\Delta S=1)}$ is conventionally chosen well above m_c while the μ that appears in $\mathcal{H}^{(\Delta S=1)}$ should be chosen above m_s. (Of course, in both cases we would like to choose μ in a region where perturbation theory can be used.) In the notation of Ref. [32], operators in the effective theory are given by O_i for the five-quark theory which includes the up, down, strange, charm, and bottom quarks, by P_i for the effective four-quark theory, and by Q_i for the effective three-quark theory including only the up, down, and strange quarks explicitly. We follow this notation, but since we will not deal with the effective five-quark theory, we also use O_i to represent a generic operator. Using the operator basis defined below and following Refs. [32,23,24] the effective Hamiltonians can be written as

$$\mathcal{H}_c^{(\Delta S=1)}=\frac{G_F}{\sqrt{2}}V_{ud}V_{us}^*\left\{\sum_{i=1}^{2}C_i(\mu)[P_i+(\tau-1)P_i^c]+\tau\sum_{i=3}^{10}C_i(\mu)P_i\right\},\tag{2}$$

$$\mathcal{H}^{(\Delta S=1)}=\frac{G_F}{\sqrt{2}}V_{ud}V_{us}^*\left\{\sum_{i=1}^{10}[z_i(\mu)+\tau y_i(\mu)]Q_i\right\}.\tag{3}$$

Here G_F is the Fermi coupling constant, V_{kl} are elements of the CKM matrix, $\lambda_k\equiv V_{kd}V_{ks}^*$ for $k=u$, c, t, and $\tau=-\lambda_t/\lambda_u$. For the four-flavor theory, we denote the Wilson coefficients by real numbers $C_i(\mu)$ and the four-quark operators by P_i and P_i^c. In general, charm quark fields will appear in the operators P_i as well as P_i^c. For the three-flavor theory, we denote the Wilson coefficients by the real numbers $y_i(\mu)$ and $z_i(\mu)$ and use Q_i to represent the four-quark operators, which are made of up, down, and strange quark fields only. The dependence of the Wilson coefficients on the other parameters shown in Eq. (1) is suppressed.

Before describing the operator basis in detail, a few important features of the effective $\Delta S=1$ Hamiltonians should be noted.

(1) In these Hamiltonians, CP violation enters entirely through the parameter τ, since we choose the standard representation of the CKM matrix of Ref. [34] where V_{td}, and thus τ, is complex.

(2) Of the 12 operators entering $\mathcal{H}_c^{(\Delta S=1)}$, only nine are linearly independent in a regularization that preserves Fierz transformations. Similarly, for the ten operators entering $\mathcal{H}^{(\Delta S=1)}$, only seven are linearly independent. The calculations of the Wilson coefficients most commonly use an overcomplete basis, since this allows one to transparently see how the original physics is inherited by the operators in the low-energy effective theory.

(3) The Wilson coefficients, which can be thought of as the couplings for the low-energy theory, vary markedly in size. The Wilson coefficient for the vector boson exchange term is of $\mathcal{O}(1)$. The QCD penguin terms are naively of $\mathcal{O}(\alpha_s)$ while the electroweak penguins are naively of $\mathcal{O}(\alpha)$. This simple counting is influenced by the large logarithms generated from QCD running, which we will discuss further in Sec. VII.

The numerical results reported here are for the three-flavor theory, where the charm quark mass has been integrated out. In the remainder of this section we summarize the relevant low-energy four-fermion operators for the three- and four-flavor theories and establish notation for both cases.

As mentioned above, charged vector boson exchange gives rise to left-left current interactions, with a particular color trace structure (Q_2, P_2, and P_2^c below). Mixing under renormalization produces a left-left operator with the other possible color trace (Q_1, P_1, and P_1^c below). Letting (L,R) denote the $\mathrm{SU}(3)_L\otimes\mathrm{SU}(3)_R$ representation of an operator and I its isospin, we give the quantum numbers of the opera-

tors as (L, R) I. Then with α and β denoting color indices, the charged vector boson exchange operators in our basis are [32,24]

Current–current operators:

$$Q_1 \equiv P_1 = (\bar{s}_\alpha d_\alpha)_{V-A}(\bar{u}_\beta u_\beta)_{V-A} \quad (8,1)\ 1/2 \quad (27,1)\ 1/2 \quad (27,1)\ 3/2, \tag{4}$$

$$P_1^c = (\bar{s}_\alpha d_\alpha)_{V-A}(\bar{c}_\beta c_\beta)_{V-A} \quad (8,1)\ 1/2, \tag{5}$$

$$Q_2 \equiv P_2 = (\bar{s}_\alpha d_\beta)_{V-A}(\bar{u}_\beta u_\alpha)_{V-A} \quad (8,1)\ 1/2 \quad (27,1)\ 1/2 \quad (27,1)\ 3/2, \tag{6}$$

$$P_2^c = (\bar{s}_\alpha d_\beta)_{V-A}(\bar{c}_\beta c_\alpha)_{V-A} \quad (8,1)\ 1/2. \tag{7}$$

Here the subscript $(V-A)$ refers to a quark bilinear of the form $\bar{q}\gamma_\mu(1-\gamma_5)q$. Operators with color trace structure similar to Q_1 are referred to as color diagonal operators while Q_2 is an example of a color mixed operator. Note that the exchange operators in Eqs. (4) and (6) get a contribution from more than one representation of $\mathrm{SU}(3)_L \otimes \mathrm{SU}(3)_R$ and contain both $I=1/2$ and 3/2 parts.

In addition to the simple exchange diagrams which lead to the operators of Eqs. (4)–(7), loop diagrams in the standard model (the penguin diagrams) produce additional four-fermion terms in the effective theory. In the penguin diagrams relevant to this paper, a top quark loop appears in the full electroweak theory. QCD penguins involve gluon exchange with this top quark loop, while electroweak penguins involve Z^0 and photon exchange with the top quark loop. The resulting four-fermion operators in the effective theory include interactions between left-handed and right-handed currents and both color diagonal and color mixed operators arise. For effective operators generated by the QCD penguin diagrams, all quarks which are present in the effective theory enter with equal weight, since the strong interactions couple equally to each flavor.

QCD penguin operators:

$$Q_3 = (\bar{s}_\alpha d_\alpha)_{V-A} \sum_{q=u,d,s} (\bar{q}_\beta q_\beta)_{V-A} \quad (8,1)\ 1/2, \tag{8}$$

$$P_3 = (\bar{s}_\alpha d_\alpha)_{V-A} \sum_{q=u,d,s,c} (\bar{q}_\beta q_\beta)_{V-A} \quad (8,1)\ 1/2, \tag{9}$$

$$Q_4 = (\bar{s}_\alpha d_\beta)_{V-A} \sum_{q=u,d,s} (\bar{q}_\beta q_\alpha)_{V-A} \quad (8,1)\ 1/2, \tag{10}$$

$$P_4 = (\bar{s}_\alpha d_\beta)_{V-A} \sum_{q=u,d,s,c} (\bar{q}_\beta q_\alpha)_{V-A} \quad (8,1)\ 1/2, \tag{11}$$

$$Q_5 = (\bar{s}_\alpha d_\alpha)_{V-A} \sum_{q=u,d,s} (\bar{q}_\beta q_\beta)_{V+A} \quad (8,1)\ 1/2, \tag{12}$$

$$P_5 = (\bar{s}_\alpha d_\alpha)_{V-A} \sum_{q=u,d,s,c} (\bar{q}_\beta q_\beta)_{V+A} \quad (8,1)\ 1/2, \tag{13}$$

$$Q_6 = (\bar{s}_\alpha d_\beta)_{V-A} \sum_{q=u,d,s} (\bar{q}_\beta q_\alpha)_{V+A} \quad (8,1)\ 1/2, \tag{14}$$

$$P_6 = (\bar{s}_\alpha d_\beta)_{V-A} \sum_{q=u,d,s,c} (\bar{q}_\beta q_\alpha)_{V+A} \quad (8,1)\ 1/2. \tag{15}$$

Here the subscript $(V+A)$ refers to a quark bilinear of the form $\bar{q}\gamma_\mu(1+\gamma_5)q$. As the list above shows, the QCD penguin operators all have $I=1/2$ and are singlets under $\mathrm{SU}(3)_R$, even though they contain right-handed quark fields.

The electroweak penguin operators have the same quark flavors as the QCD penguins, but each quark bilinear is multiplied by its electric charge e_q.

Electroweak penguin operators:

$$Q_7 = \frac{3}{2}(\bar{s}_\alpha d_\alpha)_{V-A} \sum_{q=u,d,s} e_q (\bar{q}_\beta q_\beta)_{V+A} \quad (8,8)\ 1/2 \quad (8,8)\ 3/2, \tag{16}$$

$$P_7 = \frac{3}{2}(\bar{s}_\alpha d_\alpha)_{V-A} \sum_{q=u,d,s,c} e_q (\bar{q}_\beta q_\beta)_{V+A} \quad (8,8)\ 1/2 \quad (8,8)\ 3/2 \quad (8,1)\ 1/2, \tag{17}$$

$$Q_8 = \frac{3}{2}(\bar{s}_\alpha d_\beta)_{V-A} \sum_{q=u,d,s} e_q (\bar{q}_\beta q_\alpha)_{V+A} \quad (8,8)\ 1/2 \quad (8,8)\ 3/2, \tag{18}$$

$$P_8 = \frac{3}{2}(\bar{s}_\alpha d_\beta)_{V-A} \sum_{q=u,d,s,c} e_q (\bar{q}_\beta q_\alpha)_{V+A} \quad (8,8)\ 1/2 \quad (8,8)\ 3/2 \quad (8,1)\ 1/2, \tag{19}$$

$$Q_9 = \frac{3}{2}(\bar{s}_\alpha d_\alpha)_{V-A} \sum_{q=u,d,s} e_q (\bar{q}_\beta q_\beta)_{V-A} \quad (8,1)\ 1/2 \quad (27,1)\ 1/2 \quad (27,1)\ 3/2, \tag{20}$$

$$P_9 = \frac{3}{2}(\bar{s}_\alpha d_\alpha)_{V-A} \sum_{q=u,d,s,c} e_q (\bar{q}_\beta q_\beta)_{V-A} \quad (8,1)\ 1/2 \quad (27,1)\ 1/2 \quad (27,1)\ 3/2, \tag{21}$$

$$Q_{10} = \frac{3}{2}(\bar{s}_\alpha d_\beta)_{V-A} \sum_{q=u,d,s} e_q (\bar{q}_\beta q_\alpha)_{V-A} \quad (8,1)\ 1/2 \quad (27,1)\ 1/2 \quad (27,1)\ 3/2, \tag{22}$$

$$P_{10} = \frac{3}{2}(\bar{s}_\alpha d_\beta)_{V-A} \sum_{q=u,d,s,c} e_q (\bar{q}_\beta q_\alpha)_{V-A} \quad (8,1)\ 1/2 \quad (27,1)\ 1/2 \quad (27,1)\ 3/2. \tag{23}$$

Note that Q_7 and Q_8 are in a single representation of $\mathrm{SU}(3)_L \otimes \mathrm{SU}(3)_R$, so their $I=1/2$ and 3/2 matrix elements can be related by the Wigner-Eckert theorem. This is not true

for P_7 and P_8, since the addition of the charm quark brings in a contribution from a different $SU(3)_L \otimes SU(3)_R$ representation.

These operators can also be decomposed into irreducible representations of isospin and $SU(3)_L \otimes SU(3)_R$ and the details are given in Appendix B. For the left-left operators made of *u*, *d*, and *s* quarks, there is a single (27,1) and two (8,1) irreducible representations. Thus there are only three matrix elements needed to determine Q_1, Q_2, Q_3, Q_4, Q_9, and Q_{10}.

With these definitions and knowledge of the Wilson coefficients, $K \to \pi\pi$ processes in the standard model can be expressed in terms of the matrix elements $\langle \pi\pi | P_i(\mu) | K \rangle$ defined in the four-quark effective theory or the three-quark effective theory matrix elements $\langle \pi\pi | Q_i(\mu) | K \rangle$. Notice that here we have shown explicitly the dependence of the operator on the scale μ, which cancels the μ dependence of the Wilson coefficients. Since the Wilson coefficients are calculated in continuum perturbation theory using dimensional regularization and we will calculate the hadronic matrix elements using a lattice regularization, we must relate, or match, operators normalized on the lattice and the continuum operators. This matching will also involve operator mixing, so in general one has

$$O_i^{\rm cont}(\mu) = Z_{ij}(\mu, a) O_j^{\rm lat}(a), \tag{24}$$

where a is the lattice spacing. In this work, we employ a relatively new technique, nonperturbative renormalization, as part of the calculation of the Z_{ij}'s. This is explained in detail in Sec. VIII. Before turning to our lattice determination of $\langle \pi\pi | O_i(\mu) | K \rangle$ matrix elements, we summarize the effective Hamiltonian for $\Delta S = 2$ transitions in the standard model.

B. K^0-$\overline{K^0}$ mixing in the standard model

In the development of the standard model, the K^0-$\overline{K^0}$ system has played an important role. The GIM mechanism [35] provided a natural theoretical explanation for the small mass difference between the K_L and K_S and was subsequently used to give an estimate for the charm quark mass [36]. These calculations were done for the case of only four quarks, where there is no imaginary part to the K^0-$\overline{K^0}$ mass matrix and no *CP* violation. For the six-quark standard model, this system should in general exhibit *CP* violation and the low energy theory describing these effects, including QCD corrections to leading logarithm order, was first given in [37,38]. Subsequent work has determined the Wilson coefficients to next-to-leading order [39,40].

We write the $\Delta S = 2$ Hamiltonian for the effective three-flavor theory to NLO as [39]

$$\begin{aligned}\mathcal{H}^{(\Delta S=2)} = & \frac{G_F^2}{16\pi^2} M_W^2 [\lambda_c^2 \eta_1 S_0(x_c) + \lambda_t^2 \eta_2 S_0(x_t) \\ & + 2\lambda_c \lambda_t \eta_3 S_0(x_c, x_t)] \\ & \times [\alpha_S^{(3)}]^{-2/9} \left[1 + \frac{\alpha_S^{(3)}(\mu)}{4\pi} J_3 \right] Q^{(\Delta S=2)} + \text{H.c.}, \end{aligned} \tag{25}$$

where

$$Q^{(\Delta S=2)} = (\overline{s}_\alpha d_\alpha)_{V-A} (\overline{s}_\beta d_\beta)_{V-A} \quad (27,1) \quad 1, \tag{26}$$

$x_q = m_q^2 / M_W^2$ and the functions $S_0(x_i)$ and $S_0(x_i, x_j)$ are the Inami-Lim functions [41]. J_3 is defined as

$$J_3 \equiv \frac{\gamma^{(0)} \beta_1}{2\beta_0^2} - \frac{\gamma^{(1)}}{2\beta_0}, \tag{27}$$

where $\gamma^{(i)}$ is the ith-order contribution to the anomalous dimension for $Q^{(\Delta S=2)}$ and β_j are the jth-order coefficients for the QCD beta function in a three flavor theory. In addition, $\alpha_S^{(3)}(\mu)$ is the QCD running coupling for a three flavor theory.

The coefficients η_i are known to NLO [39,40] and have the values

$$\eta_1 = 1.38 \pm 0.20, \quad \eta_2 = 0.57 \pm 0.01, \quad \eta_3 = 0.37 \pm 0.04. \tag{28}$$

CP violating processes involving K^0-$\overline{K^0}$ mixing in the standard model are then known if the CKM matrix elements are known and the matrix element $\langle \overline{K^0} | Q^{(\Delta S=2)} | K^0 \rangle$ is known. Since for three degenerate quarks, $Q^{(\Delta S=2)}$ is part of the same (27,1) irreducible representation as Q_1 and Q_2, one can relate the $\langle \overline{K^0} | Q^{(\Delta S=2)} | K^0 \rangle$ matrix element to $\langle \pi^+ | Q_1 | K^+ \rangle$ and $\langle \pi^+ | Q_2 | K^+ \rangle$.

C. Connecting experiment and theory

The previous two sections have given the $\Delta S = 1$ and $\Delta S = 2$ effective Hamiltonians in the notation we will use in this paper. To further establish our notation and conventions, we now collect the relevant formulas to connect these Hamiltonians with the experimentally measured quantities. For a more comprehensive review, the reader is referred to [42,43].

Considering only the strong Hamiltonian, a neutral kaon, the K^0, containing an antistrange and down quark and its antiparticle, the $\overline{K^0}$, containing an antidown and strange quark are energy eigenstates. We adopt the conventional definitions of parity P and charge conjugation C for quark fields in the standard model, giving $CP|K^0\rangle = -|\overline{K^0}\rangle$. While charge conjugation and parity are valid symmetries of the strong interactions, they are violated by the weak interactions. Allowing for the weak interactions to also violate *CP*, for the neutral kaons seen in nature one writes

$$|K_S\rangle = p|K^0\rangle - q|\overline{K^0}\rangle, \tag{29}$$

$$|K_L\rangle = p|K^0\rangle + q|\overline{K^0}\rangle, \tag{30}$$

with $p^2 + q^2 = 1$. *CP* is not a valid symmetry if the resulting physical states have $p \neq q$. Provided *CP* violating effects are small, K_S, being predominantly *CP* even, has a much shorter lifetime than K_L, since K_S decay to two pions, where more phase space is available, conserves *CP*.

The quantities measured experimentally to determine *CP* violation are

$$\eta_{+-}=|\eta_{+-}|e^{i\phi_{+-}}=\frac{A(K_L\to\pi^+\pi^-)}{A(K_S\to\pi^+\pi^-)}, \tag{31}$$

$$\eta_{00}=|\eta_{00}|e^{i\phi_{00}}=\frac{A(K_L\to\pi^0\pi^0)}{A(K_S\to\pi^0\pi^0)}. \tag{32}$$

The current values for these quantities are [34] $|\eta_{+-}|\approx|\eta_{00}|=2.28\times10^{-3}$ and $|\phi_{+-}|\approx|\phi_{00}|=44°$.

It is important to distinguish between *CP* violation due to mixing, also known as indirect *CP* violation, and *CP* violation in decays, also referred to as direct *CP* violation. *CP* violation due to mixing refers to $K_L\leftrightarrow K_S$ transitions (or alternately $K^0\leftrightarrow\overline{K^0}$) and if all *CP* violation came from this source, one would find $\eta_{+-}=\eta_{00}$. The initial states would mix and the decay processes would preserve *CP*. Allowing for *CP* violation in decays, one defines

$$\eta_{+-}=\epsilon+\epsilon', \quad \eta_{00}=\epsilon-2\epsilon' \tag{33}$$

and a nonzero value for ϵ' signals *CP* violation in decays. The current value for ϵ is $(2.271\pm0.017)\times10^{-3}$ and for ϵ'/ϵ is $(2.1\pm0.5)\times10^{-3}$ [34].

To relate the experimental quantities to the theoretical matrix elements calculated here, it is conventional to define the isospin amplitudes by

$$A(K^0\to\pi\pi(I))=A_Ie^{i\delta_I}, \tag{34}$$

$$A(\overline{K^0}\to\pi\pi(I))=-A_I^*e^{i\delta_I}, \tag{35}$$

where I gives the isospin state of the pions and δ_I is the final-state phase shift determined from $\pi\pi$ scattering. In general, $A[K^0\to\pi\pi(I)]=\langle\pi\pi(I)|-i\mathcal{H}|K^0\rangle$. Defining $\overline{\epsilon}$ through

$$\frac{p}{q}=\frac{(1+\overline{\epsilon})}{(1-\overline{\epsilon})} \tag{36}$$

and using the isospin decomposition

$$|\pi^0\pi^0\rangle=\sqrt{\frac{2}{3}}|\pi\pi(I=2)\rangle-\sqrt{\frac{1}{3}}|\pi\pi(I=0)\rangle, \tag{37}$$

$$\sqrt{\frac{1}{2}}(|\pi^+\pi^-\rangle+|\pi^-\pi^+\rangle)=\sqrt{\frac{1}{3}}|\pi\pi(I=2)\rangle+\sqrt{\frac{2}{3}}|\pi\pi(I=0)\rangle \tag{38}$$

one can show [42]

$$\epsilon=\overline{\epsilon}+i\left(\frac{\mathrm{Im}\,A_0}{\mathrm{Re}\,A_0}\right) \tag{39}$$

$$\epsilon'=\frac{ie^{i(\delta_2-\delta_0)}}{\sqrt{2}}\frac{\mathrm{Re}\,A_2}{\mathrm{Re}\,A_0}\left[\frac{\mathrm{Im}\,A_2}{\mathrm{Re}\,A_2}-\frac{\mathrm{Im}\,A_0}{\mathrm{Re}\,A_0}\right]. \tag{40}$$

We define

$$\omega\equiv\frac{\mathrm{Re}\,A_2}{\mathrm{Re}\,A_0}, \tag{41}$$

$$P_0\equiv\frac{\mathrm{Im}\,A_0}{\mathrm{Re}\,A_0}, \tag{42}$$

$$P_2\equiv\frac{\mathrm{Im}\,A_2}{\mathrm{Re}\,A_2}, \tag{43}$$

and simplify Eqs. (39) and (40) to

$$\epsilon=\overline{\epsilon}+iP_0, \tag{44}$$

$$\epsilon'=\frac{ie^{i(\delta_2-\delta_0)}}{\sqrt{2}}\omega[P_2-P_0]. \tag{45}$$

The equations above assume that both $\overline{\epsilon}$ and ω are small quantities, which is true for the physical values of quark masses. In particular, the small value of ω (0.045) is the quantitative expression of the $\Delta I=1/2$ rule. For our quenched QCD simulations, we must be careful to only use these formulas for situations where both $\overline{\epsilon}$ and ω are small.

There are corrections to Eq. (45) from isospin violations. These will not be included in our current calculation but have been estimated by [44,45].

From Eq. (45) one sees that *CP* violation in decays comes from a nonzero value of P_2-P_0. This in turn arises through isospin-dependent imaginary parts of A_I. In the standard model, *CP*-violating imaginary contributions to A_0 and A_2 enter only through the CKM matrix element V_{td}. The effects of V_{td} enter through the penguin operators and in particular, the major contribution to $\mathrm{Im}\,A_2$ is expected to come from the electroweak penguin operators, while the QCD penguin operators should produce most of $\mathrm{Im}\,A_0$. Given that P_2-P_0 determines the size of direct *CP* violation effects, estimates of the generic size of P_0 and P_2 do not tightly constrain ϵ'.

Since a nonperturbative lattice calculation of $K\to\pi\pi$ matrix elements yields A_0 and A_2, the calculation also produces a value for ω. The value of ω is an interesting quantity in its own right and because of its dependence only on the real parts of the amplitudes, it probes standard model physics that is quite different from *CP* violation.

To determine ϵ, one needs the value for $\overline{\epsilon}$ which in turn comes from a determination of the off-diagonal elements of the two by two matrix governing the evolution of the K^0-$\overline{K^0}$ system [43]. These off-diagonal contributions are commonly parameterized by defining $B_K(\mu)$ through

$$\langle\overline{K^0}|Q^{(\Delta S=2)}(\mu)|K^0\rangle\equiv\frac{8}{3}B_K(\mu)f_K^2m_K^2 \tag{46}$$

and the renormalization group invariant parameter $\hat{B}_K$ by

$$\hat{B}_K\equiv B_K(\mu)[\alpha_s^{(3)}(\mu)]^{-2/9}\left[1+\frac{\alpha_s^{(3)}(\mu)}{4\pi}J_3\right]. \tag{47}$$

With these definitions, one finds that

$$\epsilon = \hat{B}_K \,\mathrm{Im}\,\lambda_t \frac{G_F^2 f_K^2 m_K M_W^2}{12\sqrt{2}\pi^2 \Delta M_K} \times \{\mathrm{Re}\,\lambda_c[\eta_1 S_0(x_c) - \eta_3 S_0(x_c, x_t)] - \mathrm{Re}\,\lambda_t \eta_2 S_0(x_t)\} \times \exp(i\pi/4), \quad (48)$$

where ΔM_K is the mass difference between K_L and K_S.

Thus a determination from lattice QCD simulations of $\langle \pi\pi | Q_i(\mu) | K \rangle$ and $\langle \overline{K^0} | Q^{(\Delta S=2)}(\mu) | K^0 \rangle$ matrix elements, coupled with experimental measurements of ϵ' and ϵ, gives constraints on the elements of the CKM matrix in the standard model. Additionally, the lattice calculations should also yield a value for ω which is expected to be essentially independent of the elements of the CKM matrix. We now turn to some of the issues faced in the lattice determinations of the matrix elements.

III. CONTINUUM CHIRAL PERTURBATION THEORY AND KAON MATRIX ELEMENTS

The calculation of decay amplitudes with multiparticle final states presents a challenge to the Euclidean-space techniques of lattice QCD. In a general field-theoretic context, Euclidean space and Minkowski space are related by an analytic continuation. Such an analytic continuation in a numerical calculation is extremely difficult, given that a discrete set of data points with statistical errors does not define an analytic function. Fortunately, there are matrix elements we can calculate directly from lattice QCD using the usual lattice projection technique of evaluating the large time limit of the operator $e^{\{-H_{\mathrm{QCD}}t\}}$. For single particle matrix elements, we directly achieve the matrix element at the desired kinematic values. However, for multiparticle states with nonzero relative momentum, the state will not be the lowest energy state with a specific set of quantum numbers and, therefore, cannot be isolated by the large time limit of the operator $e^{\{-H_{\mathrm{QCD}}t\}}$, the Maiani-Testa theorem [46]. As a result, $K \to \pi\pi$ transition amplitudes with physical masses cannot be directly measured on the lattice with current techniques. (There is a recent promising proposal [47] to tune the finite volume of a Euclidean-space simulation so that the physical, multiparticle final state corresponds to a next-lowest energy, finite-volume eigenstate of H_{QCD}—a state that might be extracted from the time dependence given by $e^{\{-H_{\mathrm{QCD}}t\}}$.)

Even before the formalization of the Maiani-Testa theorem, it was realized [12] that chiral perturbation theory could be used to relate $K \to \pi\pi$ amplitudes to $K \to \pi$ and $K \to |0\rangle$ amplitudes (here $|0\rangle$ is the vacuum). In addition to circumventing the Maiani-Testa theorem, these amplitudes should be easier to measure numerically, since they involve fewer interpolating operators to produce the mesons. Chiral perturbation theory uses the effective Lagrangian representing the pseudo-Goldstone boson degrees of freedom for QCD to determine relations between the desired matrix elements. It should be noted that the chiral effective Lagrangian automatically satisfies the relevant Ward-Takahashi identities of QCD, in the limit when these identities are dominated by arbitrarily light pseudo-Goldstone bosons.

Our use of chiral perturbation theory in the calculation of the $K \to \pi\pi$ weak matrix elements requires that we address a number of issues. We cannot currently calculate lattice matrix elements for arbitrarily small quark mass, where the quark mass dependence is linear, since such small masses require large volumes and computer resources beyond those currently available. Since our quark masses will be as large as the strange quark mass, we must understand the nonlinear dependence expected from continuum chiral perturbation theory for $K \to \pi$ and $K \to |0\rangle$ matrix elements. Such an understanding will allow us to see if our data matches these expectations and to permit us to accurately extract the low-energy chiral perturbation theory parameters needed to make the connection to the desired two pion decay. (As we will discuss in Sec. IV we can also get nonlinearities from a lattice effect, domain wall fermion zero modes in quenched QCD for finite volume.) Since our calculation is done in the quenched approximation, we must also look for the pathologies expected from quenched chiral perturbation theory. Finally, our results for $K \to \pi\pi$ weak matrix elements in the chiral limit must be compared with the physical values measured for nonzero quark mass. Estimates of the effects of higher order terms in chiral perturbation theory are crucial to estimating the systematic errors in extrapolating to the physical kaon mass. We now turn to the results from chiral perturbation theory relevant to our determination of weak matrix elements.

A. Lowest order chiral perturbation theory

Following [12] and adopting their conventions for states and normalizations (see Appendix A for a summary), one must represent the various operators listed in Eqs. (4)–(23) in terms of the fields used in chiral perturbation theory. One starts with a unitary chiral matrix field, Σ, defined by

$$\Sigma \equiv \exp\left[\frac{2i\phi^a t^a}{f}\right], \quad (49)$$

where ϕ^a are the real pseudo-Goldstone boson fields, t^a are proportional to the Gell-Mann matrices, with $\mathrm{Tr}(t_a t_b) = \delta_{ab}$, and f is the pion decay constant. In chiral perturbation theory, the lowest order Lagrangian for QCD, of $\mathcal{O}(p^2)$, is

$$\mathcal{L}^{(2)}_{\mathrm{QCD}} = \frac{f^2}{8}\mathrm{Tr}(\partial_\mu \Sigma \partial^\mu \Sigma^\dagger) + v\ \mathrm{Tr}[M\Sigma + (M\Sigma)^\dagger]. \quad (50)$$

Here M is the quark mass matrix and

$$v = \frac{f^2 m_{\pi^+}^2}{4(m_u + m_d)}. \quad (51)$$

Thus v is the chiral condensate at zero quark mass and, as shown in Appendix A $\langle \overline{u}u \rangle (m_q = 0) = -2v$. Note that the matrix field Σ has $\mathrm{SU}(3)_L \otimes \mathrm{SU}(3)_R$ quantum numbers $(L,R) = (3,\overline{3})$. Here f is the pion decay constant in the limit $m_q \to 0$ and we use a normalization where f_π is 131 MeV.

Working to lowest order in chiral perturbation theory, one finds [12] that there are two possible (8, 1) operators with

$\Delta S=1$ and $\Delta D=-1$, denoted by $\tilde{\Theta}_1^{(8,1)}$ and $\tilde{\Theta}_2^{(8,1)}$, and a single (27, 1) operator $\tilde{\Theta}^{(27,1)}$. These three operators are all that is required to represent the matrix elements of the operators in Eqs. (4)–(23), except Q_7, Q_8, P_7, and P_8. Other work [33] showed that there is a single (8, 8) operator. Thus the correspondence between an operator $\Theta^{(L,R)}$ given in terms of quark fields and its representation in chiral perturbation theory is given by

$$\Theta^{(8,1)} \to \alpha_1^{(8,1)} \tilde{\Theta}_1^{(8,1)} + \alpha_2^{(8,1)} \tilde{\Theta}_2^{(8,1)}, \tag{52}$$

$$\Theta^{(27,1)} \to \alpha^{(27,1)} \tilde{\Theta}^{(27,1)}, \tag{53}$$

$$\Theta^{(8,8)} \to \alpha^{(8,8)} \tilde{\Theta}^{(8,8)}, \tag{54}$$

where the α's are constants and

$$\tilde{\Theta}_1^{(8,1)} \equiv \mathrm{Tr}[\Lambda(\partial_\mu \Sigma)(\partial^\mu \Sigma^\dagger)], \tag{55}$$

$$\tilde{\Theta}_2^{(8,1)} \equiv \frac{8v}{f^2} \mathrm{Tr}[\Lambda \Sigma M + \Lambda (\Sigma M)^\dagger], \tag{56}$$

$$\tilde{\Theta}^{(27,1)} \equiv T^{ij}_{kl} (\Sigma \partial_\mu \Sigma^\dagger)^k_i (\Sigma \partial^\mu \Sigma^\dagger)^l_j, \tag{57}$$

$$\tilde{\Theta}^{(8,8)} \equiv \mathrm{Tr}[\Lambda \Sigma T_R \Sigma^\dagger]. \tag{58}$$

Here $\Lambda_{ij} \equiv \delta_{i3}\delta_{j2}$, T^{ij}_{kl} is symmetric in i, j and k, l and traceless on any pair of upper and lower indices, and $T_R \equiv \mathrm{diag}(2,-1,-1)$. Further detail is given in Appendixes B and D, along with precise values for T^{ij}_{kl} for both the $\Delta I = 1/2$ and $\Delta I = 3/2$ components.

There is a unique set of α's for each four-quark operator that is in an irreducible representation of $\mathrm{SU}(3)_L \otimes \mathrm{SU}(3)_R$. The operators in Eqs. (4)–(23) are generally in reducible representations, so we will determine the α's for each operator individually. The matrix elements of the effective operators $\tilde{\Theta}$ given in Eqs. (55)–(58) between states composed of pions and kaons can be easily evaluated in chiral perturbation theory. For the $K \to 0$ matrix elements one finds

$$\langle 0|\Theta^{(8,1)}|K^0\rangle = \frac{16iv}{f^3}(m_s' - m_d')\alpha_2^{(8,1)}, \tag{59}$$

$$\langle 0|\Theta^{(27,1)}|K^0\rangle = 0, \tag{60}$$

$$\langle 0|\Theta^{(8,8)}|K^0\rangle = 0, \tag{61}$$

where m_s' and m_d' are the quark masses used in the construction of the K^0. Similarly

$$\langle \pi^+|\Theta^{(8,1)}|K^+\rangle = \frac{4m_M^2}{f^2}(\alpha_1^{(8,1)} - \alpha_2^{(8,1)}), \tag{62}$$

$$\langle \pi^+|\Theta^{(27,1)}\rangle K^+\rangle = -\frac{4m_M^2}{f^2}\alpha^{(27,1)}, \tag{63}$$

$$\langle \pi^+|\Theta^{(8,8)}|K^+\rangle = \frac{12}{f^2}\alpha^{(8,8)}, \tag{64}$$

where m_M is the common meson mass of the π^+ and K^+. Following [12], one then finds that the desired $K \to \pi\pi$ matrix elements are given by

$$\langle \pi^+\pi^-|\Theta^{(8,1)}|K^0\rangle = \frac{4i}{f^3}(m_{K^0}^2 - m_{\pi^+}^2)\alpha_1^{(8,1)}, \tag{65}$$

$$\langle \pi^+\pi^-|\Theta^{(27,1)}|K^0\rangle = -\frac{4i}{f^3}(m_{K^0}^2 - m_{\pi^+}^2)\alpha^{(27,1)}, \tag{66}$$

$$\langle \pi^+\pi^-|\Theta^{(8,8)}|K^0\rangle = \frac{-12i}{f^3}\alpha^{(8,8)}. \tag{67}$$

Since the (27,1) and (8,8) operators contain both $\Delta I = 1/2$ and $\Delta I = 3/2$ parts, which we will need to measure to determine $K \to \pi\pi$ amplitudes of definite isospin, we give the isospin decomposition of Eqs. (63), (64), (66), and (67) in Appendix D.

These simple relations form the heart of the calculation we have performed and a few important points are worth highlighting.

(1) The current calculation is a determination of the physical parameters $\alpha_1^{(8,1)}$, $\alpha^{(27,1)}$, and $\alpha^{(8,8)}$ for a fixed lattice spacing and volume in the quenched approximation. As such, $K \to \pi\pi$ amplitudes are determined to lowest order in chiral perturbation theory in the quenched approximation.

(2) The $K^+ \to \pi^+$ matrix elements of (8,1) and (27,1) operators vanish in the chiral limit, while for (8,8) operators the matrix element is nonzero. Thus, for small enough quark masses, the electroweak penguin operators will dominate all amplitudes. Since the electroweak penguin operators are suppressed by the electroweak coupling constant, the quark mass where they dominate is quite small.

(3) The term $\alpha_2^{(8,1)}$ is determined by the unphysical $K^0 \to 0$ matrix element and in general is quadratically divergent for regularizations which preserve chiral symmetry. To determine $\alpha_1^{(8,1)}$, and hence the physical $K \to \pi\pi$ amplitude, requires canceling this quadratic divergence against the quadratic divergence in $\langle \pi^+|\Theta^{(8,1)}|K^+\rangle$. This first-principles cancellation arises in the relevant Ward-Takahashi identities of QCD and is reflected in chiral perturbation theory, which respects these identities. For the most extreme cases, the physical result is only 5% of the size of the divergent terms. This $\alpha_2^{(8,1)}$ subtraction will be extensively discussed in Sec. XI A.

(4) The $\alpha_2^{(8,1)}$ subtraction is determined by matrix elements of four-quark operators in hadronic states. As part of the renormalization of lattice four-quark operators, a related subtraction must be done for matrix elements of these operators in off-shell Green's functions involving quark fields. Only the momentum independent divergent parts of these two subtractions are the same. This issue is discussed further in Sec. VIII.

(5) In these lowest order chiral perturbation theory expressions, only $\alpha_2^{(8,1)}$ is divergent. However, higher order

terms in chiral perturbation theory can be multiplied by divergent coefficients, as happens for (8,8) operators. Thus Eq. (64) is modified at next order by the addition of a divergent term of the form

$$\langle \pi^+ | \Theta^{(8,8)} | K^+ \rangle = \frac{12}{f^2} \{ \alpha^{(8,8)} + m_M^2 \alpha_{\rm div}^{(8,8)} + \cdots \}, \quad (68)$$

where the dots represent possible nondivergent higher order terms. Even though the matrix element is nonzero when $m_q = 0$, the finite quark mass corrections enter with a power divergent coefficient. One way to find the $m_q = 0$ value is to extrapolate in quark mass. For domain wall fermions at finite L_s, the zero quark mass limit is not precisely known for power divergent operators. This, coupled with the power divergent slope, makes the extrapolation problematic. One can use a subtraction to remove the divergent slope. However, an even simpler approach is to use the $\Delta I = 3/2$ part of the (8,8) operator, which does not have divergent coefficients, to determine $\alpha^{(8,8)}$.

B. Full QCD one loop chiral perturbation theory: $K \to \pi\pi$

An important early calculation in QCD revealed that in the small quark mass limit m_π^2 deviates from simple linear dependence on the quark mass, m_q, due to chiral logarithm terms of the form $m_q \ln m_q$ [48]. In the language of chiral perturbation theory such logarithms arise from higher order loop effects, which for m_π^2 come from calculating loop corrections using $\mathcal{L}_{\rm QCD}^{(2)}$. To work to a consistent order in chiral perturbation theory requires that if loop effects in the $\mathcal{O}(p^2)$ effective Lagrangian are included, one must also include the effects of the $\mathcal{O}(p^4)$ terms in the effective Lagrangian, denoted $\mathcal{L}_{\rm QCD}^{(4)}$. Unfortunately, $\mathcal{L}_{\rm QCD}^{(4)}$ introduces new, unknown parameters, but for on-shell particles at rest these parameters are multiplied by m_q^2. Thus the general form for a quantity like m_π^2 in full QCD is

$$m_\pi^2 = a_1 m_q + a_l m_q^2 \ln m_q + a_2 m_q^2. \quad (69)$$

Systematic calculations of higher loop effects in chiral perturbation theory [49,50] have been done including the up, down, and strange quarks. We will give these results in terms of the lowest order chiral perturbation theory, or bare, meson masses, which are given, for example, by $m_{\pi^+}^2 = 4v(m_u + m_d)/f^2$ where f and v are constants. We will set $m_u = m_d$ and denote the subtraction point for chiral perturbation theory by $\Lambda_{\chi PT}$. Calculating the one-loop terms in $\mathcal{L}_{\rm QCD}^{(2)}$ gives [50]

$$(m_\pi^2)^{(1\ \rm loop)} = m_\pi^2 \left\{ 1 + L_\chi(m_\pi) - \frac{1}{3} L_\chi(m_\eta) + \cdots \right\}, \quad (70)$$

$$(m_K^2)^{(1\ \rm loop)} = m_K^2 \left\{ 1 + \frac{2}{3} L_\chi(m_\eta) + \cdots \right\}, \quad (71)$$

$$(f_\pi)^{(1\ \rm loop)} = f\{ 1 - 2L_\chi(m_\pi) - L_\chi(m_K) + \cdots \}, \quad (72)$$

$$(f_K)^{(1\ \rm loop)} = f\left\{ 1 - \frac{3}{4} L_\chi(m_\pi) - \frac{3}{2} L_\chi(m_K) - \frac{3}{4} L_\chi(m_\eta) + \cdots \right\}, \quad (73)$$

where

$$L_\chi(m) \equiv \frac{m^2}{(4\pi f)^2} \ln\left(\frac{m^2}{\Lambda_{\chi PT}^2} \right) \quad (74)$$

and the dots represent terms quadratic in the pseudoscalar masses. The coefficients of these terms depend on parameters entering $\mathcal{L}_{\rm QCD}^{(4)}$.

To study matrix elements in chiral perturbation theory, one starts from the lowest order QCD Lagrangian in Eq. (50) and adds terms representing the effective four-fermion operators at low energies. To $\mathcal{O}(p^2)$ this yields

$$\mathcal{L}_{\rm eff}^{\mathcal{O}(p^2)} = \mathcal{L}_{\rm QCD}^{(2)} + \mathcal{L}_{\Delta S=1}^{(0)} + \mathcal{L}_{\Delta S=1}^{(2)} + \mathcal{L}_{\Delta S=2}^{(2)} \quad (75)$$

for the $\Delta S = 1$ and $\Delta S = 2$ processes of interest here. Note that there are terms at $\mathcal{O}(p^0)$ that enter the $\Delta S = 1$ part of the chiral Lagrangian. These are the (8,8) operators mentioned in the previous section which represent the electroweak penguins Q_7 and Q_8 for $\mu < m_c$, or a part of P_7 and P_8 for $\mu > m_c$. The term $\mathcal{L}_{\Delta S=1}^{(0)}$ depends on the single parameter $\alpha^{(8,8)}$ for each operator, while $\mathcal{L}_{\Delta S=1}^{(2)}$ depends on $\alpha_1^{(8,1)}$, $\alpha_2^{(8,1)}$, $\alpha^{(27,1)}$ and the coefficients for higher order (8,8) operators. The single operator appearing in $\mathcal{L}_{\Delta S=2}^{(2)}$ enters with a parameter which can be shown to be related to $\alpha^{(27,1)}$.

The chiral logarithm terms in $\Delta S = 1$ and $\Delta S = 2$ matrix elements can be calculated using $\mathcal{L}_{\rm eff}^{\mathcal{O}(p^2)}$. Amplitudes involving $\Theta^{(8,8)}$, which are nonzero at $\mathcal{O}(p^0)$ due to $\mathcal{L}_{\Delta S=1}^{(0)}$, have chiral logarithms at $\mathcal{O}(p^2)$ due to interaction terms in $\mathcal{L}_{\rm eff}^{\mathcal{O}(p^2)}$. These chiral logarithms have not yet been calculated explicitly, but should modify Eq. (68) to the form

$$\langle \pi^+ | \Theta^{(8,8)} | K^+ \rangle = \frac{12}{f^2} \{ \alpha^{(8,8)} [1 + \xi^{(8,8)} L_\chi(m_M) + \cdots] + m_M^2 \alpha_{\rm div}^{(8,8)} + \cdots \}, \quad (76)$$

where $\xi^{(8,8)}$ is a calculable coefficient and m_M is the common mass for the π^+ and K^+ in this matrix element. (For full QCD, these terms were calculated after this paper was finished in [51].) As previously mentioned, unless only the $\Delta I = 3/2$ amplitude is considered, there are higher order terms in chiral perturbation theory with power divergent coefficients, given collectively in Eq. (76) by $\alpha_{\rm div}^{(8,8)}$.

The effective Lagrangian to the next order, $\mathcal{L}_{\rm eff}^{\mathcal{O}(p^4)}$, includes all possible $\mathcal{O}(p^4)$ terms and introduces many unknown coefficients. This Lagrangian takes the form

$$\mathcal{L}_{\rm eff}^{\mathcal{O}(p^4)} = \mathcal{L}_{\rm eff}^{\mathcal{O}(p^2)} + \mathcal{L}_{\rm QCD}^{(4)} + \mathcal{L}_{\Delta S=1}^{(4)} + \mathcal{L}_{\Delta S=2}^{(4)}. \quad (77)$$

For $\Delta S=1$ processes at $\mathcal{O}(p^4)$, amplitudes will include loop effects coming from $\mathcal{L}^{(2)}_{\rm QCD}$ and $\mathcal{L}^{(2)}_{\Delta S=1}$. There are also $\mathcal{O}(p^4)$ contributions from two-loop corrections to $\mathcal{L}^{(0)}_{\Delta S=1}$.

For $\Theta^{(8,1)}$ and $\Theta^{(27,1)}$ $\Delta S=1$ operators, the chiral logarithm corrections to the matrix elements of interest in this work have been calculated [52–56]. The results for $K^+\to\pi^+$ are

$$\langle\pi^+|\Theta^{(8,1)}|K^+\rangle=\frac{4m_M^2}{f^2}\left\{\alpha_1^{(8,1)}\left[1+\frac{1}{3}L_\chi(m_M)\right]-\alpha_2^{(8,1)}[1+2L_\chi(m_M)]\right\},\tag{78}$$

$$\langle\pi^+|\Theta^{(27,1)}|K^+\rangle=-\frac{4m_M^2}{f^2}\left\{\alpha^{(27,1)}\left[1-\frac{34}{3}L_\chi(m_M)\right]\right\}.\tag{79}$$

Similarly for $K\to|0\rangle$ one finds

$$\begin{aligned}\langle 0|\Theta^{(8,1)}|K^0\rangle=&\frac{4i\alpha_2^{(8,1)}}{f}(m_K^2-m_\pi^2)\left\{1-\frac{3}{4}L_\chi(m_\pi)-\frac{3}{2}L_\chi(m_K)-\frac{1}{12}L_\chi(m_\eta)\right\}\\&+\frac{4i\alpha_1^{(8,1)}}{f}(m_K^2-m_\pi^2)\\&\times\left\{\frac{1}{3}L_\chi(m_\eta,m_K)-2L_\chi(m_\eta,m_\pi)\right\},\end{aligned}\tag{80}$$

$$\begin{aligned}\langle 0|\Theta^{(27,1)}|K^0\rangle=&\frac{4i\alpha^{(27,1)}}{f}(m_K^2-m_\pi^2)\\&\times\{-2L_\chi(m_\eta,m_K)+2L_\chi(m_\eta,m_\pi)\},\end{aligned}\tag{81}$$

where

$$L_\chi(m_1,m_2)\equiv\frac{1}{(4\pi f)^2}\frac{1}{m_1^2-m_2^2}\times\left[m_1^4\ln\left(\frac{m_1^2}{\Lambda_{\chi PT}^2}\right)-m_2^4\ln\left(\frac{m_2^2}{\Lambda_{\chi PT}^2}\right)\right].\tag{82}$$

One of the most important aspects of using these formulas to determine $K\to\pi\pi$ matrix elements is the determination of the coefficients $\alpha_2^{(8,1)}$, which are in general quadratically divergent in a regularization which preserves chiral symmetry. [Since (8,1) operators are pure $\Delta I=1/2$, we cannot avoid $\alpha_2^{(8,1)}$ by measuring only $\Delta I=3/2$ amplitudes, as we can avoid $\alpha_{\rm div}^{(8,8)}$.] However, as the equations above show, $\alpha_2^{(8,1)}$ is multiplied by chiral logarithm corrections at subleading order. Given the large difference possible in $\alpha_1^{(8,1)}$ and $\alpha_2^{(8,1)}$, $\alpha_1^{(8,1)}$ can be much smaller than $\alpha_2^{(8,1)}\,L_\chi(m_\pi)$.

The power divergent part of the four-quark operators can be written as a quark bilinear times a momentum-independent coefficient. Thus the chiral logarithm corrections to the power divergent parts of four-quark operators must be the same as the chiral logarithm corrections to the corresponding quark bilinears. That this is indeed the case for full QCD can be seen explicitly, since the chiral logarithms for the bilinears are known and can be compared with Eqs. (78)–(81). Following [53], we define

$$\Theta^{(3,\bar3)}=\bar s(1-\gamma_5)d=\alpha^{(3,\bar3)}{\rm Tr}(A\Sigma)\tag{83}$$

to lowest order in chiral perturbation theory. Here A is a three by three matrix with $A_{i,j}=\delta_{i,3}\delta_{j,2}$ and with our conventions, $\alpha^{(3,\bar3)}=-2iv$. Then the chiral logarithm corrections for the matrix elements of $\langle\pi^+|\Theta^{(3,\bar3)}|K^+\rangle$ and $\langle 0|\Theta^{(3,\bar3)}|K^0_{\bar{}}\rangle$ are given in [53]. We will use the value for $\langle\pi^+|\Theta^{(3,\bar3)}|K^+\rangle$ from [53], since here there is a single meson mass, m_M. For $\langle 0|\Theta^{(3,\bar3)}|K^0\rangle$, where the meson masses are not degenerate, the formula in [53] does not include separate chiral logarithms for each of the possible meson masses, m_π, m_K, and m_η. Thus, for this matrix element, we make use of the fact that

$$\langle 0|\Theta^{(3,\bar3)}|K^0\rangle\sim(m_K^2)^{(1\ \rm loop)}(f_K)^{(1\ \rm loop)}/m_q\tag{84}$$

and use Eqs. (71) and (73) to determine the chiral logarithms. This gives

$$\langle\pi^+|\Theta^{(3,\bar3)}|K^+\rangle=\frac{2}{f^2}\alpha^{(3,\bar3)}\{1+2L_\chi(m_M)\},\tag{85}$$

$$\langle 0|\Theta^{(3,\bar3)}|K^0\rangle=\frac{2i}{f}\alpha^{(3,\bar3)}\left\{1-\frac{3}{4}L_\chi(m_\pi)-\frac{3}{2}L_\chi(m_K)-\frac{1}{12}L_\chi(m_\eta)\right\}.\tag{86}$$

Thus we have

$$\begin{aligned}\frac{\langle 0|\Theta^{(8,1)}|K^0\rangle}{\langle 0|\Theta^{(3,\bar3)}|K^0\rangle}=&2\frac{\alpha_2^{(8,1)}}{\alpha^{(3,\bar3)}}(m_K^2-m_\pi^2)\{1+\cdots\}\\&+2\frac{\alpha_1^{(8,1)}}{\alpha^{(3,\bar3)}}(m_K^2-m_\pi^2)\{\text{chiral logs}+\cdots\},\end{aligned}\tag{87}$$

where the dots represent nonlogarithmic higher order terms. The ''chiral logs'' in Eq. (87) are those given in the second line of Eq. (80) and in Eq. (86). As expected, the chiral logarithms from the power divergent part of the four-quark operator are the same as for the corresponding quark bilinear. The logarithms in the $\alpha_1^{(8,1)}$ term in Eq. (87) are higher order in chiral perturbation theory and are suppressed by the relative sizes of $\alpha_1^{(8,1)}$ and $\alpha_2^{(8,1)}$. For m^2 corrections which come from loops in the $\mathcal{O}(p^2)$ Lagrangian, one also expects a cancellation between the bilinears and the four-quark op-

erators. This analysis leads us to expect that the ratio in Eq. (87) is a linear function of $m_K^2 - m_\pi^2$ with very small corrections. We will investigate this numerically in Sec. XI A.

It is also important to note that once $\alpha_2^{(8,1)}$ has been determined, we must numerically evaluate

$$\langle \pi^+ | \Theta^{(8,1)} | K^+ \rangle + \alpha_2^{(8,1)} \frac{4 m_M^2}{f^2} [1 + 2 L_\chi(m_M)] \qquad (88)$$

to determine $\alpha_1^{(8,1)}$ if we are not working with arbitrarily small quark masses. If we could work close enough to the chiral limit, the chiral logarithm terms in Eq. (88) would make an arbitrarily small contribution. This is not the case for the data presented here, where the minimum pseudoscalar mass is 390 MeV. Equation (88) involves large cancellations between divergent quantities. Notice that the chiral logarithms are very important in this determination, since they multiply the divergent coefficient $\alpha_2^{(8,1)}$. A simple way to do this is to recall that the power divergent part of four-quark operators should also have the same chiral logarithms as the corresponding quark bilinear. Equation (85) shows this to be the case. Thus the combination

$$\langle \pi^+ | \Theta^{(8,1)} | K^+ \rangle + 2 m_M^2 \frac{\alpha_2^{(8,1)}}{\alpha^{(3,3)}} \langle \pi^+ | \Theta^{(3,\bar{3})} | K^+ \rangle = \frac{4 m_M^2}{f^2} \alpha_1^{(8,1)} \left[1 + \frac{1}{3} L_\chi(m_M) \right] \qquad (89)$$

yields a result only involving the physical coefficient $\alpha_1^{(8,1)}$, with corrections in chiral perturbation theory that do not involve the power divergent coefficient. The chiral logarithms which multiply power divergent coefficients have been removed, without having to know their precise values. (This subtraction technique was originally discussed in Ref. [57], although its ability to remove power divergent terms multiplied by chiral logarithm corrections was not discussed.) Note, this complete cancellation of the quadratic divergence will hold as well in the quenched theory. This is important, since our actual calculation is done in the quenched approximation where the coefficients of the chiral logarithms are not known.

C. Quenched one-loop chiral perturbation theory: $K \to \pi$ and $K \to 0$

The discussion in the previous section focused on the chiral logarithms present in various full QCD masses and matrix elements. Similar techniques can be used to calculate the nonanalytic dependence on the quark mass for quenched simulations [13–15]. A surprising aspect of these calculations is the appearance of quenched chiral logarithms, where in addition to the $m_\pi^2 \ln m_\pi^2$ form of a conventional QCD chiral logarithm, terms of the form $\delta \ln m_\pi^2$ also appear. Here δ is a constant given in terms of the parameters which enter the low-energy effective Lagrangian for quenched QCD. These effects are larger for small quark masses than the corresponding conventional QCD logarithms, since they lack a factor of m_π^2. Such effects may also appear in the matrix elements studied in this paper and in this section we discuss the current state of analytic results and how we will handle these effects in our simulation data.

For quenched chiral perturbation theory, a Lagrangian framework has been developed [15] and two new parameters enter, α and m_0. Calculating one-loop effects for the pion mass gives

$$(m_\pi^2)^{(1\ \mathrm{loop})} = m_\pi^2 \left\{ 1 + \frac{1}{8\pi^2 f^2} \left[\frac{\alpha}{3} \Lambda_{Q\chi PT}^2 - \frac{m_0^2}{3} - \left[\frac{m_0^2}{3} - \frac{2\alpha}{3} m_\pi^2 \right] \times \ln(m_\pi^2 / \Lambda_{Q\chi PT}^2) \right] \right\}, \qquad (90)$$

where $\Lambda_{Q\chi PT}$ is the scale used to renormalize the quenched theory. From loops in the $\mathcal{O}(p^2)$ Lagrangian, one gets an $\mathcal{O}(m_\pi^4)$ term of $\alpha m_\pi^4 / 24\pi^2 f^2$, which is not shown in Eq. (90). It is common to define the coefficient of the quenched chiral logarithm by δ, where

$$\delta \equiv \frac{m_0^2}{24\pi^2 f^2}. \qquad (91)$$

It is important to note that, in addition to the appearance of the $m_0^2 \ln m_\pi^2$ term, the only conventional chiral logarithm appears multiplied by α. In Sec. VI we discuss the determination of m_0 and α from our measurements of the dependence of pion mass squared on the quark mass for quenched domain wall fermion simulations.

For the kaon matrix elements of primary interest in this work, quenching is also expected to modify the quark mass dependence from the full QCD forms given in the previous section. A recent calculation of the quenched chiral logarithms for the (8,1) and (27,1) operators has been presented in Ref. [55]. Calculations of this type, including the (8,8) operators, are very useful in the analysis of matrix elements from QCD simulations. Unfortunately, the currently available calculations completely remove all quark loops, including those in the effective low energy four-quark operators. For the $\mathcal{O}(p^2)$ $\Delta S = 1$ Lagrangian of quenched chiral perturbation theory, Eq. (2.2) of [55] shows that the authors have used a supertrace to represent the operators in chiral perturbation theory. The supertrace introduces ghost quarks to cancel loop effects of real quarks, which is an unconventional definition of the quenched approximation.

However, for actual numerical QCD calculations, quark loops which can be made through self-contractions of the low-energy four-quark operators of Eqs. (4)–(23) are included. Only disconnected quark loops, generated through the quark determinant in QCD and connected solely by gluon exchange with the four-quark operators, are discarded. The numerical simulations correspond to evaluating all relevant four-quark operators, at low energies, in background gluon fields generated without explicit vacuum polarization quark loops. In the quenched approximation these vacuum quark loop effects are partially included by using an appropriately

shifted value of the bare QCD coupling β. The existing analytic calculations for the quenched theory correspond to evaluating all relevant four-quark operators, including ghost quark self-contractions, in a quenched gluon background. Since these situations are quite distinct, formula presented in [55] are not generally applicable to our simulation results.

There is one result from [55] and earlier calculations which is applicable to our simulations, the amplitude for $K^+ \to \pi^+$ for the (27,1) operators. Since there are no self-contractions of the four-quark operators in this amplitude, it is unaffected by the ghost-quark loops discussed in the previous paragraphs. Quenched chiral perturbation theory predicts that this amplitude has the form

$$\langle \pi^+ | \Theta^{(27,1)} | K^+ \rangle = -\frac{4 m_M^2 \alpha^{(27,1)}}{f^2} \left[1 - 6 L_{Q\chi}(m_M) - \frac{(m_0^2 - 2\alpha m_M^2)}{24\pi^2 f^2} \ln(m_M^2/\Lambda_{Q\chi PT}^2) \right] + O(m_M^4), \tag{92}$$

where $L_{Q\chi}(m)$ is the same as L_χ defined in Eq. (82) except that $\Lambda_{\chi PT}$ is replaced by $\Lambda_{Q\chi PT}$. Note that Eq. (92) contains both a conventional chiral logarithm and a quenched chiral logarithm. The conventional chiral logarithm is quite large (its coefficient is 6) but markedly smaller than the conventional chiral logarithm in full QCD, Eq. (79) (its coefficient is 34/3). It is fortunate that this quenched formula is known, since, as we will discuss in Sec. X, the value of $\alpha^{(27,1)}$ we can determine from our data is strongly dependent on the known analytic value for the coefficient of the conventional chiral logarithm in quenched QCD.

For our quenched simulations, we must still perform a subtraction of power divergent quantities to get the quenched values for $\alpha_1^{(8,1)}$. As we discussed in the previous section for full QCD, it is vital to do the subtraction in a way which correctly removes power divergent coefficients times both conventional and quenched logarithms. If the quenched formula analogous to Eqs. (78)–(81) existed, one could in principle fit individual amplitudes to the formulas, including logarithms, and extract the desired coefficients. Even with the formula, such a process could prove difficult due to the statistical errors on the data.

However, we can make use of the fact that in chiral perturbation theory, the power divergent parts of operators appear as lower dimensional operators. Thus the logarithmic corrections, both conventional and quenched, should be the same for the power divergent parts of a four-quark operator and the appropriate quark bilinear. This is the basis for the cancellation of the chiral logarithms in Eqs. (87) and (89). Thus for the subtractions of power divergent operators, the analytic coefficients of the logarithms are not needed. It would, however, be useful to know the coefficients of the logarithms for the remaining finite terms. (As this paper was being completed, such a calculation was reported for some of the operators of interest here [58].) We will have to rely on the behavior of our data to estimate the size of these effects.

It is important to stress that this cancellation of the quadratic divergence in the logarithmic corrections to the chiral limit discussed above provides a concrete example of the general cancellation of quadratic divergences implied by the form of the subtraction term which we adopt. As will be discussed in Sec. XI A, we choose to implement the subtraction required by chiral perturbation theory in a fashion which removes the quadratic divergence completely from the resulting $\langle \pi^+ | \Theta^{(8,1)} | K^+ \rangle$ amplitude in the limit $m_{\rm res} \to 0$. The cancellation of the quadratic divergence is guaranteed by standard renormalization arguments and does not rely on chiral perturbation theory.

IV. DOMAIN WALL FERMION MODIFICATIONS TO CHIRAL PERTURBATION THEORY

In the previous section, results relevant to the current calculation from both quenched and full QCD continuum chiral perturbation theory were discussed. In addition to the basic lowest order relations, chiral perturbation theory gives the logarithmic corrections for both full and quenched QCD. For domain wall fermions with finite extent in the fifth dimension, exact chiral symmetry does not exist, even if only the fermionic modes relevant for low-energy QCD physics are studied, due to the mixing between the left- and right-handed fermion surface states that form at the boundaries of the fifth dimension. However, for low energy physics this mixing appears as an additional contribution to the fermion mass, the residual mass $m_{\rm res}$, in the low-energy effective Lagrangian describing domain wall fermion QCD at finite values for the fifth dimension [21,22].

For the calculation at hand, we must include power divergent operators, which are also affected by the residual chiral symmetry breaking. However, due to their dependence on scales up to the cutoff, chiral symmetry breaking effects here cannot be precisely described in terms of an extra additional mass in the low-energy effective Lagrangian. As we will see in Sec. IV A below, these effects modify the formula in Eqs. (52)–(67). These modifications will be important in the analysis of our numerical data.

A second modification to the chiral perturbation theory formula of the previous section comes from the presence of unsuppressed topological near-zero modes in our quenched QCD calculation. Without the fermionic determinant, these modes need not occur with the distribution of full QCD and the light-quark mass limit of quenched QCD has been seen to be pathological [21]. The effects of such modes are suppressed for large volumes, but can be important for the volumes used in the matrix element calculations discussed here. Since the zero modes can lead to nonlinear dependence on the input quark mass, just as the chiral logarithms can, it is important to quantify their effects. We do this through a discussion of some of the relevant Ward-Takahashi identities in Sec. IV B.

The notation we use for domain wall fermions is given in [21]. In particular, we use $\Psi_i(x,s)$ to represent a five-dimensional fermion field with four spin components and flavor i. A generic four-dimensional fermion field with four spin components and flavor i will be given by $\psi_i(x)$, while

the specific four-dimensional field defined from $\Psi_i(x,s)$ will be given by $q_i(x)$. For quark fields of specific flavor, *u, d, s,* and *c* will be used to represent four-dimensional fields defined from $\Psi_i(x,s)$.

A. Residual mass effects

Residual chiral symmetry breaking effects for domain wall fermions at finite L_s can be easily discussed by introducing a new term into the action containing a special-unitary flavor matrix Ω [59]. This term connects four-dimensional planes at the midpoint of the fifth dimension and has the form

$$S_\Omega = -\sum_x \{\overline{\Psi}_{x,L_s/2-1} P_L(\Omega^\dagger - 1)\Psi_{x,L_s/2} + \overline{\Psi}_{x,L_s/2} P_R(\Omega - 1)\Psi_{x,L_s/2-1}\}. \quad (93)$$

If we let Ω transform as

$$\Omega \to U_R \Omega U_L^\dagger \quad (94)$$

under $SU(3)_L \otimes SU(3)_R$, then the domain wall fermion Dirac operator possesses exact chiral symmetry. When $L_s \to \infty$, this extra midpoint term in the action should not matter for low-energy physics, so any Green's function that contains a power of Ω should also contain a factor of $\exp(-\alpha L_s)$. (Here we assume that in the $L_s \to \infty$ limit the residual chiral symmetry vanishes exponentially. For the quenched theory, the numerical data is not conclusive on this point, but does show that the residual chiral symmetry breaking effects can be made quite small.) Since Ω is a $(\overline{3},3)$ under $SU(3)_L \otimes SU(3)_R$, it transforms "like a mass term."

Consider a continuum effective Lagrangian description of QCD with domain wall fermions at finite L_s. The presence of the parameter Ω implies the mass term in this Lagrangian will be

$$Z_m m_f \overline{\psi}\psi + c\{\overline{\psi}\Omega^\dagger P_R \psi + \overline{\psi}\Omega P_L \psi\}, \quad (95)$$

to leading order. Here Z_m is a mass renormalization constant and c is a constant with dimensions of mass that is $\mathcal{O}[\exp(-\alpha L_s)/a]$ where a is the lattice spacing. With the conventional choice $\Omega_{a,b} = \delta_{a,b}$, Eq. (95) reduces to the form

$$Z_m(m_f + m_{\rm res})\overline{\psi}\psi \quad (96)$$

where $m_{\rm res} \approx 10^{-3}$ for quenched lattices with $a^{-1} \sim 2$ GeV and $L_s = 16$.

A simple case where power divergences are involved is given by the determination of $\langle \overline{q}q \rangle$ on the lattice with domain wall fermions. Since this transforms as a $(\overline{3},3)$ plus $(3,\overline{3})$ in chiral perturbation theory, its dependence on explicit chiral symmetry breaking terms is given by

$$\langle \overline{q}q \rangle(m_f, L_s) \sim c_1(M + M^\dagger) + c_1'(\Omega + \Omega^\dagger) \quad (97)$$

where c_1 and c_1' are two constants. Since c_1 depends on high momentum scales and behaves as $1/a^2$, c_1' also depends on high momentum and is thus not simply equal to $c_1 m_{\rm res}$. In particular, $c_1' \sim \exp(-\alpha L_s)/a^3$. For the case with SU(3) flavor symmetry and the conventional choice $\Omega_{ab} = \delta_{ab}$, the chiral condensate for domain wall fermions should have the form

$$\langle \overline{q}q \rangle(m_f, L_s) = \langle \overline{q}q \rangle_0 + c_1 m_f + c_1'. \quad (98)$$

Notice that the value of $\langle \overline{q}q \rangle(m_f, L_s)$ for $m_f = -m_{\rm res}$ is not equal to $\langle \overline{q}q \rangle(m_f = 0, L_s = \infty)$ since there is no simple relation between c_1 and c_1'. Thus the residual chiral symmetry breaking effects in a power divergent quantity are small for large L_s, but they cannot be cancelled by a simple choice for the input quark mass.

The presence of the new parameter Ω for domain wall fermions means that there is an additional operator needed to represent $\Theta^{(8,1)}$ in chiral perturbation theory. In particular, replacing M in Eq. (56) by $m_{\rm res}\Omega$ yields the operator

$$\tilde{\Theta}_3^{(8,1)} \equiv \frac{8v}{f^2} m_{\rm res} {\rm Tr}[\Lambda\Sigma\Omega + \Lambda(\Sigma\Omega)^\dagger] \quad (99)$$

and the representation of $\Theta^{(8,1)}$ in Eq. (52) is modified to

$$\Theta^{(8,1)} \to \alpha_1^{(8,1)}\tilde{\Theta}_1^{(8,1)} + \alpha_2^{(8,1)}\tilde{\Theta}_2^{(8,1)} + \alpha_3^{(8,1)}\tilde{\Theta}_3^{(8,1)}. \quad (100)$$

As mentioned in the previous section, the coefficient $\alpha_2^{(8,1)}$ is power divergent and consequently so is $\alpha_3^{(8,1)}$. Because we have used an explicit factor of $m_{\rm res}$ in the definition of $\tilde{\Theta}_3^{(8,1)}$, which involves power divergences, $\alpha_3^{(8,1)} \neq \alpha_2^{(8,1)}$. Similar to the behavior of $\langle \overline{q}q \rangle$ at finite L_s, the chiral limit of $\Theta^{(8,1)}$ is not given by setting $m_f = -m_{\rm res}$.

The presence of this additional term in the representation of $\Theta^{(8,1)}$ does not change Eq. (59), since Ω is flavor symmetric and $\alpha_3^{(8,1)}$ is defined in the zero quark mass limit. (There can be quark mass dependence in the residual chiral symmetry breaking effects, but this is a higher order effect. Such quark mass dependence has been seen in quenched simulations, but is a small effect [21,22].) This new term does change Eq. (62) for finite L_s to

$$\langle \pi^+ | \Theta^{(8,1)} | K^+ \rangle = \frac{4m_M^2}{f^2}(\alpha_1^{(8,1)} - \alpha_2^{(8,1)}) - \frac{32v}{f^4} m_{\rm res} \alpha_3^{(8,1)}, \quad (101)$$

where we have also taken $\Omega_{ab} = \delta_{ab}$. Thus we see that $\langle \pi^+ | \Theta^{(8,1)} | K^+ \rangle$ will not vanish at $m_f = 0$, nor at $m_f = -m_{\rm res}$, since there is no simple relation between $\alpha_2^{(8,1)}$ and $\alpha_3^{(8,1)}$. However, since all we require from simulations is the value of $\alpha_1^{(8,1)}$, we see that it can be determined from the slope of $\langle \pi^+ | \Theta^{(8,1)} | K^+ \rangle$ with respect to m_f and the value of $\alpha_2^{(8,1)}$ from $\langle 0 | \Theta^{(8,1)} | K^0 \rangle$.

It is true that $\langle \pi^+ | \Theta^{(8,1)} | K^+ \rangle$ should reach its chiral limit at $m_f = \mathcal{O}(-m_{\rm res})$, since the residual chiral symmetry breaking effects still depend on the overlap between the surface states at the ends of the fifth dimension. We will be able to check that our numerical results show this behavior. In general, the chiral limit for any divergent quantity is uncertain at finite L_s. As previously mentioned, this directly impacts the

determination of $\alpha^{(8,8)}$ from the $\Delta I=1/2$ matrix elements of $\langle \pi^+|\Theta^{(8,8)}|K^+\rangle$. Fortunately, here we can use the finite $\Delta I=3/2$ matrix elements and the Wigner-Eckart theorem to determine $\alpha^{(8,8)}$.

B. Topological near-zero modes and Ward-Takahashi identities

In the previous section we discussed how residual chiral symmetry breaking effects from finite L_s values can enter the operators of interest in this work. These effects make the chiral limit uncertain for divergent operators. A second difficulty with the chiral limit arises for quenched domain wall simulations in finite volumes from fermionic topological near-zero modes which are unsuppressed due to neglecting the fermionic determinant. The presence of these zero modes is an important feature of domain wall fermions, but it does lead to additional complications in the quenched simulations reported here. Since these modes distort the chiral limit, they can produce nonlinear behavior in Green's functions that may, in a range of small quark masses, be difficult to distinguish from the chiral logarithm effects discussed earlier. For the remainder of this section, we will refer to the topological near-zero modes as zero modes, with the understanding that their eigenvalues are not precisely zero for finite L_s.

The presence of zero modes in quenched simulations has been extensively discussed in [21], where their effects were seen in the chiral condensate and hadronic masses. In this calculation we will be subtracting large, power divergent lattice quantities to achieve our final physical results; it is important that the zero mode effects be well understood for the subtraction process. Since zero mode effects are suppressed as the volume increases, naively down by a factor of $1/\sqrt{V}$ relative to the fermionic modes responsible for chiral symmetry breaking and low energy QCD physics, their effects are not included in the infinite volume chiral perturbation theory results of Sec. III.

To gain a quantitative understanding of the zero mode effects, we will use the Ward-Takahashi identities of domain wall fermion QCD. Since these identities are true in the quenched theory for any quark mass and volume, they must include the effects of zero modes. Continuum chiral perturbation theory is the simplest way to represent the Ward-Takahashi identities in the infinite volume limit with arbitrarily small quark masses. In this limit, where zero modes do not enter, saturating intermediate states with light pseudoscalars gives the relations of lowest order chiral perturbation theory. Thus the Ward-Takahashi identities can detail how zero mode effects alter the lowest order chiral perturbation theory we are using to determine $K\to\pi\pi$ matrix elements. Of course, the chiral logarithm corrections to lowest order chiral perturbation theory are also included in the Ward-Takahashi identities, but these are more easily handled through chiral perturbation theory techniques.

The Ward-Takahashi identity for domain wall fermions with SU(3) flavor symmetry is [18,21]

$$\Delta_\mu\langle \mathcal{A}^a_\mu(x)O(y)\rangle = 2m_f\langle J^a_5(x)O(y)\rangle + 2\langle J^a_{5q}(x)O(y)\rangle + i\langle \delta^a O(y)\rangle. \tag{102}$$

Here $\mathcal{A}^a_\mu$ is the conserved axial current which involves all points in the fifth dimension, $J^a_5\equiv\bar{q}t^a\gamma_5 q$ and J^a_{5q} is a similar pseudoscalar density defined at the midpoint of the fifth dimension. Summing over x yields the integrated form of this identity

$$\sum_x \left[\langle [2m_f J^a_5(x)+2J^a_{5q}(x)]O(y)\rangle + i\langle \delta^a O(y)\rangle\right]=0 \tag{103}$$

which we will use extensively.

We first consider the simple case where $O(y)=J^a_5(y)$. Then Eq. (103) becomes

$$\sum_x \langle [m_f J^a_5(x)+J^a_{5q}(x)]J^a_5(y)\rangle = \langle \bar{u}u(y)\rangle \equiv 12\langle \bar{u}u(y)\rangle_{\text{lat norm}} \quad \text{(no sum on a)}, \tag{104}$$

where the factor of 12 is needed since we normalize $\langle \bar{u}u(y)\rangle_{\text{lat norm}}$ per spin and color. [We are considering the case with SU(3) flavor symmetry, making the chiral condensate for u, d, and s quarks the same.] Working in Euclidean space with correlators evaluated through the Feynman path integral, we break the sum over x into the points with $x\neq y$ and the point with $x=y$. For the points with $x\neq y$, the correlator is a sum of exponentials, with the overlap between the operators $J^a_5(x)$ and $J^a_{5q}(x)$ and the different mass states conventionally represented as a matrix element. For $x=y$ a "contact" term is generated. Using the normalizations for the states given in Appendix A gives

$$\sum_{x,n}\langle 0|m_f J^a_5(\mathbf{x},0)+J^a_{5q}(\mathbf{x},0)|n\rangle \frac{\exp[-E_n(|x_0-y_0|)]}{2V_s E_n} \times\langle n|J^a_5(\mathbf{y},0)|0\rangle + C(y) - \langle \bar{u}u(y)\rangle = 0, \tag{105}$$

where V_s is the spatial volume and $C(y)$ is the contact term generated when $x=y$. The pseudo-Goldstone boson term in the sum over n gives

$$\langle 0|m_f J^a_5(0)+J^a_{5q}(0)|\pi^a\rangle \frac{1}{m^2_\pi}\langle \pi^a|J^a_5(0)|0\rangle = -\frac{m_f+m_{\text{res}}}{m^2_\pi}|\langle 0|J^a_5(0)|\pi\rangle|^2 \tag{106}$$

since for the low energy physics described by the state $|\pi^a\rangle$ we have $J^a_{5q}=m_{\text{res}}J^a_5$. This term in the sum is not suppressed for light quark masses due to the m^2_π term which appears in the denominator. For a general integrated Ward-Takahashi identity, keeping only the leading terms in the $m_f\to 0$ limit, which includes such "pion pole saturation" contributions, leads to the relations of lowest order chiral perturbation theory [49]. To apply this procedure here, we must first note that the other states in the sum and the contact term give a contribution of $\mathcal{O}(m_f)/a^2+\mathcal{O}(m_{\text{res}})/a^2$. Here high momen-

tum modes can enter and the midpoint pseudoscalar density J^a_{5q} is not simply related to J^a_5. Thus, without any effects of zero modes, we have

$$-\frac{m_f+m_{\rm res}}{m_\pi^2}|\langle 0|J^a_5(0)|\pi\rangle|^2+\frac{\mathcal{O}(m_f)}{a^2}+\frac{\mathcal{O}(m_{\rm res})}{a^2}$$
$$=\langle\overline{u}u\rangle(m_f,L_s). \tag{107}$$

This relation is the same as Eq. (98) and once again demonstrates that the chiral limit cannot be achieved at finite L_s by setting $m_f=-m_{\rm res}$ when divergent quantities are involved. However, since the Ward-Takahashi identities include zero mode effects, we can investigate their contributions to this relation.

To simplify the discussion of zero modes, we consider the $L_s\to\infty$ limit where the contribution of the J^a_{5q} term to the Ward-Takahashi identity vanishes. Following [21] we work with generic fermion fields ψ, the continuum four-dimensional Dirac operator $\not{D}^{(4)}$ with eigenvalues and eigenvectors given by $(\not{D}^{(4)}+m)\psi_\lambda=(i\lambda+m)\psi_\lambda$ and write the quark propagator as

$$S^{(4)}_{x,y}=\sum_\lambda\frac{\psi_\lambda(x)\psi^\dagger_\lambda(y)}{i\lambda+m}. \tag{108}$$

[Here we are considering a particular gauge field $U_\mu(x)$ and the eigenvalues λ, eigenvectors $\psi_\lambda(x)$, and quark propagator are functions of $U_\mu(x)$. Green's functions result from averaging over an appropriate distribution of gauge fields.] The integrated Ward-Takahashi identity, Eq. (104), then becomes

$$-m_f\sum_{x,\lambda,\lambda'}\ {\rm Tr}\left(\frac{\psi_\lambda(y)\psi^\dagger_\lambda(x)}{-i\lambda+m_f}\,\frac{\psi_{\lambda'}(x)\psi^\dagger_{\lambda'}(y)}{i\lambda'+m_f}\right)$$
$$+\sum_\lambda\ {\rm Tr}\left(\frac{\psi_\lambda(y)\psi^\dagger_\lambda(y)}{i\lambda+m_f}\right)=0. \tag{109}$$

Performing the sum over x in the first term gives $\delta_{\lambda,\lambda'}$ and we are left with

$$-m_f\sum_\lambda\ {\rm Tr}\left(\frac{\psi_\lambda(y)\psi^\dagger_\lambda(y)}{\lambda^2+m_f^2}\right)+\sum_\lambda\ {\rm Tr}\left(\frac{\psi_\lambda(y)\psi^\dagger_\lambda(y)}{i\lambda+m_f}\right)=0. \tag{110}$$

This relation is easily seen to be true, since for $\lambda\neq 0$, there is also an eigenvalue $-\lambda$. Also, the zero mode contributions cancel between the two terms. Zero modes in the left term will alter numerical measurements of pion properties in moderate volumes, while the right term contains the zero modes which enter in the chiral condensate.

Consider working in moderate sized volumes where zero mode effects may be present but enter only as small corrections to the infinite volume results. We decompose the sums in Eq. (109) into terms without zero modes and terms with zero modes. The terms without zero modes will give Eq. (107). Including zero mode effects changes Eq. (107) for small m_f in the $L_s\to\infty$ limit to

$$-m_f\left\{\frac{|\langle 0|J^a_5(0)|\pi\rangle|^2}{m_\pi^2}\right.$$
$$\left.+\sum_{\substack{x,\lambda=0\\ \text{or }\lambda'=0}}\ {\rm Tr}\left(\frac{\psi_\lambda(y)\psi^\dagger_\lambda(x)}{-i\lambda+m_f}\,\frac{\psi_{\lambda'}(x)\psi^\dagger_{\lambda'}(y)}{i\lambda'+m_f}\right)\right\}+\frac{\mathcal{O}(m_f)}{a^2}$$
$$=\langle\overline{\psi}\psi\rangle(m_f)-\sum_{\lambda=0}\ {\rm Tr}\left(\frac{\psi_\lambda(y)\psi^\dagger_\lambda(y)}{i\lambda+m_f}\right). \tag{111}$$

For finite L_s, the modifications to Eq. (111) come from including the midpoint term J^a_{5q} and a residual chiral symmetry breaking term for each eigenvector, referred to as δm_i in [21]. In [21] it was found that a histogram of δm_i values for modes with eigenvalues below $\approx\Lambda_{\rm QCD}$ was peaked very close to $m_{\rm res}$. It is certainly possible that as $a\to 0$ the low lying eigenvalues all show a common residual chiral symmetry breaking of $m_{\rm res}$, although this has not been demonstrated. To proceed with our general analysis including finite L_s effects, we make this reasonable assumption and in the sums over eigenvalues replace m_f by $m_f+m_{\rm res}$ for modes with eigenvalues below $\approx\Lambda_{\rm QCD}$. For such terms, the factor of m_f multiplying the quantity in braces on the left-hand side is also modified to $m_f+m_{\rm res}$. For terms with eigenvalues above $\approx\Lambda_{\rm QCD}$, such a simple modification does not seem likely. However, these terms do not produce any effects which diverge as $m_f\to 0$ since the $1/m_f$ from the zero mode is cancelled by the explicit m_f multiplying the terms in braces on the left-hand side of Eq. (111). This gives us the finite L_s result

$$-(m_f+m_{\rm res})\left\{\frac{|\langle 0|J^a_5(0)|\pi\rangle|^2}{m_\pi^2}\right.$$
$$\left.+\sum_{\substack{x,\lambda=0\\ \text{or }\lambda'=0}}^{\lambda,\lambda'<\Lambda_{\rm QCD}}\ {\rm Tr}\left(\frac{\psi_\lambda(y)\psi^\dagger_\lambda(x)}{-i\lambda+m_f+m_{\rm res}}\,\frac{\psi_{\lambda'}(x)\psi^\dagger_{\lambda'}(y)}{i\lambda'+m_f+m_{\rm res}}\right)\right\}$$
$$+\frac{\mathcal{O}(m_f)}{a^2}+\frac{\mathcal{O}(m_{\rm res})}{a^2}$$
$$=\langle\overline{u}u\rangle(m_f,L_s)-\sum_{\lambda=0}\ {\rm Tr}\left(\frac{\psi_\lambda(y)\psi_\lambda(y)^\dagger}{i\lambda+m_f+m_{\rm res}}\right). \tag{112}$$

When $\langle 0|J^a_5(0)|\pi\rangle$ and m_π are measured from the correlator $\langle iJ^a_5(x)iJ^a_5(y)\rangle$ in a numerical simulation, some zero mode effects can be present depending on the range of $x-y$ used. The effects of zero modes [the second term in braces in Eq. (112)] will enter in the measured values $\langle 0|J^a_5(0)|\pi'\rangle$ and $m_{\pi'}$, where the primes indicate quantities deviating slightly from their infinite volume values. We can replace the quantity in braces in Eq. (112) by

$$\frac{|\langle 0|J^a_5(0)|\pi'\rangle|^2}{m^2_{\pi'}} \tag{113}$$

which is bounded by the values for $\langle \bar{u}u\rangle(m_f,L_s)$ measured with and without zero mode effects.

We can now do a similar analysis for the matrix element $\langle \pi^+|\bar{s}d|K^+\rangle$. This is an instructive example since we want to use measured values of $\langle \pi^+|Q_i|K^+\rangle$ matrix elements on the lattice to determine physical quantities and we seek some understanding of the role of zero modes in matrix elements of this form. We start from Eq. (103) taking $J_5^a(x) = [\bar{d}\gamma_5 u](x)$ and letting $O(y)\to[\bar{s}d](y)[i\bar{u}\gamma_5 s](z)$. We define the pseudoscalar densities $P_{K^-}(x)\equiv[i\bar{u}\gamma_5 s](x)$ and $P_{\pi^+}(x)\equiv[i\bar{d}\gamma_5 u](x)$ and the scalar density $S(x)\equiv[\bar{s}d](x)$. [We adopt the notation $P_{K^-}(x)$ to distinguish these pseudoscalar operators from the operators like $K^-(x)$ of chiral perturbation theory, as in Eqs. (A9) and (A10), which have a different normalization.] We can then write Eq. (103) as

$$\sum_x \langle [2m_f P_{\pi^+}(x) + 2P^{\rm MP}_{\pi^+}(x)] S(y) P_{K^-}(z)\rangle - \langle P_{K^+}(y)P_{K^-}(z)\rangle + \langle S(y)S^\dagger(z)\rangle = 0 \qquad (114)$$

where $P^{\rm MP}_{\pi^+}(x)$ is the ''midpoint'' pseudoscalar density with the π^+ quantum numbers formed from $\Psi_i(x,s)$ for $s = L_s/2-1$ and $L_s/2$. Considering the case where $L_s\to\infty$, $y-z$ is large, there are no zero modes present and $m_f\to 0$ gives

$$\frac{2m_f}{m_\pi^2}\langle \pi^+|\bar{s}d|K^+\rangle - 1 = 0. \qquad (115)$$

The term $\langle S(y)S^\dagger(z)\rangle$ plays no role in this case, since it does not contain any contribution from the massless pseudoscalars.

We now consider the role of zero modes for the $L_s=\infty$ case. We start with the complete spectral decomposition of Eq. (114), which is

$$2m_f \sum_{x,\lambda,\lambda',\lambda''} {\rm Tr}\left(\frac{\psi_\lambda(y)\psi_\lambda^\dagger(z)}{i\lambda+m_f}\frac{\psi_{\lambda'}(z)\psi_{\lambda'}^\dagger(x)}{-i\lambda'+m_f}\frac{\psi_{\lambda''}(x)\psi_{\lambda''}^\dagger(y)}{i\lambda''+m_f}\right) - \sum_{\lambda,\lambda'} {\rm Tr}\left(\frac{\psi_\lambda(y)\psi_\lambda^\dagger(z)}{i\lambda+m_f}\frac{\psi_{\lambda'}(z)\psi_{\lambda'}^\dagger(y)}{-i\lambda'+m_f}\right) - \sum_{\lambda,\lambda'} {\rm Tr}\left(\frac{\psi_\lambda(y)\psi_\lambda^\dagger(z)}{i\lambda+m_f}\frac{\psi_{\lambda'}(z)\psi_{\lambda'}^\dagger(y)}{i\lambda'+m_f}\right) = 0. \qquad (116)$$

The sum over x allows this to be written as

$$\sum_{\lambda,\lambda'} {\rm Tr}\left(\frac{\psi_\lambda(y)\psi_\lambda^\dagger(z)}{i\lambda+m_f}\psi_{\lambda'}(z)\psi_{\lambda'}^\dagger(y) \times\left[\frac{2m_f}{(\lambda')^2+m_f^2} - \frac{1}{-i\lambda'+m_f} - \frac{1}{i\lambda'+m_f}\right]\right) = 0. \qquad (117)$$

The term in brackets is easily seen to be zero. As must be the case, the zero modes entering the spectral decomposition also satisfy the Ward-Takahashi identity.

We now consider the modifications to Eq. (115) from zero modes, when $\langle \pi^+|S|K^+\rangle$ is measured on the lattice from the correlator $\langle P_{\pi^+}(x)S(y)P_{K^-}(z)\rangle$, with $x>y>z$. Provided the zero modes are localized, their effects will predominantly enter the quark propagators $D^{-1}(x,y)$ and $D^{-1}(y,z)$, since $x-z$ can exceed the size of the zero mode. Thus our measured quantities will not include the $\lambda'=0$ term in the first summation of Eq. (116). Separating out this term and again letting primes denote states where some zero mode contamination is possible gives the following result for the Ward-Takahashi identity when $m_f\to 0$:

$$\begin{aligned}\frac{2m_f}{m_{\pi'}^2}\langle 0|P_{\pi^+}|(\pi^+)'\rangle\langle(\pi^+)'|S(y)P_{K^-}(z)\rangle &= \langle P_{K^+}(y)P_{K^-}(z)\rangle - \langle S(y)S^\dagger(z)\rangle \\ &\quad - 2\sum_{\substack{\lambda'=0\\ x,\lambda,\lambda''}} {\rm Tr}\left(\frac{\psi_\lambda(y)\psi_\lambda^\dagger(z)}{i\lambda+m_f}\psi_{\lambda'}(z)\psi_{\lambda'}^\dagger(x)\frac{\psi_{\lambda''}(x)\psi_{\lambda''}^\dagger(y)}{i\lambda''+m_f}\right) \\ &= \langle P_{K^+}(y)P_{K^-}(z)\rangle - \langle S(y)S^\dagger(z)\rangle \\ &\quad - 2\sum_{\lambda'=0,\lambda} {\rm Tr}\left(\frac{\psi_\lambda(y)\psi_\lambda^\dagger(z)}{i\lambda+m_f}\frac{\psi_{\lambda'}(z)\psi_{\lambda'}^\dagger(y)}{m_f}\right). \qquad (118)\end{aligned}$$

The combination $\langle P_{K^+}(y)P_{K^-}(z)\rangle - \langle S(y)S^\dagger(z)\rangle$ has zero mode effects. These arise from a zero mode in either one or both quark propagators. The $\lambda=0$ term in the sum cancels the contribution from $\langle P_{K^+}(y)P_{K^-}(z)\rangle - \langle S(y)S^\dagger(z)\rangle$ when both quark propagators have a zero mode. When $\lambda\neq 0$, the additional term cancels half of the zero mode contribution from $\langle P_{K^+}(y)P_{K^-}(z)\rangle - \langle S(y)S^\dagger(z)\rangle$ due to a zero mode in only one propagator. Since zero mode effects enter $\langle P_{K^+}(y)P_{K^-}(z)\rangle$ and $\langle S(y)S^\dagger(z)\rangle$ identically, the right-hand side of Eq. (118) becomes

$$\langle P_{K^+}(y)P_{K^-}(z)\rangle_{\rm no\ zero} + \langle P_{K^+}(y)P_{K^-}(z)\rangle_{\rm one\ zero} - \langle S(y)S^\dagger(z)\rangle_{\rm no\ zero}. \qquad (119)$$

Here ''no zero'' means no zero modes included in the spectral sum and ''one zero'' means one of the two quark propagators is a zero mode. For small m_f, $\langle S(y)S^\dagger(z)\rangle_{\rm no\ zero}$ plays no role leaving us with

$$\frac{2m_f}{m_{\pi'}^2}\langle 0|P_{\pi^+}|(\pi^+)'\rangle\langle(\pi^+)'|S(y)P_{K^-}(z)\rangle = \langle P_{K^+}(y)P_{K^-}(z)\rangle_{\rm no\ zero} + \langle P_{K^+}(y)P_{K^-}(z)\rangle_{\rm one\ zero}. \qquad (120)$$

For finite L_s, Eq. (120) is modified by replacing $2m_f$ with $2(m_f+m_{\rm res})$ since no divergent terms appear.

For the range of $y-z$ where our matrix elements calculations are done, we have explicit results for $\langle P_{K^+}(y)P_{K^-}(z)\rangle$ and $\langle S(y)S^\dagger(z)\rangle$. Since

$$\langle P_{K^+}(y)P_{K^-}(z)\rangle_{\rm no\ zero} = \langle P_{K^+}(y)P_{K^-}(z)\rangle + \langle S(y)S^\dagger(z)\rangle \qquad (121)$$

we can estimate the effects of the one zero mode term on the right side of Eq. (120). We can compare our numerical data to the Ward-Takahashi identity with no zero modes [Eq. (115)] and with zero modes [Eq. (120)]. We will discuss our numerical results for the Gell-Mann–Oakes–Renner (GMOR) relation in Sec. VI B and for the $\bar{s}d$ Ward-Takahashi identity in Sec. VI C.

C. Topological near-zero modes and operator subtraction

A final part of this calculation where the features of domain wall fermions in quenched QCD are important is the role of zero modes in the subtraction of power divergence operators required to determine $K\to\pi\pi$ matrix elements using chiral perturbation theory. As discussed in Sec. III B and shown in Eq. (87), the ratio

$$\frac{\langle 0|\Theta^{(8,1)}|K^0\rangle}{\langle 0|\Theta^{(3,\bar{3})}|K^0\rangle} \tag{122}$$

has no chiral logarithms multiplying power divergent quantities. This is due to the locality of the power divergent part of the operator $\Theta^{(8,1)}$. The situation for zero mode effects is identical since in the denominator they only enter the quark propagators connecting the K^0 to the operator. For the power divergent part of the numerator, zero modes also only enter the propagators connecting the K^0 to the operator and their effects cancel in the ratio. Thus the linearity in $(m_K^2-m_\pi^2)$ given in Eq. (87) should also be true for the $\alpha_2^{(8,1)}$ term when zero mode effects are included. This linearity will make the determination of $\alpha_2^{(8,1)}$ much more accurate and our results will not be influenced by a small zero mode effect times a power divergent contribution.

Once $\alpha_2^{(8,1)}$ is known, we can use the combination of matrix elements given on the left-hand side of Eq. (89) to determine $\alpha_1^{(8,1)}$. Here we take a linear combination of two $K\to\pi$ matrix elements and zero modes may enter in both. However, once again the power divergent part of $\langle\pi^+|\Theta^{(8,1)}|K^+\rangle$ and $\alpha_2^{(8,1)}\langle\pi^+|\Theta^{(3,\bar{3})}|K^+\rangle$ are altered identically by zero mode effects in the quark propagators between the operators creating the pion and kaon and the Θ's. Thus our results will not be altered by small zero mode effects multiplied by power divergent terms. There can, however, be zero mode effects left in the finite part of the left-hand side of Eq. (89). These should be similar to the zero mode effects discussed in the preceding section for $\langle\pi^+|\bar{s}d|K^+\rangle$, whose size we will estimate from our data in Sec. VI C.

V. BASIC FEATURES OF NUMERICAL SIMULATIONS

A. Simulation parameters

The quenched gauge field ensemble used to calculate expectation values in this study was generated at gauge coupling $\beta=6.0$ with lattice four-volume $16^3\times 32$ (space $\times$time). The ensemble comprises 400 configurations separated by 10 000 sweeps, with each sweep consisting of a simple two-subgroup heat-bath update of each link. The gauge coupling corresponds to a lattice cutoff of $a^{-1}=1.922$ GeV set by the ρ mass [21]. The domain wall fermion fifth dimension was $L_s=16$ sites with a domain wall height $M_5=1.8$. These parameters yield a residual quark mass of about 3% of the strange quark mass [21].

The light quark masses in units of the lattice spacing were taken to be $m_f=0.01$, 0.02, 0.03, 0.04, and 0.05. The value of m_f corresponding to a pseudoscalar state made of degenerate quarks with mass equal to the physical kaon at $\beta=6.0$ is 0.018 [21]. Heavier quarks were also included to allow matrix elements to be calculated in the 4-flavor case where a charm quark is present. These heavy masses, with values of $m_f=0.1$, 0.2, 0.3, and 0.4 will not be discussed in this paper but rather in a subsequent publication. Quark propagators were calculated using the conjugate gradient method with a stopping residual $r=10^{-8}$.

Quark propagators were calculated from Coulomb gauge fixed wall sources at time slices $t_K=5$ and $t_\pi=27$. The resulting propagators were fixed to lattice Coulomb gauge (on the ''sink'' end) to reduce fluctuations in gauge averages and to allow construction of wall-wall correlators. Forward and backward in time propagators were constructed from linear combinations of propagators computed with periodic and antiperiodic boundary conditions. This amounts to using an unphysical doubled lattice in the time direction with periodicity 64. The random wall sources used to calculate eye diagrams were spread over times $t=14$–17, and the corresponding propagators had periodic boundary conditions.

Before starting the production simulation, all correlation functions were computed for a single common configuration on each of the QCDSP machines that were to be used in the calculation. They agreed bit by bit. During the production simulation, we checkpointed every tenth configuration. All quark propagators and contractions were calculated twice on this checkpointed configuration in order to detect any hardware errors. If the output from the repeated calculation did not agree with the original, the node responsible for the failure was tracked down and replaced. The process was repeated until bit by bit agreement was obtained. Such hardware errors occurred very infrequently (less than 1% of the configurations).

B. Computer code details

We have written two completely separate production computer programs to calculate weak matrix elements. The first is based on the general purpose QCD code written by the Columbia University lattice group and runs primarily on the QCDSP supercomputers at the RIKEN-BNL Research Center and Columbia University. The second program is based on the general purpose QCD code written by the MILC Collaboration which was extended by us to use domain wall fermions. We only have a single code which calculates the propagators necessary to compute renormalization (Z) factors, which is part of the QCDSP version. In addition we have three independently written analysis packages that run on workstations which take the raw matrix elements and combine them with Z factors and Wilson coefficients to yield physical amplitudes.

We have performed several checks of these codes. Most importantly, a completely independent check code was written to compare with the two production versions (this does not include the Z factors). Output generated on the same configuration from each code was compared for several test cases. In each case one code was run on a scalar workstation and the other on a parallel machine. The expected agreement was obtained in each test. We also checked the production simulation by calculating all of the required correlation functions with the check code on a single common gauge field configuration. All of the production simulation parameters (volume, gauge coupling, quark masses, sources, etc.) were used in this test. The Z factor code, which runs on a workstation, has not been exhaustively checked by second independent code.

As a final useful check, note that we work explicitly with the operators defined in Eqs. (4)–(23). The $(V-A)\times(V-A)$ operators go into themselves under a Fierz transformation. Thus color-mixed contractions can be compared to corresponding color-diagonal ones. We find perfect agreement in all cases.

VI. BASIC TESTS OF THE CHIRAL PROPERTIES OF DOMAIN WALL FERMIONS

In the earlier sections we have discussed the changes in full QCD, chiral perturbation theory relations due to quenching and using domain wall fermions at finite L_s. In this section, we will present our numerical results for simple cases and check their consistency with the theoretical expectations. The cases we consider are: (1) the presence of quenched chiral logarithms in m_π^2, (2) tests of the Gell-Mann–Oakes–Renner relation for finite L_s domain wall fermions, and (3) the Ward identity satisfied by the matrix element of $\langle \pi^+|\bar{s}d|K^+\rangle$.

A. Quenched chiral logarithms in m_π^2

Numerous simulations have looked for the presence of quenched chiral logarithms in m_π^2 versus m_f of the form given in Eq. (90). Recent values for δ are ≈ 0.1 [60] using Wilson fermions, the Wilson gauge action, and lattice spacings in the range 0.1–0.05 fm, 0.065 ± 0.013 [61] using clover-improved Wilson fermions, the modified quenched approximation, and a lattice spacing of 0.17 fm, and 0.07 ± 0.04 [21] using domain wall fermions, the Wilson action, and a lattice spacing of 0.2 fm. Since δ is a parameter of low-energy quenched QCD, the general agreement between the results from the different lattice formulations quoted above is encouraging and expected.

All the values for δ are below the initial estimates of ~ 0.2, based on the value for the η' mass in full QCD. This suggests that the effects of quenched chiral logarithms will only be evident at quite small quark masses. In this section we want to revisit the determination of δ from m_π^2 versus m_f for domain wall fermions, but at a smaller lattice spacing (0.104 fm) than our earlier determination at 0.197 fm [21]. We will then be able to assess the importance of quenched chiral logarithms in our determination of kaon matrix elements.

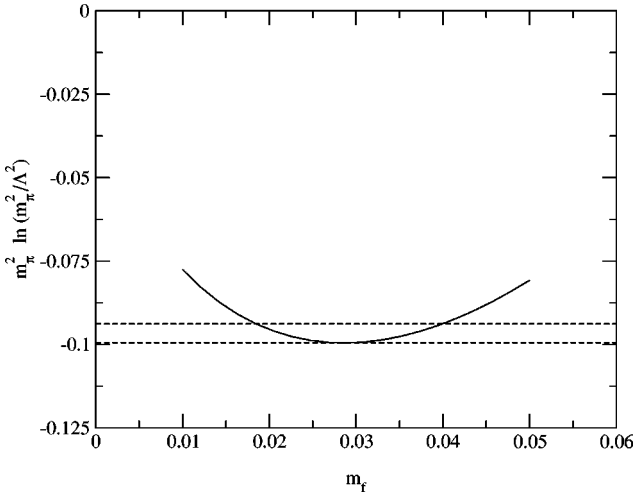

FIG. 1. The value of $m_\pi^2 \ln(m_\pi^2/\Lambda_{Q\chi PT}^2)$ vs m_f for the range of quark masses used in our simulations. The dashed lines have $m_\pi^2 \ln(m_\pi^2/\Lambda_{Q\chi PT}^2) = -0.0938$ and -0.0996. For $0.02 \leqslant m_f \leqslant 0.04$ the variation in $m_\pi^2 \ln(m_\pi^2/\Lambda_{Q\chi PT}^2)$ is about 5%.

In our earlier work on the chiral limit of domain wall fermions, we found that by working on large enough volumes to suppress the effects of topological near-zero modes, our data was consistent with the presence of a quenched chiral logarithm and that the point where m_π^2 vanished for such a fit was also in agreement with our value of $m_{\rm res}$ determined independently. For our current simulations, where the volumes are not as large, we will use the previously measured value $m_{\rm res} = 0.00124(5)$ as an input and neglect the $m_f = 0.01$ point in our analysis. This should exclude the dominant effects of topological near-zero modes and will also allow us to determine a value for δ.

In fitting to the general form of Eq. (90) we must decide how to handle the presence of the parameter α as well as δ. We first note an important consequence of our range of pion masses, which is that $m_\pi^2 \ln(m_\pi^2/\Lambda_{Q\chi PT}^2)$ only varies by 5% for $0.02 \leqslant m_f \leqslant 0.04$ with $\Lambda_{Q\chi PT} = 1$ GeV. This is shown in Fig. 1 where we have used $m_\pi^2 = 0.0098(20) + 3.14(9) m_f$ from [21]. Thus the term $\alpha m_\pi^2 \ln(m_\pi^2/\Lambda_{Q\chi PT}^2)$ will be approximately constant over our range of quark masses and we cannot expect to resolve it with our data. The small variation in $m_\pi^2 \ln(m_\pi^2/\Lambda_{Q\chi PT}^2)$ over our pion mass range will be an important point in fits to much of our data.

Thus we fit our lattice data to the form

$$(m_\pi^2)^{\rm lat} = a_\pi (m_f + m_{\rm res}) \left[1 - \delta \ln\left(\frac{a_\pi (m_f + m_{\rm res})}{\Lambda_{Q\chi PT}^2} \right) \right]. \quad (123)$$

We have used this functional form to fit m_π^2 from the 85 configurations used in [21], where quark masses 0.015, 0.02, 0.025, 0.03, 0.035, and 0.04 were used for the fits. These values for m_π^2 come from the axial current correlator $\langle A_0^a(x) A_0^a(0) \rangle$ to reduce the effects of topological near-zero modes. We have also done fits for the 400 configuration data set generated for this matrix elements calculation, where quark masses 0.02, 0.03, 0.04, and 0.05 were used in the fits.

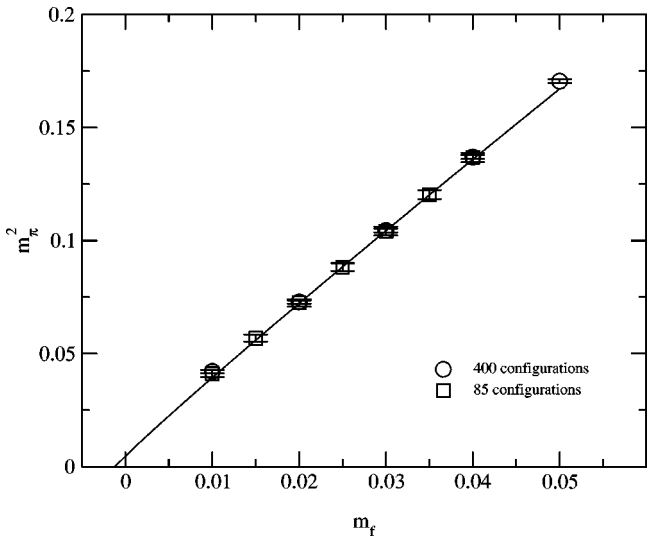

FIG. 2. The data for m_π^2 from 85 configurations and 400 configurations. The line is a fit to the 85 configuration data, excluding the $m_f=0.01$ point, and gives $\delta=0.05(2)$.

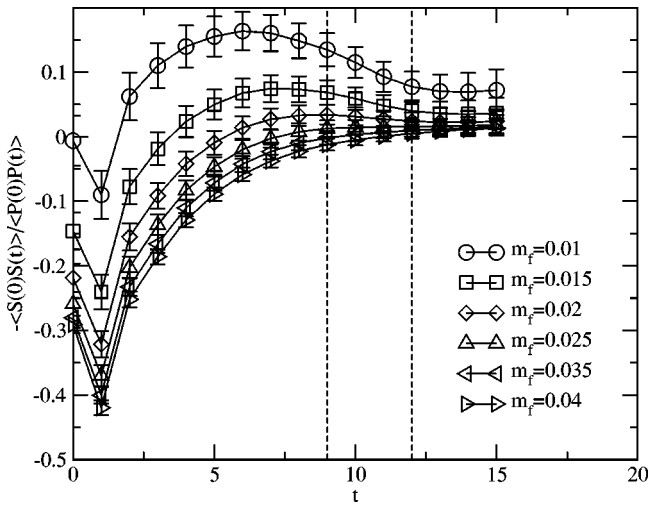

FIG. 3. The ratio $-\langle S^{\text{wall}}(0)S^\dagger(t)\rangle/\langle P^{\text{wall}}_{K^+}(0)P_{K^-}(t)\rangle$ of the scalar and pseudoscalar correlators, as a function of temporal separation. Without zero mode effects the ratio should be zero for m_f small, since the pseudoscalar mass is vanishing. Zero mode effects are present at the $\sim$10% level for $t=9-12$. This is the separation used in our evaluation of lattice matrix elements.

The pion masses for this data set come from $\langle \pi^a(x)A_0^a(0)\rangle$ correlators, since we only have pseudoscalar sinks in our matrix elements programs. We choose to quote results for $\Lambda_{Q\chi PT}=1$ GeV and have also done fits for $\Lambda_{Q\chi PT}=0.77$ and 1.2 GeV.

Figure 2 shows the data for both data sets and the curve is the fit to the 85 configuration set. For the 400 configuration data set we find $a_\pi=3.27(2)$ and $\delta=0.029(7)$ with $\chi^2/\text{DOF}=2.3$, while for the earlier 85 configuration data set we find $a_\pi=3.18(6)$ and $\delta=0.05(2)$ with $\chi^2/\text{DOF}=0.3$. Since these are uncorrelated fits to correlated data, the values of χ^2 are of limited validity, but, particularly for the 85 configuration data set, show the data is consistent with a quenched chiral logarithm form. Varying $\Lambda_{Q\chi PT}$ only changes a_π by $\pm 2\%$ and does not change δ within errors. The difference in the value of δ between the two data sets is due to the $m_f=0.015$ point only being present in the 85 configuration set. Without this point a smaller curvature is needed, and hence a smaller δ, to make m_π^2 vanish at $m_f=-m_{\text{res}}$. Also notice that the $m_f=0.05$ value for m_π^2 lies substantially above the fit line, which neglects this point. Since we are interested in quenched pathologies appearing at small quark masses, we have not included $\mathcal{O}[(m_f+m_{\text{res}})^2]$ terms in our fit. Given that $m_\pi=790$ MeV for this heaviest quark mass, such higher order terms are expected to be important.

Notice that we cannot determine the one loop effects on the value of a_π. The combination of constants in the braces in Eq. (90), the almost precise constancy of $m_\pi^2\ln(m_\pi^2/\Lambda_{Q\chi PT}^2)$, and the uncertainty in $\Lambda_{Q\chi PT}$ provide too many similar effects to be distinguished in our data. Since δ is small, it is reasonable to expect that ignoring these terms is a good approximation. Also note that a large value for α should make the αm_π^4 term give a noticeable nonlinearity for larger m_π^2. This is not seen, implying either a small value for α or a cancellation with terms from the $\mathcal{O}(p^4)$ Lagrangian.

Thus we have consistency with other measurements of δ and will use a value of 0.05 for the remainder of this work. The fact that this value is small means the effects are not pronounced for the scales of masses where we are currently simulating.

B. Gell-Mann–Oakes–Renner relation for domain wall fermions

In Secs. IV A and IV B we discussed the role of residual mass and zero mode effects in the Ward-Takahashi identity which is the basis for the Gell-Mann–Oakes–Renner (GMOR) relation. The result is given by Eq. (112). In this section we show our numerical results for the quantities in this equation.

The zero mode effects in Eq. (112) are associated with $\langle\bar{u}u\rangle$ and $\langle J_5^a(x)J_5^a(y)\rangle$. For $\langle\bar{u}u\rangle$, the effects produce a $1/m_f$ pole, as shown in [21], which can be separated out by doing an extrapolation to $m_f=0$ from heavy quark masses. For $\langle J_5^a(x)J_5^a(y)\rangle$, we can see the size of the zero mode effects as a function of $x-y$ by comparing the correlator $\langle S(y)S^\dagger(z)\rangle$ to $\langle P_{K^+}(y)P_{K^-}(z)\rangle$. We plot this ratio in Fig. 3, using the wall source, point sink propagators from [21]. In the figure one sees that this ratio is essentially zero for $x-y>8$ and $m_f\geqslant 0.02$, as it should be since the pseudoscalar mass is much smaller than the scalar mass. However, for $m_f=0.01$ or 0.015, the scalar correlator changes sign and is a measurable fraction of the pseudoscalar correlator even for $x-y>8$. We attribute this effect to zero modes and note that zero mode effects are identical in the two correlators. Thus, in discussing the GMOR relation, we can easily remove the effects of zero modes in $\langle\bar{u}u\rangle$, but zero modes in the pseudoscalar correlator become $\sim$5% effects only for separations greater than 12.

Since many of the terms in Eq. (112) have been measured in [21] for two different values of L_s with the quenched

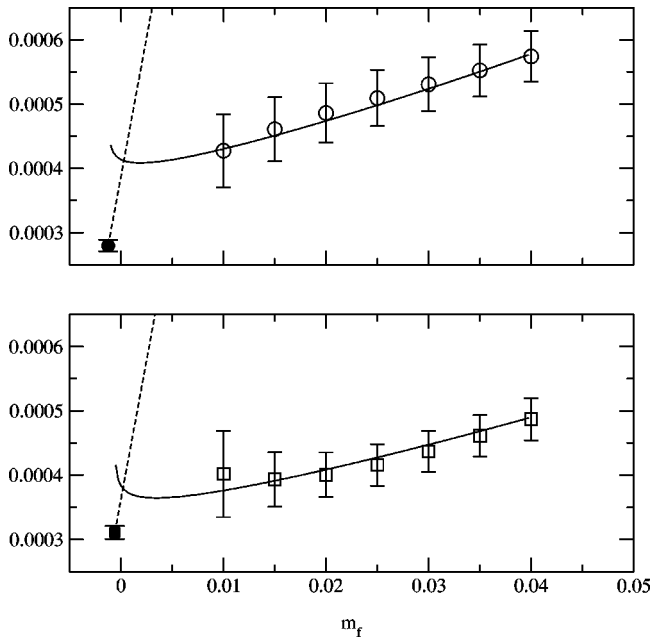

FIG. 4. The GMOR relation for $L_s=16$ (upper panel) and $L_s=24$ (lower panel). The open symbols are $(m_f+m_{\rm res})|\langle 0|J_5^a(0)|\pi'\rangle|^2/(12m_{\pi'}^2)$ and the closed symbols are $-\langle\bar{u}u\rangle_{\rm lat\ norm}(m_f=0,L_s)$. The prime on the states and masses indicates that zero mode effects may be present. The dashed line gives the m_f/a^2 dependence of $-\langle\bar{u}u\rangle_{\rm lat\ norm}(m_f,L_s)$ as determined from large quark masses where zero mode effects are absent. The solid line includes the effects of quenched chiral logarithms in m_π^2.

Wilson gauge action at $\beta=6.0$, we can discuss how well the GMOR relation is satisfied. Figure 4 shows the terms in the GMOR relation using these measured values. The upper panel is for $L_s=16$ and the lower is for $L_s=24$. The closed symbols are the values for $-\langle\bar{u}u\rangle_{\rm lat\ norm}(m_f=0,L_s)$ and the dashed line gives the m_f/a^2 dependence of this quantity. The zero mode term [the sum on the right-hand side of Eq. (112)] has been excluded by extrapolating to $m_f=0$ from large values of m_f where zero mode effects play no role. The open circles are

$$|\langle 0|J_5^a(0)|\pi'\rangle|^2\left(\frac{m_f+m_{\rm res}}{12m_{\pi'}^2}\right) \tag{124}$$

as measured from pseudoscalar correlators $\langle P_{\pi^+}(y)P_{\pi^-}(z)\rangle$ using values of $|y-z|$ from 7 to 16. Since this ratio contains zero mode effects, some of the zero mode terms from $\langle J_5^a(x)J_5^a(y)\rangle$ are included. The solid lines are the same quantity where a quenched chiral logarithm is included in $m_{\pi'}^2$.

For the $L_s=16$ case, we expect the quantity in Eq. (124) to differ from $-\langle\bar{u}u\rangle_{\rm lat\ norm}(m_f=0,L_s)$ due to the presence of zero modes in this quantity and the $m_{\rm res}$ terms on the left-hand side of Eq. (112). In Fig. 4 one sees that the $m_f\to 0$ extrapolation of the heavier mass points lies considerably above $-\langle\bar{u}u\rangle_{\rm lat\ norm}(m_f=0,L_s)$, revealing the size of the $\mathcal{O}(m_{\rm res})/a^2$ term. Since the slope of $-\langle\bar{u}u\rangle_{\rm lat\ norm}(m_f,L_s)$ with m_f is power divergent (the dashed line), a small value for $m_{\rm res}$ has a large effect. Any zero mode effects for small m_f are not visible within our statistical errors. Since $x-y$ in the range 7–16 has been used in determining the quantities in Eq. (124), Fig. 3 shows that the effects should be at the few percent level. For $L_s=24$ the residual mass is much smaller, and the $m_f=0$ extrapolation from heavy quark masses agrees quite well with $-\langle\bar{u}u\rangle_{\rm lat\ norm}(m_f=0,L_s)$. Some nonlinearity at small quark masses is seen, but the errors are too large for a definite conclusion.

Thus we see that for $L_s=16$, the naive GMOR relation is noticeably modified by the presence of $m_{\rm res}$, while for $L_s=24$ the $m_{\rm res}$ effects for this power divergent case appear to be smaller than 10%. It is important to note that $m_{\rm res}$ is small for $L_s=16$, but $m_{\rm res}/a^2$ effects are not. We now turn to a similar comparison of our numerical results with the Ward-Takahashi identity for $\langle\pi^+|\bar{s}d|K^+\rangle$.

C. Ward-Takahashi identity for $\bar{s}d$

In contrast to the GMOR relation discussed in the previous section, the Ward-Takahashi identity for $\bar{s}d$ does not contain any power divergent terms. Thus we can work in the large L_s limit and then replace m_f with $m_f+m_{\rm res}$ at the end. We can use Eq. (120) to understand the size of the zero mode effects in $\langle\pi^+|\bar{s}d|K^+\rangle$. Such zero mode effects will appear identically in the power divergent part of $\langle\pi^+|Q_i|K^+\rangle$ and will be removed in the subtraction procedure given in Eq. (89). The remaining finite terms in the subtracted matrix element will have zero mode effects, whose source we will understand more clearly after investigating $\langle\pi^+|\bar{s}d|K^+\rangle$.

To measure $\langle\pi^+|\bar{s}d|K^+\rangle$, one can start with the ratio

$$R_1\equiv\frac{\langle P_{\pi^+}^{\rm wall}(x_0)[\bar{s}d](y)P_{K^-}^{\rm wall}(z_0)\rangle}{\langle P_{\pi^+}^{\rm wall}(x_0)P_{\pi^-}(y)\rangle\langle P_{K^+}(y)P_{K^-}^{\rm wall}(z_0)\rangle}, \tag{125}$$

where $P_{\pi^+}^{\rm wall}(x)$, etc. are Coulomb gauge fixed, pseudoscalar wall sources and x_0 is the time coordinate at the point x. (For more details on the measurement of three-point correlators, please see Sec. IX.) We plot this ratio in Fig. 5 where we take $x_0=5$, $z_0=27$, and average over $14\leqslant y_0\leqslant 17$. For $x\gg y\gg z$ and without zero-mode effects, this ratio should be

$$R_1=\frac{\langle\pi^+|\bar{s}d|K^+\rangle}{\langle\pi^+|P_{\pi^-}|0\rangle\langle 0|P_{K^+}|K^+\rangle} \tag{126}$$

which is finite and nonzero in the chiral limit. From the Ward-Takahashi identity, without zero modes and chiral logarithms, this ratio is $2m_f/(m_\pi^2 f^2)$, which is ≈ 120 in lattice units. [In this section, we consider the case of SU(3) flavor symmetry so that $m_\pi=m_K=m_M$, where m_M is the common meson mass first used in Eq. (62).] One sees from the figure that for smaller m_f the points actually are decreasing, rather than increasing towards ≈ 120.

Since our measurements are made with $9\leqslant x_0-y_0\leqslant 12$ and $10\leqslant y_0-z_0\leqslant 13$, zero mode effects do enter the terms in the denominator. Consider a zero mode with support at x and y. It produces a power of $1/m_f$ in the numerator of R_1 and contributions of order $1/m_f^2$ and $1/m_f$ in the first term in the

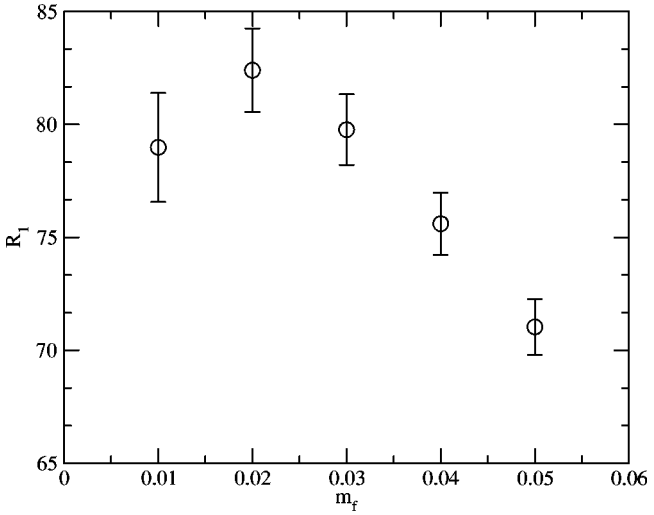

FIG. 5. A plot of R_1, the ratio of a three point correlator to two, two-point correlators, defined in Eq. (125). The larger zero mode effects in the two-point correlators should make this quantity vanish in the $m_f \to 0$ limit, a marked change from the chiral limit value of ≈ 120 expected without these chiral pathologies.

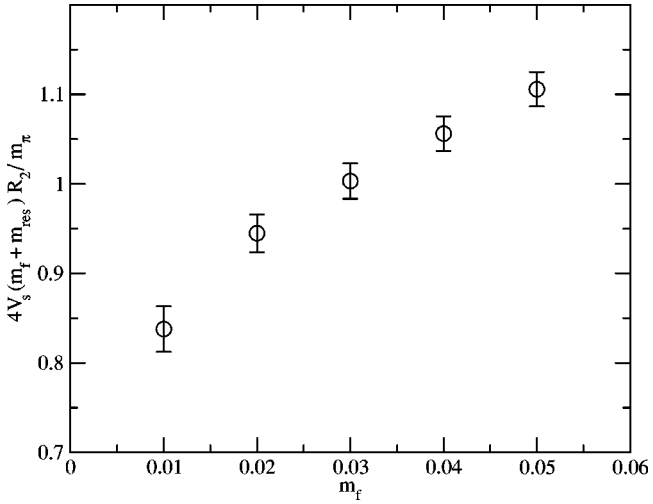

FIG. 6. A plot of $4V_s(m_f+m_{\rm res})R_2/m_\pi$ vs m_f, where R_2 is defined in Eq. (127). The Ward-Takahashi identity determines that this value should be 1 for $m_f \to 0$ if there are no zero mode effects present. The deviation from 1 for small m_f is consistent with estimates of the different effective pseudoscalar masses entering in the Green's functions in the numerator and denominator of R_2. The different effective pseudoscalar masses arise through zero mode effects, as discussed in Secs. IV B and VI C.

denominator of R_1. A similar argument is also true for a quark propagator containing a zero mode at y and z. Thus, for very small m_f, the ratio R_1 will go to zero due to zero modes. We believe this to be the source of the turnover in Fig. 5 for small values of m_f.

One can also determine $\langle \pi^+ | \bar{s}d | K^+ \rangle$ from the ratio

$$R_2 \equiv \frac{\langle P^{\rm wall}_{\pi^+}(x_0)[\bar{s}d](y) P^{\rm wall}_{K^-}(z_0)\rangle}{\langle P^{\rm wall}_{\pi^+}(x_0) P^{\rm wall}_{\pi^-}(z_0)\rangle}. \tag{127}$$

In the denominator of R_2, zero modes should be negligible, since $x_0 - z_0 = 22$ and the lattice has been doubled to make propagation around the ends unimportant. Thus we are not introducing zero mode effects into the ratio through the denominator. Zero modes in the numerator enter through the propagators $D^{-1}(x-y)$ and $D^{-1}(y-z)$. Without zero mode effects, we have

$$R_2 = \frac{\langle \pi^+ | \bar{s}d | K^+ \rangle}{2 m_\pi V_s}, \tag{128}$$

where V_s is the spatial volume. To precisely describe our numerical situation, we again use primes to describe states and masses which can have zero mode effects. For the current case, only one of the quark propagators in the pseudoscalars in the numerator can have a zero mode. With this notation, we insert complete sets of states in Eq. (127) and find

$$R_2 = \langle (\pi^+)' | \bar{s}d | (K^+)' \rangle \frac{|\langle 0 | P_{\pi^+} | (\pi^+)' \rangle|^2}{|\langle 0 | P_{\pi^+} | \pi^+ \rangle|^2} \frac{2 m_\pi V_s}{(2 m_{\pi'} V_s)^2} \times e^{(m_\pi - m_{\pi'})(x_0 - z_0)}. \tag{129}$$

The Ward-Takahashi identity result given in Eq. (120) can be similarly written as

$$\frac{2 m_f}{m^2_{\pi'}} \langle 0 | P_{\pi^-} | (\pi^+)' \rangle \langle (\pi^+)' | \bar{s}d | (K^+)' \rangle \times \langle (K^+)' | P_{K^-} | 0 \rangle \frac{e^{-m_{K'}(y-z_0)}}{2 m_{K'} V_S} = \frac{|\langle 0 | P_{\pi^-} | (\pi^+)' \rangle|^2}{2 m_{\pi'} V_s} e^{-m_{\pi'}(y-z_0)}, \tag{130}$$

which reduces to

$$\frac{2 m_f}{m^2_{\pi'}} \langle (\pi^+)' | \bar{s}d | (K^+)' \rangle = 1. \tag{131}$$

We now let L_s be finite and change $m_f \to m_f + m_{\rm res}$. We are left with

$$R_2 \frac{4 V_s (m_f + m_{\rm res})}{m_\pi} \frac{|\langle 0 | P_{\pi^-} | \pi^+ \rangle|^2}{|\langle 0 | P_{\pi^-} | (\pi^+)' \rangle|^2} e^{(m_{\pi'} - m_\pi)(x_0 - z_0)} = 1. \tag{132}$$

When there are no zero mode effects, $m_\pi = m_{\pi'}$ and $|\pi^+\rangle = |(\pi^+)'\rangle$ leaving $R_2 4 V_s (m_f + m_{\rm res})/m_\pi = 1$. Notice that a small difference in m_π and $m_{\pi'}$ is multiplied by $x_0 - z_0$, which can lead to larger effects in R_2. This is a result of the simple fact that zero modes effect the pseudoscalar propagators in the numerator of R_2 differently than they effect the propagators in the denominator.

Figure 6 is a plot of the value of $4 R_2 V_s (m_f + m_{\rm res})/m_\pi$ versus quark mass. We use a value for m_π that is not effected by zero modes. One sees that for the smaller values of m_f

this ratio deviates substantially from 1, being 16% below 1 for $m_f=0.01$. We would like to see if this is consistent with the prediction of Eq. (132). We do not have direct measurements of $m_{\pi'}$, since this is a mass which comes from correlators with at most one zero mode. However, the effective mass plots shown in Fig. 21 of [21] give values for $m_{\pi''}$, the mass from the pseudoscalar correlator where any number of zero modes is allowed, for $m_f=0.01$. In the range of separations 9–12, $m_{\pi''}=0.211(6)$, compared with $m_\pi=0.199$, our best estimate for m_π without zero mode effects for $m_f=0.01$. This gives $m_{\pi''}-m_\pi=0.014$ and $\exp[(m_{\pi''}-m_\pi)(x_0-z_0)]=1.36$ for $x-z=22$.

We do not know the relative contributions of one and two zero mode terms to $m_{\pi''}$. However, the zero modes have eigenvectors where the product $\psi_\lambda(x)\psi_\lambda^\dagger(y)$ is going to zero in the range of separations we are considering. It is reasonable to argue that the falloff in the eigenvectors with $x-y$ is producing $m_{\pi''}>m_{\pi'}$, since the two zero mode contribution should dominate for small m_f, they involve $|\psi_\lambda(x)|^2|\psi_\lambda(y)|^2$ and the pseudoscalar correlator is positive definite. For $m_{\pi'}$, only terms with at most one zero mode contribution are included. In this case $\psi_\lambda(x)\psi_\lambda(y)$ enters not $|\psi_\lambda(x)|^2|\psi_\lambda(y)|^2$ and there is no positivity for the one zero mode contribution alone. However, naively one could expect $m_{\pi''}>m_{\pi'}>m_\pi$. Thus it is reasonable that $1<\exp[(m_{\pi'}-m_\pi)(x_0-z_0)]<1.36$. From the determination of f_π in [21] using pseudoscalar and axial vector correlators, the zero mode effects in $\langle 0|P_{\pi^-}|(\pi^+)'\rangle$ are at the few percent level. Thus the deviation of $4R_2V_s(m_f+m_{\rm res})/m_\pi$ from 1 in Fig. 6 is consistent with the estimates based on the difference in the mass of the pseudoscalar states relevant to the numerator and denominator of R_2. From Eq. (131), the zero mode effects in $\langle(\pi^+)'|\overline{sd}|(K^+)'\rangle$ are at most a few percent. The small differences in the "masses," $m'_\pi-m_\pi$ indicate a substantial effect of zero modes for time separations of the order of 10. We believe that these effects are responsible for the large deviation seen from the predictions of chiral symmetry for these $\overline{sd}$ matrix elements (Fig. 6).

We now turn to the question of the extraction of matrix elements from our lattice correlators. As we have discussed, in the subtraction of divergent terms zero mode effects cancel. In the ratio R_1, large zero mode effects are introduced into the denominator through the pseudoscalar correlators acting over moderate distances. This produces a different effective pseudoscalar mass in the numerator and denominator. In the ratio R_2, no zero modes are introduced in the denominator, but there is a similar mismatch in pseudoscalar masses since the numerator can contain zero modes. However, this mismatch is most pronounced for the power divergent terms, which behave like the $\overline{sd}$ matrix element above. In the finite, subtracted operator, a similar mass mismatch can occur for eye type diagrams, but will not in general occur for figure eight diagrams due to the way gamma matrices enter the traces and the fact that all zero modes have the same chirality. Thus the ratio R_2 will not eliminate all the effects of zero modes in the desired physical quantities, but it minimizes them. We will use R_2 for the determination of our desired $K\to\pi$ matrix elements.

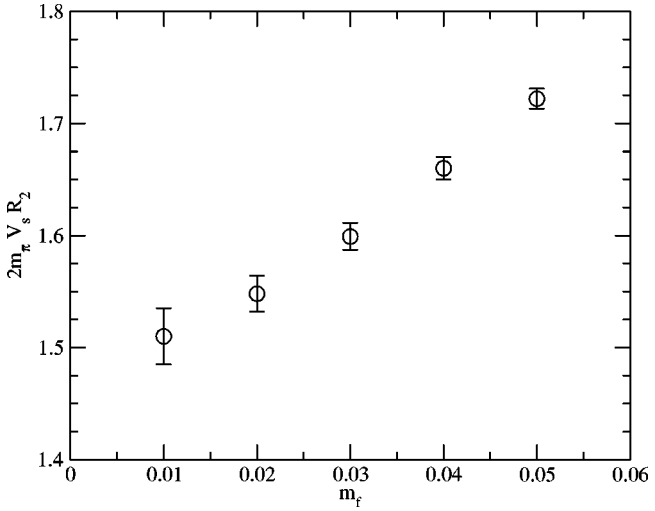

FIG. 7. A graph of $2m_\pi V_s R_2$ vs m_f. Without zero mode effects, this quantity is $\langle\pi^+|\overline{sd}|K^+\rangle$. In the operator subtraction, any nonlinearities in the power divergent parts of $\langle\pi^+|Q_i|K^+\rangle$ will exactly match the nonlinearities in this plot. The resulting subtracted operator will not have chiral logarithm and zero mode effects multiplied by power divergent terms.

Figure 7 shows $2m_\pi V_s R_2$ versus m_f. With no zero mode effects this equals $\langle\pi^+|\overline{sd}|K^+\rangle$. For $m_f=0.01$, the zero modes should produce the same relative distortions in this quantity as are shown in Fig. 6. This matrix element is used in the operator subtraction and as discussed previously any zero mode and chiral logarithm effects in this matrix element will match those in the power divergent parts of $\langle\pi^+|Q_i|K^+\rangle$. Since the plot is not obviously linear, it is important to subtract the two matrix elements to take full advantage of the correlation of zero mode and chiral logarithm effects between them.

VII. WILSON COEFFICIENTS

The twelve-dimensional vector of Wilson coefficients $\mathbf{C}(\mu)$ has been calculated at next to leading order (NLO) in QCD and QED by the Munich [62–64] and Rome [65] groups. In those calculations the Callan-Symanzik equations are solved to determine the Wilson coefficients at an energy scale $\mu\approx 1$ GeV, appropriate for lattice calculations, starting from their values at the weak scale, $\approx M_W$. The solution is obtained within the approximation that the parameters α_s and α (the fine structure constant of electromagnetism) are small but that the products $(\alpha_s t)^n$ are of order one, where $t=\ln(M_W/\mu)$. According to this reasoning, in leading order (LO) one sums all terms of the form $\alpha_s^n t^n$ and $\alpha\alpha_s^n t^{n+1}$. These terms are identified as $\mathcal{O}(1)$ and $\mathcal{O}(\alpha/\alpha_s)$, respectively. In the next to leading order approximation (NLO) one also includes all terms of the form $\alpha_s^{n+1}t^n$ and $\alpha\alpha_s^n t^n$, identified as $\mathcal{O}(\alpha_s)$ and $\mathcal{O}(\alpha)$, respectively. Terms of order α^n for $n\geqslant 2$ are not included.

In the notation of Ref. [64] the NLO evolution of $\boldsymbol{C}(\mu)$ to a value of μ below the charm threshold is given by

TABLE I. Decomposition of the next-to-leading order (NLO) Wilson coefficients into contributions of a given order. The coefficients z_i at $\mu=1.3$ GeV (the charm quark mass) are given in the NDR scheme for the 3-flavor case where the charm quark has been integrated out.

i	$\mathcal{O}(1)$	$\mathcal{O}(\alpha_s)$	$\mathcal{O}(\alpha)$	$\mathcal{O}(\alpha/\alpha_s)$	Total
1	−0.517 171	0.119 497	0.001 607 68	−0.003 938 67	−0.400 005
2	1.266 03	−0.067 024 2	−0.002 53	0.009 641 83	1.206 12
3	0.0	0.004 210 37	0.000 032 065 3	0.0	0.004 242 43
4	0.0	−0.012 631 1	−0.000 096 195 9	0.0	−0.012 727 3
5	0.0	0.004 210 37	0.000 032 065 3	0.0	0.004 242 43
6	0.0	−0.012 631 1	−0.000 096 195 9	0.0	−0.012 727 3
7	0.0	0.0	0.000 052 588 2	0.0	0.000 052 588 2
8	0.0	0.0	0.0	0.0	0.0
9	0.0	0.0	0.000 052 588 2	0.0	0.000 052 588 2
10	0.0	0.0	0.0	0.0	0.0

$$\mathbf{C}(\mu)=\hat{U}_3(\mu,m_c,\alpha)\hat{M}_4\hat{U}_4(m_c,m_b,\alpha)\times\hat{M}_5\hat{U}_5(m_b,M_W,\alpha)\boldsymbol{C}(M_W), \tag{133}$$

where $\hat{U}_f(\mu_1,\mu_2,\alpha)$ is the renormalization group improved, evolution matrix from the scale μ_2 down to the scale μ_1 in a theory with f quark flavors. The matrix $\hat{U}_f(\mu_1,\mu_2,\alpha)$ is a 12×12 matrix for $f=4$ and 5 while it reduces to a 10×10 matrix for $f=3$. The flavor matching matrix $\hat{M}_f$ relates the Wilson coefficients that appear in the f and $f-1$ flavor effective theories. It is naturally written as a 12×12 matrix for $f=4$ and 5, while for $f=3$ it is a 10×12 array. Here $\boldsymbol{C}(M_W)$ are the 12 coefficients of the effective theory calculated at the scale M_W by matching to the full theory. Evolution down to a value of μ above the charm threshold is given by an obvious truncation of Eq. (133). The matrix $\hat{U}_f(\mu,m,\alpha)$ contains terms of order $\mathcal{O}(1)$ and $\mathcal{O}(\alpha_s)$ in QCD and includes terms of $\mathcal{O}(\alpha/\alpha_s)$ and $\mathcal{O}(\alpha)$ when QED effects are included. Following convention, we fix $\alpha=1/128$ at $\mu=M_W$ and do not include its running in the evolution of the Wilson coefficients.

Following Ref. [23], we express the contributions arising from charged W exchange as the sum of two terms. The first, which evolves with Wilson coefficients defined as $z_i(\mu)$, contains the difference of charm and up quark fields and carries the CKM coefficients $(1-\tau)$. The second evolves with Wilson coefficients defined as $v_i(\mu)$, contains the difference of the top and up quark fields, and carries the CKM coefficients τ [see Ref. [23], Eq. (4.4)]. For the three-flavor, ''charm-out'' case, only the ten operators Q_i appear and their Wilson coefficients are given by

$$C_i=\tau v_i+(1-\tau)z_i \tag{134}$$

$$=\tau y_i+z_i, \tag{135}$$

where $y_i=v_i-z_i$. With this separation, the evolution of the coefficients z_i is particularly simple: The cancellation between the charm and up quark loops (the GIM mechanism) prevents the appearance of penguin contributions until one matches to the 3-flavor, charm-out effective theory. Since, with our standard choice of phase conventions, the CP violating phase is contained in the CKM parameter τ, the larger, τ-independent terms coming from z_i will provide the dominant contribution to the CP conserving amplitudes $\mathrm{Re}\,A_{0,2}$ while y_i must appear in the CP violating amplitudes $\mathrm{Im}\,A_{0,2}$ [see Eq. (3)].

We calculate these Wilson coefficients in two steps. First we determine $\boldsymbol{C}(\mu)$ in the NDR scheme using exactly the formulas and procedures given in Refs. [23,64]. In particular, when using Eq. (133), all $\mathcal{O}(\alpha_s^2,\alpha_s\alpha)$ and higher order terms which are generated by multiplication of the evolution and matching matrices are dropped so that the final Wilson coefficients at scale μ contain all contributions up to and including $\mathcal{O}(\alpha_s,\alpha/\alpha_s,\alpha)$ and no more. An example of the breakdown of z_i and y_i at $\mu=1.3$ GeV in the NDR scheme is given in Tables I and II. In the second step, we transform these coefficients, obtained in the NDR scheme, into the coefficients of operators defined according to the RI scheme[1] in Landau gauge using

$$\mathbf{C}_{\mathrm{RI}}(\mu)=\left(1-\frac{\alpha_s(\mu)}{4\pi}(\Delta r^{\mathrm{NDR}}_{\lambda*=0})^T\right)\mathbf{C}_{\mathrm{NDR}}(\mu), \tag{136}$$

where the matching matrix $\Delta r^{\mathrm{NDR}}_{\lambda*=0}$ is given in Table VIII of Ref. [24].

[1]This matching requires a careful definition of our basis of operators in the NDR scheme associated with the difficulties of defining γ^5 in dimensional regularization. While in the RI scheme, Fierz rearrangement of the fermion fields has no effect, this is not true in the NDR scheme. In fact, for the NDR calculation and matching to RI to be described correctly, we should follow Ref. [64] and write our operators $Q_{1,2}$ in a Fierz rearranged fashion. This is the form that is used in the NDR calculation [64] we are following and in determining the matching coefficients $\Delta r^{\mathrm{NDR}}_{\lambda*=0}$ in Refs. [65,24]. However, in our own matrix element and NPR calculations, where the Fierz ordering is immaterial, we find the Fierz structure shown in Eqs. (4)–(7) to be more convenient.

TABLE II. Decomposition of the next-to-leading order (NLO) Wilson coefficients into contributions of a given order. The coefficients y_i at $\mu = 1.3$ GeV (the charm quark mass) are given in the NDR scheme for the 3-flavor case where the charm quark has been integrated out.

i	$\mathcal{O}(1)$	$\mathcal{O}(\alpha_s)$	$\mathcal{O}(\alpha)$	$\mathcal{O}(\alpha/\alpha_s)$	Total
1	0.0	0.0	0.0	0.0	0.0
2	0.0	0.0	0.0	0.0	0.0
3	0.026 693 3	−0.000 750 255	0.001 433 01	0.000 130 383	0.027 506 5
4	−0.051 399	−0.002 549 18	−0.001 071 9	−0.000 277 595	−0.055 297 6
5	0.013 273 9	−0.007 886 98	0.000 117 102	0.000 077 474 6	0.005 581 51
6	−0.077 522 2	−0.005 344 37	−0.000 868 366	−0.000 372 801	−0.084 107 7
7	0.0	0.0	0.000 700 858	−0.000 878 706	−0.000 177 847
8	0.0	0.0	0.001 236 6	−0.000 180 252	0.001 056 34
9	0.0	0.0	−0.010 766 4	−0.000 999 603	−0.011 766
10	0.0	0.0	0.004 061 02	0.000 173 261	0.004 234 29

In this paper we discuss only the three-flavor, charm-out case. Thus we naturally deal with an effective theory that describes physics at energy scales below the charm mass—the scales that dominate the matrix elements we are computing. However, we are concerned about potential errors that come from using perturbation theory so close to the nonperturbative region. We cannot avoid the use of perturbative matching to connect the four-flavor (charm-in) and three-flavor (charm-out) theories since in the lattice calculations presented in this paper we do not include a propagating charm quark. However, the connection between the NDR and RI Wilson coefficients, also done in perturbation theory, can be done at a scale above the charm quark mass, thereby reducing the perturbative uncertainties. Note, in these discussions the energy μ specifies the energy scale that appears in the normalization condition that defines the operators that appear in our effective theory. For the case at hand, we are free to choose this scale to be well above m_c where perturbation theory may be more reliable. Of course, our effective theory will not describe processes in nature in this region of energies ($\sim m_c$), but only processes involving lower energy scales. Note, we are prevented from using a very large value for μ since we do not want large lattice spacing errors to enter our nonperturbative normalization of these operators.

In order that the product of the RI Wilson coefficients times the RI operators be independent of the scale μ they must both be computed in the full or the quenched theory. Since our nonperturbative normalization is determined in the quenched approximation, the μ-dependence of the Wilson coefficients should be determined in the quenched theory. Therefore we adopt the following transition to our quenched approximation. In evolving the effective weak Hamiltonian from the W mass scale down to a form valid in the three-quark, charm-out theory, we include all required quark loop effects. Making a ''quenched'' approximation here is not necessary and would leave out physically important phenomena. We then interpret the resulting NDR scheme, 3-flavor effective weak Hamiltonian with operators and coefficients defined at $\mu = m_c$ as our quenched approximation Hamiltonian. Thus we use the Wilson coefficients without change but interpret the operators as defined in the quenched approximation. We are then free to vary the renormalization scale μ, increasing it above m_c if we choose. However, we must normalize the operators by evaluating quenched Green's functions and evolve the Wilson coefficients from

TABLE III. The Wilson coefficients $z_i(\mu)$ in the RI scheme for the 3-flavor case. Starting from the 3-flavor, NDR scheme Wilson coefficients in full QCD at the charm mass, the Wilson coefficients are evolved to the μ values in this table using the quenched three-loop value for $\Lambda_{\overline{\rm MS}}$ and the two-loop quenched α_s. At this μ they are converted to the RI scheme.

i	1.51	2.13	2.39	3.02 (GeV)
1	−0.346 301	−0.304 999	−0.292 757	−0.269 806
2	1.173 84	1.149 51	1.142 47	1.129 47
3	0.004 048 56	0.001 813 46	0.001 214 41	0.000 164 314
4	−0.012 939 7	−0.005 736 13	−0.003 686 11	0.000 066 681 1
5	0.004 763 83	0.002 815 54	0.002 223 81	0.001 098 64
6	−0.014 647 1	−0.006 561 06	−0.004 404 76	−0.000 612 69
7	0.000 053 034 8	0.000 066 681 1	0.000 073 936 1	0.000 092 251 2
8	−0.000 022 313 5	−0.000 062 572 4	−0.000 072 154 2	−0.000 087 598 8
9	0.000 041 580 3	0.000 034 010 3	0.000 035 681 3	0.000 044 365 3
10	0.000 015 928 9	0.000 042 263 6	0.000 049 355 9	0.000 061 744 2

TABLE IV. The Wilson coefficients $y_i(\mu)$ in the RI scheme for the 3-flavor case. Starting from the 3-flavor, NDR scheme Wilson coefficients in full QCD at the charm mass, the Wilson coefficients are evolved to the μ values in this table using the quenched three-loop value for $\Lambda_{\overline{\rm MS}}$ and the two-loop quenched α_s. At this μ they are converted to the RI scheme.

i	1.51	2.13	2.39	3.02 (GeV)
1	0.0	0.0	0.0	0.0
2	0.0	0.0	0.0	0.0
3	0.023 894 3	0.022 464 4	0.022 021 1	0.021 168 5
4	−0.050 515 5	−0.051 148 4	−0.051 301 4	−0.051 553 6
5	0.005 832 45	0.007 190 03	0.007 560 92	0.008 223
6	−0.091 293 5	−0.081 790 1	−0.079 262 9	−0.074 830 7
7	−0.000 176 754	−0.000 155 239	−0.000 148 013	−0.000 133 228
8	0.001 156 08	0.000 971 975	0.000 921 86	0.000 832 504
9	−0.011 419 6	−0.011 143 6	−0.011 064 9	−0.010 921
10	0.003 684 73	0.003 251 91	0.003 127 29	0.002 897 85

their $\mu = m_c$ values using quenched evolution equations.[2]

Our results in the RI scheme for the three-flavor theory are given in Tables III and IV. The scales $\mu = 1.51$, 2.13, 2.39, and 3.02 GeV correspond to those where the nonperturbative, operator renormalization Z factors were calculated. The standard model parameters used to obtain these numbers are given in Table V. Two-loop running of α_s is used throughout. We have performed several checks of our analysis. Our numerical values of $\boldsymbol{C}_{\rm NDR}(\mu)$ agree exactly with those reported in [64] when their values for the standard model parameters are used. We also agree within 20%, or much better in most cases, with the Wilson coefficients given in [24] for the NDR and RI schemes. These differences arise because the treatment of terms beyond NLO differs between that adopted in Ref. [64], which we follow, and that of [24].

We note that there is a potential ambiguity which arises when using the one-loop matching given by Eq. (136). Straight multiplication of $\mathbf{C}_{\rm NDR}(\mu)$ by the one-loop matching matrix generates an $\mathcal{O}(\alpha_s\alpha)$ contribution which is large. After matching we find $C_{8,\rm RI}(\mu \approx 2\ {\rm GeV}) \approx 0.0006$ if we drop this term, or 0.0009 if we do not. Thus this $\mathcal{O}(\alpha_s\alpha)$ term increases $C_{8,\rm RI}$ by 50%. The origin of this large correction is easily understood by examining the $\mathcal{O}(\alpha/\alpha_s)$ and $\mathcal{O}(\alpha)$ terms in $C_{8,\rm NDR}$. The subleading $\mathcal{O}(\alpha)$ term is roughly seven times the leading order $\mathcal{O}(\alpha/\alpha_s)$ term and they have opposite signs. The origin of this reversal is well known; the $\mathcal{O}(\alpha)$ term is dominated by the contribution proportional to m_t^2 which is quite large. This sum of leading (small) and subleading (large) terms is then to be multiplied by the one-loop matching for C_8 which is dominated by the diagonal term which is itself anomalously large, $(\Delta r^{\rm NDR}_{\lambda*=0})_{8,8} \approx 10$.

The above discussion may lead the reader to conclude that there is a significant uncertainty in C_8, an important quantity in ϵ'. In fact, we believe that this is not the case. The large corrections which arise from the matching calculation must be included as complete factors in the Wilson coefficients to maintain the scheme independence of the weak Hamiltonian. Arbitrarily dropping these higher order terms could potentially increase the scheme dependence of our final result (we follow the general argument given in Ref. [67] for the NDR and HV schemes which applies to the RI scheme as well). In practice, the scheme and scale dependence of the Wilson coefficients and the renormalized operators cancel when they are combined in the weak Hamiltonian. Schematically,

$$\begin{aligned} H_W &= \boldsymbol{Q}^T\boldsymbol{C} = \boldsymbol{Q}^T_{\rm RI}\boldsymbol{C}_{\rm RI} \\ &= \boldsymbol{Q}^T_{\rm NDR}\left(1 + \frac{\alpha_s(\mu)}{4\pi}(\Delta r^{\rm NDR}_{\lambda*=0})^T + \cdots\right) \\ &\quad \times \left(1 - \frac{\alpha_s(\mu)}{4\pi}(\Delta r^{\rm NDR}_{\lambda*=0})^T + \cdots\right)\boldsymbol{C}_{\rm NDR} = \boldsymbol{Q}^T_{\rm NDR}\boldsymbol{C}_{\rm NDR}. \end{aligned} \tag{137}$$

By far the largest contribution to the $\mathcal{O}(\alpha)$ part of the weak Hamiltonian is C_8Q_8 which then, by itself, must be scheme independent. As we saw, the $\mathcal{O}(\alpha\alpha_s)$ contribution to the

TABLE V. Standard model parameters used to generate the Wilson coefficients. Dimensionful parameters are in GeV.

Parameter	Value
M_W	80.419
$m_t(M_W)$	175.5
$m_b(m_b)$	4.4
$m_c(m_c)$	1.3
α	1/128
$\Lambda^{(f=5)}_{\overline{\rm MS}}$	0.208 ± 0.025
$\sin^2\theta_W$	0.23117

[2]In the results described below, we carry out this prescription only approximately. For the μ dependence of α_s we use the $f=0$ β function and the value of $\Lambda_{\rm QCD} = 238$ MeV from the quenched calculation of Ref. [66]. However, we still use the 3-flavor, two-loop anomalous dimension matrix rather than the 0-flavor matrix as required by the above discussion. Since the resulting evolution only corresponds to scale changes on the order of a factor of 2, there are no large logarithms and it is appropriate to neglect such two-loop effects in our NLO calculation.

matching matrix (which by definition is scheme dependent) was quite large. In our calculation, the renormalization of the operators is done to all orders in QCD in the RI scheme. Thus the product C_8Q_8 could implicitly contain a compensating large $\mathcal{O}(\alpha\alpha_s)$ scheme dependent contribution coming from the $\mathcal{O}(\alpha)$ term in C_8 and the $\mathcal{O}(\alpha_s)$ term implicit in the nonperturbative renormalization of Q_8. Thus it is natural to include the full matching coefficient in the RI value of C_8 so that these compensating terms will both be present in the product C_8Q_8.

Recently, partial next-next-to-leading order (NNLO) calculations have been performed [68,67]. We only examine the latter case where the complete set of $\mathcal{O}(\alpha\alpha_s)$ and $\mathcal{O}[\alpha\alpha_s \sin^2(\theta_W)m_t^2]$ corrections to the Wilson coefficients C_{7-10} of the electroweak penguins have been calculated. In Ref. [67] it is argued that these are the dominant NNLO contributions. We simply take the values in Ref. [67] for $\mu = 1.4$ GeV to estimate the change in C_{7-10} in the RI scheme, and use these values in conjunction with the ones in Tables III and IV to estimate the effects of these corrections on the $K\to\pi\pi$ amplitudes given in later sections. We conclude that the changes in the Wilson coefficients and final $K\to\pi\pi$ amplitudes are modest.

We explicitly tabulate the values of the Wilson coefficients at four different scales μ. In later sections these coefficients are combined with the nonperturbative Z factors, computed at these same four values of μ to determine the final physical results. Since these final numbers should be independent of this renormalization scale μ, this comparison gives a significant indication of how well our method is working.

VIII. OPERATOR RENORMALIZATION USING NPR

As is well known, in using the lattice to calculate matrix elements, one cannot simply transcribe the operators of the continuum theory to the lattice. The lattice operators and continuum operators have to be properly renormalized and the relationship between them explicitly known. For this we use a two step process to take advantage of existing continuum calculations for the Wilson coefficients.

(1) We use a renormalization scheme (here the RI or regularization independent scheme) to define renormalized operators which is independent of the underlying regulator. This ensures a common definition of renormalized operators on the lattice and in the continuum.

(2) We also need the relationship between operators renormalized in the RI scheme and those in the $\overline{\text{MS}}$ scheme since the existing perturbative calculations of the Wilson coefficients are done in this scheme. The matching between RI and $\overline{\text{MS}}$ with naive dimensional regularization (NDR) is known at one loop [65,24].

An additional complication in the renormalization of the operators in the $\Delta S=1$ Hamiltonian is the mixing between these operators and lower dimensional operators. This is due to the presence of quark and antiquark fields of the same flavor in the $\Delta S=1$ operators. Since this mixing in general involves power divergent coefficients, it can be quite large if the lattice formulation badly breaks chiral symmetry. Since in our calculation with domain wall fermions chiral symmetry breaking effects are small, this problem becomes tractable.

A. Mixing for $\Delta S=1$ operators

For the $\Delta S=1$ Hamiltonian, the continuum renormalized dimension-six operators can be written in terms of bare lattice operators as

$$O_i^{\text{cont,ren}}(\mu) = \sum_j Z_{ij}(\mu)\left[O_j^{\text{lat}} + \sum_k c_k^j(\mu) B_k^{\text{lat}}\right] + O(a). \tag{138}$$

We have introduced the scale μ used to define the renormalized operators. Here O_j^{lat} is also a four-quark dimension-six operator and the B_k^{lat}'s are operators that contain only two quark fields. Due to the $\Delta S=1$, $\Delta D=-1$ nature of the operators we are considering, the B_k^{lat}'s must have the $\bar{s}d$ flavor structure. These operators can mix with coefficients c_k^j that diverge as the lattice spacing tends to zero.

We will consider here the renormalization of the parity conserving part of the $\Delta S=1$ effective Hamiltonian assuming, as in the rest of this work, that chiral symmetry is respected. (We have investigated this question in detail for the renormalization of quark bilinear operators and found no significant effects due to explicit chiral symmetry breaking by domain wall fermions at finite L_s [59].) The renormalization conditions will be imposed in the massless limit and as such operators in different multiplets of $\text{SU}(3)_L \otimes \text{SU}(3)_R$ or isospin do not mix under renormalization. This imposes strong constraints on the allowed operator mixing, and in particular on the number of quark bilinear operators that need to be considered. The latter may be split into three classes [69,62].

(1) Operators that vanish on shell by the equations of motion.
(2) Gauge invariant operators that do not vanish by the equations of motion.
(3) Nongauge, but BRST, invariant operators.

Operators of types one and three do not contribute to physical processes and so do not have to be considered in the calculation of hadronic matrix elements. However, they do have to be taken into account in operator renormalization, where amplitudes with off-shell gauge-fixed external fields are used.

The bilinear operators B_k in Eq. (138) must contain an $\bar{s}$ and d quark and conserve parity. Thus their general form must be one of the following:

$$\bar{s}X^{(1)}d, \tag{139}$$

$$\bar{s}\sigma_{\mu\nu}X^{(2)}_{\mu\nu}d, \tag{140}$$

$$\bar{s}\gamma_\mu X^{(3)}_\mu d, \tag{141}$$

where $X^{(1)}$, $X^{(2)}_{\mu\nu}$, and $X^{(3)}_\mu$ are flavor singlet quantities which may include gluon, ghost, and derivative terms. It is simple to see that Eq. (139) is in a $(3,\bar{3})+(\bar{3},3)$ representation of

$SU(3)_L \otimes SU(3)_R$ and so may not mix with any of the dimension-six operators we are considering in the massless limit.

In fact, the only operator that is allowed to mix by $SU(3)_L \otimes SU(3)_R$ is Eq. (141), which transforms as an $(8,1)+(1,8)$. This gives one dimension-four operator,

$$\bar{s}(-\vec{\not{D}}+\overleftarrow{\not{D}})d, \tag{142}$$

with a mixing coefficient c_k^j that may behave as $1/a^2$ as $a \to 0$, which we must consider. BRST noninvariant operators are allowed to mix only if they vanish by the equations of motion [69]. This forbids the second possible dimension four operator, $\bar{s}\not{\partial}d$, from appearing. This argument allows operators of dimension-five to appear. However, these operators break chiral symmetry and are therefore forbidden. Several dimension-six operators (for example, those involving three $\not{D}$ operations) can also occur, although their mixing coefficients diverge at most logarithmically.

The arguments above rely on the fact the renormalization conditions that we will be imposing are defined in the chiral limit. The numerical simulations that we have done to evaluate them, however, were performed at multiple, finite values of the quark mass and the results extrapolated to the massless limit. As this is the case, it is also important to study operators that may be present due to the breaking of chiral symmetry by the quark mass and also the explicit chiral symmetry breaking from finite L_s. This allows many more operators to mix. We will focus on the most divergent one (which diverges as $1/a^2$) given by Eq. (139) with $X^{(1)}=1$ and show that its contributions are negligible in the chiral limit.

B. Nonperturbative renormalization

Although, in principle, the renormalization of lattice operators can be done by using lattice perturbation theory, in practice simple uses of lattice perturbation theory suffer from poor convergence for currently accessible gauge couplings ($\beta \sim 6.0$). Use of renormalized or boosted couplings [70] improves the perturbative behavior in many cases of interest but considerable arbitrariness remains [71]. Furthermore, for domain wall fermions lattice perturbation theory has the added complication that the renormalization coefficients can depend sensitively on M_5, the domain-wall height [59,72–74]. The nonperturbative renormalization technique pioneered by the Rome-Southampton group [26] provides a method for removing the uncertainties associated with perturbation theory. (Another approach to nonperturbative renormalization has been developed by [25].) The use of this technique here represents one of the most complicated situations where it has been applied. We now give a brief overview of the method and elaborate on its use for the $\Delta S=1$ case.

The NPR method starts with the computation of Green's functions of the bare operators in question. The Green's function is calculated using off-shell external quark fields at large Euclidean momentum. This momentum defines the renormalization scale μ. The quark fields must be in a particular gauge, and in this work we only use Landau gauge. We note that renormalization coefficients in the RI scheme can be gauge dependent. Schematically, we have

$$G^{(4)}(p_1,p_1,p_2,p_2)=\langle q_\alpha^i(p_1) q_\gamma^k(p_1) O_m \overrightarrow{q}_\beta^j(p_2) \overrightarrow{q}_\delta^l(p_2)\rangle \tag{143}$$

and, as we will discuss in more detail later, we work with $|p_1|=|p_2|=|p_1-p_2|$. This Green's function is then amputated using the full quark propagators calculated in the same gauge. A renormalization condition which fixes the Z_{ij} and c_k^j factors in Eq. (138) may then be applied by requiring that the amputated Green's function of $O_i^{\mathrm{cont,ren}}$ take on its free field value for all spin and color indices on these quark fields. This defines the RI scheme. Its relationship to other renormalization schemes requires only continuum perturbation theory, which is better behaved than lattice perturbation theory at the low scales ($\mu \sim 2$ GeV) used in the present calculations.

The success of this method requires two important conditions to be satisfied.

(1) A suitable ''window'' of momenta must exist. The window must include momenta which are large enough to make nonperturbative (condensate) effects small. It must also include momenta which are small enough to avoid artifacts due to finite lattice spacing. Such a window was seen for quark bilinears in [59].

(2) Since the method of nonperturbative renormalization must eventually make a connection with continuum perturbation theory, our approach which uses Landau gauge is potentially vulnerable to the presence of Gribov gauge copies. Such multiple gauge copies, present in Landau gauge lattice simulations, invalidate a comparison of gauge-variant quantities with perturbation theory, even when our calculations are performed at increasingly weak coupling. For the success of our method the effects of Gribov copies must therefore be small.

In principle, the Gribov copy problem can be avoided by a more complete gauge fixing procedure. For example, we could begin with a gauge transformation to a completely fixed axial gauge and then follow with the usual Landau gauge fixing. Such a procedure would guarantee that in the weak coupling, small volume regime, a comparison with continuum perturbation theory would be accurate. While we have not implemented this more sophisticated gauge choice for the NPR calculations described here, we have made a nontrivial test. We have carried out a companion calculation for both 8^4 and 16^4 lattices of the renormalization factors for both the dimension-three quark bilinear operators and the single four-quark operator that enters the calculation of B_K and found no meaningful difference between our usual Landau gauge fixing determination of the renormalization factors and the same determination using the more elaborate two-step procedure described above [75]. Thus we believe that the presence of Gribov copies is not a cause of difficulty for the work presented here.

With this overview of NPR, we now turn to the specific issues and conventions we use in the application of this technique to $\Delta S=1$ operators. We first consider the type of quark

contractions that can occur in Eq. (143) and see that there are two types. The first has each quark field in the operator contracted with an external quark field, which we will call tree contractions in this section, and the second, which we call eye contractions, have quark propagators that begin and end on the operator. This second class of contractions are both theoretically and numerically challenging. They are theoretically challenging because it is through these diagrams that the mixing with lower dimensional operators occurs. They are numerically challenging because they involve the evaluation of a spectator quark propagator $S(p,q)$ with $p \neq q$. These numerical issues will be discussed later, after the theoretical issues are outlined.

In the RI scheme, the standard condition for determining $c_k^j(\mu)$ is the requirement that the renormalized four-quark operator vanish when evaluated in a Green's function with two external quark fields. In particular

$$G^{(2)}(p,p) = \langle s_\alpha^i(p) O_m \overline{d}_\beta^j(p) \rangle \tag{144}$$

should be zero. As such, it is convenient when calculating $Z_{ij}(\mu)$ to use a two step process where first a subtracted operator is defined by evaluating the $c_k^j(\mu)$ in Eq. (138) through

$$O_i^{\text{sub}} = O_i^{\text{latt}} + \sum_k c_k^i B_k . \tag{145}$$

The second step consists of evaluating the four-quark Green's function $G_{\text{sub}}^{(4)}$ for the subtracted operator using the external quark fields in Eq. (143). We now discuss which quark bilinears we will subtract.

A full subtraction of all the bilinear operators that could potentially mix with the four-quark operators in question would be challenging and prone to numerical error due to their large number. However, in the context of the current study our accuracy is limited by the existing one-loop perturbative calculations of the matching coefficients between the RI and $\overline{\text{MS}}$ schemes and the current Wilson coefficients, for which the finite terms are also known only to one-loop accuracy. Therefore it is not necessary to subtract operators that affect the renormalization factors at order g^4 and above in perturbation theory, provided we have no *a priori* reason to expect them to give anomalously large contributions.

Consequently, we neglect the subtraction of any bilinear operator that is not power divergent and which mixes with the four-quark operators at order g^2 and above. The explanation for this is straightforward. Consider the Green's function of a generic subtracted operator $G_{\text{sub}}^{(4)}(p_1,p_1,p_2,p_2)$, evaluated in the free case. The bilinear operator will give no contribution to this Green's function, due to the choice of momenta. For interacting theories, gluon exchange can transfer momenta, allowing a nonzero contribution of the bilinear operator to this Green's function. Such effects occur at order g. If the lowest order contribution of $c_k^j(\mu)$ begins at g^2 the total contribution will be of higher order and may be neglected.

This counting is clearly not relevant for the bilinear operators of dimension below six as the needed subtraction coefficients may be power divergent as the lattice spacing tends to zero. This means we must always consider the operator given in Eq. (142), and away from the massless limit it may be useful to subtract the operator given in Eq. (139), the subtraction coefficient of which has the leading behavior m/a^2. Now we have to consider various dimension-six operators. At $\mathcal{O}(g^0)$ there are no dimension-six bilinear operators that mix. At one loop, here $\mathcal{O}(g)$, there is a single operator that can mix [62]:

$$\overline{s}\gamma_\nu d D_\mu F_{\mu\nu} . \tag{146}$$

To be consistent we should subtract this operator. However, as we will argue later, the numerical effect of neglecting this subtraction is small. At two loops additional gauge invariant operators which vanish by virtue of the equations of motion and possible gauge noninvariant operators must also be included [62]. However, as explained earlier, we can consistently ignore such order g^4 effects in the present calculation.

We will therefore consider the subtraction of only two bilinear operators

$$\begin{aligned} B_1 &\equiv \overline{s}d, \\ B_2 &\equiv \overline{s}(-\vec{\not{D}} + \overleftarrow{\not{D}} + m_s + m_d)d \\ &= \overline{s}(-\vec{\not{D}} + m_s)d + \overline{s}(\overleftarrow{\not{D}} + m_d)d. \end{aligned} \tag{147}$$

B_2 is a modification of Eq. (142) with additional mass dependent terms added such that the operator vanishes on-shell both in and out of the chiral limit, and B_1 is the operator in Eq. (139) with $X^{(1)}=1$. The two subtraction coefficients, c_1^i and c_2^i, should have leading behavior

$$c_1^i \propto \frac{m_s + m_d}{a^2} + \cdots , \tag{148}$$

$$c_2^i \propto \frac{1}{a^2} + \cdots . \tag{149}$$

As mentioned previously, we subtract these operators by requiring that Green's functions for the subtracted four-quark operators O_i^{sub} vanish between external quarks states with flavor structure $s\overline{d}$. To determine both coefficients we need to impose two linearly independent conditions which we choose as

$$\text{Tr}[\langle s(p) O_i^{\text{sub}} \overline{d}(p) \rangle_{\text{amp}}] = 0, \tag{150}$$

$$\text{Tr}[i\not{p} \langle s(p) O_i^{\text{sub}} \overline{d}(p) \rangle_{\text{amp}}] = 0, \tag{151}$$

where ''amp'' denotes the amputated vertex. The momentum p where the condition is enforced is explained in detail below.

In QCD, the operators O_i mix under renormalization. To account for this mixing we define a set of suitable color, spin, and flavor projectors which we use to implement our renormalization conditions and thus yield the Z_{ij} in the RI

scheme. First, to distinguish the flavor structure of the operators we define a set of external quark fields, denoted by $E^j_{\alpha\beta\gamma\delta}$, as

$$E^j_{\alpha\beta\gamma\delta} = f^{j,abcd} q^a_\alpha(p_1)\overline{q}^b_\beta(p_2) q^c_\gamma(p_1)\overline{q}^d_\delta(p_2), \quad (152)$$

where q is a generic quark field; the subscripts representing spin and color and the superscripts representing the flavor. Here $f^{j,abcd}$ is a set of constants defining the flavor structure of the jth set of external quark fields. We then construct the amputated Green's functions of $O^{\rm sub}_i$ between these external quark fields

$$\Lambda^{i,j}_{\alpha\beta\gamma\delta} = \langle O^{\rm sub}_i E^j_{\alpha\beta\gamma\delta}\rangle_{\rm amp} \quad (153)$$

and trace the result with a chosen set of projectors, P^j,

$$P^j\{\Lambda^{ij}\} \equiv \Gamma^j_{\alpha\beta\gamma\delta}\Lambda^{i,j}_{\beta\alpha\delta\gamma} \quad (154)$$

where Γ^j is a rank-four tensor in spin and color space that defines the projector, and there is no sum over j in the above equation. The renormalization factors Z_{ki} are then fixed by requiring that, for renormalized operators with a specific choice of the momenta appearing in Eq. (152), this set of quantities be equal to its free case value,

$$\frac{1}{Z_q^2} Z^{ki} P^j\{\Lambda^{i,j}\} = F^{kj}. \quad (155)$$

Here F^{ij} is the free case limit of $P^j\{\Lambda^{i,j}\}$ and $Z_q^{1/2}$ is the quark wave function renormalization factor from [59]. This may be conveniently be written in matrix form

$$\frac{1}{Z_q^2} Z = F M^{-1} \quad (156)$$

with $M^{ij} \equiv P^j\{\Lambda^{i,j}\}$. Z, M, and F are all real $N\times N$ matrices, where N is the number of operators in our basis.

As long as the external states and projectors are chosen such that a linearly independent set of conditions is applied (F is invertible), this completely and uniquely specifies the renormalization coefficients for any such choice of the flavor structure of the external quark fields $f^{j,abcd}$ and projectors $\Gamma^j_{\alpha\beta\gamma\delta}$.

C. Numerical implementation

We now move to a discussion of the numerics of our calculation. All the results presented were measured on quenched gauge configurations generated using the Wilson gauge action for a lattice of size $16^3\times 32$ with $\beta = 6.0$. These configurations were then fixed into Landau gauge (see [59]). On these Landau gauge-fixed configurations we then calculated the needed quark propagators using the domain wall fermion action with $L_s = 16$.

To construct the quark contractions that arise in Eqs. (150), (151), and (153) three distinct quark propagators are needed for a fixed mass.

(1) The propagator from the position of the operator to a general site x on the lattice transformed into momentum space on x.
(2) The propagator from the position of the operator back to that position.
(3) A spectator propagator transformed into momentum space on both source and sink indices with distinct momenta, $S(p,q)$ with $p \neq q$.

The first two of these require a single inversion of the Dirac operator for each mass. However, to calculate the last of these we inverted the Dirac operator using a fixed momentum source, which costs an inversion for every momenta, q, needed. For this reason we calculate this propagator for only four fixed momenta and a limited range of masses.

As we are working on a finite lattice with periodic boundary conditions, the possible values of the momenta for a given direction $i \in \{x,y,z,t\}$ are

$$ap_i = \frac{2\pi n_i}{L_i}, \quad (157)$$

where L_i is the lattice size in direction i,

$$L_x = L_y = L_z = 16, \; L_t = 32 \quad (158)$$

and

$$-\frac{L_i}{2} < n_i \leqslant \frac{L_i}{2}. \quad (159)$$

1. Bilinear operator subtractions

To evaluate the subtraction coefficients c_1^i and c_2^i the spectator propagator is not needed, a single momentum space propagator from a point being sufficient. As this is the case we have used a separate data set from that used for the full four-quark Z-factor calculation. We used an ensemble of 50 gauge configurations for which we calculated the quark propagators for bare quark masses $m_f = 0.02$, 0.03, 0.04, and 0.05.

From Eqs. (150) and (151) we obtain

$$-c_1^i - 2c_2^i \frac{{\rm Tr}[S^{-1}(p)]}{{\rm Tr}[\langle s(p)(\overline{s}d)\overline{d}(p)\rangle_{\rm amp}]} = \frac{{\rm Tr}[\langle s(p)O_i\overline{d}(p)\rangle_{\rm amp}]}{{\rm Tr}[\langle s(p)(\overline{s}d)\overline{d}(p)\rangle_{\rm amp}]} = \kappa^i, \quad (160)$$

$$-c_1^i \frac{{\rm Tr}[i\not{p}\langle s(p)(\overline{s}d)\overline{d}(p)\rangle_{\rm amp}]}{2\,{\rm Tr}[i\not{p}S^{-1}(p)]} - c_2^i = \frac{{\rm Tr}[i\not{p}\langle s(p)O_i\overline{d}(p)\rangle_{\rm amp}]}{2\,{\rm Tr}[i\not{p}S^{-1}(p)]} = \lambda^i, \quad (161)$$

where we have explicitly taken the degenerate limit, $m_s = m_d = m_f$. These two relations may be simplified by noting that

TABLE VI. The $\mathcal{O}(a)^2$ errors in the lower dimensional operator subtractions are eliminated by fitting the coefficient $A_{\kappa^i}(p)$ in Eq. (163) to the form $A_{\kappa^i}(p)=A_{\kappa^i}^{(0)}+A_{\kappa^i}^{(2)}(ap)^2$. This table gives results for $A_{\kappa^i}^{(0)}$ and $A_{\kappa^i}^{(2)}$.

i	$A_{\kappa^i}^{(0)}$	$A_{\kappa^i}^{(2)}$
1	$2.2(16)\times10^{-3}$	$-7.2(54)\times10^{-4}$
2	$8.3(89)\times10^{-3}$	$-1.3(30)\times10^{-3}$
3	$2.3(19)\times10^{-2}$	$-4.6(65)\times10^{-3}$
4	$2.9(27)\times10^{-2}$	$-5.2(92)\times10^{-3}$
5	$6.73(12)\times10^{-1}$	$1.9(31)\times10^{-3}$
6	2.037(44)	$1.3(97)\times10^{-3}$
7	$-3.330(73)\times10^{-1}$	$-1.7(13)\times10^{-3}$
8	$-9.95(20)\times10^{-1}$	$-5.6(33)\times10^{-3}$
9	$-8.3(89)\times10^{-3}$	$1.3(30)\times10^{-3}$

$$\frac{\mathrm{Tr}[S^{-1}(p)]}{\mathrm{Tr}[\langle s(p)(\bar{s}d)\bar{d}(p)\rangle_{\mathrm{amp}}]}=m_f \tag{162}$$

to within the statistical errors given in [59]. It was also found in [59] that $\mathrm{Tr}[i\not{p}\langle s(p)(\bar{s}d)\bar{d}(p)\rangle_{\mathrm{amp}}]=0$ up to $\mathcal{O}(a^2)$ contributions. As this is the case, we extract c_2^i from Eq. (161) in the chiral limit. We then substitute this value into Eq. (160) to give c_1^i.

It is instructive to investigate the mass dependence of c_1^i, since c_1^i should vanish in the chiral limit. In addition, as shown in Eqs. (148) and (149), the dominant $1/a^2$ divergences in c_1^i and c_2^i are momentum independent, although subleading terms are expected to depend on $\ln(pa)$. Thus the dominant contributions to c_1^i and c_2^i as determined through Eqs. (160) and (161) are momentum independent as long as we are in the required "window;" however, experience has shown that at the momenta accessible for the lattice parameters we are using, discretization errors may be important. To check for the above features of c_1^i and c_2^i, we first rewrite Eqs. (160) and (161) as

$$\kappa^i(p)=2m_f A_{\kappa^i}(p)+B_{\kappa^i}(p), \tag{163}$$

TABLE VII. The $\mathcal{O}(a)^2$ errors in the lower dimensional operator subtractions are eliminated by fitting the coefficient $B_{\kappa^i}(p)$ in Eq. (163) to the form $B_{\kappa^i}(p)=B_{\kappa^i}^{(0)}+B_{\kappa^i}^{(2)}(ap)^2$. This table gives results for $B_{\kappa^i}^{(0)}$ and $B_{\kappa^i}^{(2)}$.

i	$B_{\kappa^i}^{(0)}$	$B_{\kappa^i}^{(2)}$
1	$-1.6(21)\times10^{-4}$	$1.02(72)\times10^{-4}$
2	$-8(13)\times10^{-4}$	$3.5(43)\times10^{-4}$
3	$-2.0(29)\times10^{-3}$	$9.8(93)\times10^{-4}$
4	$-2.7(41)\times10^{-3}$	$1.2(13)\times10^{-3}$
5	$1.05(19)\times10^{-2}$	$-7.3(47)\times10^{-4}$
6	$2.49(62)\times10^{-2}$	$1(13)\times10^{-4}$
7	$-5.4(11)\times10^{-3}$	$4.1(21)\times10^{-4}$
8	$-1.52(30)\times10^{-2}$	$9.4(46)\times10^{-4}$
9	$8(13)\times10^{-4}$	$-3.5(43)\times10^{-4}$

TABLE VIII. The $\mathcal{O}(a)^2$ errors in the lower dimensional operator subtractions are eliminated by fitting the coefficient $A_{\lambda^i}(p)$ in Eq. (164) to the form $A_{\lambda^i}(p)=A_{\lambda^i}^{(0)}+A_{\lambda^i}^{(2)}(ap)^2$. This table gives results for $A_{\lambda^i}^{(0)}$ and $A_{\lambda^i}^{(2)}$.

i	$A_{\lambda^i}^{(0)}$	$A_{\lambda^i}^{(2)}$
1	$7(64)\times10^{-5}$	$1(21)\times10^{-5}$
2	$-1.03(29)\times10^{-2}$	$2.93(98)\times10^{-3}$
3	$-1.97(60)\times10^{-2}$	$5.7(20)\times10^{-3}$
4	$-3.02(87)\times10^{-2}$	$8.6(30)\times10^{-3}$
5	$-3.62(34)\times10^{-2}$	$8.85(96)\times10^{-3}$
6	$-1.32(12)\times10^{-1}$	$3.36(34)\times10^{-2}$
7	$1.60(14)\times10^{-2}$	$-3.85(39)\times10^{-3}$
8	$4.59(41)\times10^{-2}$	$-1.10(11)\times10^{-2}$
9	$1.03(29)\times10^{-2}$	$-2.93(98)\times10^{-3}$

$$\lambda^i(p)=2m_f A_{\lambda^i}(p)+B_{\lambda^i}(p), \tag{164}$$

where we have used notation that explicitly allows κ^i, λ^i, A_{κ^i}, B_{κ^i}, A_{λ^i}, and B_{λ^i} to depend on the momentum. (The parameters c_1^i and c_2^i are given in terms of A_{κ^i}, B_{κ^i}, A_{λ^i}, and B_{λ^i}.) Thus, for each momentum, we fit our data for κ^i and λ^i to a linear function of m_f.

Having determined $A_{\kappa^i}(p)$, $B_{\kappa^i}(p)$, $A_{\lambda^i}(p)$, and $B_{\lambda^i}(p)$, we can now remove the dominant effects of discretization errors. For the momenta we are using, these enter as $\mathcal{O}[(ap)^2]$ effects, which we can determine by fitting $A_{\kappa^i}(p)$, $B_{\kappa^i}(p)$, $A_{\lambda^i}(p)$, and $B_{\lambda^i}(p)$ to the form $A_{\kappa^i}(p)=A_{\kappa^i}^{(0)}+A_{\kappa^i}^{(2)}(ap)^2$, etc. Momenta are used in the fits such that $0.8<(ap)^2<2.0$. Tables VI and VII summarize the results of the fits for A_{κ^i} and B_{κ^i}, respectively, while Tables VIII and IX give the same information for the fits to A_{λ^i} and B_{λ^i}. All fits use 50 configurations, with jackknife blocks of size one.

Tables VI and VII show that $A_{\kappa^i}^{(2)}$ and $B_{\kappa^i}^{(2)}$ are generally zero within our statistical errors, so discretization errors for $A_{\kappa^i}(p)$ and $B_{\kappa^i}(p)$ are not resolved. In addition, the statistical errors on $A_{\kappa^i}^{(2)}$ and $B_{\kappa^i}^{(2)}$ for $i=5$, 6, 7, and 8 are small compared to $A_{\kappa^i}^{(0)}$ and $B_{\kappa^i}^{(0)}$, so any discretization errors are a

TABLE IX. The $\mathcal{O}(a)^2$ errors in the lower dimensional operator subtractions are eliminated by fitting the coefficient $B_{\lambda^i}(p)$ in Eq. (164) to the form $B_{\lambda^i}(p)=B_{\lambda^i}^{(0)}+B_{\lambda^i}^{(2)}(ap)^2$. This table gives results for $B_{\lambda^i}^{(0)}$ and $B_{\lambda^i}^{(2)}$.

i	$B_{\lambda^i}^{(0)}$	$B_{\lambda^i}^{(2)}$
1	$-2.02(48)\times10^{-3}$	$2.06(69)\times10^{-4}$
2	$1.14(14)\times10^{-2}$	$-2.31(36)\times10^{-3}$
3	$1.67(32)\times10^{-2}$	$-4.02(79)\times10^{-3}$
4	$3.01(44)\times10^{-2}$	$-6.5(11)\times10^{-3}$
5	$4(14)\times10^{-4}$	$-5.3(23)\times10^{-4}$
6	$4.26(45)\times10^{-2}$	$-8.8(12)\times10^{-3}$
7	$-5.95(95)\times10^{-4}$	$1.32(26)\times10^{-4}$
8	$-1.82(28)\times10^{-3}$	$4.13(78)\times10^{-4}$
9	$-1.14(14)\times10^{-2}$	$2.31(36)\times10^{-3}$

TABLE X. The lower dimensional operator subtraction coefficients c_1^i used in the $m_f=0.04$ subtraction.

i	c_1^i
1	$1.2(12)\times10^{-4}$
2	$-8.0(77)\times10^{-4}$
3	$-1.2(17)\times10^{-3}$
4	$-2.2(24)\times10^{-3}$
5	$-6.42(13)\times10^{-2}$
6	$-1.916(34)\times10^{-1}$
7	$3.204(65)\times10^{-2}$
8	$9.49(17)\times10^{-2}$
9	$8.0(77)\times10^{-4}$

small effect for $A_{\kappa^i}(p)$ and $B_{\kappa^i}(p)$. For $A_{\lambda^i}(p)$ and $B_{\lambda^i}(p)$, the discretization errors are statistically resolved and, for $(ap)^2=2$, alter $A_{\lambda^i}^{(0)}$ and $B_{\lambda^i}^{(0)}$, by ~30%. Given these fits to $(ap)^2$, we can determine c_1^i and c_2^i from $c_2^i=-B_{\lambda^i}^{(0)}$ and from $c_1^i=-2m_f(c_2^i+A_{\kappa^i}^{(0)})-B_{\kappa^i}^0$. Note that the combination $2m_fA_{\kappa^i}^{(0)}+B_{\kappa^i}^0$ entering c_1^i is $\kappa^i(0)$, i.e., the value of Eq. (163) for $p=0$. In our final determination of c_1^i this combination is found directly from fitting $\kappa^i(p)$ to $\kappa^{i,(0)}+\kappa^{i,(2)}(ap)^2$ and using the value of $\kappa^{i,(0)}$. This reduces any possible numerical imprecision from fitting both m_f dependence and p dependence separately. Our data is well fit by the various relations given above, which shows that the data has mass dependence predicted for c_1^i and c_2^i in Eqs. (148) and (149).

Since c_2^i shows no visible mass dependence, we have chosen to use its value in the chiral limit, as just described, for the final computation of the Z factors at nonzero quark mass. (If mass dependence were visible in c_2^i, our entire approach would be suspect.) On the other hand, since c_1^i is strongly mass dependent, we extract it at nonzero mass from Eq. (160). The values of c_1^i used for the $m_f=0.04$ subtractions are given in Table X. The quoted error is only a statistical error, which comes from the jackknife procedure.

2. Four-quark operator renormalization

For the extraction of the four-quark renormalization factors we have 100 configurations with two values of the quark mass, $m_f=0.02$ and $m_f=0.04$ and a further 390 configurations for the second mass value. The extra configurations for the heavier mass were obtained to gain increased statistics at a reasonable cost after the subtracted renormalization factors had been found to be mass independent to a good degree of accuracy on the first 100 configurations.

The renormalization condition we apply is such that all the momentum scales in the problem should be the same, i.e.,

$$p_1^2=p_2^2=(p_1-p_2)^2=\mu^2. \tag{165}$$

The values of n_i corresponding to the momenta that we used are given in Table XI. The results are averaged over equivalent orientations, and denoted by the corresponding Euclidean squared momenta $(ap)^2$.

TABLE XI. The discrete Euclidean four-momenta used in the four-quark operator renormalization calculation. Values are given in the order $[x, y, z, t]$.

$(ap)^2$	n_1	n_2
1.23		
	[0, 2, 2, 0]	[2, 2, 0, 0]
	[0, 2, 2, 0]	[−2, 2, 0, 0]
	[0, 2, 2, 0]	[2, 0, 2, 0]
	[0, 2, 2, 0]	[−2, 0, 2, 0]
	[0, 2, 2, 0]	[0, 2, 0, 4]
	[0, 2, 2, 0]	[0, 2, 0, −4]
	[0, 2, 2, 0]	[0, 0, 2, 4]
	[0, 2, 2, 0]	[0, 0, 2, −4]
1.54		
	[1, 1, 2, 4]	[1, −2, 1, 4]
	[1, 1, 2, 4]	[1, 2, −1, 4]
	[1, 1, 2, 4]	[−2, 1, 1, 4]
	[1, 1, 2, 4]	[2, 1, −1, 4]
	[1, 1, 2, 4]	[−2, 1, 2, 2]
	[1, 1, 2, 4]	[2, 1, 2, −2]
	[1, 1, 2, 4]	[1, −2, 2, 2]
	[1, 1, 2, 4]	[1, 2, 2, −2]

The operators below the charm threshold, Q_i $(i=1,...,10)$, are not linearly independent. As can be seen from Eq. (156) the method we use to calculate Z requires the inverse of M, which is singular in this case. Therefore we actually calculate Z from Eq. (156) for a linearly independent subset of these operators.

This subset was defined by eliminating Q_4, Q_9, and Q_{10}, through the identities

$$Q_4=-Q_1+Q_2+Q_3,$$

$$Q_9=\frac{3}{2}Q_1-\frac{1}{2}Q_3,$$

$$Q_{10}=\frac{1}{2}Q_1+Q_2-\frac{1}{2}Q_3. \tag{166}$$

Since conventionally the $\Delta S=1$ Hamiltonian is given in the dependent basis, after calculating the 7×7 matrix Z in the reduced basis, we reconstructed a 10×10 matrix $\hat{Z}$ in the full basis using the relations

$$\hat{Z}_{ij}=Z_{ij},\quad i,j\in\{1,2,3,5,6,7,8\}, \tag{167}$$

$$\hat{Z}_{ij}=0,\quad i\in\{1,2,3,4,5,6,7,8,9,10\}, \tag{168}$$

$$j\in\{4,9,10\}, \tag{169}$$

$$\hat{Z}_{ij}=T_k^iZ_{kj},\quad i\in\{4,9,10\}, \tag{170}$$

$$j\in\{1,2,3,5,6,7,8\}, \tag{171}$$

TABLE XII. The inverse of the four-quark renormalization matrix, MF^{-1}, in the block diagonal basis of irreducible representations of $SU(3)_L \times SU(3)_R$. Q'_1 is in the (27,1) representation, Q'_2, Q'_3, Q'_5, and Q'_6 are in (8,1) representations, and $Q'_{7,8}$ belong to (8,8) representations. Note that entries connecting the various representations are either zero within statistical errors or very small. The renormalization point is $(ap)^2=(ap)^2_{\rm diff}=1.23$.

	1	2	3
1	1.1380(35)	$3(11)\times10^{-5}$	$2.1(70)\times10^{-5}$
2	$6(245)\times10^{-8}$	1.052(12)	$7.03(98)\times10^{-2}$
3	$-8(368)\times10^{-8}$	$8.0(19)\times10^{-2}$	1.086(22)
5	$-6(45)\times10^{-20}$	$4.8(32)\times10^{-2}$	$1.8(24)\times10^{-2}$
6	$-1(112)\times10^{-20}$	$-2.1(60)\times10^{-2}$	$1.3(73)\times10^{-2}$
7	$1.11(37)\times10^{-4}$	$5.1(41)\times10^{-3}$	$9.9(50)\times10^{-3}$
8	$-1.5(20)\times10^{-5}$	$1.6(12)\times10^{-2}$	$3.0(15)\times10^{-2}$

	5	6	7
1	$1.52(80)\times10^{-5}$	$-2.87(33)\times10^{-5}$	$1.71(36)\times10^{-3}$
2	$9.7(38)\times10^{-3}$	$-8(21)\times10^{-4}$	$-2.3(18)\times10^{-4}$
3	$-2.2(61)\times10^{-3}$	$2.1(11)\times10^{-2}$	$-1.08(77)\times10^{-3}$
5	1.039(12)	$9.00(77)\times10^{-2}$	$1.1(16)\times10^{-3}$
6	$3.2(23)\times10^{-2}$	1.218(35)	$-2.2(50)\times10^{-3}$
7	$-4(15)\times10^{-4}$	$-1.8(22)\times10^{-3}$	1.0562(29)
8	$-1.3(45)\times10^{-3}$	$-5.1(64)\times10^{-3}$	$6.10(25)\times10^{-2}$

	8
1	$-5.4(15)\times10^{-4}$
2	$8(16)\times10^{-5}$
3	$7.3(65)\times10^{-4}$
5	$1.2(18)\times10^{-3}$
6	$8.5(55)\times10^{-3}$
7	$8.31(17)\times10^{-2}$
8	1.1354(43)

where T^i_k encodes Eq. (166) as $Q^i=T^i_kQ_k$ for $k=4$, 9, and 10.

As enumerated in Appendix B, the four-quark operators we are considering are composed of elements transforming according to the (8,1), (27,1), and (8,8) representations of $SU(3)_L \otimes SU(3)_R$. There are four distinct (8,1) representations, two distinct (8,8) representations and a single (27,1). Since we renormalize in the massless limit, our Z factors should not have mixings between the (8,1), (27,1), and (8,8) representations, but there can be mixings between the four distinct (8,1) representations and also between the two (8,8) representations. In particular, the calculated values for Z should be block diagonal in an operator basis where each operator is purely an (8,1), (27,1), or (8,8). This is already the case for Q_5 and Q_6, which are in distinct (8,1) representations, and Q_7 and Q_8, which are in distinct (8,8) representations. However, Q_1, Q_2, and Q_3 are mixtures of two (8,1) representations and a single (27,1). To check the chiral structure of the renormalization factors it is convenient to consider a basis with operators Q'_i in distinct $SU(3)_L \otimes SU(3)_R$ representations, given by

TABLE XIII. The same as Table XII except the renormalization point is $(ap)^2=(ap)^2_{\rm diff}=1.54$.

	1	2	3
1	1.1516(36)	$-5(99)\times10^{-6}$	$5(59)\times10^{-6}$
2	$2(235)\times10^{-8}$	1.0665(95)	$8.95(76)\times10^{-2}$
3	$-4(353)\times10^{-8}$	$7.3(15)\times10^{-2}$	1.066(18)
5	$1(13)\times10^{-20}$	$-8(23)\times10^{-3}$	$-9(21)\times10^{-3}$
6	$5(68)\times10^{-20}$	$-4.8(53)\times10^{-2}$	$-1.5(61)\times10^{-2}$
7	$7.5(31)\times10^{-5}$	$-1.9(25)\times10^{-3}$	$-4(33)\times10^{-4}$
8	$-1.0(15)\times10^{-5}$	$-6.1(76)\times10^{-3}$	$-2.1(97)\times10^{-3}$

	5	6	7
1	$1.9(78)\times10^{-6}$	$-2.25(23)\times10^{-5}$	$1.02(32)\times10^{-3}$
2	$-3(28)\times10^{-4}$	$-1.8(13)\times10^{-3}$	$1.6(11)\times10^{-4}$
3	$-9.6(63)\times10^{-3}$	$3.29(77)\times10^{-2}$	$-2.4(41)\times10^{-4}$
5	1.0684(82)	$8.65(67)\times10^{-2}$	$-3.1(10)\times10^{-3}$
6	$4.7(21)\times10^{-2}$	1.246(26)	$-8.8(31)\times10^{-3}$
7	$-6(11)\times10^{-4}$	$-2.0(18)\times10^{-3}$	1.0626(26)
8	$-1.8(33)\times10^{-3}$	$-5.8(52)\times10^{-3}$	$7.57(18)\times10^{-2}$

	8
1	$-6(12)\times10^{-5}$
2	$7(11)\times10^{-5}$
3	$2.1(62)\times10^{-4}$
5	$8(10)\times10^{-4}$
6	$2.6(40)\times10^{-3}$
7	$8.80(18)\times10^{-2}$
8	1.1234(41)

$$Q'_1=3Q_1+2Q_2-Q_3, \tag{172}$$

$$Q'_2=\frac{1}{5}(2Q_1-2Q_2+Q_3), \tag{173}$$

$$Q'_3=\frac{1}{5}(-3Q_1+3Q_2+Q_3), \tag{174}$$

$$Q'_i=Q_i;\ \ i\in\{5,6,7,8\}. \tag{175}$$

In this new basis Q'_1 is in the (27,1) representation and Q'_2 and Q'_3 are in the (8,1) representation. To display the chiral symmetry properties we tabulate elements of MF^{-1} in this basis in Tables XII and XIII. We tabulate MF^{-1} rather than FM^{-1} because the former is linear in the quark contractions, so individual contributions are more easily distinguished. In terms of the elements of MF^{-1} in the Q' basis, the restriction that operators in different multiplets cannot mix may be written

$$(MF^{-1})_{1i}=(MF^{-1})_{i1}=0;\ \ i\in\{2,3,5,6,7,8\},$$

$$(MF^{-1})_{7i}=(MF^{-1})_{i7}=0;\ \ i\in\{2,3,5,6\},$$

$$(MF^{-1})_{8i}=(MF^{-1})_{i8}=0;\ \ i\in\{2,3,5,6\}. \tag{176}$$

TABLE XIV. The four-quark operator renormalization factors $\hat{Z}_{ij}/Z_q^2$ at the renormalization point $(ap)^2=1.23$ ($\mu=2.13$ GeV) for the 3-flavor case. Values are given in the full overcomplete basis of operators as explained in the text.

	1	2	3
1	$9.466(27)\times10^{-1}$	$-6.79(26)\times10^{-2}$	$3.1(35)\times10^{-3}$
2	$-5.65(72)\times10^{-2}$	$9.353(70)\times10^{-1}$	$-4.7(59)\times10^{-3}$
3	$9.1(14)\times10^{-2}$	$-9.1(14)\times10^{-2}$	$8.79(16)\times10^{-1}$
4	$-9.13(20)\times10^{-1}$	$9.13(20)\times10^{-1}$	$8.71(19)\times10^{-1}$
5	$-1.03(51)\times10^{-2}$	$1.03(51)\times10^{-2}$	$-1.13(92)\times10^{-2}$
6	$1.4(21)\times10^{-2}$	$-1.4(21)\times10^{-2}$	$2(18)\times10^{-3}$
7	0.0(0)	0.0(0)	0.0(0)
8	0.0(0)	0.0(0)	0.0(0)
9	1.3746(73)	$-5.65(72)\times10^{-2}$	$-4.347(61)\times10^{-1}$
10	$3.715(35)\times10^{-1}$	$9.466(27)\times10^{-1}$	$-4.424(40)\times10^{-1}$

	5	6	7
1	$-9.2(37)\times10^{-3}$	$2.4(19)\times10^{-3}$	0.0(0)
2	$3.1(53)\times10^{-3}$	$-1.61(85)\times10^{-2}$	0.0(0)
3	$-2.1(12)\times10^{-2}$	$-2.5(15)\times10^{-2}$	0.0(0)
4	$-9(15)\times10^{-3}$	$-4.3(24)\times10^{-2}$	0.0(0)
5	$9.65(11)\times10^{-1}$	$-7.11(64)\times10^{-2}$	0.0(0)
6	$-2.6(18)\times10^{-2}$	$8.23(24)\times10^{-1}$	0.0(0)
7	0.0(0)	0.0(0)	$9.508(25)\times10^{-1}$
8	0.0(0)	0.0(0)	$-5.11(20)\times10^{-2}$
9	$-3.1(53)\times10^{-3}$	$1.61(85)\times10^{-2}$	0.0(0)
10	$9.2(37)\times10^{-3}$	$-2.4(19)\times10^{-3}$	0.0(0)

	8
1	0.0(0)
2	0.0(0)
3	0.0(0)
4	0.0(0)
5	0.0(0)
6	0.0(0)
7	$-6.96(12)\times10^{-2}$
8	$8.845(34)\times10^{-1}$
9	0.0(0)
10	0.0(0)

As can be seen from Tables XII and XIII, these relations are satisfied to a good degree of accuracy by our data. As such, for the calculation of the final renormalization factors we will set these elements to be exactly zero in MF^{-1}, before inverting to get Z to reduce the statistical error on the final result.

The final values for $\hat{Z}_{ij}/Z_q^2$ are given in Tables XIV–XIX where $(ap)^2$ is the square of the Euclidean momenta for the external legs and $(ap_{\mathrm{diff}})^2$ is the transferred momenta. To display the numerical importance of the various components of the calculation, three sets of renormalization coefficients are given: (1) The full renormalization coefficients (Tables XIV and XV), (2) those calculated without the eye-diagram contributions (Tables XVI and XVII), and (3) those calculated with the eye-diagrams but without the subtraction of the lower dimensional operators (Tables XVIII and XIX). All values given are with $m_f=0.04$ for 490 configurations. The quoted error is statistical, and was calculated by jackknifing the data in blocks of 10. To obtain $\hat{Z}$ we use $Z_q=0.808(3)(15)$ [59] at 2 GeV. In principle Z_q should be run to the exact scale at which we are working, however, this is a very small effect (see Ref. [59], Fig. 17).

TABLE XV. The same as Table XIV except the renormalization point is $(ap)^2=1.54$ ($\mu=2.39$ GeV).

	1	2	3
1	$9.458(23)\times10^{-1}$	$-7.74(22)\times10^{-2}$	$-9(26)\times10^{-4}$
2	$-7.14(57)\times10^{-2}$	$9.397(60)\times10^{-1}$	$1.9(48)\times10^{-3}$
3	$9.0(10)\times10^{-2}$	$-9.0(10)\times10^{-2}$	$8.70(12)\times10^{-1}$
4	$-9.28(16)\times10^{-1}$	$9.28(16)\times10^{-1}$	$8.72(15)\times10^{-1}$
5	$-2.4(33)\times10^{-3}$	$2.4(33)\times10^{-3}$	$1.9(70)\times10^{-3}$
6	$9(17)\times10^{-3}$	$-9(17)\times10^{-3}$	$9(15)\times10^{-3}$
7	0.0(0)	0.0(0)	0.0(0)
8	0.0(0)	0.0(0)	0.0(0)
9	1.3739(65)	$-7.14(57)\times10^{-2}$	$-4.361(49)\times10^{-1}$
10	$3.567(31)\times10^{-1}$	$9.458(23)\times10^{-1}$	$-4.333(31)\times10^{-1}$

	5	6	7
1	$-6(25)\times10^{-4}$	$3.5(11)\times10^{-3}$	0.0(0)
2	$9.6(53)\times10^{-3}$	$-2.57(54)\times10^{-2}$	0.0(0)
3	$1.7(12)\times10^{-2}$	$-4.1(10)\times10^{-2}$	0.0(0)
4	$2.8(16)\times10^{-2}$	$-7.0(15)\times10^{-2}$	0.0(0)
5	$9.389(70)\times10^{-1}$	$-6.54(47)\times10^{-2}$	0.0(0)
6	$-3.5(16)\times10^{-2}$	$8.05(17)\times10^{-1}$	0.0(0)
7	0.0(0)	0.0(0)	$9.464(22)\times10^{-1}$
8	0.0(0)	0.0(0)	$-6.38(14)\times10^{-2}$
9	$-9.6(53)\times10^{-3}$	$2.57(54)\times10^{-2}$	0.0(0)
10	$6(25)\times10^{-4}$	$-3.5(11)\times10^{-3}$	0.0(0)

	8
1	0.0(0)
2	0.0(0)
3	0.0(0)
4	0.0(0)
5	0.0(0)
6	0.0(0)
7	$-7.42(12)\times10^{-2}$
8	$8.951(32)\times10^{-1}$
9	0.0(0)
10	0.0(0)

D. Discussion

Having completed the renormalization of our four-quark operators, we now turn to a discussion of the size of various contributions, the effects of discretization errors, and the role of the dimension six bilinear operators which were not included in our present work. Turning first to the size of effects from our calculation, the numerical results show that the eye-diagrams, even though they have a $1/a^2$ dependence in the

TABLE XVI. The four-quark operator renormalization factors $\hat{Z}_{ij}/Z_q^2$ at the renormalization point $(ap)^2=1.23$ ($\mu=2.13$ GeV) for the 3-flavor case except that the eye diagrams (and consequently the lower dimensional operator subtractions) have been omitted in the calculation of $\hat{Z}_{ij}/Z_q^2$.

	1	2	3
1	$9.484(26)\times10^{-1}$	$-6.96(16)\times10^{-2}$	$9(380)\times10^{-8}$
2	$-6.96(16)\times10^{-2}$	$9.484(26)\times10^{-1}$	$9(380)\times10^{-8}$
3	$6.96(16)\times10^{-2}$	$-6.96(16)\times10^{-2}$	$8.787(27)\times10^{-1}$
4	$-9.484(26)\times10^{-1}$	$9.484(26)\times10^{-1}$	$8.787(27)\times10^{-1}$
5	$3.3(54)\times10^{-5}$	$-3.3(54)\times10^{-5}$	$-3.1(10)\times10^{-4}$
6	$-4.72(71)\times10^{-4}$	$4.72(71)\times10^{-4}$	$5.6(48)\times10^{-5}$
7	0.0(0)	0.0(0)	0.0(0)
8	0.0(0)	0.0(0)	0.0(0)
9	1.3877(38)	$-6.96(16)\times10^{-2}$	$-4.394(13)\times10^{-1}$
10	$3.698(24)\times10^{-1}$	$9.484(26)\times10^{-1}$	$-4.394(13)\times10^{-1}$

	5	6	7
1	$-1.29(38)\times10^{-4}$	$-1.7(13)\times10^{-5}$	0.0(0)
2	$-1.14(18)\times10^{-4}$	$1.05(16)\times10^{-4}$	0.0(0)
3	$-6.1(14)\times10^{-4}$	$1.58(50)\times10^{-4}$	0.0(0)
4	$-6.0(12)\times10^{-4}$	$2.80(55)\times10^{-4}$	0.0(0)
5	$9.510(23)\times10^{-1}$	$-7.03(11)\times10^{-2}$	0.0(0)
6	$-5.108(98)\times10^{-2}$	$8.823(31)\times10^{-1}$	0.0(0)
7	0.0(0)	0.0(0)	$9.509(23)\times10^{-1}$
8	0.0(0)	0.0(0)	$-5.103(98)\times10^{-2}$
9	$1.14(18)\times10^{-4}$	$-1.05(16)\times10^{-4}$	0.0(0)
10	$1.29(38)\times10^{-4}$	$1.7(13)\times10^{-5}$	0.0(0)

	8
1	0.0(0)
2	0.0(0)
3	0.0(0)
4	0.0(0)
5	0.0(0)
6	0.0(0)
7	$-7.02(11)\times10^{-2}$
8	$8.823(31)\times10^{-1}$
9	0.0(0)
10	0.0(0)

TABLE XVII. The same as Table XVI except the renormalization point is $(ap)^2=1.54$ ($\mu=2.39$ GeV).

	1	2	3
1	$9.465(23)\times10^{-1}$	$-7.81(16)\times10^{-2}$	$1(47)\times10^{-7}$
2	$-7.81(16)\times10^{-2}$	$9.465(23)\times10^{-1}$	$1(47)\times10^{-7}$
3	$7.81(16)\times10^{-2}$	$-7.81(16)\times10^{-2}$	$8.684(27)\times10^{-1}$
4	$-9.465(23)\times10^{-1}$	$9.465(23)\times10^{-1}$	$8.684(27)\times10^{-1}$
5	$3.3(36)\times10^{-5}$	$-3.3(36)\times10^{-5}$	$-2.07(84)\times10^{-4}$
6	$-1.47(52)\times10^{-4}$	$1.47(52)\times10^{-4}$	$3.8(35)\times10^{-5}$
7	0.0(0)	0.0(0)	0.0(0)
8	0.0(0)	0.0(0)	0.0(0)
9	1.3807(34)	$-7.81(16)\times10^{-2}$	$-4.342(13)\times10^{-1}$
10	$3.560(26)\times10^{-1}$	$9.465(23)\times10^{-1}$	$-4.342(13)\times10^{-1}$

	5	6	7
1	$-8.4(33)\times10^{-5}$	$-1.1(10)\times10^{-5}$	0.0(0)
2	$-5.7(14)\times10^{-5}$	$3.0(12)\times10^{-5}$	0.0(0)
3	$-3.6(12)\times10^{-4}$	$2.6(45)\times10^{-5}$	0.0(0)
4	$-3.4(10)\times10^{-4}$	$6.7(47)\times10^{-5}$	0.0(0)
5	$9.474(22)\times10^{-1}$	$-7.45(11)\times10^{-2}$	0.0(0)
6	$-6.07(11)\times10^{-2}$	$8.943(29)\times10^{-1}$	0.0(0)
7	0.0(0)	0.0(0)	$9.474(22)\times10^{-1}$
8	0.0(0)	0.0(0)	$-6.07(11)\times10^{-2}$
9	$5.7(14)\times10^{-5}$	$-3.0(12)\times10^{-5}$	0.0(0)
10	$8.4(33)\times10^{-5}$	$1.1(10)\times10^{-5}$	0.0(0)

	8
1	0.0(0)
2	0.0(0)
3	0.0(0)
4	0.0(0)
5	0.0(0)
6	0.0(0)
7	$-7.45(11)\times10^{-2}$
8	$8.942(29)\times10^{-1}$
9	0.0(0)
10	0.0(0)

continuum limit, are small compared to the other graphs. This is in stark contrast to the matrix element case, where as we will see in Sec. XI, such divergent graphs overshadow the physical signal by approximately two orders of magnitude, and their subtraction is an extremely delicate operation that must be performed with great precision.

In the matrix element study, when considering dimensionful quantities, an order of magnitude estimate of the size of a physical signal may be made by taking $\Lambda_{\rm QCD}$ to the relevant number of powers. If the quantity is divergent, however, the dimensions may also be made up with inverse powers of the lattice spacing. As $a^{-1}\approx 10\times\Lambda_{\rm QCD}$ at the lattice spacing we are working, the physical signal may be much smaller than the subtraction. For the renormalization factors, however, we are studying high energy quantities, so the relevant scale is $a^{-1}\approx\mu$. Thus eye-graphs involving powers of a^{-1} have a much smaller effect on the renormalization factors than corresponding eye-graphs have on physical hadronic matrix elements. In addition, the eye-graphs are suppressed as they are zero in the free case, with the nonzero signal being due to gauge interactions. The numerical evidence in Tables XIV–XIX shows that inclusion of the divergent eye graphs affects the renormalization factors on the order of a few percent.

As we are studying high energy quantities, we must also worry about the effect of discretization errors. If the momenta, although large, still allow lattice artifacts to be treated as small corrections, it is possible to describe them as $\mathcal{O}(ap^2)$ and $\mathcal{O}(ap^2_{\rm diff})$ terms. Then, with a sufficient number of different momentum configurations, they can be isolated and removed. A naive estimate of the scale at which these effects become large is $p\approx 1/a$. This is only a rough esti-

TABLE XVIII. The four-quark operator renormalization factors $\hat{Z}_{ij}/Z_q^2$ at the renormalization point $(ap)^2=1.23$ ($\mu=2.13$ GeV) for the 3-flavor case except that lower dimensional operator subtractions have been omitted in the calculation of $\hat{Z}_{ij}/Z_q^2$.

	1	2	3
1	$9.463(28)\times10^{-1}$	$-6.75(26)\times10^{-2}$	$4.2(35)\times10^{-3}$
2	$-5.52(73)\times10^{-2}$	$9.340(71)\times10^{-1}$	$-9.0(66)\times10^{-3}$
3	$9.2(14)\times10^{-2}$	$-9.2(14)\times10^{-2}$	$8.73(17)\times10^{-1}$
4	$-9.09(21)\times10^{-1}$	$9.09(21)\times10^{-1}$	$8.60(21)\times10^{-1}$
5	$-9.0(49)\times10^{-3}$	$9.0(49)\times10^{-3}$	$-1.06(93)\times10^{-2}$
6	$2.4(21)\times10^{-2}$	$-2.4(21)\times10^{-2}$	$-1.6(19)\times10^{-2}$
7	0.0(0)	0.0(0)	0.0(0)
8	0.0(0)	0.0(0)	0.0(0)
9	1.3733(75)	$-5.52(73)\times10^{-2}$	$-4.303(67)\times10^{-1}$
10	$3.719(34)\times10^{-1}$	$9.463(28)\times10^{-1}$	$-4.436(41)\times10^{-1}$

	5	6	7
1	$-7.5(36)\times10^{-3}$	$-3(19)\times10^{-4}$	0.0(0)
2	$-3.8(60)\times10^{-3}$	$-5.1(88)\times10^{-3}$	0.0(0)
3	$-3.0(13)\times10^{-2}$	$-1.1(16)\times10^{-2}$	0.0(0)
4	$-2.6(17)\times10^{-2}$	$-1.6(25)\times10^{-2}$	0.0(0)
5	$9.70(11)\times10^{-1}$	$-7.99(75)\times10^{-2}$	0.0(0)
6	$-4.1(17)\times10^{-2}$	$8.42(23)\times10^{-1}$	0.0(0)
7	0.0(0)	0.0(0)	$9.521(24)\times10^{-1}$
8	0.0(0)	0.0(0)	$-4.67(17)\times10^{-2}$
9	$3.8(60)\times10^{-3}$	$5.1(88)\times10^{-3}$	0.0(0)
10	$7.5(36)\times10^{-3}$	$3(19)\times10^{-4}$	0.0(0)

	8
1	0.0(0)
2	0.0(0)
3	0.0(0)
4	0.0(0)
5	0.0(0)
6	0.0(0)
7	$-7.32(25)\times10^{-2}$
8	$8.720(73)\times10^{-1}$
9	0.0(0)
10	0.0(0)

mate, however, and previous studies have shown that for the lattice parameters we are using, momenta as large as $(ap)^2=2$ produce discretization errors of a few percent [59]. As such in this preliminary study, for which we have only a few momenta configurations, all of which have a momenta scale of $\approx 1/a$, we will ignore these effects.

Next we consider the effect of neglecting the subtraction of the dimension six quark bilinear operators. These subtractions are needed for two reasons.

(1) Discretization errors in our expressions for B_1 and B_2 are of $\mathcal{O}(a^2)$ and may be written in terms of the dimension six quark bilinear operators we are considering. When the Green's functions of these operators are multiplied by the subtraction coefficients c_1^i and c_2^i, which have leading behavior $1/a^2$, this can lead to errors in the final results that are of $\mathcal{O}(1)$ in the lattice spacing.

TABLE XIX. The same as Table XVIII except the renormalization point is $(ap)^2=1.54$ ($\mu=2.39$ GeV).

	1	2	3
1	$9.451(24)\times10^{-1}$	$-7.67(22)\times10^{-2}$	$-8(24)\times10^{-4}$
2	$-6.86(59)\times10^{-2}$	$9.370(62)\times10^{-1}$	$1.7(48)\times10^{-3}$
3	$9.3(11)\times10^{-2}$	$-9.3(11)\times10^{-2}$	$8.69(13)\times10^{-1}$
4	$-9.21(16)\times10^{-1}$	$9.21(16)\times10^{-1}$	$8.72(16)\times10^{-1}$
5	$-3.6(29)\times10^{-3}$	$3.6(29)\times10^{-3}$	$3.0(67)\times10^{-3}$
6	$1.7(18)\times10^{-2}$	$-1.7(18)\times10^{-2}$	$1.2(15)\times10^{-2}$
7	0.0(0)	0.0(0)	0.0(0)
8	0.0(0)	0.0(0)	0.0(0)
9	1.3712(68)	$-6.86(59)\times10^{-2}$	$-4.359(49)\times10^{-1}$
10	$3.575(31)\times10^{-1}$	$9.451(24)\times10^{-1}$	$-4.333(30)\times10^{-1}$

	5	6	7
1	$-4(24)\times10^{-4}$	$1.1(11)\times10^{-3}$	0.0(0)
2	$8.7(51)\times10^{-3}$	$-1.68(57)\times10^{-2}$	0.0(0)
3	$1.6(12)\times10^{-2}$	$-3.0(11)\times10^{-2}$	0.0(0)
4	$2.5(15)\times10^{-2}$	$-4.8(16)\times10^{-2}$	0.0(0)
5	$9.407(67)\times10^{-1}$	$-6.79(53)\times10^{-2}$	0.0(0)
6	$-3.3(15)\times10^{-2}$	$8.34(18)\times10^{-1}$	0.0(0)
7	0.0(0)	0.0(0)	$9.475(23)\times10^{-1}$
8	0.0(0)	0.0(0)	$-5.98(17)\times10^{-2}$
9	$-8.7(51)\times10^{-3}$	$1.68(57)\times10^{-2}$	0.0(0)
10	$4(24)\times10^{-4}$	$-1.1(11)\times10^{-3}$	0.0(0)

	8
1	0.0(0)
2	0.0(0)
3	0.0(0)
4	0.0(0)
5	0.0(0)
6	0.0(0)
7	$-7.48(18)\times10^{-2}$
8	$8.927(58)\times10^{-1}$
9	0.0(0)
10	0.0(0)

(2) The operator in Eq. (146) mixes at $\mathcal{O}(g)$ in perturbation theory and so should be subtracted to the order at which we are working. Such a subtraction was not attempted in this first work, since it involves explicit external gluons.

Expanding on the issues raised in case one, we consider a simplified situation involving a single dimension-six opera-

TABLE XX. Values for m_π versus m_f from 85 configurations using $\langle A^a(x)A_0^a(0)\rangle$ and from the 400 configurations of this work using $\langle \pi^a(x)A_0^a(0)\rangle$.

m_f	m_π (85 configurations)	m_π (400 configurations)
0.01	0.203(3)	0.2052(17)
0.02	0.270(3)	0.2699(14)
0.03	0.324(2)	0.3231(12)
0.04	0.371(2)	0.3700(12)
0.05		0.4129(11)

tor in the continuum, $B_3^{\rm cont}$. Then we can write, for example,

$$B_2^{\rm lat}=B_2^{\rm cont}+O(a^2)B_3^{\rm cont}. \tag{177}$$

When $B_2^{\rm lat}$ is multiplied by $c_2^j(\mu)$, which behaves as $1/a^2$, then $B_3^{\rm cont}$ is multiplied by a coefficient of $\mathcal{O}(1)$ in the lattice spacing. As we have just discussed, discretization effects are small, and so is the contribution of $O(a^2)B_3^{\rm cont}$ to Eq. (177). In addition, as we have noted, the contribution of $c_k^j(\mu)B_k^{\rm lat}$ to the four-quark renormalization factors is also small. Hence we expect any effects due to these discretization errors to be negligible.

A similar argument may be put forward for case two. While this operator should be subtracted at the order in perturbation theory in which we are working, the subtraction coefficient associated with this operator will be only logarithmically divergent in the lattice spacing, rather than power divergent. Our data from the extraction of the subtraction coefficients supports the numerical dominance of B_1 and B_2 [Eqs. (148) and (149)] very well. This suggests that the power divergent terms are much more important, for this set of lattice parameters, than the logarithmically divergent terms that would multiply the dimension-six operators. Again this indicates that we are correctly treating the dominant part of the subtractions, which themselves amount to only a small correction to the final renormalization factors.

IX. LATTICE CALCULATION OF $K\to\pi$ AND $K\to|0\rangle$ MATRIX ELEMENTS

In this section we present the lattice calculation of the $K\to\pi$ and $K\to|0\rangle$ matrix elements. In the first two sections the lattice method and basic contractions are briefly described. Results for $K\to\pi$ and $K\to|0\rangle$ matrix elements obtained by using this methodology, which form the basis of our calculation, are given in the last section. We continue to label pseudoscalar states with K and π to make the discussion clear, but the matrix elements $\langle\pi^+|Q_i|K^+\rangle$ are calculated with *degenerate* quarks and have $m_{\pi^+}=m_{K^+}$. Since $K\to|0\rangle$ matrix elements vanish in this limit, we use nondegenerate quark propagators for this case. It is useful to keep in mind that when the quarks are degenerate, flavor is specified by the type of quark contraction.

A. Lattice method of matrix element calculation

In order to obtain the desired matrix elements, we work in Euclidean space-time and calculate correlation functions. For example, a typical $K\to\pi$ correlation function is

$$G_{\pi OK}(t)\equiv\sum_{z,z'}\frac{1}{V_s}\sum_y\sum_{x,x'}\langle[i\bar{d}(z',t_\pi)\gamma_5 u(z,t_\pi)]O(y,t)\times[i\bar{u}(x',t_K)\gamma_5 s(x,t_K)]\rangle, \tag{178}$$

where $\langle\rangle$ denotes an average over gauge field configurations, $t_\pi>t>t_K$ with t_π and t_K fixed, V_s is the three-dimensional spatial volume and the factors of i make the pseudoscalar correlator positive. We employ Coulomb gauge fixed wall sources which have significant overlap with the pseudoscalar ground states and the spatial average over the operator time slice enhances the statistical average. For fixed values of t_K and t_π, a "plateau" in $G_{\pi OK}(t)$ emerges when $t_\pi\gg t\gg t_K$ as then the lowest energy states ($|\pi^+\rangle$ and $|K^+\rangle$) dominate the correlation function. The correlation function becomes time independent since the meson masses are equal. Up to source matrix elements and kinematical factors, $G_{\pi OK}(t)$ then directly yields the desired matrix element

$$\lim_{t_\pi\gg t\gg t_K} G_{\pi OK}(t)\to\frac{\langle\pi^+|O|K^+\rangle}{N(2m_\pi V_s)(2m_K V_s)}e^{-m_K(t-t_K)}e^{-m_\pi(t_\pi-t)}, \tag{179}$$

which is easily seen by inserting two complete sets of relativistically normalized states between the operator and each source. The factor N represents an unknown normalization factor introduced by the wall sources.

One way to remove the kinematic factors and the unknown normalization of our wall sources is to divide by the pseudoscalar two-point correlation function from each source. For example, with the wall-point (spatially extended source-local sink) two-point correlation function

$$G_\pi(t)\equiv\frac{1}{V_s}\sum_x[i\bar{u}(x,t)\gamma_5 d(x,t)]\sum_{z,z'}[i\bar{d}(z',t_\pi)\gamma_5 u(z,t_\pi)], \tag{180}$$

and similarly for $G_K(t)$, we can form a ratio of the desired matrix element to known factors.

$$\lim_{t_\pi\gg t\gg t_K}\frac{G_{\pi OK}(t)}{G_\pi(t)G_K(t)}=\frac{\langle\pi^+|O|K^+\rangle}{\langle\pi^+|P_{\pi^-}|0\rangle\langle0|P_{K^+}|K^+\rangle}. \tag{181}$$

[We use $P_{K^-}(x)\equiv[i\bar{u}\gamma_5 s](x)$ and $P_{\pi^+}(x)\equiv[i\bar{d}\gamma_5 u](x)$ as in Sec. IV B.] We can also normalize Eq. (179) by pseudoscalar-axial vector correlators, which changes the denominator in Eq. (181) to $\langle\pi^+|\bar{u}\gamma_0\gamma_5 d|0\rangle\langle0|\bar{s}\gamma_0\gamma_5 u|K^+\rangle$. The axial current matrix elements have the normalization given in Eq. (A12). These axial current matrix elements have been calculated using point-point correlation functions in Ref. [21] and can also be extracted from a simultaneous fit to the wall-point and wall-wall two-point functions calculated in the present study. As discussed in Sec. VI C, zero mode effects are introduced through $G_\pi(t)$ and $G_K(t)$ since such effects are seen in scalar correlators at a separation t. We also determine the pion mass from pseudoscalar-axial vector correlators (wall-point) for the 400 configurations used in this work and the results are given in Table XX and plotted in Fig. 2.

Another possibility is to divide the three-point function by a different three-point function. In particular

$$\lim_{t_\pi\gg t\gg t_K}\frac{G_{\pi OK}(t)}{G_{\pi\bar{s}dK}(t)}=\frac{\langle\pi^+|O|K^+\rangle}{\langle\pi^+|\bar{s}d|K^+\rangle}=\frac{2m_f}{m_\pi^2}\langle\pi^+|O|K^+\rangle, \tag{182}$$

where we have used the Ward-Takahashi identity Eq. (115), neglecting zero mode effects, in the last step. Since as we have seen, zero modes have a noticeable effect on this Ward-Takahashi identity, we do not divide by this three-point function to extract $\langle\pi^+|O|K^+\rangle$.

Our preferred approach is to divide $G_{\pi OK}(t)$ by the wall-wall two-point function computed from the correlator from t_π to t_K,

$$G_{\rm ww}(t_\pi,t_K)\equiv\frac{1}{V_s}\sum_{x,x'}\Big\langle[i\overline{u}(x,t_\pi)\gamma_5 d(x',t_\pi)]\times\sum_{z,z'}[i\overline{d}(z',t_K)\gamma_5 u(z,t_K)]\Big\rangle. \quad (183)$$

Since we work with degenerate quarks, we have

$$\lim_{t_K\gg t\gg t_\pi}\frac{G_{\pi OK}(t)}{G_{\rm ww}(t_\pi,t_K)}=\frac{\langle\pi^+|O|K^+\rangle}{2m_\pi} \quad (184)$$

where we determine $2m_\pi$ from a covariant fit to the wall-point two-point function in the range $t=12-20$ for each quark mass. As discussed in Sec. VI C this normalization minimizes the effects of zero modes.

We have tested the various methods described above for extracting $K\to\pi$ matrix elements from three-point correlation functions and find the results generally consistent, within errors. We give results for the last method since it is the simplest, requiring only the value for m_π, does not rely on chiral perturbation theory, and minimizes zero mode effects. In addition, we have used two types of wall sources to create and destroy pseudoscalar mesons: the usual pseudoscalar source $i\overline{q}\gamma_5 t_a q$ and an axial-vector source $\overline{q}\gamma_0\gamma_5 t_a q$. They give statistically equivalent results, but the pseudoscalar source yields somewhat smaller errors; we will always quote the former unless otherwise specified.

As mentioned earlier, for $K\to|0\rangle$ matrix elements we extract the needed power divergent coefficient from the ratio

$$\lim_{t_\pi\gg t\gg t_K}\frac{G_{OK}(t)}{G_K(t)}=\frac{\langle 0|O|K^0\rangle}{\langle 0|\overline{s}\gamma_5 d|K^0\rangle}, \quad (185)$$

where

$$G_{OK}(t)=\frac{1}{V_s}\sum_y\sum_{x,x'}\langle O(y,t)[i\overline{d}(x',t_K)\gamma_5 s(x,t_K)]\rangle. \quad (186)$$

The ratio in Eq. (185) is just the parity-odd analogue of Eq. (182) if we recognize the denominator of each ratio as the parity even or odd component, respectively, of the subtraction operator $\Theta^{(3,3)}$ discussed in Secs. III and XI. However, in Eq. (185) the ratio immediately gives the needed $\mathcal{O}(1/a^2)$ coefficient without relying on the Ward-Takahashi identity.

B. Contractions

To compute the $K\to\pi$ correlation function in Eq. (178), the quark fields are Wick contracted into propagators which are calculated by inverting the five-dimensional domain wall fermion Dirac matrix on an external source and projecting to four dimensions in the usual way (see [21]). Two types of diagrams emerge: figure eight diagrams as shown in Fig. 8(a) and eye diagrams as shown in Fig. 8(b). The $K\to|0\rangle$ matrix elements are computed in an analogous fashion and require the annihilation contraction given in Fig. 8(c). The matrix element of $\langle\pi^+|\overline{s}d|K^+\rangle$, which is needed to subtract the power divergent contribution, is shown in Fig. 8(d).

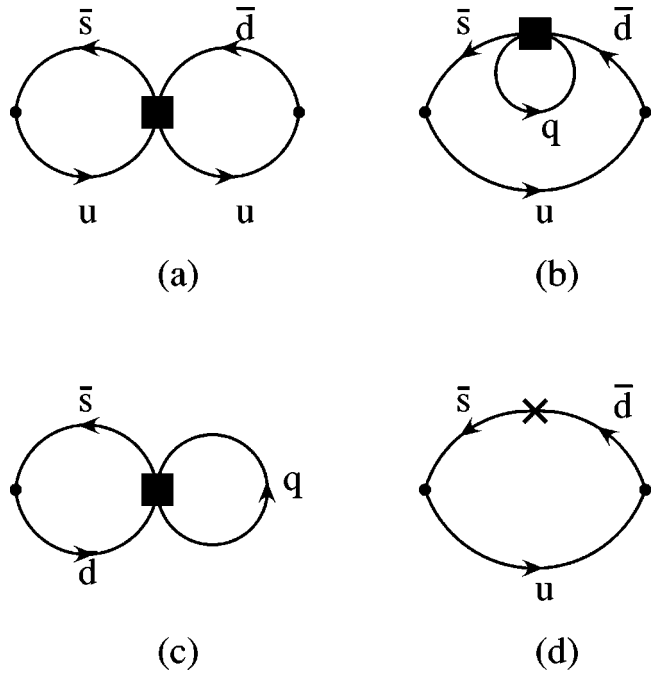

FIG. 8. The quark contractions needed for $\langle\pi^+|Q_i|K^+\rangle$ matrix elements are the figure eight (a) and eye (b) contractions. If the quark loop in (b) contains a d or s quark, there are two different eye contractions possible. This is the case for Q_3-Q_{10}. For $\langle 0|Q_i|K^0\rangle$ matrix elements, the annihilation contraction (c) is needed. For the determination of $\langle\pi^+|Q_i|K^+\rangle_{\rm sub}$ the contraction shown in (d) is needed, where the cross is an insertion of the quark bilinear $\overline{s}d$. The closed boxes represent insertions of a generic four-fermion operator, and the closed dots the creation and annhilation of the pseudoscalar states. Depending on the particular weak operator, the quark loops in (b) and (c) may contain $q=u$, d, s quarks (and c if charm is an active flavor).

The figure eight diagrams are constructed from quark propagators from the wall sources at t_K and t_π to a point $(\boldsymbol{x},t)$. Propagators from $(\boldsymbol{x},t)$ to t_π and t_K are obtained from the Hermiticity of the quark propagators, $G(x,y)=\gamma_5 G^\dagger(y,x)\gamma_5$. After the appropriate propagators are combined at a point $(\boldsymbol{x},t)$ where the weak operator is inserted, an average over $\boldsymbol{x}$ is done.

For the eye diagrams [Fig. 8(b)] and $K\to|0\rangle$ diagrams [Fig. 8(c)] we also need an additional propagator from $(\mathbf{x},t)$ to itself, since two fields in the weak operator are contracted together. To efficiently calculate this propagator we use a common technique in lattice simulations, calculating a propagator from a complex Gaussian random wall source. Since we only want the loop propagator for the weak operator in meson states, we choose the random source to be nonzero on time slices with $14\leqslant t\leqslant 17$. When the propagators are assembled to form a particular contraction, we include the complex conjugate of the random source at each sink point $(\mathbf{x},t)$ and average over random sources and gauge configurations to project out the desired diagonal contribution. This allows the spatial average of the correlation function

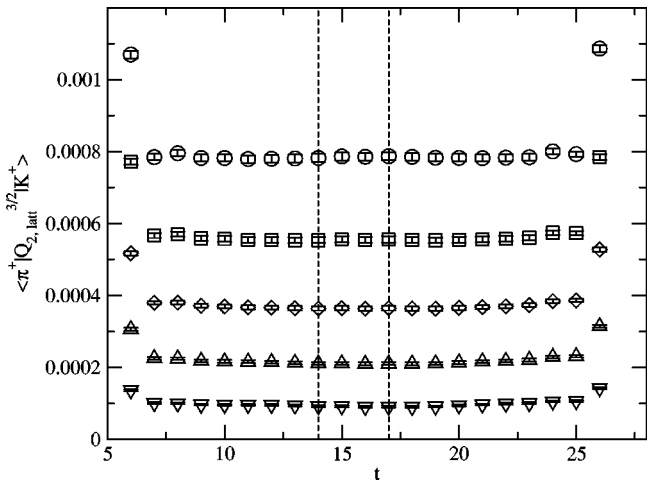

FIG. 9. $\langle \pi^+|Q^{(3/2)}_{2,\mathrm{lat}}|K^+\rangle$ for each Euclidean time slice t where the four quark operator was inserted. The different m_f values shown are: 0.01 (∇), 0.02 ($\triangle$), 0.03 ($\diamond$), 0.04 ($\square$), and 0.05 ($\bigcirc$). The matrix element is time-independent for the range $14 \leqslant t \leqslant 17$ for each mass (vertical dashed lines), showing that only the lowest energy pseudoscalar states are contributing.

over the operator time slice for any number of time slices to be done with only one (or a few) quark propagator inversion(s) on each gauge field configuration. We have chosen to calculate two independent, random source quark propagators on each configuration, corresponding to 1/3 of the computer time spent calculating propagators. The same random sources are used for all quark masses on a given configuration. The last part of the eye diagrams is the spectator quark propagator from t_K to t_π. This is constructed using the wall source propagator from t_K and using a wall sink at t_π where the spatial coordinates of the propagator are summed over before inserting the propagator into the contraction.

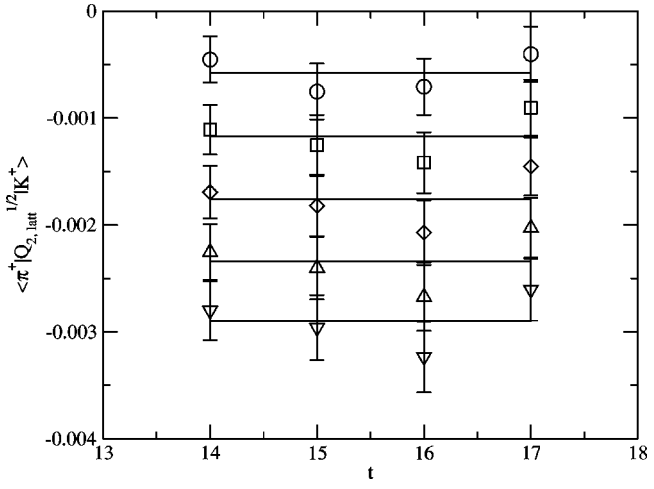

FIG. 10. $\langle \pi^+|Q^{(1/2)}_{2,\mathrm{lat}}|K^+\rangle$ for the time slices $14 \leqslant t \leqslant 17$. This matrix element involves a noisy estimator for the fermion loop in the eye contractions. The symbols denote different values for m_f, as in Fig. 9, and the lines are the average over time slices for a single m_f. The values on different time slices agree within the quoted statistical errors.

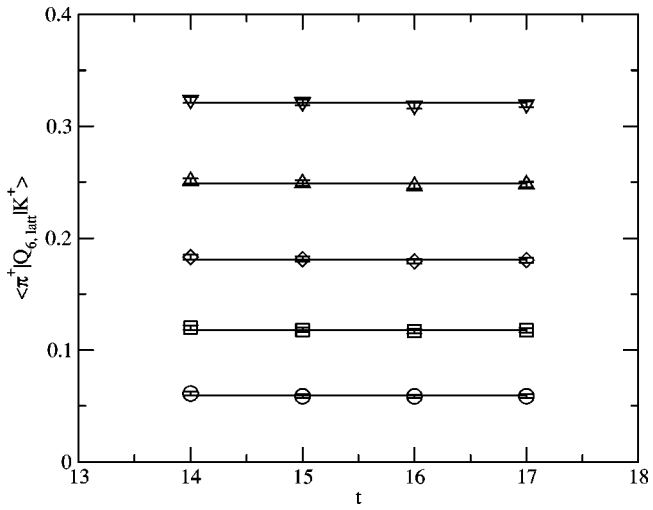

FIG. 11. The same as in Fig. 10, except that $\langle \pi^+|Q_{6,\mathrm{lat}}|K^+\rangle$ is shown. Again values agree on different time slices within errors.

C. Lattice values for $K \to \pi$ and $K \to 0$ matrix elements

We first demonstrate that for $t_\pi = 27$, $t = 14$–17, and $t_K = 5$ the ratio $2m_\pi G_{\pi OK}(t_\pi, t, t_K)/G_{\mathrm{ww}}(t_\pi, t_K)$ is t independent. If this is the case, then from Eq. (184) this ratio is the desired matrix element. In Fig. 9 we show $\langle \pi^+|Q^{3/2}_{2,\mathrm{lat}}|K^+\rangle$ as a function of t for $m_f = 0.01$, 0.02, 0.03, 0.04, and 0.05. There is no visible time dependence in the range $10 \leqslant t \leqslant 20$, demonstrating that only the lowest energy pseudoscalar state is contributing to the matrix element and justifying our choice of $14 \leqslant t \leqslant 17$ for the range over which eye contractions are calculated. The $\Delta I = 3/2$ parts of operators do not involve any eye contractions and are easier to determine with small statistical errors.

Having established that a plateau exists for t from 14 to 17, we plot the dependence on t of the $\Delta I = 1/2$ parts of operators, where random noise sources are used in the calculation of the eye diagrams. Figure 10 shows $\langle \pi^+|Q^{1/2}_{2,\mathrm{lat}}|K^+\rangle$ as a function of t for the values of m_f used and Fig. 11 is the same for $\langle \pi^+|Q^{1/2}_{6,\mathrm{lat}}|K^+\rangle$. Note the large difference in the vertical scale between Figs. 10 and 11, which is due to the larger divergent contribution in Q_6. One sees appreciable fluctuations between different times slices, but they agree within errors. This is the expectation from using a noisy estimator for the quark loops. Figures 12 and 13 show the data for the annihilation contractions needed for $\langle 0|Q_i|K^0\rangle$ matrix elements. These also involve random sources in the calculation of the quark loops and we see again that the results on different time slices agree within errors.

The results for $\langle \pi^+|(\bar{s}d)_{\mathrm{lat}}|K^+\rangle$, $\langle \pi^+|Q^{1/2}_{i,\mathrm{lat}}|K^+\rangle$, and $\langle \pi^+|Q^{(3/2)}_{i,\mathrm{lat}}|K^+\rangle$ are tabulated in Tables XXI, XXII, and XXIII, respectively. Results for the ratio $\langle 0|Q_i|K^0\rangle/\langle 0|\bar{s}\gamma_5 d|K^0\rangle$ are given in Tables XXIV and XXV. In each case the matrix elements have been averaged over time slices 14–17. The relative statistical error for the $\Delta I = 1/2$ matrix elements is almost 100% for matrix elements that are quite small (compatible with zero), i.e., $\langle \pi^+|Q_1|K^+\rangle$. For the left-left operators like Q_2 the statistical errors are 10%–20% and the errors fall to 0.5%–3% for

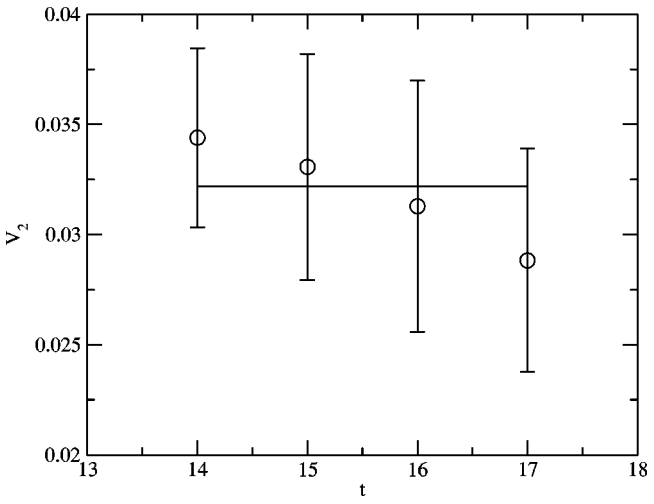

FIG. 12. A graph of $V_2 \equiv \langle 0|Q_{2,\mathrm{lat}}|K^0\rangle/[(m_s-m_d)\langle 0|\overline{s}\gamma_5 d|K\rangle]$ for each Euclidean time slice where the operator was inserted. The data is for $m_d=0.01$ and $m_s=0.02$. A noisy estimator is used for the closed fermion loop and the values on each time slice agree within errors. The line is the average over *t*.

the color-mixed left-right operators. For $\Delta I=3/2$ matrix elements the relative statistical error is 2% to 3%.

X. $\Delta I=3/2$ MATRIX ELEMENTS

In this section we discuss the lattice $K^+\to\pi^+$ matrix elements for the $\Delta I=3/2$ parts of the operators listed in Eqs. (4)–(23). In lowest order chiral perturbation theory, three constants serve to determine all of these matrix elements. A single value of $\alpha_{\mathrm{lat}}^{(27,1),(3/2)}$ fixes the $\Delta I=3/2$ parts of Q_1, Q_2, Q_9, Q_{10}, P_1, P_2, P_9, and P_{10}. For the electroweak penguin operators, $\alpha_{7,\mathrm{lat}}^{(8,8),(3/2)}$ is needed for the $\Delta I=3/2$ part of Q_7 and P_7 and $\alpha_{8,\mathrm{lat}}^{(8,8),(3/2)}$ is needed for Q_8 and P_8. [The two values for the (8,8) operators arise since Fierz transformations do not relate the electroweak operators with and without color-mixed indices.] The constants $\alpha_{\mathrm{lat}}^{(27,1),(3/2)}$, $\alpha_{7,\mathrm{lat}}^{(8,8),(3/2)}$, and $\alpha_{8,\mathrm{lat}}^{(8,8),(3/2)}$ are all finite and no subtraction is needed to determine the corresponding $K\to\pi\pi$ matrix elements. In addition, since there is a single (27,1) representation for left-left operators, the value of $\alpha_{\mathrm{lat}}^{(27,1),(3/2)}$ also provides a determination of $\langle\overline{K^0}|Q^{(\Delta S=2)}|K^0\rangle$.

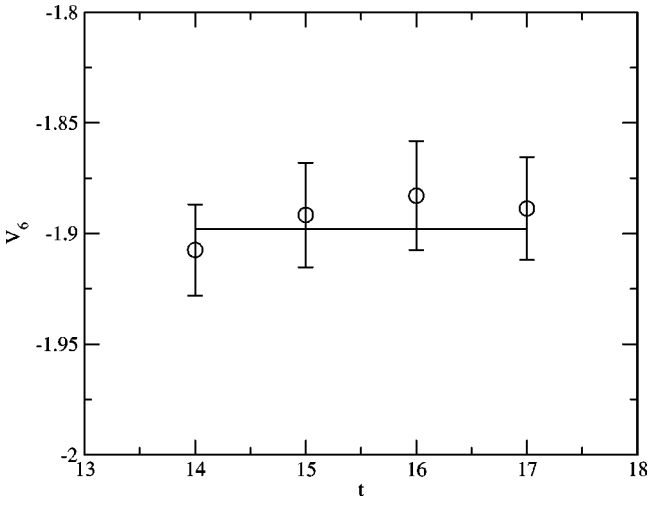

FIG. 13. A graph of $V_6 \equiv \langle 0|Q_{6,\mathrm{lat}}|K^0\rangle/[(m_s-m_d)\langle 0|\overline{s}\gamma_5 d|K\rangle]$ for each Euclidean time slice where the operator was inserted. The data is for $m_d=0.01$ and $m_s=0.02$. A noisy estimator is used for the closed fermion loop and the values on each time slice agree within errors. The line is the average over *t*.

TABLE XXI. The values for $\langle\pi^+|\overline{s}d_{\mathrm{lat}}|K^+\rangle$ for each light quark mass studied. These matrix elements are used in the subtraction needed in the determination of $K\to\pi\pi$ matrix elements from $K\to\pi$ and $K\to|0\rangle$ matrix elements.

m_f	$\langle\pi^+\|(\overline{s}d)_{\mathrm{lat}}\|K^+\rangle$
0.01	1.510(25)
0.02	1.548(16)
0.03	1.599(12)
0.04	1.660(10)
0.05	1.722(9)

A. The lattice value of $\alpha_{\mathrm{lat}}^{(27,1),(3/2)}$

We start with a determination of $\alpha_{\mathrm{lat}}^{(27,1),(3/2)}$. From Eqs. (B6), (B7), (B10), and (B11) of Appendix B, we see that we need the matrix element of $Q_{LL,S,(27,1),3/2}^{\Delta s=1,\Delta d=-1}$, defined in Eq. (B2), which is the $\Delta I=3/2$ part of $\Theta^{(27,1)}$. To follow more closely the notation of Sec. III A, in Appendix C we define $\Theta^{(27,1),(3/2)}\equiv Q_{LL,S,(27,1),3/2}^{\Delta s=1,\Delta d=-1}$. Then $\alpha_{\mathrm{lat}}^{(27,1),(3/2)}$ is defined by Eq. (D11), the generalization of Eq. (63) for a particular isospin. [For the (27,1) operator the generalization is trivial and in fact $\alpha_{\mathrm{lat}}^{(27,1),(3/2)}=\alpha_{\mathrm{lat}}^{(27,1)}$, but we will use $\alpha_{\mathrm{lat}}^{(27,1),(3/2)}$ to make it clear that this is determined from the $\Delta I=3/2$ amplitude.] The dependence of this matrix element on the parameters of low-energy quenched QCD is given in Eq. (92).

Table XXVI gives our values for $\langle\pi^+|\Theta_{\mathrm{lat}}^{(27,1),(3/2)}|K^+\rangle$ versus quark mass. The function we fit to is Eq. (92) with $\alpha=0$. For our particular lattice spacing this takes the form

$$\begin{aligned}\langle\pi^+|\Theta_{\mathrm{lat}}^{(27,1),(3/2)}|K^+\rangle &= b_1^{(27,1)}m_M^2\left[1-\left(\delta+\frac{6m_M^2}{(4\pi f)^2}\right)\ln(3.6941m_M^2)\right] \\ &\quad + b_2^{(27,1)}m_M^4 \qquad (187)\end{aligned}$$

with $m_M^2=3.18(m_f+m_{\mathrm{res}})$ and $1/(4\pi f)^2=1.246$. Here we have used the result for f from [21], which is 137(10) MeV, rather than the physical value, since we do not assume that quenched QCD at our fixed lattice spacing agrees with the physical world. The factor of 3.6941 in the logarithm is $\Lambda_{Q\chi PT}^2=1\ \mathrm{GeV}^2$ in lattice units. Figure 14 is a plot of the data and the solid line shows the result of a fit to Eq. (187). The fit uses all five values for the quark mass and sets $\delta=0.05$. The fit is again an uncorrelated fit to our correlated data, which results in a value of $\chi^2/\mathrm{DOF}=1.9$. The other lines in the figure give the contribution to the total of the

TABLE XXII. The values for $\langle \pi^+ | Q^{1/2}_{i,\mathrm{lat}} | K^+ \rangle \times 10^2$ for each light quark mass studied.

i	$m_f=0.01$	$m_f=0.02$	$m_f=0.03$	$m_f=0.04$	$m_f=0.05$
1	0.030(24)	0.024(26)	0.007(27)	−0.012(28)	−0.032(29)
2	−0.058(12)	−0.117(13)	−0.176(14)	−0.233(14)	−0.290(15)
3	−0.03(8)	−0.18(9)	−0.37(10)	−0.56(10)	−0.75(10)
4	−0.12(7)	−0.32(8)	−0.55(8)	−0.78(8)	−1.01(9)
5	2.10(8)	4.12(9)	6.28(10)	8.61(10)	11.09(11)
6	5.92(12)	11.79(14)	18.07(16)	24.84(18)	32.03(19)
7	−1.805(34)	−2.989(34)	−4.227(36)	−5.553(38)	−6.955(40)
8	−5.56(10)	−9.16(11)	−12.93(11)	−16.98(12)	−21.26(12)
9	0.063(12)	0.127(13)	0.194(14)	0.261(14)	0.329(15)
10	−0.026(24)	−0.013(26)	0.011(27)	0.040(28)	0.071(29)

various terms in Eq. (92). Of particular importance is the chiral logarithm term (the dot-dash line) $\sim m_M^4 L_{Q\chi}(m_M)$ which is very nearly linear in m_f up to $m_f=0.035$. Numerically, this term cannot be distinguished from the simple m_M^2 term and, as the graph shows, the term proportional to m_M^2 and the chiral logarithm term are of roughly equal size. Thus our value for $b_1^{(27,1)}$ is strongly dependent on the known coefficient, -6, for the chiral logarithm in Eq. (92). In particular, leaving out the chiral logarithm term makes the value of $b_1^{(27,1)}$ almost a factor of 2 larger.

In contrast to the chiral logarithm, the quenched chiral logarithm, shown by the short dashed line in Fig. 14 is contributing very little to the final result. This appears to be a consequence of the small value for δ and the fact that we are working with pseudoscalar masses above 390 MeV. This particular $\Delta I=3/2$ amplitude has quite small statistical errors and the one-loop quenched chiral perturbation theory formula is known. Since we see very little effects of the quenched chiral logarithms here, we expect them to have little effect on other amplitudes where the explicit coefficient of the quenched chiral logarithm is not known.

The full range of quark masses (0.01–0.05) has been used in the fit shown in Fig. 14. The range of pseudoscalar masses covered by this quark mass range is 390–790 MeV and from the fit it appears that one-loop quenched chiral perturbation theory is working reasonably well over this range. The χ^2/DOF is somewhat large for an uncorrelated fit, with the $m_f=0.05$ point lying somewhat above the curve from the fit. This point may be showing the limitations of one-loop chiral perturbation theory. At the other extreme, the $m_f=0.01$ point is where chiral perturbation theory should work the best, but this light quark mass is the most susceptible to the effects of finite volume and topological near-zero modes. It is worth reemphasizing that even for $m_f=0.01$, the chiral logarithm contributions are about 25% of the total value and must be included.

To test for sensitivity to the quark mass range used in the fit, we have done fits with different ranges and give the results in Table XXVII. One sees essentially no difference between the fits to $m_f=0.02$ to 0.04 and $m_f=0.01$ and 0.05. On this basis, we choose to fit to all five quark masses and find

$$\alpha_{\mathrm{lat}}^{(27,1),(3/2)} = -4.13(18)\times 10^{-6}. \tag{188}$$

B. The lattice value of $\alpha_{7,\mathrm{lat}}^{(8,8),(3/2)}$ and $\alpha_{8,\mathrm{lat}}^{(8,8),(3/2)}$

Unlike the single (27,1) operator which enters in many Q_i's and P_i's, the color diagonal (8,8) enters only in Q_7 and P_7 and the color mixed (8,8) enters only in Q_8 and P_8. We therefore define $\Theta_i^{(8,8),(3/2)} \equiv [Q_i]^{(3/2)}$ for $i=7$ and 8, as shown in more detail in Appendixes C and D. Equations (B14), (B17), and (B18) give the isospin decomposition of Q_7 in terms of quark fields. The results for Q_8 are similar, with color mixed indices on the quark fields. In lowest order chiral perturbation theory, $\alpha_{7,\mathrm{lat}}^{(8,8),(3/2)}$ and $\alpha_{8,\mathrm{lat}}^{(8,8),(3/2)}$ are determined from $\langle \pi^+ | \Theta_{7,\mathrm{lat}}^{(8,8),(3/2)} | K^+ \rangle$ and $\langle \pi^+ | \Theta_{8,\mathrm{lat}}^{(8,8),(3/2)} | K^+ \rangle$ through Eq. (D4), which is Eq. (64) decomposed into operators of definite isospin. Unlike the (27,1) operator, the chiral logarithm corrections for the (8,8) operator in quenched QCD are not currently known.

Table XXVIII gives our values for $\langle \pi^+ | \Theta_{7,\mathrm{lat}}^{(8,8),(3/2)} | K^+ \rangle$ and Table XXIX gives them for $\langle \pi^+ | \Theta_{8,\mathrm{lat}}^{(8,8),(3/2)} | K^+ \rangle$. Since

TABLE XXIII. The values for $\langle \pi^+ | Q^{3/2}_{i,\mathrm{lat}} | K^+ \rangle \times 10^4$ for each light quark mass studied.

i	$m_f=0.01$	$m_f=0.02$	$m_f=0.03$	$m_f=0.04$	$m_f=0.05$
1	0.914(30)	2.106(45)	3.64(7)	5.55(9)	7.85(12)
2	0.914(30)	2.106(45)	3.64(7)	5.55(9)	7.85(12)
7	−44.7(12)	−54.3(11)	−64.0(12)	−74.8(13)	−86.8(14)
8	−137.5(38)	−162.1(35)	−185.8(35)	−211.9(37)	−240.1(40)
9	1.370(44)	3.16(7)	5.46(10)	8.33(14)	11.78(18)
10	1.370(44)	3.16(7)	5.46(10)	8.33(14)	11.78(18)

TABLE XXIV. The values for the ratio $\langle 0|Q_{i,\mathrm{lat}}|K^0\rangle/\langle 0|(\bar{s}\gamma_5 d)_{\mathrm{lat}}|K^0\rangle$ for $i=1-6$ for each nondegenerate pair of light quark masses. These ratios are used in the determination of the subtraction coefficient required to relate $K\to\pi$ matrix elements to $K\to\pi\pi$ matrix elements.

i	m_s	$m_d=0.01$	$m_d=0.02$	$m_d=0.03$	$m_d=0.04$
1	0.02	$-0.009(43)\times10^{-3}$			
	0.03	$-0.056(50)\times10^{-3}$	$-0.013(40)\times10^{-3}$		
	0.04	$-0.098(56)\times10^{-3}$	$-0.053(43)\times10^{-3}$	$-0.019(39)\times10^{-3}$	
	0.05	$-0.138(62)\times10^{-3}$	$-0.090(47)\times10^{-3}$	$-0.054(40)\times10^{-3}$	$-0.026(38)\times10^{-3}$
2	0.02	$0.338(22)\times10^{-3}$			
	0.03	$0.663(26)\times10^{-3}$	$0.323(20)\times10^{-3}$		
	0.04	$0.979(29)\times10^{-3}$	$0.634(22)\times10^{-3}$	$0.331(20)\times10^{-3}$	
	0.05	$1.287(32)\times10^{-3}$	$0.938(24)\times10^{-3}$	$0.612(21)\times10^{-3}$	$0.301(19)\times10^{-3}$
3	0.02	$0.065(15)\times10^{-2}$			
	0.03	$0.116(18)\times10^{-2}$	$0.061(14)\times10^{-2}$		
	0.04	$0.166(21)\times10^{-2}$	$0.111(16)\times10^{-2}$	$0.056(14)\times10^{-2}$	
	0.05	$0.215(23)\times10^{-2}$	$0.160(17)\times10^{-2}$	$0.106(15)\times10^{-2}$	$0.052(14)\times10^{-2}$
4	0.02	$0.100(13)\times10^{-2}$			
	0.03	$0.187(15)\times10^{-2}$	$0.094(12)\times10^{-2}$		
	0.04	$0.273(17)\times10^{-2}$	$0.179(13)\times10^{-2}$	$0.089(12)\times10^{-2}$	
	0.05	$0.357(19)\times10^{-2}$	$0.263(15)\times10^{-2}$	$0.172(13)\times10^{-2}$	$0.085(12)\times10^{-2}$
5	0.02	$-0.635(13)\times10^{-2}$			
	0.03	$-1.293(15)\times10^{-2}$	$-0.644(12)\times10^{-2}$		
	0.04	$-1.950(18)\times10^{-2}$	$-1.302(13)\times10^{-2}$	$-0.647(12)\times10^{-2}$	
	0.05	$-2.605(19)\times10^{-2}$	$-1.958(15)\times10^{-2}$	$-1.303(12)\times10^{-2}$	$-0.648(11)\times10^{-2}$
6	0.02	$-1.870(1)\times10^{-2}$			
	0.03	$-3.775(13)\times10^{-2}$	$-1.8956(88)\times10^{-2}$		
	0.04	$-5.680(15)\times10^{-2}$	$-3.803(10)\times10^{-2}$	$-1.8970(80)\times10^{-2}$	
	0.05	$-7.576(17)\times10^{-2}$	$-5.700(12)\times10^{-2}$	$-3.7962(90)\times10^{-2}$	$-1.8900(74)\times10^{-2}$

TABLE XXV. The values for the ratio $\langle 0|Q_{i,\mathrm{lat}}|K^0\rangle/\langle 0|(\bar{s}\gamma_5 d)_{\mathrm{lat}}|K^0\rangle$ matrix elements for $i=7-10$ for each nondegenerate pair of light quark masses.

i	m_s	$m_d=0.01$	$m_d=0.02$	$m_d=0.03$	$m_d=0.04$
7	0.02	$3.4616(68)\times10^{-3}$			
	0.03	$6.911(11)\times10^{-3}$	$3.4359(47)\times10^{-3}$		
	0.04	$10.333(15)\times10^{-3}$	$6.8498(86)\times10^{-3}$	$3.4074(40)\times10^{-3}$	
	0.05	$13.723(19)\times10^{-3}$	$10.235(12)\times10^{-3}$	$6.7876(77)\times10^{-3}$	$3.3762(37)\times10^{-3}$
8	0.02	$10.402(20)\times10^{-3}$			
	0.03	$20.759(34)\times10^{-3}$	$10.316(14)\times10^{-3}$		
	0.04	$31.031(45)\times10^{-3}$	$20.563(26)\times10^{-3}$	$10.226(12)\times10^{-3}$	
	0.05	$41.207(55)\times10^{-3}$	$30.722(37)\times10^{-3}$	$20.370(23)\times10^{-3}$	$10.131(11)\times10^{-3}$
9	0.02	$-0.338(22)\times10^{-3}$			
	0.03	$-0.662(26)\times10^{-3}$	$-0.323(20)\times10^{-3}$		
	0.04	$-0.976(29)\times10^{-3}$	$-0.632(22)\times10^{-3}$	$-0.311(20)\times10^{-3}$	
	0.05	$-1.281(32)\times10^{-3}$	$-0.934(24)\times10^{-3}$	$-0.610(21)\times10^{-3}$	$-0.301(19)\times10^{-3}$
10	0.02	$0.010(43)\times10^{-3}$			
	0.03	$0.057(50)\times10^{-3}$	$0.014(40)\times10^{-3}$		
	0.04	$0.101(57)\times10^{-3}$	$0.055(43)\times10^{-3}$	$0.020(39)\times10^{-3}$	
	0.05	$0.144(62)\times10^{-3}$	$0.094(47)\times10^{-3}$	$0.056(40)\times10^{-3}$	$0.026(38)\times10^{-3}$

TABLE XXVI. Values for $\langle \pi^+|\Theta_{\rm lat}^{(27,1),(3/2)}|K^+\rangle$ versus m_f.

m_f	$\langle \pi^+|\Theta_{\rm lat}^{(27,1),(3/2)}|K^+\rangle$
0.01	0.000 274 (9)
0.02	0.000 632 (14)
0.03	0.001 092 (20)
0.04	0.001 665 (27)
0.05	0.002 356 (36)

the one-loop corrections are not known, but the general form should be as in Eq. (76), except that the m_M^2 term has a finite coefficient for the $\Delta I=3/2$ amplitudes, we will try fitting with and without a conventional chiral logarithm term. We will not include any quenched chiral logarithm effects, since these were seen to be small for the (27,1), $\Delta I=3/2$ amplitudes discussed in the previous section. Thus we will fit our data to the form

$$\langle \pi^+|\Theta_{i,\rm lat}^{(8,8),(3/2)}|K^+\rangle = b_{i,0}^{(8,8)}\left[1+\left(\frac{\xi_i^{(8,8)}m_M^2}{(4\pi f)^2}\right)\ln(3.6941 m_M^2)\right] + b_{i,1}^{(8,8)} m_M^2, \tag{189}$$

where $i=7$, 8, $m_M^2=3.18(m_f+m_{\rm res})$, $1/(4\pi f)^2=1.246$, and 3.6941 is the value of $\Lambda_{QXPT}^2=1$ GeV^2 in lattice units. Since $\xi_i^{(8,8)}$ is not known, we will do fits where it is zero and where it is a free parameter.

Figure 15 is a plot of the values for $\langle \pi^+|\Theta_{7,\rm lat}^{(8,8),(3/2)}|K^+\rangle$ and Fig. 16 is the same for $\langle \pi^+|\Theta_{8,\rm lat}^{(8,8),(3/2)}|K^+\rangle$. An obvious feature of the graphs is the nearly linear behavior of the matrix elements. To determine $\alpha_{7,\rm lat}^{(8,8),(3/2)}$ and $\alpha_{8,\rm lat}^{(8,8),(3/2)}$, we

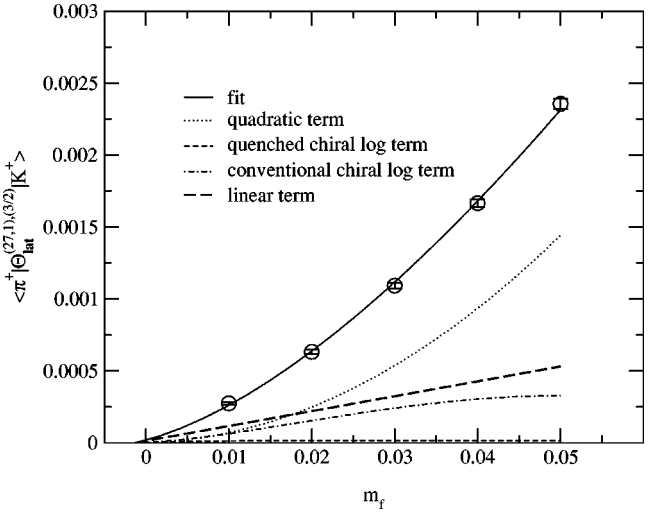

FIG. 14. The matrix element for $\Theta_{\rm lat}^{(27,1),(3/2)}$, which shows noticeable nonlinearity as a function of quark mass. The solid line is a fit to Eq. (187), using all five quark masses. The contributions from the various terms in Eq. (187) are shown, with the conventional chiral logarithm term (the dot-dashed line) of particular importance due to its essential linearity over most of our quark mass range. To extract a value of $\alpha_{\rm lat}^{(27,1),(3/2)}$ from this data, we rely on the known analytic value for the conventional chiral logarithm.

TABLE XXVII. The dependence of the fit parameters in Eq. (187) on the range of quark masses used.

m_f range	$b_1^{(27,1)}$	$b_2^{(27,1)}$	χ^2/DOF
0.01–0.04	0.003 45(16)	0.049 7(22)	1.1(4)
0.01–0.05	0.003 25(14)	0.054 2(18)	1.9(6)
0.02–0.04	0.003 20(14)	0.053 7(18)	0.4(1)
0.02–0.05	0.003 01(13)	0.057 5(15)	0.7(2)

must extrapolate to the chiral limit, $m_f=-m_{\rm res}$. Since there are no power divergences involved in these operators, their chiral limit, up to $\mathcal{O}(a^2)$, corrections should be determined by $m_{\rm res}$. Table XXX gives the results of fits to Eq. (189), where $\xi_i^{(8,8)}$ is held to zero (simple linear fit) and allowed to be a free parameter (chiral logarithm fit). In Fig. 15 and 16 the solid lines are the linear fits and the dashed lines include the chiral logarithm term with a free parameter.

One sees that the value of $b_{7,0}^{(8,8)}$ changes by about 15% with the inclusion of a chiral logarithm term, while $b_{8,0}^{(8,8)}$ moves by about 8%. Knowing $\xi_i^{(8,8)}$ analytically would decrease the uncertainty in our extrapolation. Without this knowledge, we will take the chiral logarithm fits to determine the intercepts, with the difference between the two fit choices giving an indication of our systematic uncertainty. Thus we find

$$\alpha_{7,\rm lat}^{(8,8),(3/2)} = -1.61(8)\times 10^{-6}, \tag{190}$$

$$\alpha_{8,\rm lat}^{(8,8),(3/2)} = -4.96(27)\times 10^{-6}. \tag{191}$$

XI. $\Delta I=1/2$ MATRIX ELEMENTS

In this section, we turn to the determination of the lattice $K^+\to\pi^+$ matrix elements for the $\Delta I=1/2$ parts of the operators listed in Eqs. (4)–(23). The numerical evaluation of these matrix elements is much more involved, since the physical quantities are found from the difference of two lattice quantities which contain power divergences. The basic idea behind the subtraction of the unphysical effects was discussed in Sec. III A and it is important to recall that this subtraction is done for matrix elements in hadronic states. A related subtraction was discussed in Sec. VIII, which is done in Landau gauge fixed quark states and is used for matching operator normalizations between the lattice and continuum perturbation theory. An important check of our calculation is the consistency of these two subtractions, which should

TABLE XXVIII. Values for $\langle \pi^+|\Theta_{7,\rm lat}^{(8,8),(3/2)}|K^+\rangle$ versus m_f.

m_f	$\langle \pi^+|\Theta_{7,\rm lat}^{(8,8),(3/2)}|K^+\rangle$
0.01	−0.004 47(12)
0.02	−0.005 43(11)
0.03	−0.006 40(12)
0.04	−0.007 48(13)
0.05	−0.008 68(13)

TABLE XXIX. Values for $\langle \pi^+ | \Theta_{8,\mathrm{lat}}^{(8,8),(3/2)} | K^+ \rangle$ versus m_f.

m_f	$\langle \pi^+ \vert \Theta_{8,\mathrm{lat}}^{(8,8),(3/2)} \vert K^+ \rangle$
0.01	−0.0137(4)
0.02	−0.0162(3)
0.03	−0.0186(4)
0.04	−0.0212(4)
0.05	−0.0240(4)

receive the same contribution from the leading momentum-independent power-divergent terms.

A. Subtraction of power divergent operators

All the operators in Eqs. (4)–(23) have unphysical contributions to their $\Delta I = 1/2$, $K^+ \to \pi^+$ matrix elements at finite quark mass, since an (8,1) or (8,8) representation appears in each Q_i. For the (8,1) parts of the operators, the formulas in Sec. III A show how these unphysical contributions are removed. For the operators Q_7 and Q_8, naively more options exist since they are in a single irreducible representation of $\mathrm{SU}(3)_L \otimes \mathrm{SU}(3)_R$. One can (1) find the $\Delta I = 1/2$ matrix elements from the value for $\alpha_{i,\mathrm{lat}}^{(8,8),(3/2)}$ of the previous section, (2) extrapolate the divergent $\Delta I = 1/2$ matrix elements to the chiral limit, or (3) perform a subtraction as for the (8,1) operators at finite quark mass and then extrapolate the remaining, nondivergent matrix element to the chiral limit. For domain wall fermions at finite L_s, only the first option is precisely defined, since at finite L_s the value of the input quark mass yielding the chiral limit is not well defined for divergent operators. One only knows that the chiral limit is

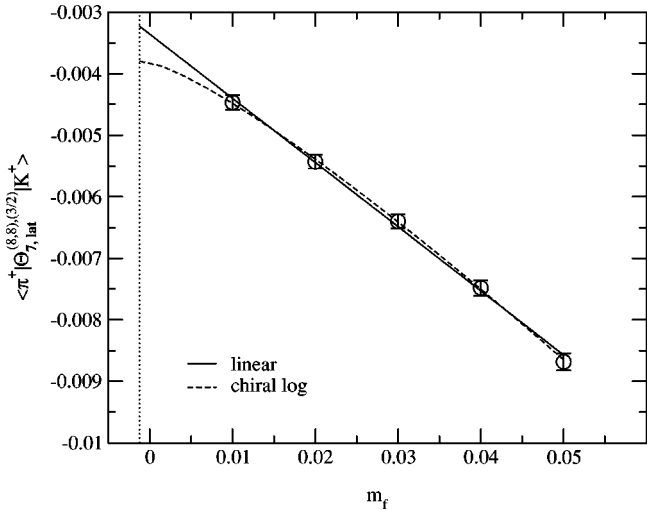

FIG. 15. The lattice matrix element for $\Theta_{7,\mathrm{lat}}^{(8,8),(3/2)}$, fit to Eq. (189). All five quark masses are used in the fit and any nonlinearity in the data is small. The vertical dashed line is drawn at $m_f = -m_{\mathrm{res}}$. There is no analytic result for the coefficient of the conventional chiral logarithm in the quenched theory for this matrix element, so we have done both simple linear fits ($\xi_7^{(8,8)} = 0$) and fits where the chiral logarithm is included with a free coefficient. The linearity of the data shows the chiral logarithm is not nearly as important here as for the fits to $\Theta_{\mathrm{lat}}^{(27,1),(3/2)}$.

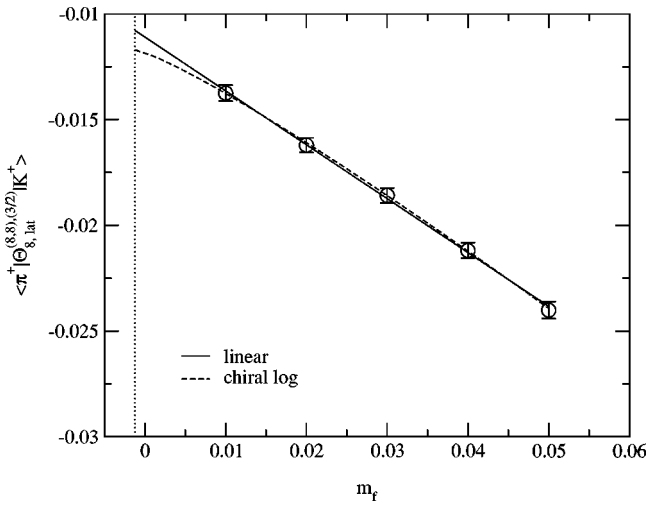

FIG. 16. The lattice matrix element for $\Theta_{8,\mathrm{lat}}^{(8,8),(3/2)}$, fit to Eq. (189). All five quark masses are used in the fit and there is little nonlinearity in the data. The vertical dashed line is drawn at $m_f = -m_{\mathrm{res}}$. Both linear fits ($\xi_8^{(8,8)} = 0$) and fits where the chiral logarithm is included with a free coefficient are shown. The linearity of the data shows that the chiral logarithm is not nearly as important here as for the fits to $\Theta_{\mathrm{lat}}^{(27,1),(3/2)}$.

achieved by setting $m_f = -O(m_{\mathrm{res}})$. For completeness and to study the effects of $\mathcal{O}(m_{\mathrm{res}})$ errors, we will include the subtraction of the $\Delta I = 1/2$ (8,8) operators in this section, but will use the values of $\alpha_{7,\mathrm{lat}}^{(8,8),(3/2)}$ and $\alpha_{8,\mathrm{lat}}^{(8,8),(3/2)}$ found previously to determine our final value for the $\Delta I = 1/2$ parts of Q_7 and Q_8.

In Sec. III B we have argued that a particular combination of matrix elements [Eqs. (87) and (89)] will not involve power divergent coefficients times higher order logarithmic terms in chiral perturbation theory. This is extremely important for our numerical subtraction, since such higher order logarithmic terms in chiral perturbation theory are not small for the pseudoscalar masses we can currently use. In addition, there is a great benefit numerically to dealing with quantities where such effects cancel, rather than canceling them through the explicit determination of extra fit parameters. We will also apply the same subtraction to Q_7 and Q_8 that we apply to the other operators. This will remove the divergent term, $m_M^2 \alpha_{\mathrm{div}}^{(8,8)}$, given in Eq. (76), since any divergent term looks like $\Theta^{(3,3)}$. The finite term proportional to m_M^2 that is left will not be related to the m_M^2 dependence of

TABLE XXX. The results for fits to $\langle \pi^+ | \Theta_{i,\mathrm{lat}}^{(8,8),(3/2)} | K^+ \rangle$ using the parametrization of Eq. (189). The data gives $O(1)$ coefficients for the chiral logarithm term, which are not currently known analytically.

i	$b_{i,0}^{(8,8)}$	$b_{i,1}^{(8,8)}$	$\xi_i^{(8,8)}$	χ^2/DOF
7	−0.003 23(13)	−0.0328(9)	set to 0	0.6(2)
7	−0.003 80(20)	−0.0334(9)	1.5(2)	0.1(3)
8	−0.0108(4)	−0.0801(27)	set to 0	0.2(1)
8	−0.0117(6)	−0.0809(25)	0.8(3)	0.1(2)

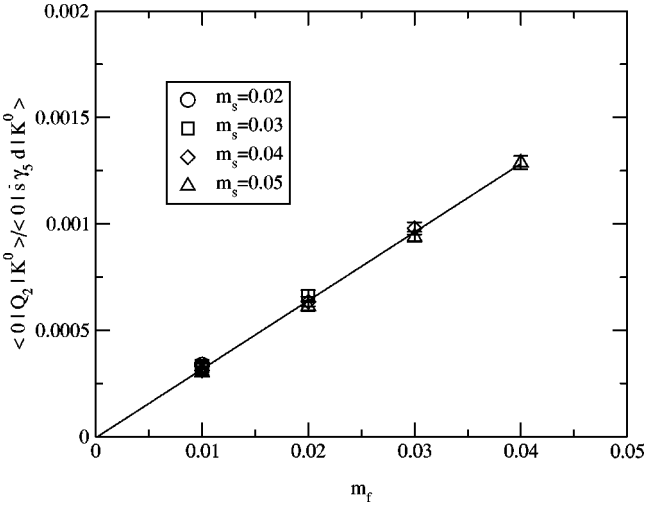

FIG. 17. The ratio $\langle 0|Q_2|K^0\rangle/\langle 0|\bar{s}\gamma_5 d|K^0\rangle$ vs $m_s'-m_d'$. The line is a linear fit of the form given in Eq. (192).

$K\to\pi\pi$ matrix elements, since this subtraction has not properly handled such finite corrections. However for these operators the physical value we seek is the extrapolation to the chiral limit, not the coefficient of the m_M^2 term, and the subtraction will only impact our ability to extrapolate to the (approximately known for finite L_s) chiral limit.

While a general approach to subtracting the power divergences is dictated by the requirement that we obtain $\langle \pi\pi|O_i|K\rangle$ to leading order in chiral perturbation theory, the specific subtraction procedure that we describe below is chosen so that all quadratic divergence is removed from the subtracted amplitude if $m_{\rm res}=0$. This ensures that our result will not be polluted by possibly large $1/a^2$ terms entering at higher order in chiral perturbation theory.

In this section, we will not report our results in terms of the various parameters $\alpha_1^{(8,1)}$ and $\alpha_2^{(8,1)}$, since there are many different (8,1) representations present in the operators in Eqs. (4)–(23) and each irreducible representation has its own values for $\alpha_1^{(8,1)}$ and $\alpha_2^{(8,1)}$. For each operator Q_i, we will determine a subtraction coefficient $\eta_{1,i}$, following the form of Eq. (87), through

$$\frac{\langle 0|Q_{i,\rm lat}|K^0\rangle}{\langle 0|(\bar{s}\gamma_5 d)_{\rm lat}|K^0\rangle}=\eta_{0,i}+\eta_{1,i}(m_s'-m_d'), \qquad (192)$$

where m_s' and m_d' are the nondegenerate quark masses used in the calculation of $K^0\to 0$ matrix elements. Corrections to this formula from higher order effects in chiral perturbation theory are free of power divergences. We expect that $\eta_{0,i}$ should be zero, but we add this free parameter to the fit to

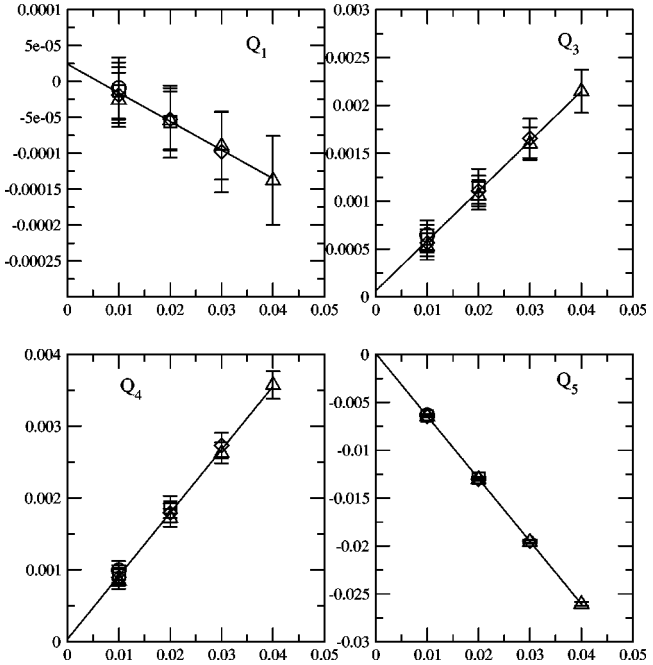

FIG. 19. The ratio $\langle 0|Q_i|K^0\rangle/\langle 0|\bar{s}\gamma_5 d|K^0\rangle$ vs $m_s'-m_d'$ for $i=1$, 3, 4, and 5. The line is a linear fit of the form given in Eq. (192). The symbols have the same meaning as in Fig. 18.

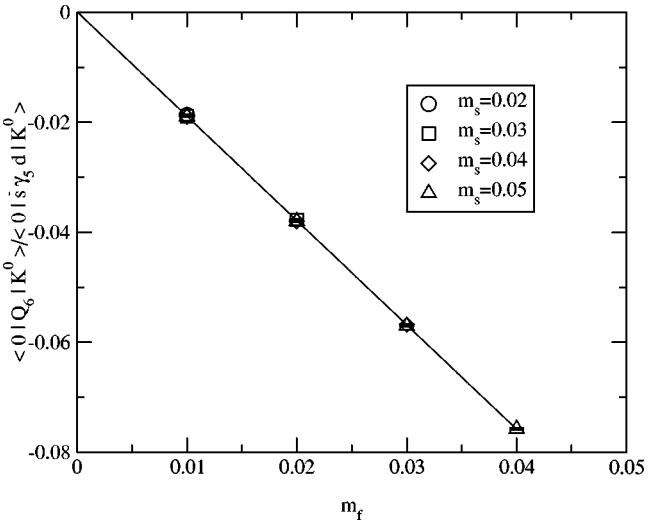

FIG. 18. The ratio $\langle 0|Q_6|K^0\rangle/\langle 0|\bar{s}\gamma_5 d|K^0\rangle$ vs $m_s'-m_d'$. The line is a linear fit of the form given in Eq. (192).

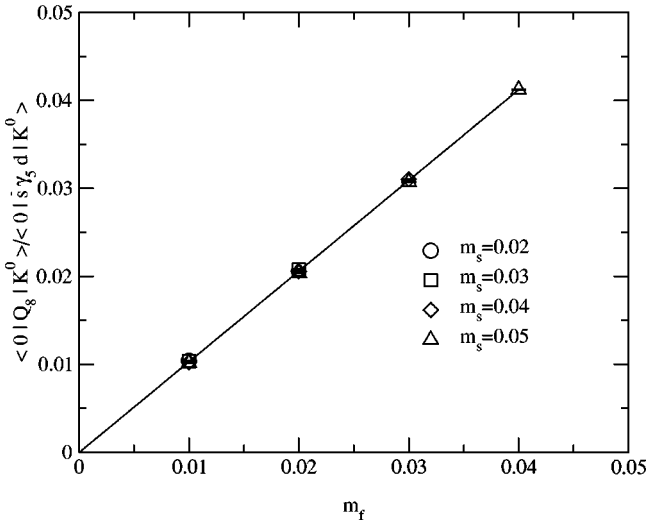

FIG. 20. The ratio $\langle 0|Q_8|K^0\rangle/\langle 0|\bar{s}\gamma_5 d|K^0\rangle$ vs $m_s'-m_d'$. The line is a linear fit of the form given in Eq. (192).

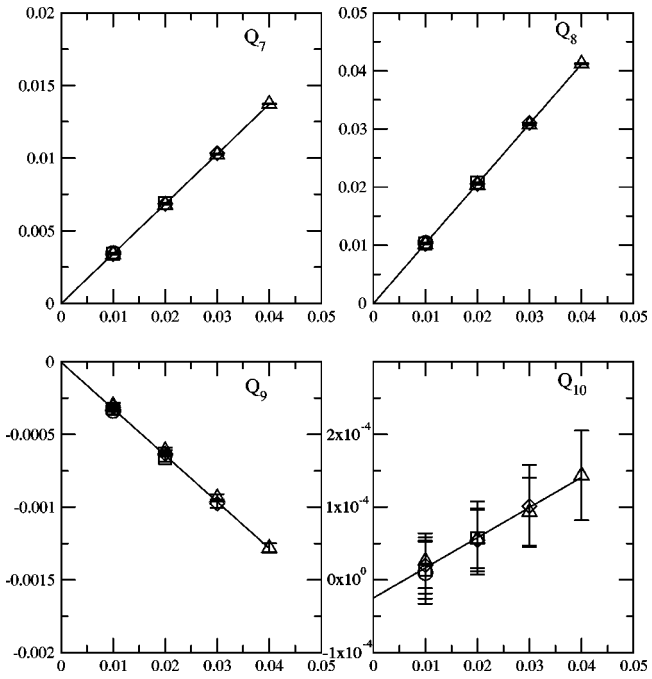

FIG. 21. The ratio $\langle 0|Q_i|K^0\rangle/\langle 0|\bar{s}\gamma_5 d|K^0\rangle$ vs $m_s'-m_d'$ for $i=7$, 8, 9, and 10. The line is a linear fit of the form given in Eq. (192). The symbols have the same meaning as in Fig. 18.

test that expectation. The arguments leading to Eq. (87) show that when, for example, $\alpha_2^{(8,1)}$ is very large, $\langle 0|Q_{i,\mathrm{lat}}|K^0\rangle/\langle 0|(\bar{s}\gamma_5 d)_{\mathrm{lat}}|K^0\rangle$ should not show the presence of chiral logarithms, since such terms appear only through $\alpha_1^{(8,1)}$. Thus, for large $\alpha_2^{(8,1)}$, where the subtraction is more delicate, the determination of the subtraction coefficient is easier since the linearity is better.

Starting from the values for $\langle 0|Q_{i,\mathrm{lat}}|K^0\rangle/\langle 0|(\bar{s}\gamma_5 d)_{\mathrm{lat}}|K^0\rangle$ given in Tables XXIV and XXV, we have plotted this ratio versus $m_s'-m_d'$ in Figs. 17–21. For Q_2, Q_6, and Q_8, graphs are shown with better resolution. Note that for Q_6 and Q_8 the y axis is a much larger scale than for Q_2. For Q_2, there is some deviation for different values of m_s' and m_d' with the same value for $m_s'-m_d'$, but within our statistics no clear conclusion can be drawn. For Q_6 and Q_8, any such deviation is much smaller, as would be expected for these operators with large power divergent contributions, but again deviations are within our statistical error.

The results for uncorrelated fits to this data are given in Table XXXI. One sees that $\eta_{1,6}$ is the largest subtraction coefficient and has a statistical error of about 0.2%. The other operators with large subtraction coefficients are Q_5, Q_7, and Q_8, which have comparable statistical precision. The good linearity of the data makes quoting such small statistical errors sensible. It is also vital that we know these subtraction coefficients to this accuracy, since there are $\mathcal{O}(a^{-2})$ divergences to cancel through this subtraction. Except for Q_7 and Q_8, $\eta_{0,i}$ is zero within statistical errors. For Q_7 and Q_8, $\eta_{0,i}$ is statistically nonzero, but very small in magnitude.

An important cross-check of our calculation is the comparison of the subtraction coefficients $\eta_{1,i}$, determined from

TABLE XXXI. Results for uncorrelated fits of $\langle 0|Q_{i,\mathrm{lat}}|K^0\rangle/\langle 0|(\bar{s}\gamma_5 d)_{\mathrm{lat}}|K^0\rangle$ to the form $\eta_{0,i}+\eta_{1,i}\ (m_s'-m_d')$. For Q_7 and Q_8 the value for $\eta_{0,i}$ is very small, but statistically nonzero.

i	$\eta_{0,i}$	$\eta_{1,i}$
1	$0.024(35)\times10^{-3}$	$-0.040(12)\times10^{-1}$
2	$-0.005(18)\times10^{-3}$	$3.220(59)\times10^{-2}$
3	$0.006(13)\times10^{-2}$	$0.521(42)\times10^{-1}$
4	$0.004(11)\times10^{-2}$	$0.883(36)\times10^{-1}$
5	$0.010(10)\times10^{-2}$	$-6.543(37)\times10^{-1}$
6	$0.077(71)\times10^{-3}$	$-18.978(36)\times10^{-1}$
7	$-1.285(74)\times10^{-5}$	$34.326(46)\times10^{-2}$
8	$-0.401(19)\times10^{-4}$	$10.307(14)\times10^{-1}$
9	$0.004(18)\times10^{-3}$	$-3.203(59)\times10^{-2}$
10	$-0.025(35)\times10^{-3}$	$0.042(12)\times10^{-1}$

properties of the operators in hadronic states, with the subtraction coefficients determined by the NPR procedure of Sec. VIII. A similar subtraction is performed there to remove the mixing between four quark operators and quark bilinears. This subtraction is done in Landau gauge fixed quark states at momentum scales $\geqslant 1.5$ GeV. Thus the two subtraction coefficients should not be identical. Only the power divergent parts should agree, since these are independent of external momenta. For the operators with the largest subtraction coefficients, the agreement should be quite close, since the large subtraction comes from the power divergent pieces dominating.

Table XXXII gives a comparison of the subtraction coefficients as determined from nonperturbative renormalization and the values from Table XXXI, which were determined from chiral perturbation theory in hadronic states. The nonperturbative renormalization subtraction coefficients are the values in the second column of Table IX minus the values in the second column of Table VI. The results in Table XXXII are also plotted in Fig. 22. For the $(V-A)\times(V+A)$ opera-

TABLE XXXII. A comparison of the subtraction coefficients in hadronic states, $\eta_{1,i}$, with those found from Landau gauge-fixed quark states. Divergent contributions, which are independent of external momenta, should give the same contribution to the two coefficients. For operators with large power divergent subtractions, like Q_6 and Q_8, the two coefficients are very similar.

i	$\eta_{1,i}$	NPR
1	−0.0040(12)	−0.0042(17)
2	0.032 20(59)	0.0031(91)
3	0.0521(42)	−0.006(20)
4	0.0883(36)	0.001(28)
5	−0.6543(37)	−0.672(12)
6	−1.8978(36)	−1.995(45)
7	0.343 26(46)	0.332(7)
8	1.0307(14)	0.993(20)
9	−0.032 03(59)	−0.0031(91)
10	0.0042(12)	

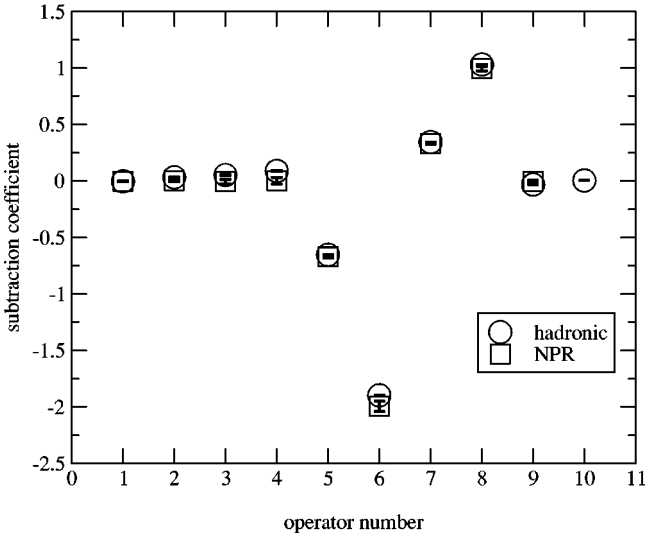

FIG. 22. The subtraction coefficients determined in hadronic states (○) compared with those determined in Landau gauge fixed quark states at $\mu = 2.13$ GeV (□). For the operators with large power divergences, the subtraction coefficients agree well since the external momentum does not enter the power divergent coefficient.

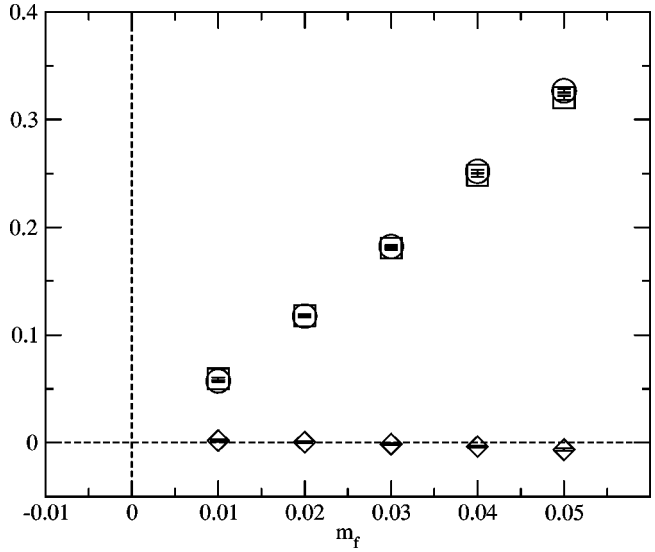

FIG. 23. The matrix elements $\langle \pi^+|Q_6|K^+\rangle$ (□), $2m_f|\eta_{1,6}|\langle \pi^+|(\bar{s}d)_{\rm lat}|K^+\rangle$ (○), and $\langle \pi^+|Q_6|K^+\rangle_{\rm sub}$ (◇) showing the noticeable, and very similar, nonlinearity in the first two quantities and the size of the subtraction for this left-right operator. The slope of the subtracted matrix element determines the desired $\alpha^{(8,1)}_{1,\rm lat}$ for Q_6 and is about 30 times smaller than the slope of the unsubtracted operator, and of opposite sign. Note that the subtracted operator does not vanish at $m_f = -m_{\rm res}$ since the divergent parts of the operator do not see only the chiral symmetry breaking of the low energy theory.

tors (Q_5, Q_6, Q_7, and Q_8) where the subtraction coefficients are the largest, the agreement between the two techniques is very good. This gives us confidence in the subtraction procedure, since the comparison is between quantities determined in entirely different ways using different computer programs for data generation and analysis. Note that the errors from the hadronic state calculation are considerably smaller.

B. Subtracted $\Delta I = 1/2$ matrix elements

The combination of terms on the left-hand side of Eq. (89) that removes chiral logarithm effects from the divergent parts of the operators can be written as

$$\langle \pi^+|Q^{(1/2)}_{i,\rm lat}|K^+\rangle_{\rm sub} \equiv \langle \pi^+|Q^{(1/2)}_{i,\rm lat}|K^+\rangle + \eta_{1,i}(m_s+m_d)\langle \pi^+|(\bar{s}d)_{\rm lat}|K^+\rangle. \tag{193}$$

It is easy to see that when written in this form, the subtraction required by chiral perturbation theory removes the entire $1/a^2$ divergence present in the original $\langle \pi^+|Q^{(1/2)}_{i,\rm lat}|K^+\rangle$ matrix element if $m_{\rm res}=0$. Usual power counting arguments, combined with exact chiral symmetry and the CPS symmetry of Ref. [12], dictate that all $1/a^2$ divergences which appear in the matrix elements of the operator $Q^{(1/2)}_{i,\rm lat}$ can be written as a divergent coefficient times matrix elements of the dimension-three operator $(m_d+m_s)\bar{s}d+(m_d-m_s)\bar{s}\gamma_5 d$. Equation (192) determines this coefficient as $\eta_{1,i}$ ensuring that the subtraction in Eq. (193) removes the entire $1/a^2$ divergent piece from the $Q^{(1/2)}_{i,\rm lat}$ matrix element.

In addition to chiral logarithm effects, we saw in Sec. VI C that the matrix element $\langle \pi^+|(\bar{s}d)_{\rm lat}|K^+\rangle$ is altered by zero modes for light quark masses. These same zero mode effects will also enter the divergent part of $\langle \pi^+|Q^{(1/2)}_{i,\rm lat}|K^+\rangle$ matrix elements. In particular, recalling Fig. 7, we are reminded that this matrix element is not well represented by a simple linear dependence on m_f. Again it is simpler to let the subtraction of matrix elements in Eq. (193) remove these nonlinear terms. Any remaining nonlinearities should be associated with the chiral logarithms on the right-hand side of Eq. (89) and near-zero mode effects in the finite terms. One once again avoids the possibility of failing to remove a divergent term which is multiplied by a higher order term in chiral perturbation theory.

With the values for the subtraction coefficients, $\eta_{1,i}$, from the previous section, we have calculated the subtracted matrix elements. To see the extent of the subtraction, in Fig. 23 we plot $\langle \pi^+|Q_{6,\rm lat}|K^+\rangle$, $2m_f|\eta_{1,6}|\langle \pi^+|(\bar{s}d)_{\rm lat}|K^+\rangle$, and $\langle \pi^+|Q_{6,\rm lat}|K^+\rangle_{\rm sub}$. The first two quantities show very similar nonlinearity and produce a subtracted matrix element which is much smaller. Given the large cancellation involved, the importance of removing divergence terms times higher order terms in chiral perturbation theory is clear.

The complete results for the subtracted matrix elements are given in Table XXXIII and are plotted versus m_f in Figs. 24–28. The subtraction is done under a jack-knife error loop, to make maximum use of any correlations in the values of $\langle \pi^+|Q^{(1/2)}_{i,\rm lat}|K^+\rangle$, $\eta_{1,i}$, and $\langle \pi^+|(\bar{s}d)_{\rm lat}|K^+\rangle$. The subtracted matrix elements for Q_2, Q_6, and Q_8 are shown on an expanded scale. Concentrating for a moment on Q_6 (Fig. 25), the graph for the subtracted operator reveals a number of important features.

TABLE XXXIII. Values of the $\Delta I=1/2$ matrix elements of the subtracted operators, $\langle \pi^+|Q^{(1/2)}_{i,\mathrm{lat}}|K^+\rangle_{\mathrm{sub}} \times 10^2$. This subtraction is done in hadronic states and removes the unphysical contribution to this matrix element for $i\neq 7$ and 8. For Q_7 and Q_8, the subtraction leaves a finite matrix element, whose value in the chiral limit is related to physical quantities.

i	$m_f=0.01$	$m_f=0.02$	$m_f=0.03$	$m_f=0.04$	$m_f=0.05$
1	0.018(24)	−0.001(27)	−0.031(29)	−0.065(32)	−0.101(36)
2	0.039(11)	0.082(13)	0.133(14)	0.194(16)	0.265(17)
3	0.123(84)	0.139(96)	0.13(10)	0.13(11)	0.14(13)
4	0.144(70)	0.222(80)	0.298(87)	0.393(96)	0.51(11)
5	0.127(74)	0.067(85)	−0.001(93)	−0.08(10)	−0.18(11)
6	0.193(75)	0.037(81)	−0.141(89)	−0.362(97)	−0.65(11)
7	−0.768(20)	−0.864(16)	−0.934(15)	−0.995(15)	−1.046(16)
8	−2.450(63)	−2.784(53)	−3.045(50)	−3.292(51)	−3.520(53)
9	−0.034(11)	−0.071(13)	−0.113(14)	−0.164(16)	−0.223(17)
10	−0.013(24)	0.013(27)	0.051(29)	0.095(32)	0.143(36)

(1) The presence of finite L_s and power divergent operators means that $\langle \pi^+|Q_{6,\mathrm{lat}}|K^+\rangle_{\mathrm{sub}}$ need not vanish at $m_f=0$ or $m_f=-m_{\mathrm{res}}$. This is obvious in the graph, where the matrix element vanishes around m_f of 0.02.

(2) For Q_i containing an (8,1) representation, only the slope of the subtracted matrix element is needed, so the ambiguities of $\mathcal{O}(m_{\mathrm{res}})$ in the chiral limit are unimportant. For (8,8) parts of an operator, such ambiguities prohibit a precise determination of the desired α's from the $\Delta I=1/2$ amplitudes.

(3) The subtracted values for Q_6 (and also Q_2 and Q_9) show some nonlinearity, although the effect is not conclusive given the statistical errors. We have not fit to the nonlinearities, since the coefficients of the chiral logarithms are not known for the (8,1) operators in quenched QCD. For the full QCD case, where they are known, the coefficient is 1/3, compared to 34/3 for the (27,1) operators. Thus we use simple linear fits and expect the corrections in the slope we seek, due to logarithms, to be small.

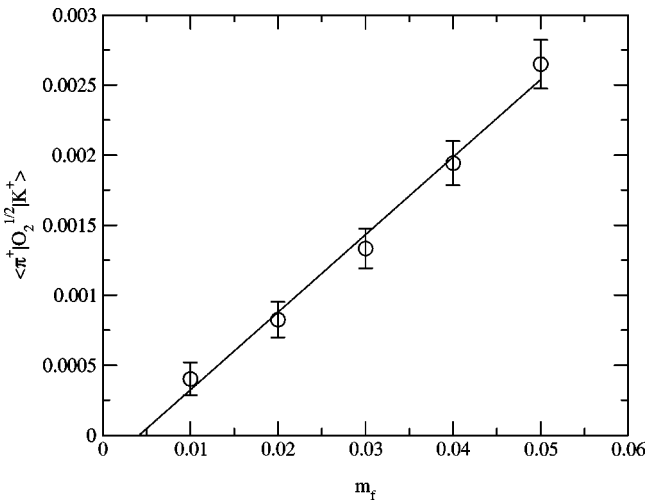

FIG. 24. The matrix element $\langle \pi^+|Q^{(1/2)}_{2,\mathrm{lat}}|K^+\rangle_{\mathrm{sub}}$ which has the divergent contribution removed. Due to the contact term in the Ward-Takahashi identity the matrix element does not vanish at $m_f=-m_{\mathrm{res}}$. The slope is related to the matrix elements we seek.

(4) Q_6 is a pure (8,1) operator, but for Q_1, Q_2, Q_9, and Q_{10}, which contain a (27,1) for which the chiral logarithm coefficient is known and large, fits could be done to incorporate this effect. However, the $\Delta I=1/2$ part of the (27,1) enters the total operator with a small coefficient (1/10 or 1/15). Also, since $\alpha^{(27,1),(1/2)}_{\mathrm{lat}}=\alpha^{(27,1),(3/2)}_{\mathrm{lat}}$ and $\alpha^{(27,1),(3/2)}_{\mathrm{lat}}$ is small, this particular chiral logarithm contribution should not be visible in our data.

(5) The lower points in the figure ($\diamond$) are the result if the subtraction in Eq. (193) has (m_s+m_d) changed to $(m_s+m_d+2m_{\mathrm{res}})$. This subtraction will also not exactly remove the $\mathcal{O}(m_{\mathrm{res}}/a^2)$ term, but the two subtractions show that chiral

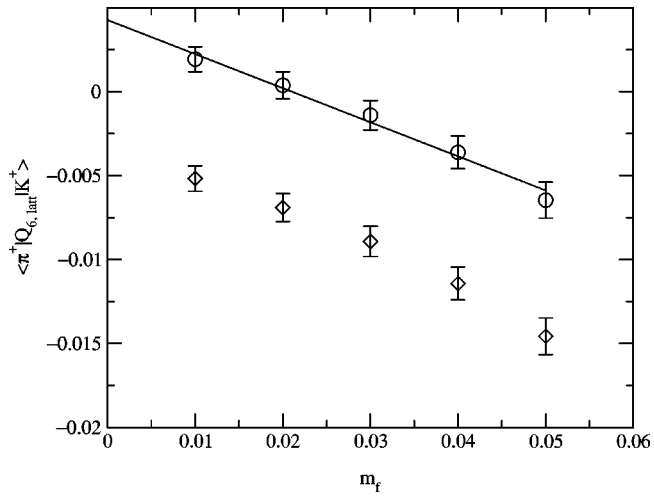

FIG. 25. The matrix element $\langle \pi^+|Q^{(1/2)}_{6,\mathrm{lat}}|K^+\rangle_{\mathrm{sub}}$ which has the divergent contribution removed (○). The subtraction does not remove the $O(m_{\mathrm{res}}/a^2)$ divergent term, so the matrix element does not vanish at $m_f=0$. The line is a linear fit to the data, since the chiral logarithm corrections are not known, and the slope of this line is related to physical matrix elements. From the data, nonlinear effects appear small. The lower points ($\diamond$) are the result if the subtraction in Eq. (193) has (m_s+m_d) changed to $(m_s+m_d+2m_{\mathrm{res}})$. This subtraction will also not exactly remove the $O(m_{\mathrm{res}}/a^2)$ term, but the two subtractions show that chiral symmetry breaking from finite L_s is quantitatively $O(m_{\mathrm{res}}/a^2)$.

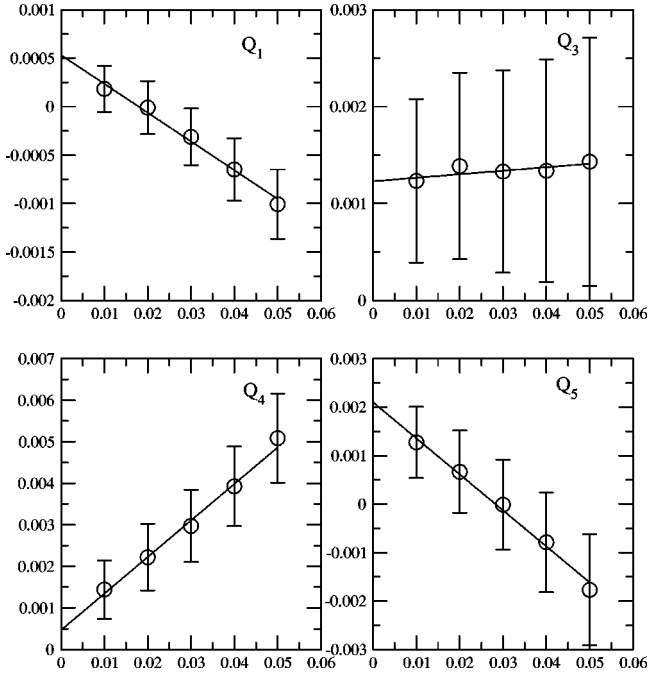

FIG. 26. The matrix element $\langle \pi^+ | Q^{(1/2)}_{i,\mathrm{lat}} | K^+ \rangle_{\mathrm{sub}}$, for $i=1$, 3, 4, and 5, which has the divergent contribution removed. Due to the contact term in the Ward-Takahashi identity the matrix element does not vanish at $m_f = -m_{\mathrm{res}}$.

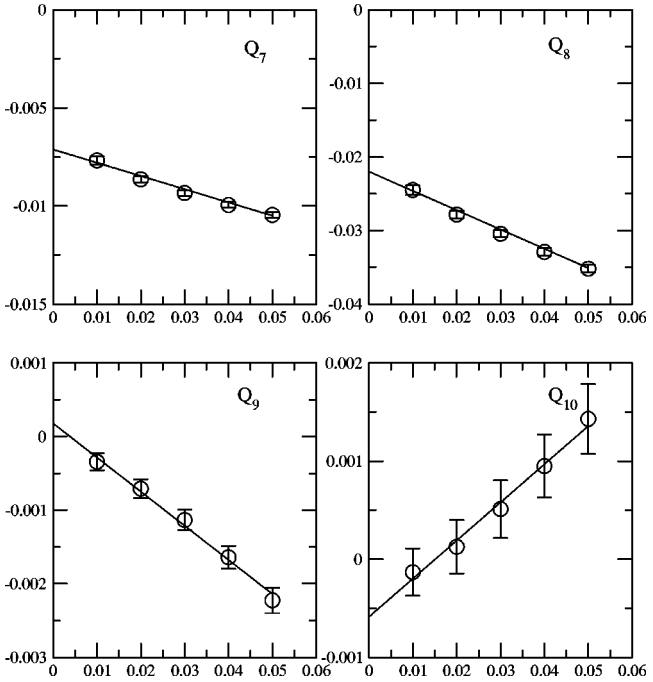

FIG. 28. The matrix element $\langle \pi^+ | Q^{(1/2)}_{i,\mathrm{lat}} | K^+ \rangle_{\mathrm{sub}}$, for $i=7$, 8, 9, and 10, which has the divergent contribution removed. For Q_9 and Q_{10}, the slope is needed to determine the $K \to \pi\pi$ matrix elements. Q_7 and Q_8 are shown for completeness.

symmetry breaking from finite L_s is quantitatively $\mathcal{O}(m_{\mathrm{res}}/a^2)$.

We have fitted the subtracted operators to a linear function parametrized by

$$\langle \pi^+ | Q^{(1/2)}_{i,\mathrm{lat}} | K^+ \rangle_{\mathrm{sub}} = c_{0,i} + c_{1,i} m_f \tag{194}$$

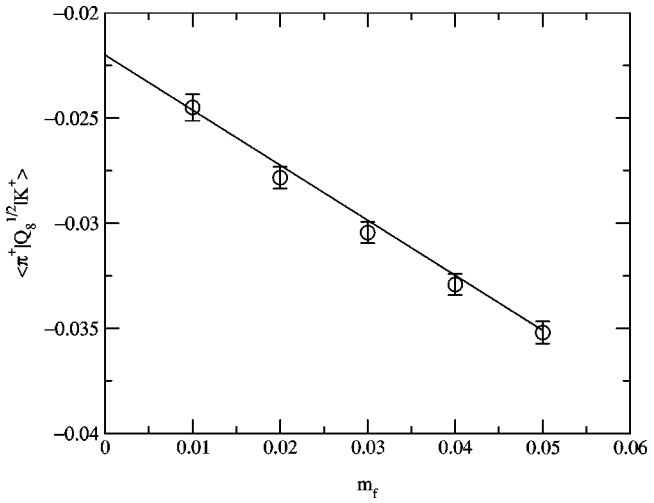

FIG. 27. The matrix element $\langle \pi^+ | Q^{(1/2)}_{8,\mathrm{lat}} | K^+ \rangle_{\mathrm{sub}}$ which has the divergent contribution removed. Due to the power divergence of this operator, the value of m_f needed to cancel the chiral symmetry breaking effects of finite L_s is not precisely known. Thus we do not know where to evaluate this matrix element to get $\alpha_8^{(8,8)}$ and must rely on the $\Delta I = 3/2$ amplitude to determine this quantity.

with the results given in Table XXXIV. These are uncorrelated linear fits to all five quark masses. We see that for Q_6, in spite of the very large subtraction involved, the slope of $\langle \pi^+ | Q^{(1/2)}_{i,\mathrm{lat}} | K^+ \rangle_{\mathrm{sub}}$ is determined with a statistical error of about 10%.

For Q_7 and Q_8, we can start from the fits given in Table XXXIV and compare the value for the $\Delta I = 1/2$ matrix elements with the value expected from the $\Delta I = 3/2$ matrix elements. Since $\alpha^{(8,8),(1/2)}_{i,\mathrm{lat}} = 2\alpha^{(8,8),(3/2)}_{i,\mathrm{lat}}$ for $i=7$ and 8, we can

TABLE XXXIV. Results for linear fits of $\langle \pi^+ | Q^{(1/2)}_{i,\mathrm{lat}} | K^+ \rangle_{\mathrm{sub}}$ to the form of Eq. (194). The slope of the fit, given by $c_{1,i}$, is related to the low energy constant needed to determine $K \to \pi\pi$ matrix elements for $i \neq 7$ and 8. For $i=7$ and 8, the matrix element in the chiral limit is the physical quantity we seek, but the chiral limit is uncertain for these power divergent operators at finite L_s. For these operators, we use the $\Delta I = 3/2$ part of the operator to determine the $\Delta I = 1/2$ part.

i	$c_{0,i}$	$c_{1,i}$	χ^2/DOF
1	0.000 53(27)	−0.0297(78)	0.05(8)
2	−0.000 24(13)	0.0555(40)	0.6(3)
3	0.001 23(97)	0.0036(284)	0.004(12)
4	0.000 47(80)	0.089(24)	0.04(6)
5	0.002 10(84)	−0.074(25)	0.02(4)
6	0.004 26(84)	−0.203(25)	0.3(2)
7	−0.007 20(21)	−0.0675(37)	0.8(3)
8	−0.0223(7)	−0.262(12)	0.4(2)
9	0.000 18(13)	−0.0464(40)	0.4(2)
10	−0.000 59(27)	0.0389(79)	0.09(10)

TABLE XXXV. The lattice values for the low energy, chiral perturbation theory constants for $\Delta I=1/2$ amplitudes for $i\neq 7$ and 8. These were determined from subtracted $K^+\to\pi^+$ matrix elements.

i	$\alpha_{i,\mathrm{lat}}^{(1/2)}$
1	$-1.19(31)\times 10^{-5}$
2	$2.22(16)\times 10^{-5}$
3	$0.15(113)\times 10^{-5}$
4	$3.55(96)\times 10^{-5}$
5	$-2.97(100)\times 10^{-5}$
6	$-8.12(98)\times 10^{-5}$
9	$-1.85(16)\times 10^{-5}$
10	$1.55(31)\times 10^{-5}$

use the values for $\alpha_{i,\mathrm{lat}}^{(8,8),(3/2)}$ given in Sec. X B to find

$$\alpha_{7,\mathrm{lat}}^{(8,8),(1/2)}=-3.22(16)\times 10^{-6}, \tag{195}$$

$$\alpha_{8,\mathrm{lat}}^{(8,8),(1/2)}=-9.92(54)\times 10^{-6}. \tag{196}$$

The unsubtracted $\Delta I=1/2$ matrix elements should have the form

$$\langle\pi^+|Q_{i,\mathrm{lat}}^{(1/2)}|K^+\rangle=c_{0,i}+c_{1,i}(m_f+m_{\mathrm{res}})+c_{1,i}^{\mathrm{div}}[m_f+O(m_{\mathrm{res}})]. \tag{197}$$

From Table XXII and Eq. (193) one sees that $c_{1,7}^{\mathrm{div}}\sim -1.3$ and $c_{1,8}^{\mathrm{div}}\sim -3.9$. Using these values and $m_{\mathrm{res}}=0.00124$ gives a m_f independent contribution to the $i=7$ and 8 matrix elements of $\mathcal{O}(0.0016)$ and $\mathcal{O}(0.0044)$ from contact terms in the Ward-Takahashi identities. The values for $c_{0,i}$ for $i=7$ and 8 are given in Table XXXIV and are $-0.00720(21)$ and $-0.0223(7)$, respectively. Thus the expected uncertainty due to finite L_s in determining $\alpha_{i,\mathrm{lat}}^{(8,8),(1/2)}$ from the subtracted $\Delta I=1/2$ amplitudes is about 20% in both cases. Using these values for $c_{0,i}$ yields

$$\alpha_{7,\mathrm{lat,sub}}^{(8,8),(1/2)}=-3.05(9)\times 10^{-6}, \tag{198}$$

$$\alpha_{8,\mathrm{lat,sub}}^{(8,8),(1/2)}=-9.44(30)\times 10^{-6}. \tag{199}$$

The agreement with the results from the $\Delta I=3/2$ matrix elements is better than might be expected. However, the $\Delta I=3/2$ fits include chiral logarithm corrections which change the results by 15% for $i=7$ and 8% for $i=8$. The change happens to improve the agreement with the values from the subtracted operators. However, this general agreement does demonstrate the reliability of the subtraction of the power divergent operators.

TABLE XXXVI. The lattice values for the $\Delta I=1/2$ and $\Delta I=3/2$ low energy, chiral perturbation theory constants determined from $K^+\to\pi^+$ matrix elements not requiring subtraction.

Parameter	Value
$\alpha_{\mathrm{lat}}^{(27,1),(1/2)}$	$-4.13(18)\times 10^{-6}$
$\alpha_{7,\mathrm{lat}}^{(8,8),(1/2)}$	$-3.22(16)\times 10^{-6}$
$\alpha_{8,\mathrm{lat}}^{(8,8),(1/2)}$	$-9.92(54)\times 10^{-6}$
$\alpha_{\mathrm{lat}}^{(27,1),(3/2)}$	$-4.13(18)\times 10^{-6}$
$\alpha_{7,\mathrm{lat}}^{(8,8),(3/2)}$	$-1.61(8)\times 10^{-6}$
$\alpha_{8,\mathrm{lat}}^{(8,8),(3/2)}$	$-4.96(27)\times 10^{-6}$

TABLE XXXVII. Central values for standard model parameters and experimental results relevant to the calculations presented in this paper. All values are from the 2000 Particle Data Book unless otherwise noted. The central values for λ_{CKM}, A_{CKM}, $\overline{\rho}_{\mathrm{CKM}}$, and $\overline{\eta}_{\mathrm{CKM}}$ are taken, without errors. Current errors on all quantities in the table which enter as inputs in our calculation have virtually no effect on our results.

Quantity	Central value	Comments and references
m_{π^+}	139.57 MeV	
m_{π^0}	134.98 MeV	
f_{π^+}	130.7 MeV	
m_{K^+}	493.68 MeV	
m_{K^0}	497.67 MeV	
f_{K^+}	159.8 MeV	
G_F	1.166×10^{-5} GeV^{-2}	
λ_{CKM}	0.2237	[89]
A_{CKM}	0.819	[89]
$\overline{\rho}_{\mathrm{CKM}}$	0.222	[89]
$\overline{\eta}_{\mathrm{CKM}}$	0.316	[89]
ρ_{CKM}	0.228	From λ_{CKM}, $\overline{\rho}_{\mathrm{CKM}}$, and $\overline{\eta}_{\mathrm{CKM}}$
η_{CKM}	0.324	From λ_{CKM}, $\overline{\rho}_{\mathrm{CKM}}$, and $\overline{\eta}_{\mathrm{CKM}}$
$\lvert V_{us}\rvert$	0.2237	$\equiv\lambda_{\mathrm{CKM}}$
$\lvert V_{ud}\rvert$	0.9747	
$\lvert V_{cb}\rvert$	0.0410	$=A_{\mathrm{CKM}}\lambda_{\mathrm{CKM}}^2$
V_{td}	$0.007\,08-0.002\,97i$	
τ	$0.001\,33-0.000\,559i$	
ϵ	2.271×10^{-3}	
$\mathrm{Re}\,A_0$	3.33×10^{-7} GeV	
ω	0.045	
$\mathrm{Re}(\epsilon'/\epsilon)$	$(20.7\pm 2.8)\times 10^{-4}$	KTEV [3]
	$(15.3\pm 2.6)\times 10^{-4}$	NA48 [5]

Defining constants $\alpha_{i,\mathrm{lat}}^{(1/2)}$ for $i\neq 7,8$ through

$$\langle\pi^+|Q_{i,\mathrm{lat}}^{(1/2)}|K^+\rangle_{\mathrm{sub}}\equiv\frac{4m_M^2}{f^2}\alpha_{i,\mathrm{lat}}^{(1/2)} \tag{200}$$

and using $m_M^2=3.18(m_f+m_{\mathrm{res}})$ gives the values in Table XXXV. We collect the α's determined without requiring subtractions in Table XXXVI. Finally Table XXXV gives the $\Delta I=1/2$ and $\Delta I=3/2$ values for α_i for the ten operators in the basis used in the three-quark effective theory. These are our results for the lattice values for the constants determining kaon matrix elements in lowest order chiral perturbation theory from quenched QCD and domain wall fermions. In the next two sections we will combine these values with the Wilson coefficients of Sec. VII, the Z factors from Sec. VIII, and known experimental quantities to give physical values for the real and imaginary parts of isospin zero and two amplitudes for $K\to\pi\pi$.

XII. PHYSICAL MATRIX ELEMENTS

The physical values for $K\to\pi\pi$ amplitudes can now be calculated from the effective Hamiltonian in Eq. (3) using the Wilson coefficients in Tables III and IV, the $\hat{Z}_{ij}^{\rm NPR}/Z_q^2$ values from nonperturbative renormalization in Tables XIV and XV, the value $Z_q=0.808(3)(15)$ from Table II of [59], the chiral perturbation theory formulas in Eqs. (65) and (67), the central values for standard model parameters in Table XXXVII, and the values for $\alpha_{j,\rm lat}^{(1/2)}$ and $\alpha_{j,\rm lat}^{(3/2)}$ from Table XXXVIII. The explicit formula is

$$\langle\pi\pi_{(I)}|-i\mathcal{H}^{(\Delta S=1)}|K^0\rangle=-i\sqrt{\frac{3}{4}}G_F V_{ud}V_{us}^*\sum_{i=1}^{10}\sum_{j=1,j\neq 4}^{8}[z_i(\mu)+\tau y_i(\mu)]\hat{Z}_{ij}^{\rm NPR}(\mu)$$
$$\times\begin{cases}\dfrac{4i}{f^3}\alpha_{j,\rm lat}^{(1/2)}(m_{K^0}^2-m_{\pi^+}^2)a^{-4} & I=0,\ j=1,2,3,5,6\\ \dfrac{-4\sqrt{2}i}{f^3}\alpha_{j,\rm lat}^{(3/2)}(m_{K^0}^2-m_{\pi^+}^2)a^{-4} & I=2,\ j=1,2,3,5,6\\ \dfrac{-12i}{f^3}\alpha_{j,\rm lat}^{(1/2)}a^{-6} & I=0,\ j=7,8\\ \dfrac{-12\sqrt{2}i}{f^3}\alpha_{j,\rm lat}^{(3/2)}a^{-6} & I=2,\ j=7,8\end{cases}, \tag{201}$$

where a^{-1}, the inverse lattice spacing, is 1.922 GeV [21]. Before discussing the numerical values produced from our data, we will outline our strategy for making the transition from the quenched QCD matrix elements we have calculated to the full QCD matrix elements needed for comparison with the physical world. We can then assess the impact of the known chiral logarithms in full QCD on our results and also discuss how sensitive our results are to the values of the standard model parameters given in Table XXXVII.

For our lattice calculation we have used a quenched value for f, which is defined in the chiral limit, of 137 MeV [21]. There is no reason why this value must agree with the full QCD value of $f_{\rm QCD}\approx 120$ MeV. In quenched chiral perturbation theory, $f_\pi^{(1\ \rm loop)}$ and $f_K^{(1\ \rm loop)}$ do not contain any conventional chiral logarithms, only quenched chiral logarithms which we have argued are small. This is consistent with the linear quark mass behavior seen in [21] in the determination of f. In relating lattice $K\to\pi$ matrix elements to lattice $K\to\pi\pi$ matrix elements, one should use this f. For small quark masses, the resulting lattice $K\to\pi\pi$ matrix elements should be equal to those explicitly calculated via a technique such as has been proposed by Lellouch and Luscher [47], provided the quenched theory does not corrupt the full QCD relations between $K\to\pi$ and $K\to\pi\pi$.

TABLE XXXVIII. The lattice values for the low energy, chiral perturbation theory constants decomposed by isospin for Q_1 to Q_{10}.

i	$\alpha_{i,\rm lat}^{(1/2)}$	$\alpha_{i,\rm lat}^{(3/2)}$
1	$-1.19(31)\times10^{-5}$	$-1.38(6)\times10^{-6}$
2	$2.22(16)\times10^{-5}$	$-1.38(6)\times10^{-6}$
3	$0.15(113)\times10^{-5}$	0.0
4	$3.55(96)\times10^{-5}$	0.0
5	$-2.97(100)\times10^{-5}$	0.0
6	$-8.12(98)\times10^{-5}$	0.0
7	$-3.22(16)\times10^{-6}$	$-1.61(8)\times10^{-6}$
8	$-9.92(54)\times10^{-6}$	$-4.96(27)\times10^{-6}$
9	$-1.85(16)\times10^{-5}$	$-2.07(9)\times10^{-6}$
10	$1.55(31)\times10^{-5}$	$-2.07(9)\times10^{-6}$

We will make the transition from the quenched theory to full QCD at the level of the matrix elements $\langle\pi\pi|Q_i|K^0\rangle$ and not at the level of the lattice constants $\alpha_{i,\rm lat}$. Since the $\alpha_{i,\rm lat}$ factors in Eq. (201) are multiplied by f^{-3}, changing from f to $f_{\rm QCD}$ would be a large effect and a factor of f^2 has already entered in the calculation of the $\alpha_{i,\rm lat}$ from our lattice data. For the $\langle\pi\pi|Q_i|K^0\rangle$ matrix elements which vanish in the chiral limit, we have actually only determined the slope of the matrix element. The matrix element itself involves using chiral perturbation theory to extrapolate to the kaon mass. This extrapolation introduces an additional choice in relating quenched matrix elements to those in full QCD.

With this strategy of using the values for quenched $K\to\pi\pi$ matrix elements as estimates for full QCD, we consider two choices for the extrapolation to the kaon scale. The first choice involves extrapolating to the kaon mass for (8,1) and (27,1) operators using lowest order chiral perturbation theory in the quenched theory. The second extrapolates to the kaon scale in the full theory and incorporates the known and estimated chiral logarithms for the $K\to\pi\pi$ matrix elements in full QCD. We now discuss these choices in detail.

(1) Physical values for $m_{K^0}^2$ and $m_{\pi^+}^2$ are used in Eq. (201). For (8,1) and (27,1) operators, this can be thought of as an extrapolation to the physical kaon mass in quenched QCD using lowest order chiral perturbation theory, since we

TABLE XXXIX. The contribution in GeV from the renormalized continuum operator $Q_{i,\mathrm{cont}}$ to the real parts of $\langle(\pi\pi)_I|-i\mathcal{H}^{(\Delta S=1)}|K^0\rangle$ for $\mu=1.51$ GeV. The central values for the standard model parameters given in Table XXXVII have been used.

	Real A_0		Real A_2	
i	choice 1	choice 2	choice 1	choice 2
1	$3.02(68)\times10^{-8}$	$4.28(97)\times10^{-8}$	$-4.11(18)\times10^{-9}$	$-4.82(22)\times10^{-9}$
2	$2.00(18)\times10^{-7}$	$2.83(25)\times10^{-7}$	$1.392(62)\times10^{-8}$	$1.635(73)\times10^{-8}$
3	$1.4(29)\times10^{-10}$	$2.0(41)\times10^{-10}$	0.0	0.0
4	$-3.80(84)\times10^{-9}$	$-5.4(12)\times10^{-9}$	0.0	0.0
5	$-6.9(29)\times10^{-10}$	$-9.8(41)\times10^{-10}$	0.0	0.0
6	$4.99(77)\times10^{-9}$	$7.1(11)\times10^{-9}$	0.0	0.0
7	$4.04(21)\times10^{-11}$	$8.00(42)\times10^{-11}$	$2.86(15)\times10^{-11}$	$3.63(19)\times10^{-11}$
8	$-5.74(32)\times10^{-11}$	$-1.137(63)\times10^{-10}$	$-4.06(22)\times10^{-11}$	$-5.15(28)\times10^{-11}$
9	$-3.91(39)\times10^{-12}$	$-5.54(56)\times10^{-12}$	$4.69(21)\times10^{-13}$	$5.51(25)\times10^{-13}$
10	$2.27(41)\times10^{-12}$	$3.23(59)\times10^{-12}$	$3.70(17)\times10^{-13}$	$4.35(20)\times10^{-13}$

have found the quenched chiral logarithms to be small and there are no conventional chiral logarithms in these masses in the quenched theory. These quenched $K\to\pi\pi$ matrix elements with $m^2_{K^0}$ and $m^2_{\pi^+}$ taking their physical values are taken as the matrix elements for full QCD. The same results would be achieved by a lowest order extrapolation in full QCD, except that the use of the physical kaon and pion masses is somewhat ambiguous, since physical masses include chiral logarithm corrections if the quark masses are taken as known input parameters. This ambiguity would change the matrix elements at the 10% level.

(2) We extrapolate to the physical kaon mass in full QCD, including the chiral logarithm corrections. For the (8,1) and $\Delta I=3/2$ part of the (27,1) operators the quenched slope is taken for the full QCD value and the known chiral logarithms in full QCD [53,76] are used in the extrapolation. For (8,8) operators, the nonzero value in the quenched chiral limit is taken directly to full QCD. Recent work on the electroweak penguins [77] allows us to estimate the coefficients of the chiral logarithm term. These authors write the matrix elements for the electroweak penguins at $\mathcal{O}(p^2)$ as $M_I=M_I^{(0)}(1+\Delta_I)$ where $M_I^{(0)}$ is the lowest order value as given in Eq. (67). They find $\Delta_0=0.98\pm0.55$ and $\Delta_2=0.27\pm0.27$ and state that Δ_I only includes the contributions from chiral logarithms. The errors they quote come from varying $\Lambda_{Q\chi PT}$. If we assume the correction is all from a chiral logarithm term $L_\chi(m_K)$, then the coefficient of this term would be ~-8.4 for $I=0$ and ~-2.3 for $I=2$.

Thus, for our second extrapolation choice, where chiral logarithms are included, we modify the second line of Eq. (201) to

$$\times\begin{cases}\dfrac{4i}{f^3}\alpha^{(1/2)}_{j,\mathrm{lat}}(m^2_{K^0}-m^2_{\pi^+})a^{-4} & \left[1-\dfrac{97}{27}L_\chi(m_K)\right] \quad I=0,\ j=1,2,3,5,6\\ \dfrac{-4\sqrt{2}i}{f^3}\alpha^{(3/2)}_{j,\mathrm{lat}}(m^2_{K^0}-m^2_{\pi^+})a^{-4} & \left[1-\dfrac{3}{2}L_\chi(m_K)\right] \quad I=2,\ j=1,2,3,5,6\\ \dfrac{-12i}{f^3}\alpha^{(1/2)}_{j,\mathrm{lat}}a^{-6} & [1-8.4L_\chi(m_K)] \quad I=0,\ j=7,8\\ \dfrac{-12\sqrt{2}i}{f^3}\alpha^{(3/2)}_{j,\mathrm{lat}}a^{-6} & [1-2.3L_\chi(m_K)] \quad I=2,\ j=7,8\end{cases}. \tag{202}$$

In these equations, the physical values for $m^2_{K^0}$ and $m^2_{\pi^+}$ should be used. We use our quenched value for f in the $1/(4\pi f)^2$ factor in the chiral logarithms. In addition to estimating the coefficient of the chiral logarithm term for the (8,8) operators, we have also used the (8,1) chiral logarithm for all of the nonelectroweak $\Delta I=1/2$ matrix elements. This is a very good approximation, since the $\Delta I=1/2$ part of the (27,1) operator contributes very little here as can be seen from the size of $\alpha^{(27,1),(1/2)}_{\mathrm{lat}}$.

XIII. REAL A_0, A_2, AND B_K

Following the procedure of the previous section, we now proceed to our results for $\mathrm{Re}(A_0)$ and $\mathrm{Re}(A_2)$ and the ΔI

TABLE XL. The contribution in GeV from the renormalized continuum operator $Q_{i,\mathrm{cont}}$ to the imaginary parts of $\langle(\pi\pi)_I|-i\mathcal{H}^{(\Delta S=1)}|K^0\rangle$ for $\mu=1.51$ GeV. The central values for the standard model parameters given in Table XXXVII have been used.

	Imaginary A_0		Imaginary A_2	
i	choice 1	choice 2	choice 1	choice 2
1	0.0	0.0	0.0	0.0
2	0.0	0.0	0.0	0.0
3	$-4.7(94)\times10^{-13}$	$-7.(13)\times10^{-13}$	0.0	0.0
4	$8.2(18)\times10^{-12}$	$1.17(26)\times10^{-11}$	0.0	0.0
5	$4.7(20)\times10^{-13}$	$6.7(28)\times10^{-13}$	0.0	0.0
6	$-1.72(27)\times10^{-11}$	$-2.45(38)\times10^{-11}$	0.0	0.0
7	$7.57(39)\times10^{-14}$	$1.498(78)\times10^{-13}$	$5.35(28)\times10^{-14}$	$6.78(35)\times10^{-14}$
8	$-1.787(98)\times10^{-12}$	$-3.54(19)\times10^{-12}$	$-1.263(70)\times10^{-12}$	$-1.602(88)\times10^{-12}$
9	$-9.45(95)\times10^{-13}$	$-1.34(14)\times10^{-12}$	$1.135(51)\times10^{-13}$	$1.334(60)\times10^{-13}$
10	$-2.25(41)\times10^{-13}$	$-3.19(58)\times10^{-13}$	$-3.66(16)\times10^{-14}$	$-4.30(19)\times10^{-14}$

$=1/2$ rule. These amplitudes are expected to come predominantly from the current–current operators Q_1 and Q_2, as seen in the relative sizes of the Wilson coefficients $z_i(\mu)$ and $y_i(\mu)$ given in Tables III and IV. (Such a statement depends on the scale μ under consideration, since the operators mix under renormalization.) As such, they are quite independent of V_{td} and CP violation effects in the standard model and provide an independent forum for comparison between our quenched lattice QCD calculations and experimental results. We conclude with our results for B_K, since it is determined by the matrix elements of the same (27, 1) operator that determines Re(A_2).

Using our data and Eqs. (201) and (202) produces the values for Re(A_0), Re(A_2), Im(A_0), and Im(A_2) in Tables XXXIX–XLVI. Here the contribution to $\langle\pi\pi_{(I)}|-i\mathcal{H}^{(\Delta S=1)}|K^0\rangle$ is decomposed into contributions for each value of the index i in Eqs. (201) and (202). We will refer to this as the full contribution to $\langle\pi\pi_{(I)}|-i\mathcal{H}^{(\Delta S=1)}|K^0\rangle$ from the continuum operator $Q_{i,\mathrm{cont}}$. These tables use the central values for standard model parameters given in Table XXXVII. The matching scale μ is 1.51 GeV for Tables XXXIX and XL, 2.13 GeV for Tables XLI and XLII, 2.39 GeV for Tables XLIII and XLIV, and 3.02 GeV for Tables XLV and XLVI. It should be noted that the continuum operators mix when this scale is changed, so the decomposition of the physical amplitudes into particular $Q_{i,\mathrm{cont}}$ contributions will change. Only the complete amplitude should be insensitive to scale and this will only occur if the Wilson coefficients and nonperturbative renormalization factors are known to all orders in α_S. In addition, we always use $Z_q(\mu)$ for $\mu=2.0$ GeV in the matching, since in the determination of $Z_q(\mu)$ the running effects were found to be quite small [59]. (The one-loop anomalous dimension for Z_q vanishes in Landau gauge.) The scale dependence of our results will be an important test of our calculation.

Results for the two choices for extrapolation discussed in Sec. XII are given in Tables XXXIX–XLVI. The first choice, a zero-loop extrapolation in quenched QCD, and the second, a one-loop extrapolation in full QCD, differ by no more than $\sim$40%, except for the contributions to A_0 coming from

TABLE XLI. The contribution in GeV from the renormalized continuum operator $Q_{i,\mathrm{cont}}$ to the real parts of $\langle(\pi\pi)_I|-i\mathcal{H}^{(\Delta S=1)}|K^0\rangle$ for $\mu=2.13$ GeV. The central values for the standard model parameters given in Table XXXVII have been used.

	Real A_0		Real A_2	
i	choice 1	choice 2	choice 1	choice 2
1	$2.69(61)\times10^{-8}$	$3.82(87)\times10^{-8}$	$-3.64(16)\times10^{-9}$	$-4.27(19)\times10^{-9}$
2	$1.81(12)\times10^{-7}$	$2.57(17)\times10^{-7}$	$1.371(61)\times10^{-8}$	$1.610(72)\times10^{-8}$
3	$1.(13)\times10^{-11}$	$2.(18)\times10^{-11}$	0.0	0.0
4	$-1.46(33)\times10^{-9}$	$-2.07(47)\times10^{-9}$	0.0	0.0
5	$-4.4(18)\times10^{-10}$	$-6.3(26)\times10^{-10}$	0.0	0.0
6	$3.09(38)\times10^{-9}$	$4.38(54)\times10^{-9}$	0.0	0.0
7	$5.32(27)\times10^{-11}$	$1.054(54)\times10^{-10}$	$3.76(19)\times10^{-11}$	$4.77(24)\times10^{-11}$
8	$-1.785(97)\times10^{-10}$	$-3.53(19)\times10^{-10}$	$-1.262(68)\times10^{-10}$	$-1.601(87)\times10^{-10}$
9	$-2.59(20)\times10^{-12}$	$-3.68(28)\times10^{-12}$	$3.43(15)\times10^{-13}$	$4.03(18)\times10^{-13}$
10	$5.14(94)\times10^{-12}$	$7.3(13)\times10^{-12}$	$8.33(37)\times10^{-13}$	$9.79(44)\times10^{-13}$

TABLE XLII. The contribution in GeV from the renormalized continuum operator $Q_{i,\mathrm{cont}}$ to the imaginary parts of $\langle(\pi\pi)_I|-i\mathcal{H}^{(\Delta S=1)}|K^0\rangle$ for $\mu=2.13$ GeV. The central values for the standard model parameters given in Table XXXVII have been used.

	Imaginary A_0		Imaginary A_2	
i	choice 1	choice 2	choice 1	choice 2
1	0.0	0.0	0.0	0.0
2	0.0	0.0	0.0	0.0
3	$-7.(87)\times10^{-14}$	$-1.(12)\times10^{-13}$	0.0	0.0
4	$7.2(16)\times10^{-12}$	$1.02(23)\times10^{-11}$	0.0	0.0
5	$6.3(26)\times10^{-13}$	$9.0(36)\times10^{-13}$	0.0	0.0
6	$-2.12(26)\times10^{-11}$	$-3.00(37)\times10^{-11}$	0.0	0.0
7	$6.95(36)\times10^{-14}$	$1.376(70)\times10^{-13}$	$4.91(25)\times10^{-14}$	$6.23(32)\times10^{-14}$
8	$-1.583(86)\times10^{-12}$	$-3.13(17)\times10^{-12}$	$-1.119(61)\times10^{-12}$	$-1.419(77)\times10^{-12}$
9	$-8.43(64)\times10^{-13}$	$-1.196(91)\times10^{-12}$	$1.114(50)\times10^{-13}$	$1.309(59)\times10^{-13}$
10	$-2.01(37)\times10^{-13}$	$-2.85(52)\times10^{-13}$	$-3.25(15)\times10^{-14}$	$-3.82(17)\times10^{-14}$

TABLE XLIII. The contribution in GeV from the renormalized continuum operator $Q_{i,\mathrm{cont}}$ to the real parts of $\langle(\pi\pi)_I|-i\mathcal{H}^{(\Delta S=1)}|K^0\rangle$ for $\mu=2.39$ GeV. The central values for the standard model parameters given in Table XXXVII have been used.

	Real A_0		Real A_2	
i	choice 1	choice 2	choice 1	choice 2
1	$2.69(59)\times10^{-8}$	$3.82(84)\times10^{-8}$	$-3.45(15)\times10^{-9}$	$-4.05(18)\times10^{-9}$
2	$1.87(11)\times10^{-7}$	$2.65(16)\times10^{-7}$	$1.346(60)\times10^{-8}$	$1.582(71)\times10^{-8}$
3	$9.(87)\times10^{-12}$	$1.(12)\times10^{-11}$	0.0	0.0
4	$-9.9(22)\times10^{-10}$	$-1.40(31)\times10^{-9}$	0.0	0.0
5	$-3.5(14)\times10^{-10}$	$-5.0(20)\times10^{-10}$	0.0	0.0
6	$2.03(25)\times10^{-9}$	$2.88(35)\times10^{-9}$	0.0	0.0
7	$5.76(29)\times10^{-11}$	$1.140(58)\times10^{-10}$	$4.07(21)\times10^{-11}$	$5.16(26)\times10^{-11}$
8	$-2.08(11)\times10^{-10}$	$-4.12(22)\times10^{-10}$	$-1.472(80)\times10^{-10}$	$-1.87(10)\times10^{-10}$
9	$-2.97(21)\times10^{-12}$	$-4.21(30)\times10^{-12}$	$3.70(17)\times10^{-13}$	$4.35(20)\times10^{-13}$
10	$6.1(11)\times10^{-12}$	$8.7(15)\times10^{-12}$	$9.46(42)\times10^{-13}$	$1.111(50)\times10^{-12}$

TABLE XLIV. The contribution in GeV from the renormalized continuum operator $Q_{i,\mathrm{cont}}$ to the imaginary parts of $\langle(\pi\pi)_I|-i\mathcal{H}^{(\Delta S=1)}|K^0\rangle$ for $\mu=2.39$ GeV. The central values for the standard model parameters given in Table XXXVII have been used.

	Imaginary A_0		Imaginary A_2	
i	choice 1	choice 2	choice 1	choice 2
1	0.0	0.0	0.0	0.0
2	0.0	0.0	0.0	0.0
3	$-9.(86)\times10^{-14}$	$-1.(12)\times10^{-13}$	0.0	0.0
4	$7.5(17)\times10^{-12}$	$1.07(23)\times10^{-11}$	0.0	0.0
5	$6.6(27)\times10^{-13}$	$9.4(38)\times10^{-13}$	0.0	0.0
6	$-1.99(24)\times10^{-11}$	$-2.83(34)\times10^{-11}$	0.0	0.0
7	$6.46(33)\times10^{-14}$	$1.279(65)\times10^{-13}$	$4.57(23)\times10^{-14}$	$5.79(30)\times10^{-14}$
8	$-1.512(82)\times10^{-12}$	$-2.99(16)\times10^{-12}$	$-1.069(58)\times10^{-12}$	$-1.356(74)\times10^{-12}$
9	$-8.76(61)\times10^{-13}$	$-1.243(87)\times10^{-12}$	$1.093(49)\times10^{-13}$	$1.285(58)\times10^{-13}$
10	$-1.99(35)\times10^{-13}$	$-2.83(50)\times10^{-13}$	$-3.09(14)\times10^{-14}$	$-3.63(16)\times10^{-14}$

TABLE XLV. The contribution in GeV from the renormalized continuum operator $Q_{i,\mathrm{cont}}$ to the real parts of $\langle(\pi\pi)_I|-i\mathcal{H}^{(\Delta S=1)}|K^0\rangle$ for $\mu=3.02$ GeV. The central values for the standard model parameters given in Table XXXVII have been used.

	Real A_0		Real A_2	
i	choice 1	choice 2	choice 1	choice 2
1	$2.46(54)\times10^{-8}$	$3.48(77)\times10^{-8}$	$-3.09(14)\times10^{-9}$	$-3.63(16)\times10^{-9}$
2	$1.72(12)\times10^{-7}$	$2.45(16)\times10^{-7}$	$1.294(58)\times10^{-8}$	$1.520(68)\times10^{-8}$
3	$-2.(13)\times10^{-12}$	$-3.(18)\times10^{-12}$	0.0	0.0
4	$-4.5(11)\times10^{-13}$	$-6.4(15)\times10^{-13}$	0.0	0.0
5	$-1.64(69)\times10^{-10}$	$-2.33(98)\times10^{-10}$	0.0	0.0
6	$3.51(42)\times10^{-10}$	$4.98(60)\times10^{-10}$	0.0	0.0
7	$6.79(35)\times10^{-11}$	$1.344(69)\times10^{-10}$	$4.80(25)\times10^{-11}$	$6.09(31)\times10^{-11}$
8	$-2.58(14)\times10^{-10}$	$-5.10(28)\times10^{-10}$	$-1.821(99)\times10^{-10}$	$-2.31(13)\times10^{-10}$
9	$-3.92(30)\times10^{-12}$	$-5.56(43)\times10^{-12}$	$5.12(23)\times10^{-13}$	$6.02(27)\times10^{-13}$
10	$7.4(13)\times10^{-12}$	$1.05(19)\times10^{-11}$	$1.127(51)\times10^{-12}$	$1.324(59)\times10^{-12}$

$Q_{7,\mathrm{cont}}$ and $Q_{8,\mathrm{cont}}$. These contributions change by almost a factor of 2, due to the large coefficient of the chiral logarithm term. As we will see, these play no role in our final results, due to the small size of $\Delta I=1/2$ effects from electroweak penguin operators compared to the $\Delta I=1/2$ effects from exchange and gluon penguin operators. Table XLVII shows the values for $\mathrm{Re}(A_0)$, $\mathrm{Re}(A_2)$, and $\mathrm{Re}(A_0)/\mathrm{Re}(A_2)=1/\omega$ for the two extrapolation choices for $\mu=2.13$ GeV. In addition, we plot $\mathrm{Re}(A_0)$, $\mathrm{Re}(A_2)$, and $\mathrm{Re}(A_0)/\mathrm{Re}(A_2)=1/\omega$ for $\mu=2.13$ GeV in Figs. 29, 30, and 31 as a function of a parameter ξ, which we introduce into Eqs. (201) and (202) by replacing all the squared pseudoscalar masses m_{PS}^2 by ξm_{PS}^2. The chiral limit is given by $\xi=0$ and the physical point corresponds to $\xi=1$. The experimental values are given by the closed triangles. The difference between the two extrapolations gives an indication of the contribution expected from including all the $\mathcal{O}(p^4)$ terms, rather than just the logarithms. We comment that the dependence of the chiral logarithms on the scale $\Lambda_{\chi PT}$ must be canceled by a similar dependence in the $\mathcal{O}(p^4)$ coefficients.

Starting with $\mathrm{Re}(A_0)$ and its dependence as a function of ξ shown in Fig. 29, we see that the chiral logarithms are producing a 42% change in the value at the physical point. Given this large correction, the close agreement between our choice 2 value of $2.96(17)\times10^{-7}$ GeV and the experimental value of 3.33×10^{-7} GeV must be viewed as coincidental, but it is encouraging that the chiral logarithms move the quenched theoretical prediction closer to the experimental value. Similar consideration of $\mathrm{Re}(A_2)$ and Fig. 30 shows that inclusion of the chiral logarithms only changes the extrapolated value by 18%, also in the direction of the experimental value. Our choice 2 extrapolation value of $1.172(53)\times10^{-8}$ GeV is 22% below the experimental value of 1.50×10^{-8} GeV.

For $\mathrm{Re}(A_0)/\mathrm{Re}(A_2)$, the differences in the extrapolations are smaller. The chiral logarithms for the (8,1) and (27,1) operators which dominate $\mathrm{Re}(A_0)$ and $\mathrm{Re}(A_2)$, respectively, have the same sign but different amplitudes. From Fig. 31, it is readily apparent that the logarithms have little effect on the answer and it is in good agreement with the experimental value of 22.2.

TABLE XLVI. The contribution in GeV from the renormalized continuum operator $Q_{i,\mathrm{cont}}$ to the imaginary parts of $\langle(\pi\pi)_I|-i\mathcal{H}^{(\Delta S=1)}|K^0\rangle$ for $\mu=3.02$ GeV. The central values for the standard model parameters given in Table XXXVII have been used.

	Imaginary A_0		Imaginary A_2	
i	choice 1	choice 2	choice 1	choice 2
1	0.0	0.0	0.0	0.0
2	0.0	0.0	0.0	0.0
3	$1.2(80)\times10^{-13}$	$2.(11)\times10^{-13}$	0.0	0.0
4	$6.7(16)\times10^{-12}$	$9.5(23)\times10^{-12}$	0.0	0.0
5	$6.8(29)\times10^{-13}$	$9.6(41)\times10^{-13}$	0.0	0.0
6	$-2.06(25)\times10^{-11}$	$-2.93(35)\times10^{-11}$	0.0	0.0
7	$5.49(28)\times10^{-14}$	$1.087(56)\times10^{-13}$	$3.88(20)\times10^{-14}$	$4.92(25)\times10^{-14}$
8	$-1.386(75)\times10^{-12}$	$-2.74(15)\times10^{-12}$	$-9.80(53)\times10^{-13}$	$-1.243(67)\times10^{-12}$
9	$-8.01(62)\times10^{-13}$	$-1.137(88)\times10^{-12}$	$1.049(47)\times10^{-13}$	$1.232(55)\times10^{-13}$
10	$-1.82(33)\times10^{-13}$	$-2.58(46)\times10^{-13}$	$-2.78(12)\times10^{-14}$	$-3.27(15)\times10^{-14}$

TABLE XLVII. The dependence of physical quantities on the extrapolation choice for $\mu = 2.13$ GeV.

Quantity	Choice 1 (zero-loop quenched)	Choice 2 (one-loop full)
$\mathrm{Re}\,A_0$	$2.09(12)\times10^{-7}$	$2.96(17)\times10^{-7}$
$\mathrm{Re}\,A_2$	$9.98(45)\times10^{-9}$	$1.172(53)\times10^{-8}$
$\mathrm{Im}\,A_0$	$-1.60(28)\times10^{-11}$	$-2.35(40)\times10^{-11}$
$\mathrm{Im}\,A_2$	$-9.91(56)\times10^{-13}$	$-1.264(72)\times10^{-12}$
$\mathrm{Re}\,A_0/\mathrm{Re}\,A_2$	$2.09(15)\times10^{1}$	$2.53(18)\times10^{1}$
$(\epsilon'/\epsilon)_{\omega\ \mathrm{exp}}$	$-3.2(22)\times10^{-4}$	$-4.0(23)\times10^{-4}$
$(\epsilon'/\epsilon)_{\omega\ \mathrm{th}}$	$-3.4(23)\times10^{-4}$	$-3.5(19)\times10^{-4}$

We choose to quote as our best estimates for $\mathrm{Re}(A_0)$, $\mathrm{Re}(A_2)$, and $\mathrm{Re}(A_0)/\mathrm{Re}(A_2)$ the values using the choice 2 extrapolation (one-loop full QCD). This extrapolation includes the most information currently available for corrections to lowest order chiral perturbation theory, but is not a complete higher order calculation. The value of μ to use for our final answer should, in principle, not matter. However, for $\mu = 1.51$ GeV, nonperturbative low-energy QCD effects could be causing a systematic shift in the values for Z_{ij}^{NPR}. For $\mu = 3.02$ GeV, finite lattice spacing effects could begin to play a role. In Table XLVIII we give the μ dependence of our results. For $\mathrm{Re}(A_0)$ and $\mathrm{Re}(A_2)$, the μ dependence is plotted in Fig. 32, while for $\mathrm{Re}(A_0)/\mathrm{Re}(A_2)$ the μ dependence is plotted in Fig. 40. No statistically significant μ dependence is seen, so choosing to quote results at $\mu = 2.13$ GeV, where systematic effects should be smallest, does not alter the quoted values

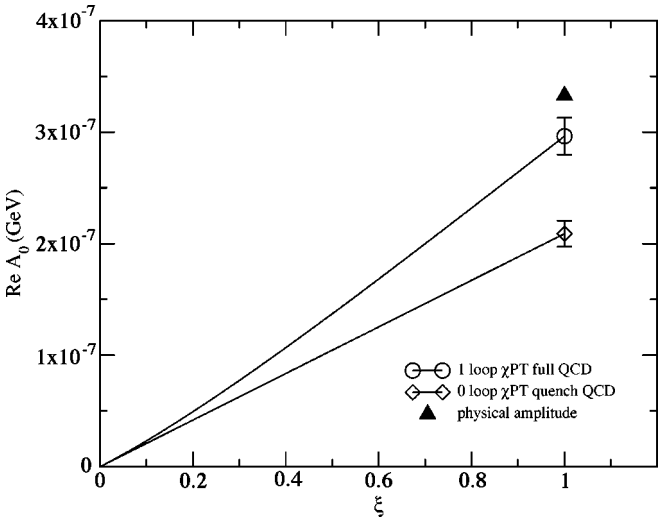

FIG. 29. $\mathrm{Re}(A_0)$ plotted vs ξ, where ξ multiplies the pseudoscalar masses appearing in Eqs. (201) and (202). The chiral limit is $\xi = 0$ and the physical point corresponds to $\xi = 1$. Two ways of extrapolating to the physical point are shown: (1) zero-loop chiral perturbation theory in quenched QCD and (2) one-loop chiral perturbation theory in full QCD. The difference between them gives an indication of the contribution expected from including all $O(p^4)$ terms in chiral perturbation theory. Since all $O(p^4)$ terms are not included in our results, the close agreement with the experimental value should be regarded as fortuitous. The data is for $\mu = 2.13$ GeV.

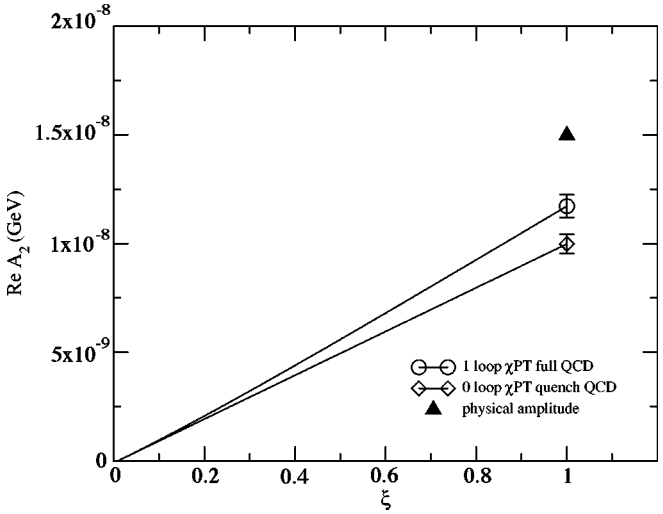

FIG. 30. As in Fig. 29, except that $\mathrm{Re}(A_2)$ is plotted vs ξ. Here the one-loop chiral perturbation theory extrapolation in full QCD differs from the experimental result by ~18%. This is well within the general expectation for higher order effects in chiral perturbation theory at scales around m_K. The data is for $\mu = 2.13$ GeV.

Our final results for $\mathrm{Re}(A_0)$, $\mathrm{Re}(A_2)$, and $\mathrm{Re}(A_0)/\mathrm{Re}(A_2)$ for the choice 2 extrapolation (one-loop full QCD chiral perturbation theory) with $\mu = 2.13$ GeV are given in Table XLIX. Figure 33 shows a breakdown of the contribution of $Q_{i,\mathrm{cont}}$ to $\mathrm{Re}(A_0)$ (upper panel) and $\mathrm{Re}(A_2)$ (lower panel). The solid filled bars in the graph denote positive quantities and the hashed represent negative quantities. One clearly sees that the dominant contributions are from $Q_{i,\mathrm{cont}}$ for $i = 1, 2$. The good agreement with experiment is very encouraging, although better than might be expected given the approxima-

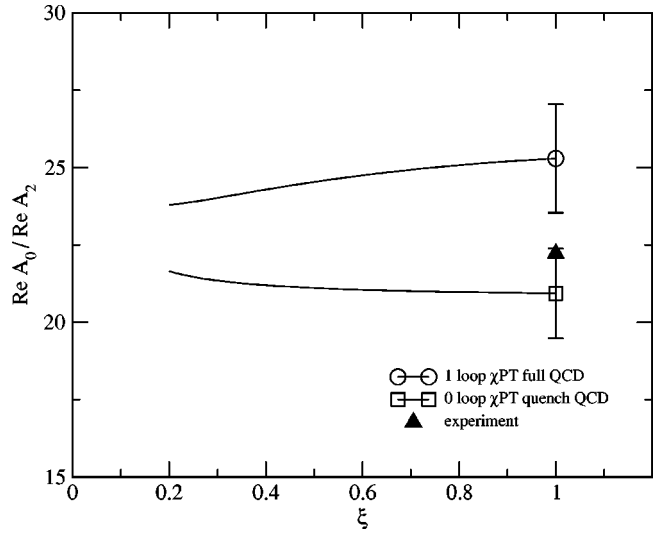

FIG. 31. As in Fig. 29, except that $\mathrm{Re}(A_0)/\mathrm{Re}(A_2)$ is plotted vs ξ. The two extrapolations are only slightly different due to the chiral logarithms having coefficients with the same sign for the dominant operators contributing to $\mathrm{Re}(A_0)$ and $\mathrm{Re}(A_2)$. The data is for $\mu = 2.13$ GeV.

TABLE XLVIII. The dependence of the physical quantities we have calculated on the scale used to match from continuum perturbation theory to the lattice calculation for extrapolation choice 2. The dependence on μ indicates the reliability of the combination of using continuum perturbation theory below 1.3 GeV (needed to define the three-quark effective theory), one-loop matching from the NDR to RI schemes, and our implementation of nonperturbative renormalization.

Quantity	$\mu=1.51$ GeV	$\mu=2.13$ GeV	$\mu=2.39$ GeV	$\mu=3.02$ GeV
$\mathrm{Re}\,A_0$	$3.27(25)\times10^{-7}$	$2.96(17)\times10^{-7}$	$3.04(16)\times10^{-7}$	$2.79(17)\times10^{-7}$
$\mathrm{Re}\,A_2$	$1.151(52)\times10^{-8}$	$1.172(53)\times10^{-8}$	$1.163(52)\times10^{-8}$	$1.140(51)\times10^{-8}$
$\mathrm{Im}\,A_0$	$-1.78(44)\times10^{-11}$	$-2.35(40)\times10^{-11}$	$-2.12(37)\times10^{-11}$	$-2.26(39)\times10^{-11}$
$\mathrm{Im}\,A_2$	$-1.444(83)\times10^{-12}$	$-1.264(72)\times10^{-12}$	$-1.206(68)\times10^{-12}$	$-1.103(63)\times10^{-12}$
$\mathrm{Re}\,A_0/\mathrm{Re}\,A_2$	$2.84(24)\times10^{1}$	$2.53(18)\times10^{1}$	$2.61(17)\times10^{1}$	$2.45(18)\times10^{1}$
$(\epsilon'/\epsilon)_{\omega\ \mathrm{exp}}$	$-9.9(23)\times10^{-4}$	$-4.0(23)\times10^{-4}$	$-4.8(20)\times10^{-4}$	$-2.2(24)\times10^{-4}$
$(\epsilon'/\epsilon)_{\omega\ \mathrm{th}}$	$-7.8(16)\times10^{-4}$	$-3.5(19)\times10^{-4}$	$-4.1(16)\times10^{-4}$	$-2.0(21)\times10^{-4}$

tions inherent in the current calculation.

We end this section with our results for the kaon B parameter, B_K, discussed in Sec. II C and defined in Eq. (46). In the SU(3) flavor limit, one has

$$\langle\overline{K^0}|Q_{\mathrm{lat}}^{(\Delta S=2)}|K^0\rangle=3\langle\pi^+|[Q_1+Q_2]_{\mathrm{lat}}^{(3/2)}|K^+\rangle$$
$$=2\langle\pi^+|\Theta_{\mathrm{lat}}^{(27,1),(3/2)}|K^+\rangle. \qquad (203)$$

For the determination of B_K, we need $\langle\pi^+|\Theta_{\mathrm{lat}}^{(27,1),(3/2)}|K^+\rangle$ at $m_f=0.018$, a quark mass which gives a kaon made from degenerate quarks its physical mass. This matrix element has been fit to the form given in Eq. (187) with the fit parameters given in the second line of Table XXVII. To convert from the lattice matrix element to one with a continuum $\overline{\mathrm{MS}}$ normalization we use $Z_{Q^{\Delta S=2}}(2\ \mathrm{GeV})/Z_A^2=0.928$ [78], $Z_A=0.7555$ [21], and the one-loop matching between the RI and $\overline{\mathrm{MS}}$ schemes from [79]. This one-loop matching has a value of 1.02 in this case.

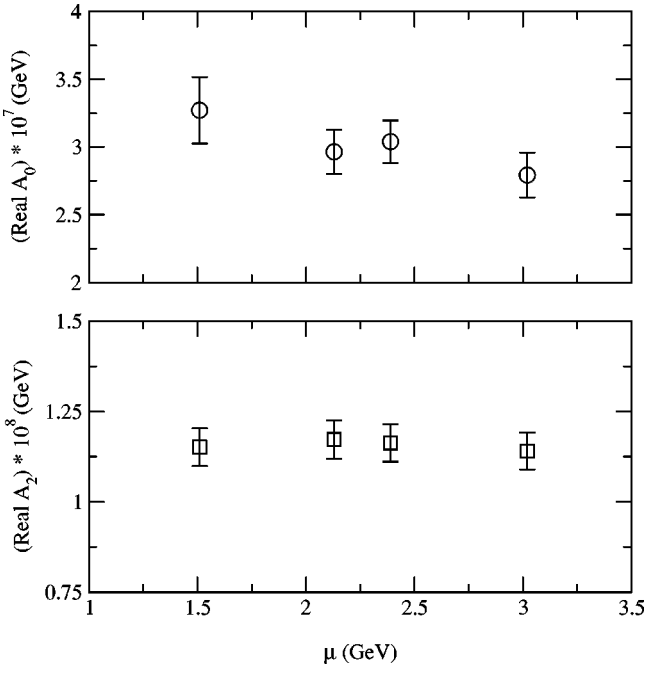

FIG. 32. A plot of $\mathrm{Re}(A_0)$ (upper panel) and $\mathrm{Re}(A_2)$ (lower panel) vs μ for the physical values obtained using one-loop full QCD chiral perturbation theory for the extrapolation to the physical kaon mass. The results show no statistically significant μ dependence. We choose to quote final values with $\mu=2.13$ GeV.

To complete the determination of B_K, values for m_K and f_K are needed [Eq. (46)]. Although f_K and m_K are given in Tables XIX and XXXI in [21], the current calculation contains 400 configurations compared to the 85 of [21], producing a reduced statistical error. To extract f_K and m_K, we simultaneously fit wall-wall pseudoscalar correlators and wall-point pseudoscalar axial-current correlators to determine the pseudoscalar mass, $\langle 0|P_{K^+,\mathrm{wall}}|K^+\rangle$ and $\langle 0|A_{0,\mathrm{pt}}|K^+\rangle$. The fits use correlators a distance $t=12-19$ from the wall source and, as can be seen in Fig. 3, in this range zero mode effects should be small.

From the 400 configuration data set of this work, the values we find for m_{PS} and f_{PS} are given in Table L for $m_f=0.01-0.05$. (Here the subscript PS added to the mass, decay constant, and B parameter is a label for a generic pseudoscalar meson which could be the π, K, etc.) Including the determinations of m_{PS}, f_{PS} and the fit to $\langle\pi^+|\Theta_{\mathrm{lat}}^{(27,1),(3/2)}|K^+\rangle$ under a jackknife loop produces the values for B_{PS}^{wall} in the fifth column of Table L. Adding an interpolation to $m_f=0.018$ in the jackknife loop, we find $B_{K,\overline{\mathrm{MS}}}^{\mathrm{wall}}(2\ \mathrm{GeV})=0.532(11)$ where the error is statistical only. We can also calculate the value in the chiral limit, $m_f=-m_{\mathrm{res}}$, and this gives $B_{PS,\overline{\mathrm{MS}}}^{\mathrm{wall}}(2\ \mathrm{GeV})(m_f=-m_{\mathrm{res}})=0.267(14)$. This method of extracting B_K using wall-wall

TABLE XLIX. Our final values for physical quantities using one-loop full QCD extrapolations to the physical kaon mass (choice 2) and a value of $\mu=2.13$ GeV for the matching between the lattice and continuum. The errors for our calculation are statistical only.

Quantity	Experiment	This calculation (statistical errors only)
$\mathrm{Re}\,A_0$(GeV)	3.33×10^{-7}	$(2.96\pm0.17)\times10^{-7}$
$\mathrm{Re}\,A_2$(GeV)	1.50×10^{-8}	$(1.172\pm0.053)\times10^{-8}$
ω^{-1}	22.2	(25.3 ± 1.8)
$\mathrm{Re}(\epsilon'/\epsilon)$	$(15.3\pm2.6)\times10^{-4}$(NA 48) $(20.7\pm2.8)\times10^{-4}$(KTEV)	$(-4.0\pm2.3)\times10^{-4}$

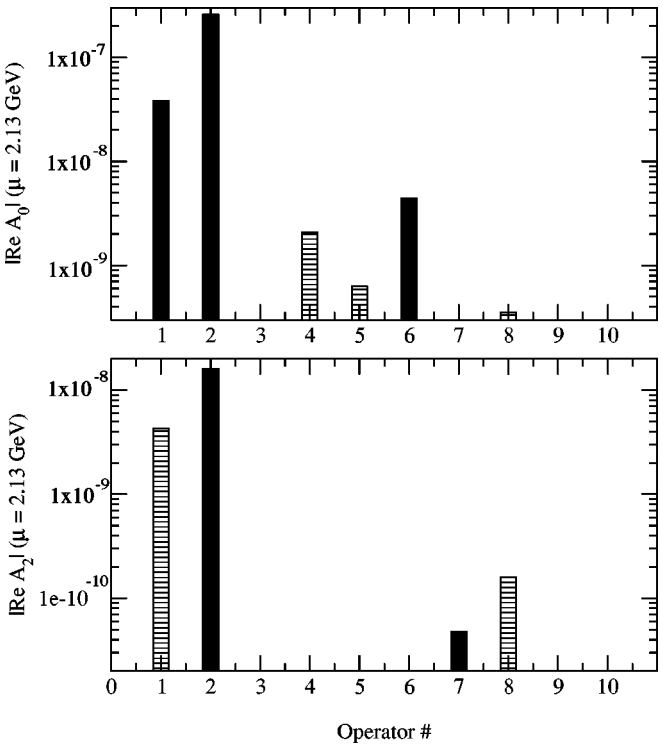

FIG. 33. A breakdown of the contribution of $Q_{i,\mathrm{cont}}$ to $\mathrm{Re}(A_0)$ (upper panel) and $\mathrm{Re}(A_2)$ (lower panel). The solid filled bars in the graph denote positive quantities and the hashed represent negative quantities. The data is for $\mu=2.13$ GeV.

correlators for the matrix element avoids introducing zero mode effects through normalization factors in a similar fashion to the techniques we have used in the analysis of $K\rightarrow\pi$ matrix elements.

This result agrees within errors with the value 0.538(8) that we obtained on a subset of 200 configurations from the present ensemble [80]. There the traditional method of calculating B_K was used, where a $\Delta S=2$ Green's function is normalized with axial current-pseudoscalar correlators. This ratio of Green's functions should be free of quenched chiral logarithms, but the axial current correlator can introduce zero modes for small quark masses. We revisit this earlier determination here with the full 400 configuration data set and use B_{PS}^{AA} to denote the result from this method. To get the value in the $\overline{\mathrm{MS}}$ scheme at $\mu=2$ GeV, the lattice $\Delta S=2$ matrix element must be multiplied by the value of $Z_{Q^{\Delta S=2}}/Z_A^2$ given above and a factor of 1.02, which is the value for the one-loop matching between the RI and $\overline{\mathrm{MS}}$ schemes. In the fourth column of Table L, our values for B_{PS}^{AA} in the $\overline{\mathrm{MS}}$ scheme at $\mu=2$ GeV are given for $m_f=0.01-0.05$. Fitting this data to the form given by one-loop quenched chiral perturbation theory for degenerate mesons [81,55],

$$B_{PS}^{\mathrm{AA}}=b_0^{\mathrm{AA}}\left[1.0-\frac{1}{(4\pi f)^2}\left(6m_{PS}^2\log\frac{m_{PS}^2}{\Lambda_{Q\chi PT}^2}\right)\right]+b_1^{\mathrm{AA}}m_{PS}^2, \tag{204}$$

we find

$$B_{K,\overline{\mathrm{MS}}}^{\mathrm{AA}}(2\ \ \mathrm{GeV})=0.536(6) \tag{205}$$

which is in very good agreement with our earlier result on 200 configurations. The fit gives $b_0^{\mathrm{AA}}=0.285(4)$ and $b_1^{\mathrm{AA}}=1.44(6)$ and we note that b_0^{AA} is the chiral limit value for

TABLE L. Values for the pseudoscalar mass m_{PS} and decay constants f_{PS} (both in lattice units) versus the quark mass m_f, along with the pseudoscalar B parameter, B_{PS}, determined from two different normalizations. B_{PS}^{AA} is found by normalizing the desired $\Delta S=2$ Green's function by axial current-pseudoscalar Green's functions, which may introduce zero mode effects. B_{PS}^{wall} is determined by normalizing with the wall-wall correlators used for the $K\rightarrow\pi$ matrix elements, which we have argued should not introduce zero modes through the normalization. Values for B_{PS} are given in the MS scheme at $\mu=2$ GeV. The results for each value of m_f are averaged over the time-slice range $14\leqslant t\leqslant 17$. The physical value $B_K=0.532(11)$ is found by choosing $m_f=0.018$ so that a kaon made with degenerate quarks has its physical mass.

m_f	m_{PS}	f_{PS}	B_{PS}^{AA}	B_{PS}^{wall}
0.01	0.2073(19)	0.0769(7)	0.478(10)	0.466(14)
0.02	0.2713(16)	0.0797(6)	0.554(6)	0.547(11)
0.03	0.3245(15)	0.0837(6)	0.602(5)	0.600(10)
0.04	0.3716(14)	0.0876(6)	0.636(4)	0.635(9)
0.05	0.4147(13)	0.0915(7)	0.662(3)	0.662(9)

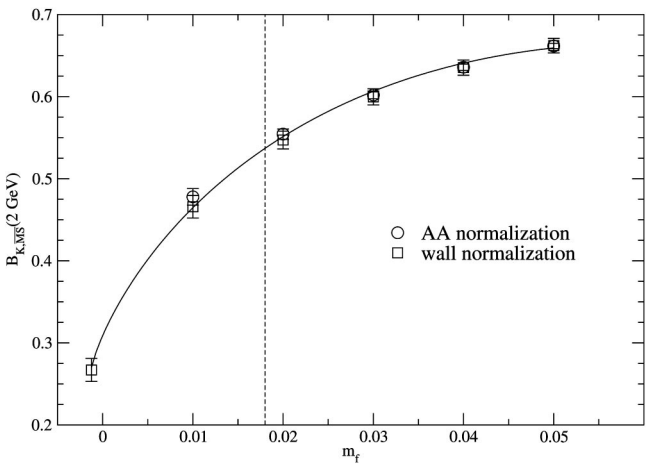

FIG. 34. Values for $B_{PS,\overline{\mathrm{MS}}}(2\ \mathrm{GeV})$ vs m_f. The points labeled AA normalization (○) are determined by normalizing with two-point functions which may introduce zero mode effects for small quark mass. The wall normalization points (□) determine B_{PS} from a $K\rightarrow\pi$ matrix element, where a wall normalization is used, and zero mode effects should not be introduced through the normalization. Some difference can be seen for the smaller quark masses. The wall normalization point at $m_f=-m_{\mathrm{res}}$ is the value of B_{PS} in the chiral limit. The solid line is the result of fitting the AA norm points to the form given in Eq. (204). Since the fit goes below the AA norm point at $m_f=0.01$, the extrapolated value agrees with the wall normalization value. The dashed line has $m_f=0.018$ and marks the point where a kaon made of degenerate quarks has its physical mass. Using the value of B_{PS} at this point, we find $B_{K,\overline{\mathrm{MS}}}(2\ \mathrm{GeV})=0.532(11)$.

the unrenormalized B parameter using this method. Including renormalization factors yields $B^{\mathrm{AA}}_{PS,\overline{\mathrm{MS}}}(2\ \mathrm{GeV})(m_f=-m_{\mathrm{res}}) = 0.270(4)$. The details of the fit are the same as those following Eq. (187) in Sec. X where the extraction of $\alpha^{(27,1),(3/2)}_{\mathrm{lat}}$ was discussed. The one difference is that no quenched chiral logarithm appears in Eq. (204), since they cancel in the ratio of the matrix element and its vacuum saturation approximation.

The two methods described above have produced quite similar results for B_K; 0.536(6) using the axial current-pseudoscalar normalization and 0.532(11) using the wall-wall correlator normalization. The results given in Table L and plotted in Fig. 34 show very good agreement in B^{AA}_{PS} and B^{wall}_{PS} for $m_f=0.03$, 0.04, and 0.05. For smaller quark masses, differences at the one standard deviation level occur. Since both analysis methods use the same raw data, the difference may be correlated and have statistical significance, but we have not pursued this question. The solid line in Fig. 34 is a fit of B^{AA}_{PS} to the form given in Eq. (204). This fit goes below the $m_f=0.01$ data point and agrees well in the chiral limit with the value determined from the wall normalization. Since the nonlinearity due to the chiral logarithm is quite pronounced near the chiral limit, the extrapolation to this limit likely requires further study to understand all the systematic effects.

Because the wall-wall normalization does not introduce additional zero mode effects and it is the technique we have used for all the $K\to\pi$ matrix elements, we will use the results from this approach for our final values. Therefore for our single lattice spacing [$a^{-1}=1.922(40)$ GeV] and volume ($16^3\times 32$) we find $B_{K,\overline{\mathrm{MS}}}(2\ \mathrm{GeV})=0.532(11)$ and the value for B_{PS} in the chiral limit is 0.267(14). Our value for B_K is smaller than that found in Ref. [82] using the RG-improved gauge action of Iwasaki at a similar lattice spacing and volume. In the $\overline{\mathrm{MS}}$ scheme at 2 GeV they find $B_K(q^*=1/a)=0.564(14)$, where perturbation theory has been used to determine the renormalization factors. (The dependence of their result on q^* is smaller than the error quoted above.) The two central values differ by about 6%, while the quoted errors are about 2% to 3%. The difference between the calculations is small and could be merely a statistical fluctuation. However, there are also systematic differences between the two calculations that are not reflected in the statistical errors; the gauge actions are different and Ref. [82] uses perturbation theory to calculate Z factors, whereas this work has used NPR. The smaller value for m_{res} for the Iwasaki action seems unlikely to effect B_K, given that no power divergent operators are involved and the large mass of the kaon. For Z factors for this four-quark operator, a direct comparison has not been done due to the difference in gauge actions. A direct comparison of perturbative and nonperturbative Z factors for quark bilinears was given in Ref. [59] where agreement at the 5% level was found between mean field perturbative results and NPR. This could be responsible for much of the difference in the central values for B_K with domain wall fermions.

Our value for B_{PS} in the chiral limit, 0.267(14), is markedly lower than the value of 0.412 given in Ref. [82] for the chiral and continuum limit. The continuum limit extrapolation in Ref. [82] is likely not responsible for this difference; rather, it is the form of the extrapolation to the chiral limit. Our data uses the analytically calculated coefficient of the chiral logarithm term as a fixed input parameter, whereas Ref. [82] fits for this coefficient, using data with the AA normalization. Their fit results in a coefficient ~ 3 times smaller than the analytic result, which will have a pronounced effect on the chiral limit and explains much of the difference in the two results. We find that our data is well fit using the analytically known coefficient, provided zero mode effects are minimized, and have used this coefficient consistently in both the determination of the (27,1) $\Delta I=3/2$ $K\to\pi$ matrix elements and the extrapolation of B_{PS} to the chiral limit.

Our domain wall fermion result is more than one standard deviation lower than the continuum limit quenched value of 0.628(42) [83] computed with Kogut-Susskind fermions. For Kogut-Susskind fermions, large $\mathcal{O}(a^2)$ effects are seen. Our result does not include an extrapolation to the continuum, but in Ref. [82] this extrapolation is done for domain wall fermions, yielding 0.5746(61) [Eq. (191)]. Thus it appears that domain wall fermions are giving a quenched value of B_K about 10% smaller than the quenched value computed with Kogut-Susskind fermions and slightly more than one standard deviation away. Given the relatively small statistical errors currently possible, these systematic differences need to be reconciled.

XIV. IMAGINARY A_0 AND A_2

In the previous section, we saw that the results for the real $K\to\pi\pi$ amplitudes from this single lattice spacing, quenched calculation were quite consistent with the known experimental values. We now present our results for the imaginary $K\to\pi\pi$ amplitudes and $\mathrm{Re}(\epsilon'/\epsilon)$. These are all directly proportional to the parameter η in the CKM matrix and we will use the central value for η from Table XXXVII.

Values for $\mathrm{Im}(A_0)$ and $\mathrm{Im}(A_2)$ are given in Tables XL, XLII, XLIV, and XLVI for $\mu=1.51$, 2.13, 2.39, and 3.02 GeV, respectively. The tables include both extrapolation choices. The values in the tables reflect the long-standing expectation that the dominant part of $\mathrm{Im}(A_0)$ is produced by $Q_{6,\mathrm{cont}}$, although $Q_{4,\mathrm{cont}}$ is $\sim$35% of the size of $Q_{6,\mathrm{cont}}$ and of the opposite sign and $Q_{8,\mathrm{cont}}$ is $\sim$10% of $Q_{6,\mathrm{cont}}$ and of the same sign. Since we choose to work in a basis where $Q_{4,\mathrm{cont}}$ is linearly dependent, most of its value is coming from $Z^{\mathrm{NPR}}_{41}\langle\pi^+|Q^{(1/2)}_{1,\mathrm{lat}}|K^+\rangle_{\mathrm{sub}}$ and $Z^{\mathrm{NPR}}_{42}\langle\pi^+|Q^{(1/2)}_{2,\mathrm{lat}}|K^+\rangle_{\mathrm{sub}}$. Since the values for $\alpha^{(1/2)}_{1,\mathrm{lat}}$ and $\alpha^{(1/2)}_{2,\mathrm{lat}}$ in Table XXXVIII have opposite sign and Z^{NPR}_{41} and Z^{NPR}_{42} also have opposite sign, these contributions add in $Q_{4,\mathrm{cont}}$. Finally we note that $y_4(\mu)$ and $y_6(\mu)$ are of similar size, resulting in the sizable contribution of $Q_{4,\mathrm{cont}}$ to $\mathrm{Im}(A_0)$. $\mathrm{Im}(A_2)$ is dominated by $Q_{8,\mathrm{cont}}$ and receives only $\sim$10% contributions from the next largest source, $Q_{9,\mathrm{cont}}$.

The values for $\mathrm{Im}(A_0)$ and $\mathrm{Im}(A_2)$ and their dependence on the choice of extrapolation to the physical kaon mass is given in Table XLVII for $\mu=2.13$ GeV. Figures 35 and 36 show $\mathrm{Im}(A_0)$ and $\mathrm{Im}(A_2)$, respectively, as a function of ξ for

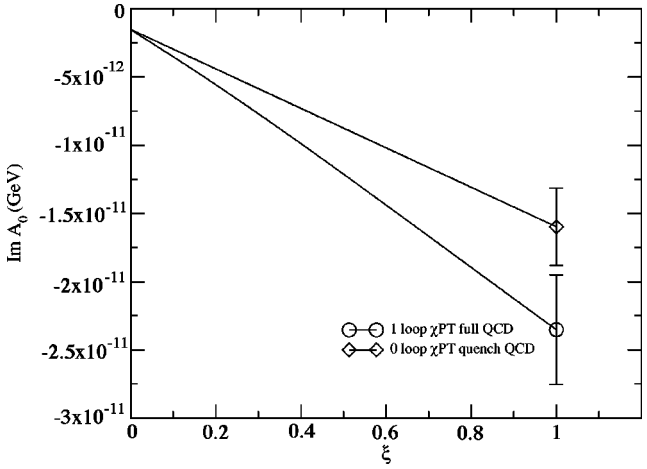

FIG. 35. As in Fig. 29, except that Im(A_0) is plotted vs ξ. Here a physical value is not directly known. The one-loop chiral perturbation extrapolation in full QCD is a 47% correction to the zero-loop extrapolation. The data is for $\mu = 2.13$ GeV.

$\mu = 2.13$ GeV. We note that Im(A_0) does not vanish as $\xi \to 0$, due to the contribution from the electroweak penguins. The chiral logarithms change the extrapolated value of Im(A_0) by 47% and Im(A_2) by 28%. The μ dependence of Im(A_0) and Im(A_2), using extrapolation choice 2, is given in Table XLVIII and plotted in Fig. 37. The results for Im(A_0) show no statistically significant μ dependence, while Im(A_2) varies by about 25% over this range of μ.

We can now discuss our results for Re(ϵ'/ϵ). Considering only the contribution from the dominant operators Q_2, Q_6, and Q_8 (represented by $Q_2 \sim \alpha_2 m_{K^0}^2 \xi$, $Q_6 \sim \alpha_6 m_{K^0}^2 \xi$, and $Q_8 \sim \alpha_8$) and assuming $Z_{i,j}^{\rm NPR}$ has small off-diagonal elements yields a schematic formula for Re(ϵ'/ϵ) giving the rough size and mass dependence of the various contributions.

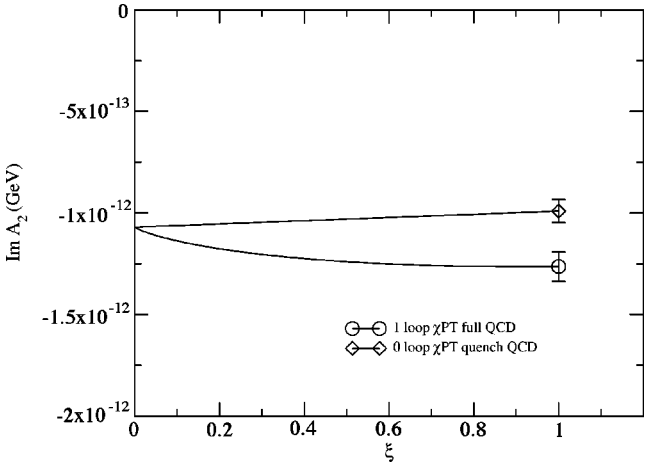

FIG. 36. As in Fig. 29, except that Im(A_2) is plotted vs ξ. Here a physical value is not directly known. The one-loop chiral perturbation extrapolation in full QCD is a 28% correction to the zero-loop extrapolation. The data is for $\mu = 2.13$ GeV.

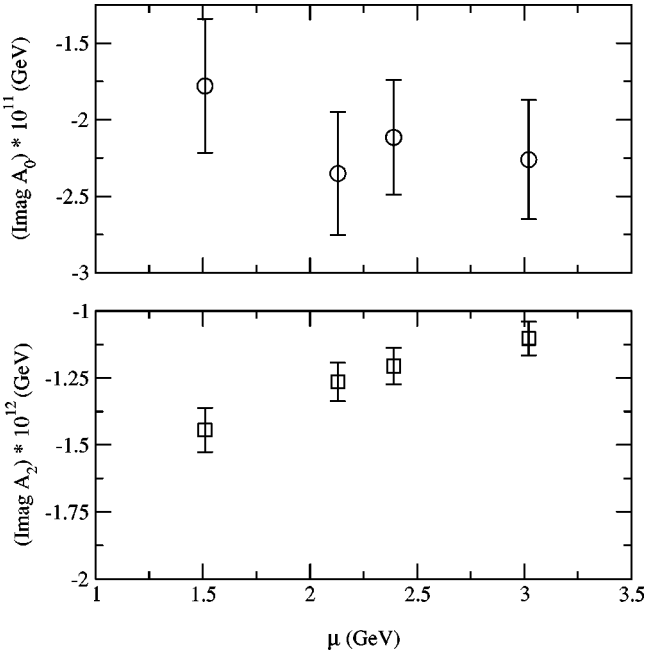

FIG. 37. A plot of Im(A_0) (upper panel) and Im(A_2) (lower panel) vs μ for the physical values obtained using one-loop full QCD chiral perturbation theory for the extrapolation to the physical kaon mass. The results for Im(A_0) show no statistically significant μ dependence, while Im(A_2) varies by 25% over this range of μ. We choose to quote final values with $\mu = 2.13$ GeV.

$$\mathrm{Re}(\epsilon'/\epsilon) = \left(\frac{\omega}{\sqrt{2}|\epsilon|}\right)_{\rm exp} \left\{ \left[\frac{\alpha_{\rm W}\alpha_8}{\alpha_{\rm W}\alpha_8 + \alpha_2 m_{K^0}^2 \xi}\right]^{(3/2)} - \left[\frac{\alpha_{\rm W}\alpha_8 + \alpha_{\rm S}\alpha_6 m_{K^0}^2 \xi}{\alpha_{\rm W}\alpha_8 + \alpha_2 m_{K^0}^2 \xi}\right]^{(1/2)} \right\}, \tag{206}$$

where $\alpha_{\rm W}$ is the electroweak fine structure constant and $\alpha_{\rm S}$ is for QCD. Here we take ω and $|\epsilon|$ from experiment, since we will concentrate on the mass dependence of $P_2 - P_0$. Recalling the $\Delta I = 1/2$ rule gives

$$[\alpha_2 m_{K^0}^2 \xi]^{(3/2)} = \omega [\alpha_2 m_{K^0}^2 \xi]^{(1/2)}, \tag{207}$$

which makes the $I = 3/2$ contribution at the physical point ($\xi = 1$) $\mathcal{O}(\alpha_{\rm W}/\omega)$ rather than $\mathcal{O}(\alpha_{\rm W})$. Equation (206) shows that in the chiral limit ($\xi = 0$), the electroweak penguins dominate Re(A_0), Re(A_2), Im(A_0), and Im(A_2) and produce Re(ϵ'/ϵ)=0. Since in this limit, both the $I = 1/2$ and $I = 3/2$ amplitudes come from the same source, there is no phase difference between them. This limit is quite different from the case with physical quark masses, where the source of Im(A_0) is primarily the gluonic penguins, Im(A_2) the electroweak penguins, and Re(A_0) and Re(A_2) the exchange operators.

To examine the ξ dependence of $P_2 - P_0$ when the operators important to the physically relevant case are noticeable, we plot in Fig. 38 the quantity

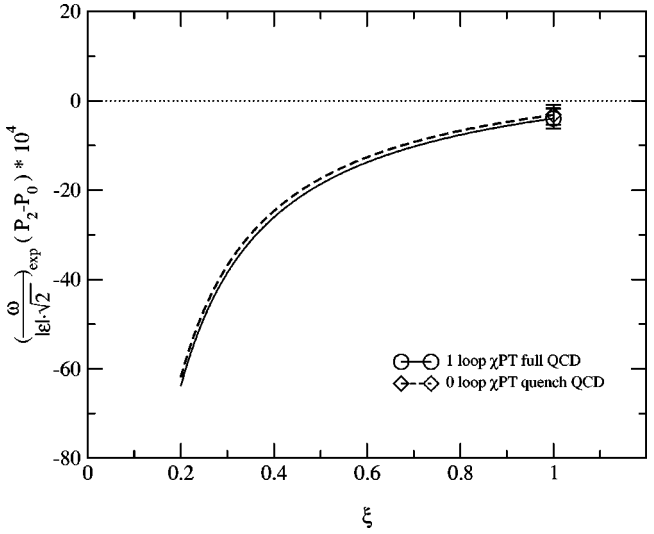

FIG. 38. A plot of $[\omega/(\sqrt{2}|\epsilon|)]_{\rm exp}(P_2-P_0)$ vs ξ, where $\xi=0$ is the chiral limit and $\xi=1$ is the physical point. We only plot points for $\xi\geqslant 0.2$, since in the chiral limit only the electroweak (8,8) operators contribute and $P_2-P_0=0$. As masses increase from zero, the contributions to P_2-P_0 of current–current, gluon penguin, and electroweak penguin operators for $\xi<0.2$ are quite different from the physical world. As explained in the text, for $0.2<\xi<0.5$, the electroweak penguins continue to dominate by making $|P_2|$ large. As one approaches the physical point, the electroweak and gluonic penguins are canceling almost completely. Higher order terms in chiral perturbation theory could be expected to alter this large cancellation. The data is for $\mu=2.13$ GeV.

$$\left(\frac{\omega}{\sqrt{2}|\epsilon|}\right)_{\rm exp}[P_2(\xi)-P_0(\xi)] \tag{208}$$

starting at $\xi=0.2$. The data is for $\mu=2.13$ GeV and we remark that for $\xi=1$, the quantity in Eq. (208) is $\mathrm{Re}(\epsilon'/\epsilon)$. One sees that for both extrapolation choices, Eq. (208) starts out large and negative and becomes very small for $\xi=1$. The large negative value arises when $\mathrm{Re}(A_2)$ is receiving very little contribution from the exchange operators and this diminishes as $\mathrm{Re}(A_2)$ grows with ξ. For the one-loop full QCD extrapolation, we show the individual contributions $[\omega/(\sqrt{2}|\epsilon|)]_{\rm exp}P_2$ and $-[\omega/(\sqrt{2}|\epsilon|)]_{\rm exp}P_0$ in Fig. 39 for $\mu=2.13$ GeV. The contribution proportional to P_2 is going to zero with increasing ξ due to the increase in $\mathrm{Re}(A_2)$. The term proportional to $-P_0$ is constant in lowest order chiral perturbation theory, once ξ is large enough that the electroweak penguins play no role, and has no chiral logarithm corrections. At the physical point $\xi=1$, the two terms are largely canceling. The μ dependence of $\mathrm{Re}(\epsilon'/\epsilon)$ is given in Table XLVIII and plotted in Fig. 40. The μ dependence is coming largely from the μ dependence of $\mathrm{Im}(A_2)$. We will take the value for $\mathrm{Re}(\epsilon'/\epsilon)$ at $\mu=2.13$ GeV for our final result.

We can also study the contribution of the individual continuum operators to the imaginary amplitudes entering $\mathrm{Re}(\epsilon'/\epsilon)$. To do this, we define P_I^i by $P_I^i \equiv \mathrm{Im}(\langle(\pi\pi)_I|-i\mathcal{H}^{(\Delta S=1)}|K^0\rangle)_i/\mathrm{Re}(A_I)$, where the subscript

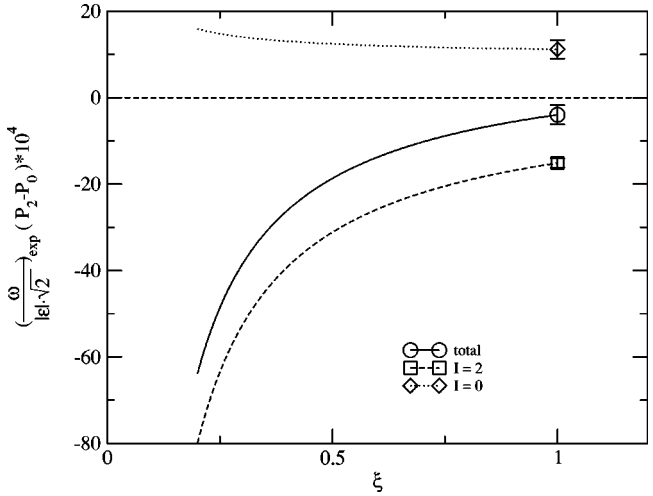

FIG. 39. The values for $-[\omega/(\sqrt{2}|\epsilon|)]_{\rm exp}P_0$, $[\omega/(\sqrt{2}|\epsilon|)]_{\rm exp}P_2$, and their sum, using the one-loop chiral perturbation theory extrapolation in full QCD, are plotted vs ξ. The contribution proportional to P_2 is going to zero with increasing ξ due to the increase in $\mathrm{Re}(A_2)$. $-P_0$ is constant in lowest order chiral perturbation theory, once ξ is large enough that the electroweak penguins play no role, and has no chiral logarithm corrections. At the physical point $\xi=1$, the two terms are almost canceling, producing the small value for $\mathrm{Re}(\epsilon'/\epsilon)$. The data is for $\mu=2.13$ GeV.

i on the matrix element in the numerator means that only the contribution from the renormalized continuum operator $Q_{i,\rm cont}$ is included. Figure 41 shows a breakdown of the contributions of $-[\omega/(\sqrt{2}|\epsilon|)]_{\rm exp}P_0^i$ (upper panel) and $[\omega/(\sqrt{2}|\epsilon|)]_{\rm exp}P_2^i$ (lower panel) to $\mathrm{Re}(\epsilon'/\epsilon)$ and Table LI gives the numerical values. The solid filled bars in the graph denote positive quantities and the hashed bars represent negative quantities. This figure shows the importance of $Q_{4,\rm cont}$ and $Q_{6,\rm cont}$ to $-[\omega/(\sqrt{2}|\epsilon|)]_{\rm exp}P_0$ and that $[\omega/(\sqrt{2}|\epsilon|)]_{\rm exp}P_2$ comes primarily from $Q_{8,\rm cont}$.

In spite of the near cancellation in P_2-P_0 visible in Fig. 39, the statistical error on the final answer, $\pm 2.3\times 10^{-4}$ is quite encouraging. The figure also shows that the magnitude of the contribution to $\mathrm{Re}(\epsilon'/\epsilon)$ from the term proportional to P_2 is about the magnitude of the experimental value, as is also true for P_0. In Table XLIX we give our final values for the main physical quantities calculated in this work. Whether ω is taken from experiment or from this calculation is not very significant in $\mathrm{Re}(\epsilon'/\epsilon)$, as can be seen from Table XLVIII. Given the general agreement with the experimental values for real $K\to\pi\pi$ amplitudes and the relatively small statistical error on $\mathrm{Re}(\epsilon'/\epsilon)$, the difference between the current calculation for $\mathrm{Re}(\epsilon'/\epsilon)$ and experiment is surprising.

XV. CONCLUSIONS

A. Summary

We have reported the details and results of our calculation of the $K\to\pi\pi$ matrix elements relevant for the $\Delta I=1/2$ rule and ϵ'/ϵ in quenched lattice QCD using domain wall fermions. In addition, we have also reported a value for B_K, which is needed to determine ϵ from the standard model. Our

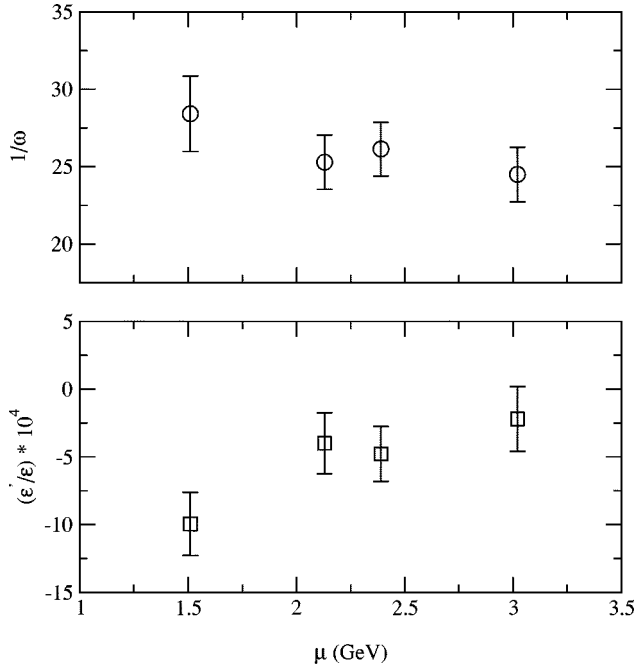

FIG. 40. A plot of $\mathrm{Re}(A_0)/\mathrm{Re}(A_2)=1/\omega$ (upper panel) and $\mathrm{Re}(\epsilon'/\epsilon)$ (lower panel) vs μ for the physical values obtained using one-loop full QCD chiral perturbation theory for the extrapolation to the physical kaon mass. The results for $1/\omega$ show some μ dependence beyond the statistical errors. For $\mathrm{Re}(\epsilon'/\epsilon)$ the μ dependence is noticeable, reflecting the visible μ dependence in $\mathrm{Im}(A_2)$. We choose to quote final values with $\mu=2.13$ GeV.

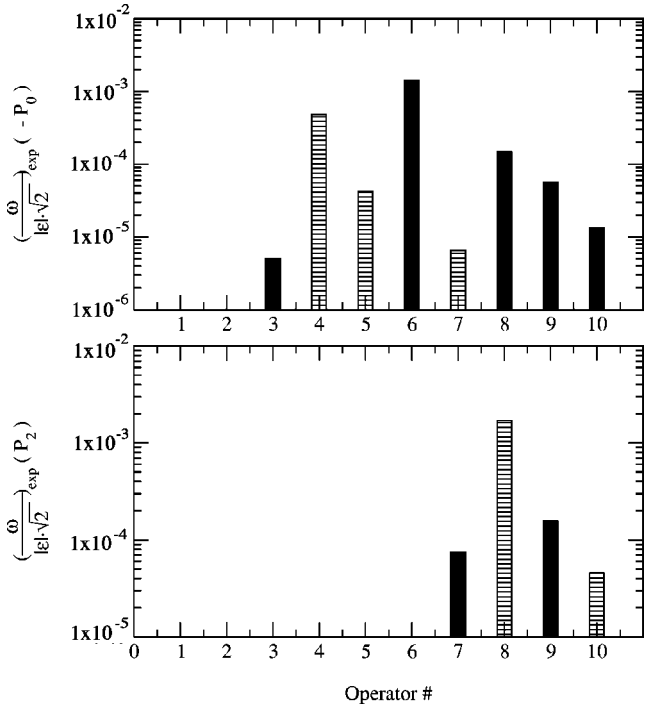

FIG. 41. A breakdown of the contribution of $Q_{i,\mathrm{cont}}$ to the imaginary amplitudes entering $-[\omega/(\sqrt{2}|\epsilon|)]_{\mathrm{exp}}P_0$ (upper panel) and $[\omega/(\sqrt{2}|\epsilon|)]_{\mathrm{exp}}P_2$ (lower panel). The solid filled bars in the graph denote positive quantities and the hashed bars represent negative quantities. The experimental values for ω and $|\epsilon|$ are used here and the data is for $\mu=2.13$ GeV.

value for B_K is slightly smaller than with other approaches, but the differences are at the 10% percent level. Our results for $\mathrm{Re}(A_0)$ and $\mathrm{Re}(A_2)$ are 10%–20% smaller than experimental values, but our value for their ratio is within 10% of the experimental value. This is a very encouraging result, since a large enhancement of the $I=0$ amplitude is being seen from the nonperturbative hadronic matrix elements, calculated using a technique where the current approximations can be reduced in the future. (The perturbative enhancement through the QCD running of the $I=0$ and $I=2$ Wilson coefficients is almost an order of magnitude smaller than the experimentally observed enhancement.) Improvements of these calculations will provide reliable systematic errors and fewer approximations, leading to a more precise test of this initial agreement between theory and experiment.

For ϵ'/ϵ, the situation is more complex and more interesting. Our results quantitatively support the long standing expectation from simple estimates that the two isospin contributions to ϵ'/ϵ are of the same order and opposite sign. Of course, such a large cancellation may be dramatically altered by removing the approximations in the current calculation. While a subtraction of power divergences is needed for $\mathrm{Re}(A_0)$, it is quantitatively much smaller than the subtraction for Q_6, which is the major contribution to $\mathrm{Im}(A_0)$. [No subtraction is required for the contributions to $\mathrm{Im}(A_2)$.] As we have shown, the dominant term in the subtraction procedure is not affected by chiral logarithm and zero mode effects, making the subtraction seem quite robust given our current understanding. Thus it appears that domain wall fermions, with their small chiral symmetry breaking for finite lattice spacing, have removed the problems found in earlier attempts where chiral symmetry breaking effects were large.

The many approximations in this calculation could affect the real and imaginary amplitudes in different ways, although at present we have no insight into how this might occur. We can estimate the size of the effects introduced by the approximations acting singly. The quenched approximation has been generally found to agree with experimental results at the 10%–20% level, except for QCD near the finite temperature phase transition where light quarks play a large role. The lowest order chiral perturbation theory results for the $K\rightarrow\pi\pi$ matrix elements are altered at the $\sim$30% level when the extrapolation to the physical kaon mass includes the known chiral logarithms. We see a $\sim$25% variation in $\mathrm{Im}(A_i)$ with the scale μ, which indicates the reliability of the combination of: using continuum perturbation theory below 1.3 GeV, one-loop matching from the NDR to RI schemes, and our implementation of nonperturbative renormalization where some operators, of order g_S^2 which are argued to be small, are neglected. We have used linear fits to our lattice data in many cases, since analytic results for the chiral logarithm terms are not known, and this could easily contribute errors on the 10% scale. We have not included any effects of isospin breaking in our results. Finally, we have only worked at one lattice spacing, but our experience with hadron masses calculated with domain wall fermions makes it likely that changes of no more than 10% will be encountered in taking the continuum limit.

TABLE LI. The contribution from the renormalized continuum operator $Q_{i,\mathrm{cont}}$ to the imaginary parts of $\langle(\pi\pi)_I|i\mathcal{H}^{(\Delta S=1)}|K^0\rangle$ is used to calculate $P_I^i \equiv \mathrm{Im}(\langle(\pi\pi)_I|-i\mathcal{H}^{(\Delta S=1)}|K^0\rangle)_i/\mathrm{Re}(A_I)$. Here we tabulate $-[\omega/(\sqrt{2}|\epsilon|)]_{\mathrm{exp}}P_0^i$ and $[\omega/(\sqrt{2}|\epsilon|)]_{\mathrm{exp}}P_2^i$ for our two extrapolation choices for $\mu=2.13$ GeV. One sees that the largest contribution to the $I=0$ channel is from $Q_{6,\mathrm{cont}}$ and the largest contribution to the $I=2$ channel is from $Q_{8,\mathrm{cont}}$. The very small errors for the contribution of $Q_{9,\mathrm{cont}}$ and $Q_{10,\mathrm{cont}}$ to $[\omega/(\sqrt{2}|\epsilon|)]_{\mathrm{exp}}P_2^i$ is due to the fact that the (27,1) operator is dominating the numerator and denominator. Since the errors in the $Q_{i,\mathrm{cont}}$ are correlated, the error for $\mathrm{Re}(\epsilon'/\epsilon)$ is not simply related to the errors from the individual contributions in this table. The experimental values for ω and $|\epsilon|$ are used here.

	$-[\omega/(\sqrt{2}\|\epsilon\|)]_{\mathrm{exp}}P_0^i$		$[\omega/(\sqrt{2}\|\epsilon\|)]_{\mathrm{exp}}P_2^i$	
i	choice 1	choice 2	choice 1	choice 2
1	0.0	0.0	0.0	0.0
2	0.0	0.0	0.0	0.0
3	$5.(58)\times10^{-6}$	$5.(58)\times10^{-6}$	0.0	0.0
4	$-4.8(11)\times10^{-4}$	$-4.8(11)\times10^{-4}$	0.0	0.0
5	$-4.2(17)\times10^{-5}$	$-4.2(17)\times10^{-5}$	0.0	0.0
6	$1.42(19)\times10^{-3}$	$1.42(19)\times10^{-3}$	0.0	0.0
7	$-4.66(36)\times10^{-6}$	$-6.50(50)\times10^{-6}$	$6.90(33)\times10^{-5}$	$7.45(35)\times10^{-5}$
8	$1.061(84)\times10^{-4}$	$1.48(12)\times10^{-4}$	$-1.571(77)\times10^{-3}$	$-1.697(84)\times10^{-3}$
9	$5.65(23)\times10^{-5}$	$5.65(23)\times10^{-5}$	$1.563\,83(69)\times10^{-4}$	$1.564\,93(75)\times10^{-4}$
10	$1.35(24)\times10^{-5}$	$1.35(24)\times10^{-5}$	$-4.5635(20)\times10^{-5}$	$-4.5668(22)\times10^{-5}$

Each of these approximations could individually produce a ~25% change in $\mathrm{Re}(A_0)$, $\mathrm{Re}(A_2)$, $\mathrm{Im}(A_0)$, or $\mathrm{Im}(A_2)$. Cumulatively, these approximations could markedly alter our result for ϵ'/ϵ, but there is currently no identified single approximation that could easily explain the discrepancy between our results and the experimental value. Lacking a single ''worst'' approximation to focus on we do not have enough information at present to even estimate how these effects act in concert for a quantity like ϵ'/ϵ, which is the difference of the ratio of amplitudes. With further work, improved calculations involving fewer approximations and reliable systematic errors will be possible.

Removing the uncontrolled effects introduced by the quenched approximation will simplify the calculation in addition to deleting a significant possible systematic error. The simplification comes from the removal of the effects of unsuppressed zero modes present in quenched QCD and the change from quenched chiral perturbation theory, where new free parameters appear in the Lagrangian, to full or partially quenched chiral perturbation theory. A recent calculation in quenched chiral perturbation theory [58] has shown that a quenched chiral logarithm appears in the determination of the subtraction coefficient $\alpha_2^{(8,1)}$, multiplied by a new free parameter. From the linearity of our data with m_s-m_d, we conclude that this parameter is small, but the presence of such terms makes fitting to numerical results less precise and offers new ways in which the quenched approximation can exhibit pathologies.

We have also calculated all the lattice matrix elements and renormalization coefficients necessary to repeat the current calculation in the context of the four-flavor effective low-energy theory, where the charm quark is not integrated out. For the four-flavor theory, continuum perturbation theory need only be used to a scale of ~2 GeV to match to our lattice. This should decrease the errors coming from the Wilson coefficients. However, the quenched lattice calculation is now required to well approximate full QCD running between the scales of 2 GeV and ~500 MeV, the scale of the kaon physics we are studying. This will clearly be a worse approximation than in the current calculation where the quenched running must approximate full QCD only between 1.3 GeV and ~500 MeV. Finally, in the four-flavor theory, operators with dimension greater than six in the effective Lagrangian are suppressed by powers of ~(0.5 GeV/5.0 GeV) compared to powers of ~(0.5 GeV/1.3 GeV) in the current calculation. The different systematic errors inherent in the use of the four-flavor theory will provide insight into the stability of our current results from the three-flavor theory.

B. Outlook

We would like to close by discussing the prospects for improving this calculation in the immediate future. It is important to note that attempts to use lattice QCD to calculate $K\to\pi\pi$ matrix elements have been ongoing for almost 20 years and without at least some chiral symmetry on the lattice these calculations were not successful. The current calculation demonstrates that all the theoretical tools are in place for these first-principles calculations and that reasonable statistical accuracy can be achieved in the quenched approximation. One consequence of the statistical accuracy achieved is increased interest in the unknown systematic errors in the calculation. We would like to address the outlook for improving the calculation by determining, and reducing, these systematic errors.

In addition to the results in this paper, the CP-PACS Collaboration has also reported results for the same observables using domain wall fermions [84]. There is general agreement in the results for ϵ'/ϵ, while our value for $\mathrm{Re}(A_0)/\mathrm{Re}(A_2)$ is

about a factor of 2 larger than their result. For both quantities, there are differences in the details of the analysis steps leading from the unrenormalized lattice matrix elements to the physical results. [A large part of the difference in $\mathrm{Re}(A_0)/\mathrm{Re}(A_2)$ is due to our use of the analytically known coefficient for the chiral logarithm in the fits for $\mathrm{Re}(A_2)$.] There are also differences in the gauge actions and volumes used and the general agreement for ϵ'/ϵ indicates that the systematic errors from such effects are not large. In particular, the CP-PACS calculations have a smaller m_{res}, due to the different gauge actions used, but, as we have argued, the m_{res} effects should be under good control. This seems to be supported by comparing the work of the two groups. The rough agreement between the groups indicates that this complicated calculation is tractable and that subsequent calculations should be able to refine these results.

In the previous section, we have mentioned estimates for the systematic errors in a single amplitude $[\mathrm{Re}(A_0),\mathrm{Re}(A_2),\mathrm{Im}(A_0),\mathrm{Im}(A_2)]$ due to the approximations employed, when each approximation is considered singly. These are only estimates, based on calculations of other observables using quenched lattice QCD, and there is no theoretical framework for addressing how these approximations, taken together, affect ϵ'/ϵ. We also do not know how a single approximation, i.e., quenching, impacts the combination of amplitudes that yields ϵ'/ϵ. However, near-term calculations, some already underway, can show how large the errors due to any single approximation are. With increasing computer power, the desired full-QCD calculations in large volumes will be possible.

The RBC Collaboration is currently repeating the calculation presented here using weaker coupling ($a^{-1}\sim 3$ GeV) and a similar size physical volume. This calculation is being performed with an improved gauge action (DBW2 [85]) which will reduce m_{res} by about a factor of 10 compared to the calculation presented here. This will allow a determination of how the quenched calculation depends on the lattice spacing and allow a check that we have correctly handled the m_{res} affects in the current calculation. In addition, at this weaker coupling the domain wall formulation may be sensible for a quark as heavy as the charm quark. This allows us the possibility of also calculating $K\to\pi\pi$ matrix elements in a four-flavor effective theory, which includes internal charm quark loops. If possible, this would check another important systematic uncertainty, the use of the three-flavor effective theory and continuum perturbation theory down to a scale of $\sim$1.3 GeV.

We are also generating full QCD lattices, with 2 flavors of dynamical domain wall quarks, at a lattice spacing of $a^{-1}\sim 1.7$ GeV, with physical volumes similar to those used here. Measuring $K\to\pi\pi$ matrix elements on these lattices will give some indication about the size of quenching effects. The volumes will not be asymptotically large and the input dynamical quark masses will be around half the strange quark mass, but these calculations should provide direct information about the importance of quenching. Larger volumes and smaller quark masses will be achieved with the next generation of computers.

To improve beyond lowest order chiral perturbation theory requires either the calculation of the higher order coefficients in the chiral expansion, and/or the direct calculation of $K\to\pi\pi$ matrix elements [47]. Both are the subject of active research in the field and require considerable numerical and analytical work to implement. While we have made extensive use of known chiral perturbation theory expressions in fitting our data, with generally good agreement, the data is too correlated and over too limited a range of quark masses to determine the coefficients of the chiral logarithms. An important aspect of trying to incorporate higher orders in chiral perturbation theory into this calculation is to have sufficient data to allow extraction of the additional low energy constants of chiral perturbation theory. Additionally, doing either higher order chiral perturbation theory or a direct calculation of $K\to\pi\pi$ in quenched QCD may be problematic due to the pathologies of the quenched approximation. Of course, for the long run, both of these methods hold promise for full QCD calculations.

We conclude by reiterating that the entire framework for successful calculations is in place and all the current approximations can be steadily improved. Accompanying this improvement will be a more quantitative understanding of our systematic errors, allowing for greater clarity in the comparison of these first principles calculations with experiment. Starting from continuum calculations of the Wilson coefficients, a very substantial effort, the lattice is used to calculate low energy matrix elements and the matching between the lattice and continuum normalizations. The current calculation demonstrates that: statistical errors are not a limiting factor; the domain wall fermion formulation, in addition to being a major theoretical advance, can be used in practical simulations; and that the complicated matching of continuum and lattice $\Delta S=1$ operators can be done with nonperturbative renormalization and domain wall fermions. This presents a very exciting future for precise calculations of experimentally important quantities using analytic techniques and lattice QCD.

ACKNOWLEDGMENTS

The authors would like to thank Andrzej Buras, Mike Creutz, Maarten Golterman, and Yigal Shamir for useful discussions. We also acknowledge use of the MILC Collaboration software (http://physics.indiana.edu/~sg/milc.html) for some of the tests we performed on our computer programs. We would like to thank T. D. Lee for valuable scientific discussions and his support in all phases of this work. The calculations reported here[3] were done on the 400 Gflops QCDSP computer [86] at Columbia University and the 600 Gflops QCDSP computer [87] at the RIKEN-BNL Research Center. We thank the Information Technology Division at BNL for their support, particularly the technical support staff

[3]A preliminary report of this calculation contained serious errors which we subsequently found and corrected. Those errors were in analysis and codes and not related to the QCDSP computer and do not affect the present paper.

led by Ed McFadden. We thank RIKEN, Brookhaven National Laboratory, and the U.S. Department of Energy for providing the facilities essential for the completion of this work. This research was supported in part by the DOE under grant No. DE-FG02-92ER40699 (Columbia), in part by the NSF under grant No. NSF-PHY96-05199 (Vranas), in part by the DOE under grant DE-AC02-98CH10886 (Soni-Dawson), in part by the RIKEN-BNL Research Center (Blum-Wingate-Ohta), and in part by the Max-Kade Foundation (Siegert).

APPENDIX A: CONVENTIONS FOR STATES AND OPERATORS

Comparing the Lagrangian of chiral perturbation theory described in Sec. III A with the Lagrangian of QCD defines the relationship between quantities expressed in terms of the pseudoscalar fields of chiral perturbation theory and the quark fields used in our simulations. Our conventions follow [88], where more details can be found. We start with the Lagrangian given in Eq. (50) and the Minkowski space QCD Lagrangian

$$\mathcal{L}_{\rm QCD} = -\frac{1}{4}(F^a_{\mu\nu})^2 + \overline{\psi}(i\not{D} - m)\psi. \tag{A1}$$

We use the conventional assignment of pseudoscalars to the chiral perturbation theory fields

$$\overline{\pi} \equiv \phi^a t^a = \begin{pmatrix} \pi^0/\sqrt{2} + \eta/\sqrt{6} & \pi^+ & K^+ \\ \pi^- & -\pi^0/\sqrt{2} + \eta/\sqrt{6} & K^0 \\ K^- & \overline{K}^0 & -2\eta/\sqrt{6}. \end{pmatrix}. \tag{A2}$$

We work with relativistically normalized states

$$\langle \pi^a(\boldsymbol{p})|\pi^b(\boldsymbol{p}')\rangle = \delta^{ab}(2E_{\boldsymbol{p}})(2\pi)^3\delta^3(\boldsymbol{p}-\boldsymbol{p}') \xrightarrow[\text{lattice}]{} \delta^{ab}(2E_{\boldsymbol{p}})V_s\delta_{\boldsymbol{p},\boldsymbol{p}'}. \tag{A3}$$

By considering global axial transformations with $U_L = \exp(-ia_a t_a)$ and $U_R = \exp(ia_a t_a)$, we find for the axial currents A^a_μ

$$A^\mu_a = \frac{if^2}{4}[\mathrm{Tr}(\Sigma t_a \partial^\mu \Sigma^\dagger) - \mathrm{Tr}(\Sigma^\dagger t_a \partial^\mu \Sigma)], \quad \chi PT, \tag{A4}$$

$$A^\mu_a = \overline{\psi}\gamma^\mu\gamma_5 t_a \psi, \qquad \text{QCD}. \tag{A5}$$

The divergence of the axial currents is

$$\partial_\mu A^\mu_a = iv\ \mathrm{Tr}[t_a(\{M,\Sigma\} - \{M^\dagger,\Sigma^\dagger\})], \quad \chi PT, \tag{A6}$$

$$\partial_\mu A^\mu_a = 2m[i\overline{\psi}\gamma_5 t_a \psi], \qquad \text{QCD}. \tag{A7}$$

For degenerate quark masses, Eq. (A6) becomes

$$\partial_\mu A^\mu_a = 2imv\ \mathrm{Tr}[t_a(\Sigma - \Sigma^\dagger)], \quad \chi PT. \tag{A8}$$

Thus, in lowest order in chiral perturbation theory, we can make the associations

$$i\overline{d}(x)\gamma_5 u(x) = i\overline{\psi}(x)\gamma_5 \frac{t_1 + it_2}{\sqrt{2}}\psi(x) \Leftrightarrow \frac{-4v}{f}\pi^+(x), \tag{A9}$$

$$i\overline{s}(x)\gamma_5 u(x) = i\overline{\psi}(x)\gamma_5 \frac{t_4 + it_5}{\sqrt{2}}\psi(x) \Leftrightarrow \frac{-4v}{f}K^+(x). \tag{A10}$$

States $|K^+\rangle$ created by the operator $K^-(x)$ therefore have

$$\langle 0|i\overline{s}\gamma_5 u|K^+\rangle = -\frac{4v}{f} \tag{A11}$$

and to lowest order in chiral perturbation theory

$$\langle 0|\overline{d}(x)\gamma^\mu\gamma_5 u(x)|\pi^+\rangle = -ifp^\mu e^{-ip\cdot x} \tag{A12}$$

where $f > 0$.

We define a pseudoscalar density in chiral perturbation theory by

$$P^{\chi PT}_a \equiv -\frac{4v}{f}\phi_a \tag{A13}$$

and a corresponding QCD pseudoscalar density as

$$P^{\rm QCD}_a \equiv i\overline{\psi}\gamma_5 t_a \psi. \tag{A14}$$

Then for degenerate quark masses, the Minkowski space Ward-Takahashi identity governing the pseudoscalar masses is

$$i\partial^x_\mu\langle A^\mu_a(x)P_b(y)\rangle = 2mi\langle P_a(x)P_b(y)\rangle - 4v\,\delta_{a,b}\delta^4(x-y), \qquad \chi PT, \tag{A15}$$

$$i\partial^x_\mu(A^\mu_a(x)P_b(y)) = 2mi\langle P_a(x)P_b(y)\rangle + 2\langle\overline{u}u(x)\rangle\delta_{a,b}\delta^4(x-y), \quad \text{QCD}, \tag{A16}$$

where the chiral perturbation theory result is valid in lowest order. Here we see the relation $\langle\overline{u}u\rangle = -2v$ between the chiral condensate in QCD and in chiral perturbation theory.

APPENDIX B: FLAVOR AND ISOSPIN DECOMPOSITION OF FOUR-QUARK OPERATORS

As discussed in [88], one can apply the tensor method for finding irreducible representations of groups to the operators in Eqs. (4)–(23). We start first with the left-left operators and note the general term $\overline{q}_{L,i}, \overline{q}_{L,j}, q_{L,k}, q_{L,l}$, where i, j, k, and l are flavor indices, is a member of a representation of $\mathrm{SU}(3)_L$ with dimension 81. Denoting this term by $(T_L)^{i,j}_{k,l}$, the irreducible representations are found by appropriately symmetrizing T_L.

Symmetry of T_L	$(T_L)^{\{i,j\}}_{\{k,l\}}$	$(T_L)^{\{i,j\}}_{[k,l]}$	$(T_L)^{[i,j]}_{\{k,l\}}$	$(T_L)^{[i,j]}_{[k,l]}$
Dimension	36	18	18	9
Irrep. dimension	27,8,1	8,8,1,1	8,8,1,1	8,1

The irreducible representations in the last line are found by tracing on pairs of upper and lower indices. For example, the 27 representation is completely symmetric in all indices and traceless on any pair of upper and lower indices, while the completely symmetric representation, which has a nonzero trace, is dimension 8.

We can now determine the number of irreducible representations that $Q_1=(\bar{s}d)_{V-A}(\bar{u}u)_{V-A}$ enters. Here we will suppress the color indices and only consider the color unmixed case, so the terms in parentheses will have their color indices contracted together. Since $(\bar{s}d)_{V-A}$ and $(\bar{u}u)_{V-A}$ commute with each other, left-left four quark current operators are symmetric under simultaneous exchange of quark and antiquark indices. Thus, left-left operators must belong to $(T_L)^{\{i,j\}}_{\{k,l\}}$ or $(T_L)^{[i,j]}_{[k,l]}$ and they have either $(L,R)=(8,1)$ or $(L,R)=(27,1)$. We will also want to simultaneously separate the operators into representations of definite isospin.

The operator

$$(\bar{s}d)_{V-A}(\bar{u}u)_{V-A}+(\bar{s}u)_{V-A}(\bar{u}d)_{V-A} \tag{B1}$$

is completely symmetric on all indices. To get a (27,1) with $I=3/2$, we must add terms so it is simultaneously traceless in $SU(3)_L$ and isospin. Equation (B1) has $(T_L)^{3,1}_{2,1}=(T_L)^{3,1}_{1,2}=(T_L)^{1,3}_{2,1}=(T_L)^{1,3}_{1,2}=1/2$, so if we add $(T_L)^{3,2}_{2,2}=(T_L)^{2,3}_{2,2}=-1/2$ with all other elements zero, we have tracelessness in $SU(3)_L$ and isospin. Thus, we have for left-left operators, symmetric in all indices, a (27,1) representation with $I=3/2$ given by

$$Q^{\Delta s=1,\Delta d=-1}_{LL,S,(27,1),3/2}=(\bar{s}d)_{V-A}(\bar{u}u)_{V-A}+(\bar{s}u)_{V-A}(\bar{u}d)_{V-A} -(\bar{s}d)_{V-A}(\bar{d}d)_{V-A}. \tag{B2}$$

Returning again to Eq. (B1) we can find the $I=1/2$ operator by making Eq. (B1) symmetric under $u\leftrightarrow d$ and then making the results traceless on pairs of upper and lower indices. This gives

$$Q^{\Delta s=1,\Delta d=-1}_{LL,S,(27,1),1/2}=(\bar{s}d)_{V-A}(\bar{u}u)_{V-A}+(\bar{s}u)_{V-A}(\bar{u}d)_{V-A} +2(\bar{s}d)_{V-A}(\bar{d}d)_{V-A}-3(\bar{s}d)_{V-A}(\bar{s}s)_{V-A} \tag{B3}$$

corresponding to $(T_L)^{3,1}_{2,1}=(T_L)^{3,1}_{1,2}=(T_L)^{1,3}_{2,1}=(T_L)^{1,3}_{1,2}=1/2$, $(T_L)^{3,2}_{2,2}=(T_L)^{2,3}_{2,2}=1$, and $(T_L)^{3,3}_{2,3}=(T_L)^{3,3}_{3,2}=-3/2$, with other elements zero.

For the (8,1) from $(T_L)^{\{i,j\}}_{\{k,l\}}$ we start again from Eq. (B1), again symmetrizing Eq. (B1) under $u\leftrightarrow d$ to get $I=1/2$. However, demanding that the operator not be traceless on contraction of upper and lower indices while still being symmetric on exchange of upper or lower indices gives

$$Q^{\Delta s=1,\Delta d=-1}_{LL,S,(8,1),1/2}=(\bar{s}d)_{V-A}(\bar{u}u)_{V-A}+(\bar{s}u)_{V-A}(\bar{u}d)_{V-A} +2(\bar{s}d)_{V-A}(\bar{d}d)_{V-A}+2(\bar{s}d)_{V-A}(\bar{s}s)_{V-A}. \tag{B4}$$

The final (8,1) comes from $(T_L)^{[i,j]}_{[k,l]}$, which is antisymmetric on pairs of upper and lower indices, and is easily seen to be

$$Q^{\Delta s=1,\Delta d=-1}_{LL,A,(8,1),1/2}=(\bar{s}d)_{V-A}(\bar{u}u)_{V-A}-(\bar{s}u)_{V-A}(\bar{u}d)_{V-A}. \tag{B5}$$

Thus, we have found that there are three irreducible representations of left-left, $\Delta s=1$, $\Delta d=-1$ four-quark operators under $SU(3)_L\otimes SU(3)_R$; a (27,1) and two (8,1) representations. The (27,1) contains both $I=1/2$ and $I=3/2$ parts. We can write Q_1, Q_2, Q_3, Q_4, Q_9, and Q_{10} in terms of these representations, yielding

$$Q_1=\frac{1}{10}Q^{\Delta s=1,\Delta d=-1}_{LL,S,(8,1),1/2}+\frac{1}{2}Q^{\Delta s=1,\Delta d=-1}_{LL,A,(8,1),1/2}+\frac{1}{15}Q^{\Delta s=1,\Delta d=-1}_{LL,S,(27,1),1/2} +\frac{1}{3}Q^{\Delta s=1,\Delta d=-1}_{LL,S,(27,1),3/2}, \tag{B6}$$

$$Q_2=\frac{1}{10}Q^{\Delta s=1,\Delta d=-1}_{LL,S,(8,1),1/2}-\frac{1}{2}Q^{\Delta s=1,\Delta d=-1}_{LL,A,(8,1),1/2}+\frac{1}{15}Q^{\Delta s=1,\Delta d=-1}_{LL,S,(27,1),1/2} +\frac{1}{3}Q^{\Delta s=1,\Delta d=-1}_{LL,S,(27,1),3/2}, \tag{B7}$$

$$Q_3=\frac{1}{2}Q^{\Delta s=1,\Delta d=-1}_{LL,S,(8,1),1/2}+\frac{1}{2}Q^{\Delta s=1,\Delta d=-1}_{LL,A,(8,1),1/2}, \tag{B8}$$

$$Q_4=\frac{1}{2}Q^{\Delta s=1,\Delta d=-1}_{LL,S,(8,1),1/2}-\frac{1}{2}Q^{\Delta s=1,\Delta d=-1}_{LL,A,(8,1),1/2}, \tag{B9}$$

$$Q_9=-\frac{1}{10}Q^{\Delta s=1,\Delta d=-1}_{LL,S,(8,1),1/2}+\frac{1}{2}Q^{\Delta s=1,\Delta d=-1}_{LL,A,(8,1),1/2} +\frac{1}{10}Q^{\Delta s=1,\Delta d=-1}_{LL,S,(27,1),1/2}+\frac{1}{2}Q^{\Delta s=1,\Delta d=-1}_{LL,S,(27,1),3/2}, \tag{B10}$$

$$Q_{10}=-\frac{1}{10}Q^{\Delta s=1,\Delta d=-1}_{LL,S,(8,1),1/2}-\frac{1}{2}Q^{\Delta s=1,\Delta d=-1}_{LL,A,(8,1),1/2} +\frac{1}{10}Q^{\Delta s=1,\Delta d=-1}_{LL,S,(27,1),1/2}+\frac{1}{2}Q^{\Delta s=1,\Delta d=-1}_{LL,S,(27,1),3/2}, \tag{B11}$$

For left-right operators, we can perform a similar construction. For the gluonic penguins, the right-handed currents are singlets under $SU(3)_R$ due to the sum over u, d, and s quarks, with equal weight for each quark. Including the charm quark still produces an (8,1) since the charm quark is also an $SU(3)_R$ singlet.

For the left-right electroweak penguins, a bit more work is required. Now we have three representation matrices for each operator, $(T_L)^i_j$, $(T_R)^k_l$, and $(T_I)^k_{j,l}$, for $SU(3)_L$, $SU(3)_R$, and isospin, respectively. For the isospin case, we

restrict j, k, and l to be 1 or 2. Notice that both left- and right-handed quarks appear in the T for isospin and to get the desired isospin decomposition we will have to symmetrize, antisymmetrize, and trace on these indices. To get (8,8) representations, we must have $(T_L)^i_i=0$ and $(T_R)^k_k=0$.

We start with a part of Q_7 and see how many irreducible representations it enters by appropriate symmetrizations, etc. on the quarks. The first term in Q_7 is

$$(\bar{s}d)_{V-A}(\bar{u}u)_{V+A}. \tag{B12}$$

To make an $I=3/2$ operator $(T_I)^k_{j,l}$ must be symmetric on j and l and traceless on k and either j or l. Symmetrizing gives

$$(\bar{s}d)_{V-A}(\bar{u}u)_{V+A}+(\bar{s}u)_{V-A}(\bar{u}d)_{V+A} \tag{B13}$$

and tracelessness in both isospin and $SU(3)_R$ gives

$$Q^{\Delta s=1,\Delta d=-1}_{L,R,(8,8),S,3/2}=(\bar{s}d)_{V-A}(\bar{u}u)_{V+A}+(\bar{s}u)_{V-A}(\bar{u}d)_{V+A} -(\bar{s}d)_{V-A}(\bar{d}d)_{V+A}. \tag{B14}$$

From Eq. (B12) we can make an $I=1/2$ operator by putting the quarks in an $I=1$ state and then adding the antiquark such that the total isospin is 1/2. We symmetrize $(T_I)^k_{j,l}$ on j and l and require that $(T_I)^1_{j,1}=(T_I)^2_{j,2}$ to get isospin 1/2. This yields

$$(\bar{s}d)_{V-A}(\bar{u}u)_{V+A}+(\bar{s}u)_{V-A}(\bar{u}d)_{V+A}+2(\bar{s}d)_{V-A}(\bar{d}d)_{V+A}. \tag{B15}$$

The last step requires tracelessness on only the $SU(3)_R$ index, to give an 8_R. Thus we get

$$Q^{\Delta s=1,\Delta d=-1}_{LR,(8,8),S,1/2}=(\bar{s}d)_{V-A}(\bar{u}u)_{V+A}+(\bar{s}u)_{V-A}(\bar{u}d)_{V+A} +2(\bar{s}d)_{V-A}(\bar{d}d)_{V+A}-3(\bar{s}d)_{V-A}(\bar{s}s)_{V+A}. \tag{B16}$$

From Eq. (B12) we can make a second $I=1/2$ operator by putting the quarks in an $I=0$ state and then adding the antiquark. We antisymmetrize $(T_I)^k_{j,l}$ on j and l and require that $(T_R)^k_l=0$ to produce an 8_R. This yields

$$Q^{\Delta s=1,\Delta d=-1}_{LR,(8,8),A,1/2}=(\bar{s}d)_{V-A}(\bar{u}u)_{V+A}-(\bar{s}u)_{V-A}(\bar{u}d)_{V+A} -(\bar{s}d)_{V-A}(\bar{s}s)_{V+A}. \tag{B17}$$

With these isospin representations of an (8,8) color unmixed operator, we can write

$$Q_7=\frac{1}{2}Q^{\Delta s=1,\Delta d=-1}_{LR,(8,8),S,3/2}+\frac{1}{2}Q^{\Delta s=1,\Delta d=-1}_{LR,(8,8),A,1/2}. \tag{B18}$$

The result for Q_8 is identical, except the color indices are mixed.

APPENDIX C: DEFINITIONS OF Θ OPERATORS

In this section we give the relations between the Θ operators of chiral perturbation theory and the four-quark operators defined in Appendix B. We define

$$\Theta^{(27,1),(3/2)}\equiv Q^{\Delta s=1,\Delta d=-1}_{LL,S,(27,1),3/2} \quad [\text{Eq.(B2)}], \tag{C1}$$

$$\Theta^{(27,1),(1/2)}\equiv Q^{\Delta s=1,\Delta d=-1}_{LL,S,(27,1),1/2} \quad [\text{Eq.(B3)}], \tag{C2}$$

$$\Theta_7^{(8,8),(3/2)}\equiv\frac{1}{2}Q^{\Delta s=1,\Delta d=-1}_{LR,(8,8),S,3/2} \quad [\text{Eq.(B14)}], \tag{C3}$$

$$\Theta_7^{(8,8),(1/2)}\equiv\frac{1}{2}Q^{\Delta s=1,\Delta d=-1}_{LR,(8,8),A,1/2} \quad [\text{Eq.(B17)}]. \tag{C4}$$

The definitions for $\Theta_8^{(8,8),(3/2)}$ and $\Theta_8^{(8,8),(1/2)}$ are the same as in Eqs. (C3) and (C4), except that the four-quark operator has color mixed indices. For $i=7$, 8 this gives

$$Q_i=\Theta_i^{(8,8)}=\Theta_i^{(8,8),(3/2)}+\Theta_i^{(8,8),(1/2)}. \tag{C5}$$

In terms of the parameters $\alpha^{(27,1)}$ and $\alpha^{(8,8)}$ defined in Eqs. (52), (53), and (54) we have

$$\Theta^{(27,1),(1/2)}=\alpha^{(27,1)}\tilde{\Theta}^{(27,1),(1/2)}, \tag{C6}$$

$$\Theta^{(27,1),(3/2)}=\alpha^{(27,1)}\tilde{\Theta}^{(27,1),(3/2)}, \tag{C7}$$

$$\Theta^{(8,8),(1/2)}=\alpha^{(8,8)}\tilde{\Theta}^{(8,8),(1/2)}, \tag{C8}$$

$$\Theta^{(8,8),(3/2)}=\alpha^{(8,8)}\tilde{\Theta}^{(8,8),(3/2)}. \tag{C9}$$

APPENDIX D: ISOSPIN DECOMPOSITION OF OPERATORS IN CHIRAL PERTURBATION THEORY

In Appendix B we have given the decomposition of our $\Delta S=1$, $\Delta D=-1$ four-quark operators into irreducible representations of $SU(3)_L\otimes SU(3)_R$ with well-defined isospin. In this section, we give the explicit decomposition of the chiral perturbation theory operators $\tilde{\Theta}^{(27,1)}$ and $\tilde{\Theta}^{(8,8)}$ into definite isospin components. From this one can easily work out the relations between the $\Delta I=1/2$ and $\Delta I=3/2$ parts of matrix elements.

For $\tilde{\Theta}^{(8,8)}$, we use the definition in [33] and write

$$\tilde{\Theta}^{(8,8)}=\mathrm{Tr}\left[\begin{pmatrix}0&0&0\\0&0&0\\0&1&0\end{pmatrix}\Sigma\begin{pmatrix}2&0&0\\0&-1&0\\0&0&-1\end{pmatrix}\Sigma^\dagger\right]. \tag{D1}$$

The nonzero element of the first matrix in the equation above reproduces the $\bar{s}d$ factor in Eq. (16) while the diagonal terms in the second matrix represent the terms in the sum over quarks in Eq. (16). The isospin decomposition can be immediately read off from Eqs. (B14) and (B17) giving

$$\tilde{\Theta}^{(8,8),(3/2)} = \mathrm{Tr}\left[\begin{pmatrix}0&0&0\\0&0&0\\0&1&0\end{pmatrix}\Sigma\begin{pmatrix}1&0&0\\0&-1&0\\0&0&0\end{pmatrix}\Sigma^\dagger\right] + \mathrm{Tr}\left[\begin{pmatrix}0&0&0\\0&0&0\\1&0&0\end{pmatrix}\Sigma\begin{pmatrix}0&1&0\\0&0&0\\0&0&0\end{pmatrix}\Sigma^\dagger\right], \quad \text{(D2)}$$

$$\tilde{\Theta}^{(8,8),(1/2)} = \mathrm{Tr}\left[\begin{pmatrix}0&0&0\\0&0&0\\0&1&0\end{pmatrix}\Sigma\begin{pmatrix}1&0&0\\0&0&0\\0&0&-1\end{pmatrix}\Sigma^\dagger\right] + \mathrm{Tr}\left[\begin{pmatrix}0&0&0\\0&0&0\\1&0&0\end{pmatrix}\Sigma\begin{pmatrix}0&-1&0\\0&0&0\\0&0&0\end{pmatrix}\Sigma^\dagger\right], \quad \text{(D3)}$$

where $\tilde{\Theta}^{(8,8)} = \tilde{\Theta}^{(8,8),(1/2)} + \tilde{\Theta}^{(8,8),(3/2)}$.

With this explicit isospin decomposition, one finds

$$\langle \pi^+ | \Theta^{(8,8),(3/2)} | K^+ \rangle \equiv \frac{12}{f^2}\alpha^{(8,8),(3/2)} = \frac{4}{f^2}\alpha^{(8,8)}, \quad \text{(D4)}$$

$$\langle \pi^+ | \Theta^{(8,8),(1/2)} | K^+ \rangle \equiv \frac{12}{f^2}\alpha^{(8,8),(1/2)} = \frac{8}{f^2}\alpha^{(8,8)}, \quad \text{(D5)}$$

which yields $\alpha^{(8,8),(1/2)} = 2\alpha^{(8,8),(3/2)}$ where $\alpha^{(8,8)} = \alpha^{(8,8),(1/2)} + \alpha^{(8,8),(3/2)}$. Similarly one finds

$$\langle \pi^+\pi^- | \Theta^{(8,8),(3/2)} | K^0 \rangle = -\frac{12i}{f^3}\alpha^{(8,8),(3/2)} = \frac{-4i}{f^3}\alpha^{(8,8)}, \quad \text{(D6)}$$

$$\langle \pi^+\pi^- | \Theta^{(8,8),(1/2)} | K^0 \rangle = \frac{-12i}{f^3}\alpha^{(8,8),(1/2)} = \frac{-8i}{f^3}\alpha^{(8,8)}. \quad \text{(D7)}$$

For $\tilde{\Theta}^{(27,1)}$, we use the definition in [12] and write

$$\tilde{\Theta}^{(27,1),(3/2)} = \mathrm{Tr}\left[\begin{pmatrix}0&0&0\\0&0&0\\0&1&0\end{pmatrix}\Sigma\partial_\mu\Sigma^\dagger\right]\mathrm{Tr}\left[\begin{pmatrix}1&0&0\\0&-1&0\\0&0&0\end{pmatrix}\Sigma\partial^\mu\Sigma^\dagger\right] + \mathrm{Tr}\left[\begin{pmatrix}0&0&0\\0&0&0\\1&0&0\end{pmatrix}\Sigma\partial_\mu\Sigma^\dagger\right]\mathrm{Tr}\left[\begin{pmatrix}0&1&0\\0&0&0\\0&0&0\end{pmatrix}\Sigma\partial^\mu\Sigma^\dagger\right], \quad \text{(D8)}$$

$$\tilde{\Theta}^{(27,1),(1/2)} = \mathrm{Tr}\left[\begin{pmatrix}0&0&0\\0&0&0\\0&1&0\end{pmatrix}\Sigma\partial_\mu\Sigma^\dagger\right]\mathrm{Tr}\left[\begin{pmatrix}1&0&0\\0&2&0\\0&0&-3\end{pmatrix}\Sigma\partial^\mu\Sigma^\dagger\right] + \mathrm{Tr}\left[\begin{pmatrix}0&0&0\\0&0&0\\1&0&0\end{pmatrix}\Sigma\partial_\mu\Sigma^\dagger\right]\mathrm{Tr}\left[\begin{pmatrix}0&1&0\\0&0&0\\0&0&0\end{pmatrix}\Sigma\partial^\mu\Sigma^\dagger\right]. \quad \text{(D9)}$$

Working in lowest order chiral perturbation theory then gives

$$\langle \pi^+ | \Theta^{(27,1),(3/2)} | K^+ \rangle \equiv -\frac{4m_M^2}{f^2}\alpha^{(27,1),(3/2)} = -\frac{4m_M^2}{f^2}\alpha^{(27,1)}, \quad \text{(D10)}$$

$$\langle \pi^+ | \Theta^{(27,1),(1/2)} | K^+ \rangle \equiv -\frac{4m_M^2}{f^2}\alpha^{(27,1),(1/2)} = -\frac{4m_M^2}{f^2}\alpha^{(27,1)}, \quad \text{(D11)}$$

and

$$\langle \pi^+\pi^- | \Theta^{(27,1),(3/2)} | K^0 \rangle = -\frac{4i}{f^3}(m_{K^0}^2 - m_{\pi^+}^2)\alpha^{(27,1),(3/2)} = -\frac{4i}{f^3}(m_{K^0}^2 - m_{\pi^+}^2)\alpha^{(27,1)}, \quad \text{(D12)}$$

$$\langle \pi^+\pi^- | \Theta^{(27,1),(1/2)} | K^0 \rangle = -\frac{4i}{f^3}(m_{K^0}^2 - m_{\pi^+}^2)\alpha^{(27,1)(1/2)} = -\frac{4i}{f^3}(m_{K^0}^2 - m_{\pi^+}^2)\alpha^{(27,1)}. \quad \text{(D13)}$$

APPENDIX E: DEFINITIONS FOR STANDARD MODEL PARAMETERS

We follow [34] and define the Cabibbo-Kobayashi-Maskawa matrix as

$$V \equiv \begin{pmatrix} V_{ud} & V_{us} & V_{ub} \\ V_{cd} & V_{cs} & V_{cb} \\ V_{td} & V_{ts} & V_{tb} \end{pmatrix} \approx \begin{pmatrix} 1-\lambda^2/2 & \lambda & A\lambda^3(\rho - i\eta) \\ -\lambda & 1-\lambda^2/2 & A\lambda^2 \\ A\lambda^3(1-\rho-i\eta) & -A\lambda^2 & 1 \end{pmatrix}. \quad \text{(E1)}$$

Outside of this section, we use $\lambda_{\rm CKM}=\lambda$, $A_{\rm CKM}=A$, and $\rho_{\rm CKM}=\rho$ to avoid confusion. Recent reviews have quoted values for

$$\overline{\rho}\equiv\rho\left(1-\frac{\lambda^2}{2}\right), \tag{E2}$$

$$\overline{\eta}\equiv\eta\left(1-\frac{\lambda^2}{2}\right). \tag{E3}$$

Our values for V_{td} are determined from

$$V_{td}=A\lambda^3(1-\rho-i\eta). \tag{E4}$$

[1] J. H. Christenson, J. W. Cronin, V. L. Fitch, and R. Turlay, Phys. Rev. Lett. **13**, 138 (1964).
[2] KTeV Collaboration, A. Alavi-Harati *et al.*, Phys. Rev. Lett. **83**, 22 (1999).
[3] KTeV Collaboration, http://kpasa.fnal.gov:8080/public
[4] NA48 Collaboration, V. Fanti *et al.*, Phys. Lett. B **465**, 335 (1999).
[5] NA48 Collaboration, http://na48.web.cern.ch/NA48
[6] M. Kobayashi and T. Maskawa, Prog. Theor. Phys. **49**, 652 (1973).
[7] S. Bertolini, M. Fabbrichesi, and J. O. Eeg, Rev. Mod. Phys. **72**, 65 (2000).
[8] C. W. Bernard, T. Draper, G. Hockney, A. M. Rushton, and A. Soni, Phys. Rev. Lett. **55**, 2770 (1985).
[9] M. Bochicchio, L. Maiani, G. Martinelli, G. C. Rossi, and M. Testa, Nucl. Phys. **B262**, 331 (1985).
[10] D. Pekurovsky and G. Kilcup, Phys. Rev. D **64**, 074502 (2001).
[11] S. R. Sharpe and A. Patel, Nucl. Phys. **B417**, 307 (1994).
[12] C. Bernard, T. Draper, A. Soni, H. D. Politzer, and M. B. Wise, Phys. Rev. D **32**, 2343 (1985).
[13] A. Morel, SACLAY-PhT/87-020.
[14] S. R. Sharpe, Phys. Rev. D **41**, 3233 (1990).
[15] C. W. Bernard and M. F. L. Golterman, Phys. Rev. D **46**, 853 (1992).
[16] D. B. Kaplan, Phys. Lett. B **288**, 342 (1992).
[17] Y. Shamir, Nucl. Phys. **B406**, 90 (1993).
[18] V. Furman and Y. Shamir, Nucl. Phys. **B439**, 54 (1995).
[19] R. Narayanan and H. Neuberger, Phys. Lett. B **302**, 62 (1993).
[20] R. Narayanan and H. Neuberger, Phys. Rev. Lett. **71**, 3251 (1993).
[21] T. Blum *et al.*, Phys. Rev. D (to be published), hep-lat/0007038.
[22] CP-PACS Collaboration, A. Ali Khan *et al.*, Phys. Rev. D **63**, 114504 (2001).
[23] A. Buras, M. Jamin, and M. E. Lautenbacher, Nucl. Phys. **B408**, 209 (1993).
[24] M. Ciuchini, E. Franco, G. Martinelli, L. Reina, and L. Silvestrini, Z. Phys. C **68**, 239 (1995).
[25] M. Luscher, S. Sint, R. Sommer, and H. Wittig, Nucl. Phys. **B491**, 344 (1997).
[26] G. Martinelli, C. Pittori, C. T. Sachrajda, M. Testa, and A. Vladikas, Nucl. Phys. **B445**, 81 (1995).
[27] G. Altarelli and L. Maiani, Phys. Lett. **52B**, 351 (1974).
[28] M. K. Gaillard and B. W. Lee, Phys. Rev. Lett. **33**, 108 (1974).
[29] A. I. Vainshtein, V. I. Zakharov, and M. A. Shifman, JETP Lett. **22**, 55 (1975).
[30] M. A. Shifman, A. I. Vainshtein, and V. I. Zakharov, Nucl. Phys. **B120**, 316 (1977).
[31] F. J. Gilman and M. B. Wise, Phys. Lett. **83B**, 83 (1979).
[32] F. J. Gilman and M. B. Wise, Phys. Rev. D **20**, 2392 (1979).
[33] J. Bijnens and M. B. Wise, Phys. Lett. **137B**, 245 (1984).
[34] Particle Data Group, D. Groom *et al.*, Eur. Phys. J. C **15**, 1 (2000), URL http://pdg.lbl.gov
[35] S. L. Glashow, J. Iliopoulos, and L. Maiani, Phys. Rev. D **2**, 1285 (1970).
[36] M. K. Gaillard and B. W. Lee, Phys. Rev. D **10**, 897 (1974).
[37] F. J. Gilman and M. B. Wise, Phys. Lett. **93B**, 129 (1980).
[38] F. J. Gilman and M. B. Wise, Phys. Rev. D **27**, 1128 (1983).
[39] A. J. Buras, M. Jamin, and P. H. Weisz, Nucl. Phys. **B347**, 491 (1990).
[40] S. Herrlich and U. Nierste, Nucl. Phys. **B476**, 27 (1996).
[41] T. Inami and C. S. Lim, Prog. Theor. Phys. **65**, 297 (1981).
[42] B. Winstein and L. Wolfenstein, Rev. Mod. Phys. **65**, 1113 (1993).
[43] A. J. Buras, hep-ph/9806471.
[44] A. J. Buras and J. M. Gerard, Phys. Lett. B **192**, 156 (1987).
[45] G. Ecker, G. Isidori, G. Muller, H. Neufeld, and A. Pich, Nucl. Phys. **B591**, 419 (2000).
[46] L. Maiani and M. Testa, Phys. Lett. B **245**, 585 (1990).
[47] L. Lellouch and M. Luscher, Commun. Math. Phys. **219**, 31 (2000).
[48] P. Langacker and H. Pagels, Phys. Rev. D **8**, 4595 (1973).
[49] J. Gasser and H. Leutwyler, Ann. Phys. (N.Y.) **158**, 142 (1984).
[50] J. Gasser and H. Leutwyler, Nucl. Phys. **B250**, 465 (1985).
[51] V. Cirigliano and E. Golowich, Phys. Rev. D **65**, 054014 (2002).
[52] J. Bijnens, H. Sonoda, and M. B. Wise, Phys. Rev. Lett. **53**, 2367 (1984).
[53] J. Bijnens, Phys. Lett. **152B**, 226 (1985).
[54] M. F. L. Golterman and K.-C. Leung, Phys. Rev. D **57**, 5703 (1998).
[55] M. Golterman and E. Pallante, J. High Energy Phys. **08**, 023 (2000).
[56] J. Bijnens, E. Pallante, and J. Prades, Nucl. Phys. **B521**, 305 (1998).
[57] S. R. Sharpe, A. Patel, R. Gupta, G. Guralnik, and G. W. Kilcup, Nucl. Phys. **B286**, 253 (1987).
[58] M. Golterman and E. Pallante, J. High Energy Phys. **10**, 037 (2001).
[59] T. Blum *et al.*, Phys. Rev. D **66**, 014504 (2002).
[60] CP-PACS Collaboration, S. Aoki *et al.*, Phys. Rev. Lett. **84**, 238 (2000).
[61] W. Bardeen, A. Duncan, E. Eichten, and H. Thacker, Phys. Rev. D **62**, 114505 (2000).

[62] A. J. Buras, M. Jamin, M. E. Lautenbacher, and P. H. Weisz, Nucl. Phys. **B400**, 37 (1993).
[63] A. J. Buras, M. Jamin, and M. E. Lautenbacher, Nucl. Phys. **B400**, 75 (1993).
[64] G. Buchalla, A. J. Buras, and M. E. Lautenbacher, Rev. Mod. Phys. **68**, 1125 (1996).
[65] M. Ciuchini, E. Franco, G. Martinelli, and L. Reina, Nucl. Phys. **B415**, 403 (1994).
[66] ALPHA Collaboration, S. Capitani, M. Luscher, R. Sommer, and H. Wittig, Nucl. Phys. **B544**, 669 (1999).
[67] A. J. Buras, P. Gambino, and U. A. Haisch, Nucl. Phys. **B570**, 117 (2000).
[68] C. Bobeth, M. Misiak, and J. Urban, Nucl. Phys. **B574**, 291 (2000).
[69] C. Dawson *et al.*, Nucl. Phys. **B514**, 313 (1998).
[70] G. P. Lepage and P. B. Mackenzie, Phys. Rev. D **48**, 2250 (1993).
[71] A. Donini, V. Gimenez, G. Martinelli, M. Talevi, and A. Vladikas, Eur. Phys. J. C **10**, 121 (1999).
[72] S. Aoki and Y. Kuramashi, Phys. Rev. D **63**, 054504 (2001).
[73] S. Aoki, T. Izubuchi, Y. Kuramashi, and Y. Taniguchi, Phys. Rev. D **60**, 114504 (1999).
[74] T. Blum, A. Soni, and M. Wingate, Phys. Rev. D **60**, 114507 (1999).
[75] Y. Zhestkov, Ph.D. thesis, Columbia University, 2001.
[76] M. F. L. Golterman and K. C. Leung, Phys. Rev. D **56**, 2950 (1997).
[77] V. Cirigliano and E. Golowich, Phys. Lett. B **475**, 351 (2000).
[78] RIKEN-Brookhaven-Columbia Collaboration (in preparation).
[79] M. Crisafulli *et al.*, Phys. Lett. B **369**, 325 (1996).
[80] RBC Collaboration, T. Blum *et al.*, Nucl. Phys. B (Proc. Suppl.) **94**, 291 (2001).
[81] S. R. Sharpe, Phys. Rev. D **46**, 3146 (1992).
[82] CP-PACS Collaboration, A. Ali Khan *et al.*, Phys. Rev. D **64**, 114506 (2001).
[83] JLQCD Collaboration, S. Aoki *et al.*, Phys. Rev. Lett. **80**, 5271 (1998).
[84] CP-PACS Collaboration, J. I. Noaki *et al.*, Phys. Rev. D **68**, 014501 (2003).
[85] Y. Aoki *et al.*, hep-lat/0211023.
[86] D. Chen *et al.*, Nucl. Phys. B (Proc. Suppl.) **73**, 898 (1999).
[87] R. D. Mawhinney, Parallel Comput. **25**, 1281 (1999).
[88] C. Bernard, Lectures given at TASI'89, Boulder, CO, 1989.
[89] M. Ciuchini *et al.*, J. High Energy Phys. **07**, 013 (2001).